COMPARATIVE EXPERIMENTAL STUDIES FOR GLOBAL DAMAGE DETECTION IN PLATES USING THE SCANNING LASER VIBROMETER TECHNIQUES

A Thesis

Presented to

The Graduate Faculty of The University of Akron

In Partial Fulfillment

of the Requirements for the Degree

Master of Science

Dabit Acharya

August, 2006

COMPARATIVE EXPERIMENTAL STUDIES FOR GLOBAL DAMAGE DETECTION IN PLATES USING THE SCANNING LASER VIBROMETER TECHNIQUES

Dabit Acharya

Thesis

Approved:	Accepted:
_____	_____
Advisor Dr. Atef Saleeb	Dean of the College Dr. George K. Haritos
_____	_____
Department Chair Dr. Wieslaw K. Binienda	Dean of the Graduate School Dr. George R. Newkome
_____	_____
Committee Member Dr. Wieslaw K. Binienda	Date

ABSTRACT

The main objective of this study is to show the specific capabilities of the Scanning Laser Vibrometer (SLV) for global damage detection using a recent defect energy parameter technique proposed by Saleeb and coworkers. The experimental technique used for extraction of signature is the first and most important part in any damage detection technique. Signatures considered here are full-field SLV measurements for modal shapes and associated frequencies of plated structures. The damage feature extraction capability was studied extensively by analyzing various simulation and experimental results. The practical significance in structural health monitoring is that the detection at early stages of small-size defects is always desirable. The amount of changes in the structure's response due to these small defects was determined to show the needed level of accuracy in the experimental methods.

The signal – noise ratio of experiment shows the capability of the same experiment to be used for damage detection purpose. Various experiments were performed to verify a significant signal – noise ratio for a successful detection. Very high number of scanning points, for optical experimental measurement, for any civil structure can be impractical and uneconomical. So, a pragmatic direction for the development of

new experimental measurement tools was studied where different number of scanning points and different types of statically loaded simulations were performed to verify the specific capabilities of the defect energy parameter technique. It was further observed that powerful graphic user interface should also be an integral part in any present in the damage detection scheme for successful and more accurate detection. Furthermore, some potential use of SLV techniques in detection are provided, both for dynamic and static applications.

ACKNOWLEDGEMENTS

I would like to express my deepest sense of gratitude to my advisor Professor Atef Saleeb, who has the substance of genius. He continually and convincingly conveyed a spirit of adventure in regard to research and an excitement in regard to teaching. Without his guidance and persistent help this thesis would not have been possible.

I would like to thank my committee member Dr. Wieslaw K. Binienda for his valuable help. Partial financial support during the course of this study by NASA Glenn Research Center, under Grand No. NCC3-808 to the University of Akron is gratefully acknowledged. I like to thank Dr. Steve Arnold, Life Prediction Branch, NASA, for providing help in this project.

My special thanks to Dr. Pizong Qiao, Dr. Wahyu Lestari and Mr. David McVaney for their continuous help and encouragement to complete the experimental part of this thesis. Sincere thanks to Mr. Krishna C. Vakada, my group members and friends for their support and moral encouragement.

Finally, I would like to thank my wife Pratibha for supporting me with her endless love and sound computer knowledge. My heartfelt gratitude to my parents, Mrs.

Manohari and Engr. Bed Nath Acharya for their selfless sacrifice, love, and support throughout my life. This thesis is dedicated to them in appreciation.

TABLE OF CONTENTS

Page

LIST OF TABLES

LIST OF FIGURES

CHAPTER I

INTRODUCTION

1.1 General

Damage is defined as change introduced into a structure which adversely affects its performance. Damage can also be defined as a phenomenon where the weakening of the structure takes place. Deviation in the structure's material property or geometry causing unwanted vibrations, displacements and stresses can also be termed as Damage.

Study of damage is very important since great amount of loss to property and life can be prevented by discovering the damage earlier. The tendency to use structures continually even after aging and deterioration, failure to make appropriate renovations on timely basics and natural hazards, places the study of damage in even more demanding position. Damage study can help designers to come up with more efficient designs, health monitoring of structures and even predict future failures.

There has been significant amount of research performed on damage detection schemes, but many factors still remain to be tested before the scheme can be judged and termed as an ideal procedure for damage detection. Limitations in accuracy of sensors

and instruments for measurement, omissions of experimental errors and disturbances, feature extraction capabilities and complexity of structure are to name a few.

1.2 Problem Statement

Extensive research work has been performed over past years to develop a reliable damage detection and non destructive evaluation (NDE) technique. Despite the effort, scheme with wide application and supporting practical situations are lacking. For any successful scheme, the following items should be studied.

1) The ability of damage detection scheme to be used in natural conditions withstanding noise: Practical application of any damage detection scheme has to face disturbances produced by sound, light, wind and vibrations. Filters used in the scheme should not affect the physics of the specimen.

2) Practicality of the density of Scanning Points: Any large structure undergoing divisions for the purpose of experiment and study should be divided into manageable and economical divisions. Excessive divisions would result in impractical time of study. Again, damage being small in nature should be detected with the scheme where the possibility of the area of damage not being intersected or touched by the scanning points has been considered.

4) Repeatability of experiments to verify results: Due to the complexity of natural conditions detection scheme should allow and compare the repeated experiments where the differences and errors in experiment could be measured.

5) Feature extraction and graphical user interface. Results of experiment should be studied and state – of – the – art graphical user interface should be used to finalize the detection.

In the present study, the focus will be on the detailed assessment of the items listed above in connection with the specific defect energy parameter technique developed recently for global damage detection by Saleeb, et al. [41,42] using Scanning Laser Vibrometer (SLV).

1.3 Objective of the Study

The objective of this study is the assessment of the capabilities of the global damage detection technique developed by Saleeb and coworkers using Scanning Laser Vibrometer and also the assessment of Scanning Laser Vibrometer itself. This study presents the work of damage identification on plates when subjected to out of plane vibrations for variety of cases. Damage identification on plates with various static loading cases with different loading locations is also presented. The assessment includes the validation of the technique by considering different types of high and ultra high damage modes obtained from Scanning Laser Vibrometer, repeatability of the experiments,

density of the scanning points and its significance, and feature extraction and representation of the cases mentioned above.

1.4 Outline

The introductory chapter is followed by background and review on literature in the areas of damage detection, Scanning Laser Vibrometer, Delta Mode Shapes and Graphical User Interface in Chapter II. Chapter III reports experimental procedures and results. Chapter IV describes the experimental results, compares physical experimental results with computer experimental results, limitations of the procedures and experiments, and density of scanning points. Finally, summary and future research areas are presented in Chapter V.

CHAPTER II

BACKGROUND AND LITERATURE REVIEW

2.1 Background

Damage detection is a challenging problem that is under vigorous investigation by numerous research groups using a variety of analytical and experimental techniques. A significant amount of research work over the years has dealt with general topic of structural health monitoring. Health monitoring techniques may be classified as global or local. Global methods attempt to simultaneously assess the condition of the whole structure, whereas local methods provide information about a relatively small region of the system by using local measurements. Clearly, these approaches are complementary to each other, with the choice of methods being dependent on the scope of the problem at hand and nature of the sensor network on the structure. The damage detection procedure depends on the level of damage and deterioration of concern, the nature of the instruments, the spatial resolution of the sensors, the degree of the measurement noise, the configuration of topology of the test structures, complexity of the detection scheme, and the depth of knowledge concerning the failure modes of the structure.

The effect of damage on a structure can be classified as linear or nonlinear. A linear damage situation is defined as the case when the initially linear-elastic structure remains linear-elastic after damage. The changes in modal properties are a result of changes in the geometry and/or the material properties of the structure, but the structural response can still be modeled using linear equations of motion. Linear methods can be further classified as model-based and non-model-based. Model-based methods assume that the monitored structure responds in some predetermined manner that can be accurately discretized by finite element analysis, such as the response described by Euler-Bernoulli theory.

Nonlinear damage is defined as the case when the initially linear-elastic structure behaves in a nonlinear manner after the damage has been introduced. One example of nonlinear damage is the formation of a fatigue crack that subsequently opens and closes under the normal operating vibration environment. Other examples include loose connections that rattle and nonlinear material behavior such as that exhibited by polymers. The majority of the studies reported in the technical literature address only the problem of linear damage detection.

Another confounding factor is the fact that damage typically is a local phenomenon. Local response is captured by higher frequency modes whereas lower frequency modes tend to capture the global response of the structure and are less sensitive to local changes in a structure. From a testing standpoint it is more difficult to excite the

higher frequency response of the structure, as more energy is required to produce measurable response at these higher frequencies than at the lower frequencies. These factors coupled with the loss of information resulting from the necessary reduction of time-history measurements to modal properties add difficulties to the process of vibration-based damage identification.

The Non Destructive Evaluation (NDE) methods for detection of damage in structural systems have received increasing attention in the recent past for different classes of structural components using the signature analysis of the system response. While there are many approaches that have been investigated, or still being developed for signature based NDE of structure, the class of health-monitoring approaches that do not require detailed knowledge of the vulnerable parts of the structure, or of the failure mode of the structure, have a significant advantage in that they have the potential to cope with unforeseen failure patterns. Classes of NDE schemes that are less sensitive to the effects of initial assumptions are certainly of significant advantage. Considering the details of the NDE technique, focus is placed on the response signature-analysis, providing a global approach for fault diagnosis, as opposed to other local methods that require one to look directly at the location of suspected defects.

2.2 Literature Review – An Overview

The term damage refers to degradation or a failure of material. It can originate from diverse phenomena such as oxidation, carbonation, mechanical work, or any type or

disintegration or weakening from aging or mechanical process. Within the framework of damage mechanics, only that which causes the loss of area, associated with change in local material properties such as Young's modulus E, moment of inertia I, stiffness and flexibility and energy dissipation, is considered. When such changes occur there is a change of the entire physical system. This change leads to a change in vibration characteristics in physical space and also in material space.

Experimental techniques in damage detection play a vital role. Effective measurement techniques are in high demand. Optical measurement is one of the effective measuring techniques since sensor contact with the specimen is not present which results in better measurement. High and Ultra high frequencies and associated mode shapes could be performed experimentally using optical measurement technique. However the fundamental quality of an experiment for detection remains the same where signal – noise ratio should be significant.

2.3 Literature Review – Scanning Laser Vibrometer and Delta Mode Shape

Leong, Staszewski, Lee and Scarpa [1] used piezoceramic transducers of 10 volts to activate Lamb wave. Aluminum Plate specimen with two sides fixed was introduced with dynamic loading of 10 KN and static loading of 13.5 KN. Specimen was fatigued up to 196000 cycles. Spark – eroded notch of 1mm diameter and 3 mm length was introduced in the middle of the plate in order to initiate a crack in fatigue testing. Microscope was used to measure and monitor the crack growth. Conclusion of the study

was cracks longer than 6 mm were detected and future research was indicated towards higher frequencies of excitation and better signal processing in order to increase the sensitivity to damage.

Halkon, Frizzel, Rothberg [2] used Polytec OFV323 laser Vibrometer and a pair of GSI Lumonics M3 galvanometers. Each galvanometers could drive the mirror angular displacement by 15^0. The model enabled the prediction of the laser Vibrometer output for any measurement configuration on any target. The experimental validation confirmed that additional component appearing in rotating target measurements were associated with both the scanning system configuration and any misalignment between the scanning system and targeted rotational axes. The use of velocity sensitivity model for the vibration engineer to make laser Doppler Vibrometer measurements reliable.

Pai, Kim and Chung [3] studied an actual aircraft wing panel for damage detection with scanning laser Vibrometer. PZT was used as an actuator and place near the clamped end of the cantilever experiment set up. Specimen was damaged in two ways. Nuts were glued to the specimen for first type of damage and placed on the sluts for the second type of damage. Ultra high frequencies were used for detection and in house software were used for processing.

Pai and Jin [4] used operational deflection shapes measured by scanning laser Vibrometer for damage detection. Two symmetric PZT patches were used at the fixed

end of the cantilever beam specimen with symmetric open crack at the center of the beam. Delta Mode Shapes were compared in one dimension for damage detection.

Khan, Stanbridge and Ewins [5] used operational deflection shapes measured by scanning laser Vibrometer for damage detection. PZT patches was used at the fixed end of the cantilever beam specimen with open crack near the fixed end of the beam. Delta Mode Shapes were compared in one dimension for damage detection. Similar approach were performed for two dimensional plate specimen.

Pai and Young [6][7] used operational deflection shapes measured by scanning laser Vibrometer for damage detection. Two symmetric PZT patches were used at the fixed end of the cantilever beam specimen with three symmetric open crack at different locations of the beam. Delta Mode Shapes were compared in one dimension for damage detection.

Choi, Park,Yoon and Stubbs [8] obtained the changes in the modal compliance distribution using the mode shapes of the pre-damaged and post-damaged states of the structure. Experiment were performed on steel test plate with all sides fixed by welding. Impact hammer was used for the loading and the experiment was repeated for verification of the results. Response accelerometer was glued on the specimen, 4 channel signal analyzer and computer was used to collect the data. Four different types of damage configuration were studied and damage detection was concluded with strain energy approach.

Swamidas and Chen [9] concluded that, by monitoring the changes in the local strain frequency response functions and the difference between the strain mode shapes, the location and severity of the crack that occurs in the structure could be determined. Modal analysis was performed on a cantilever plate with a small crack using finite element analysis. It was also observed from other parallel studies that the use of a proper and careful experimental procedure would eliminate the noise problems always present in strain gauge instrumentation.

Titurus, Friswell and Starek [10] developed a method for the estimation of damage location and apply it to the experimental case study. Modal sensitivity and changes in the measured modal quantities arising from the structural damage were studied.

Vanlanduit, Guillaume, Schoukens and Parloo [11] defined linear and nonlinear damage detection techniques. The location and size of the damage used was compared to the location and size of the damage experimented and presented in this thesis. After receiving a very rough delta mode shape it was concluded in this paper that a smooth delta mode shape with significant signal – noise ratio is required for a detectable scheme.

Gordon and Douglas [12] used ultrasonic lamb waves for damage detection. Types of damage were compared in this thesis with the type of damage explained in this

literature. Double winged indentation damage was introduced in a plate specimen and damage parameter distribution was compared with simulated ideal case.

2.4 Literature Review – Detection Methods of System Identification Type

Difficult challenges in formulating damage parameters possessing all these and other desirable attributes (e.g. applicability to different materials, multiple damage sites, various support condition, different vibration modes, etc.) are indicated by the numerous proposals made over the years (e.g., natural frequencies, mode shapes, influence flexibility coefficients, strain mode shape, curved mode shapes, as well as ratios, differences, fractions obtained form them). Basically, the performance of these measures was found to be heavily problem-dependent, with several conflicting conclusions often reached, when using the same measure under different conditions.

Zimmerman and Simmermacher [13] computed the stiffness perturbation resulting from multiple static load and vibration tests. This technique is proposed partially as a method for circumventing the mismatch in the number of models between test and FEM. They applied this technique to a FEM of a structure similar to a NASA test article. They also presented two techniques for overcoming the rank deficiency that exists in the residual vectors when the results of one static or modal test are linear combinations of the results of previous tests.

Kaouk and Zimmerman [14] extended the MRPT algorithm to estimate mass, stiffness, and proportional damping perturbation matrices simultaneously. The computation of these individual perturbation matrices is accomplished by exploiting the cross-orthogonally conditions of the measured mode shapes with respect to the damage property matrices. The authors examined the results by computing a cumulative damage vector.

Chen and Garba [15] presented a method for minimizing the norm of the model property perturbations with a zero modal force error constraint. They also enforce a connectivity constraint to impose a known set of load paths onto the allowable perturbations. The updates are thus obtained at the element parameter level, rather than at the matrix level. This method is demonstrated on a truss FEM.

McGowan, et al.[16] report ongoing research that examines stiffness matrix adjustment algorithms for application to damage identification. Based on the measured mode shape information from sensor locations that are typically fewer than the DOF in an analytical model, mode shape expansion algorithms are employed to extrapolate the measured mode shapes such that they can be compared with analytical model results. These results are used to update the stiffness matrix while maintaining the connectivity and the sparsity of the original matrix.

Ricles [17] presented a methodology for sensitivity-based matrix update, which take into account variations in system mass and stiffness, center of mass locations, changes in natural frequency and mode shapes, and statistical confidence factors for structural parameters and experimental instrumentation. The method uses a hybrid analytical / experimental sensitivity matrix, where the modal parameter sensitivities are computed from the experimental data, and the matrix sensitivities are computed from the analytical model. This method is further developed and applied to more numerical examples by Ricles and Kosmatka.

Sanayei and Onipede [18] presented a technique for updating the stiffness parameters of a FEM using results of a static load-displacements test. A sensitivity-based, element-level parameter update scheme is used to minimize the error between the applied forces and forces produced by applying the measured displacements to the model stiffness matrix. The sensitivity matrix is computed analytically. The structural DOF are partitioned such that the locations of the applied loads and the locations of the measured displacements are completely independent. The technique is demonstrated on two FEM examples.

Zimmer and Kaouk [19] implemented an eigenstructure assignment technique for damage detection. They included algorithms to improve the assignability of the mode shapes and preserve sparsity in the updated model. They applied their technique to the identification of the elastic modulus of a cantilevered beam.

Schulz, et al. [20] presented a technique similar to eigenstructure assignment known as “FRF assignment”. The authors formulated the problem as a liner solution for element-level stiffness and mass perturbation factors. They pointed out that using FRF measurements directly to solve the problem is more straightforward than extracting mode shapes. They used measured mobility functions (FRFs from velocity measurements) to obtain higher numerical accuracy, since the velocity response is flatter over the entire spectrum than either the displacement or acceleration response. The technique is applied to an FEM of a bridge structure.

Stubbs and Osegueda [21] evaluated non-destructive damage detection. The damage was modeled by reduced modulus in the element. A finite element model was used to establish the sensitivity matrix. Laboratory experiments were performed for supporting the concept. As far as the damage location is concerned, false predictions still occurred. Moreover, from the experimental results, small damage levels cannot be detected.

West [22] presented what is possibly the first systematic use of mode shape information for the location of structural damage without the use of a prior FEM. The author uses the Modal Assurance Criteria (MAC) to determine the level of correlation between modes from the test of an undamaged Space Shuttle Orbiter body flap and the modes from the test of the flap after it has been exposed to acoustic loading. The mode

shapes are partitioned using various schemes, and the change in MAC across the different partitioning techniques is used to localize the structural damage.

Stubbs and Topole [23] proposed a formulation that localizes and determines the size changes in the stiffness of the structure. Generally such changes are a reduction in stiffness and are associated with some type of structural damage. Serious damage will change the stiffness locally and globally. Thus a reduction in stiffness is generally interpreted as damage. However, reductions in stiffness do not necessarily relate to damage. Therefore, the algorithm is a conservative method to determine potential locations of damage.

Stubbs, et al [24] presented a method based on the decrease in modal strain energy between two structural DOF, as defined by the curvature of the measured mode shapes. Topole and Stubbs [23, 24] examined the feasibility of using a limited set of modal parameters for structural damage detection. They studied several dynamic parameters for damage detection using full scale modal testing. A probable failure due to a large fatigue crack was simulated by unfastening a set of high-strength bolts in a splice connection of a steel highway bridge. Experimental modal testing was performed for intact case as well as the cracked case. Results indicate the presence of detectable changes in some of the response data to a simulated physical failure. Non-parametric information, i.e., time records, frequency spectra, transfer functions as well as parametric information, i.e., modal frequencies and mode shapes had been examined. The Modal

Assurance Criteria (MAC) and modal frequencies can detect the damage in higher modes; otherwise the modal frequencies were not sensitive. In more recent publications, Stubbs and Kim examined the feasibility of localizing damage using this technique without baseline modal parameters.

2.5 Concluding remarks

A great deal of research in the past thirty years has been aimed at establishing an effective method for health monitoring in civil, mechanical, and aerospace structures. The objective is to determine the existence, location, and degree of damage in a structure. The development of a successful technology for structural health monitoring has enormous potential for application in evaluation of offshore structures and bridges subject to fatigue, corrosion, impact and earthquakes as well as buildings and aerospace structures subject to severe loads or structural deterioration. A variety of methods for evaluating damage in structural systems have emerged and evolved. All of these methods require a parameter estimation algorithm to drive them; i.e. the selection of an appropriate "measure" or suitable perturbation in system properties. To this end, recent work by Saleeb, et al. [25, 26, 27, 28] has been directed towards the development of appropriate global indices of this type, based on a more fundamental approach in structural mechanics.

Types of indentation damage in plate structures, size of the damage, boundary condition of the specimen, various techniques in the excitation of the actuator and

limitation in using Scanning Laser Vibrometer were observed from the above listed literatures and used for the experimental and analytical observation in this thesis.

CHAPTER III

TEST SET-UP AND EXPERIMENTAL RESULTS USING SCANNING LASER VIBROMETER (SLV)

3.1 Scope of Presentation

To check the validity of the physical experiment using Scanning Laser Vibrometer, computer experiments were performed. MS Excel was used for the generation of coordinates and C#.NET was used as a driver to generate input files for Damage Detection Code. SAP2000 was used for initial estimate of input frequencies for Scanning Laser Vibrometer. Specified displacements obtained from the experiment were used to create input files for Damage Detection Code using the same driver. Eview and Sigma Plot were used for processing and post processing damage parameter distribution. Figure 3.1 illustrates the Scope of work and presentation.

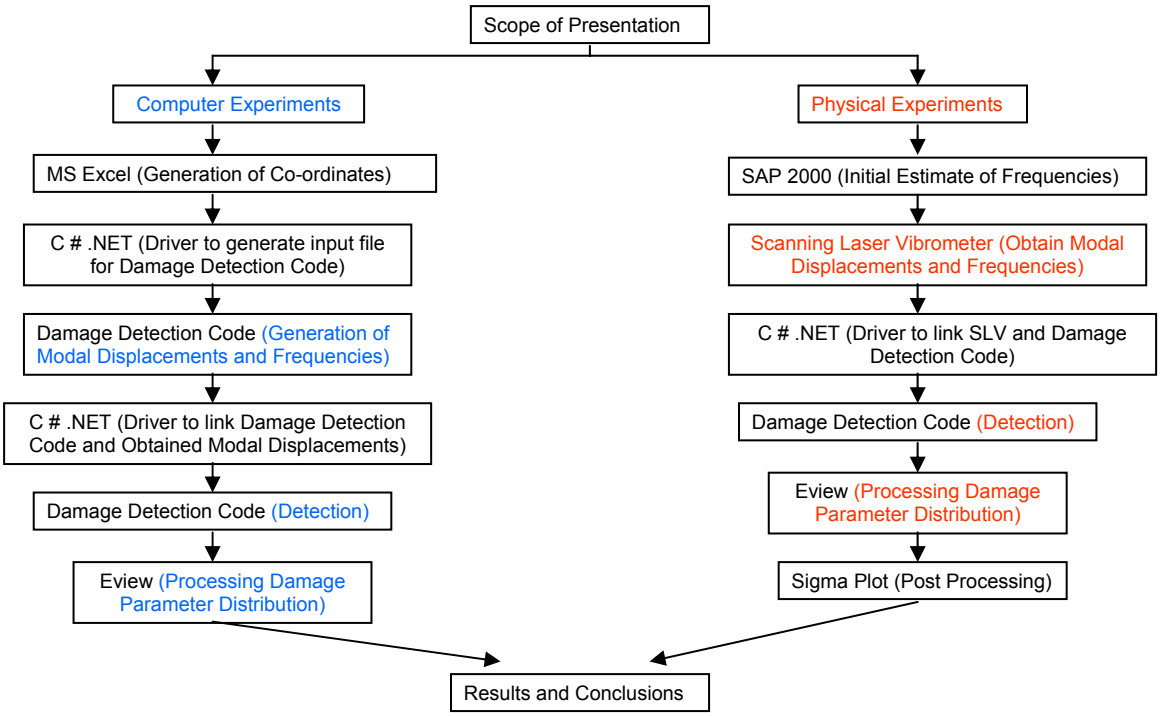

Figure 3.1 System Diagram for Damage Detection

3.2 Scanning Laser Vibrometer

Scanning Laser Vibrometer consists of Laser Head, Controller Box and Screen. Laser Head is equipped with 72 times zoom video camera for measuring large and small objects without repositioning. Controller Box has decoding of measurement signal. It can generate an analog voltage signal proportional to vibration velocity. B, H4, M2, M4, M2-20 are different types of controller for Scanning Laser Vibrometer. One used for study in this thesis is PSV-400H4.

Figure 3.2 Scanning Laser Vibrometer (Laser Head on tripod and computer screen on the top of controller)

Laser Head generates a laser beam which is divided into object beam and reference beam. Object beam reflects after hitting the object (specimen) and coincides with reference beam. Difference in the reference and object beam is analyzed by the controller and modal shapes are displayed on computer screen. Figure 3.3 illustrates the laser head work flow.

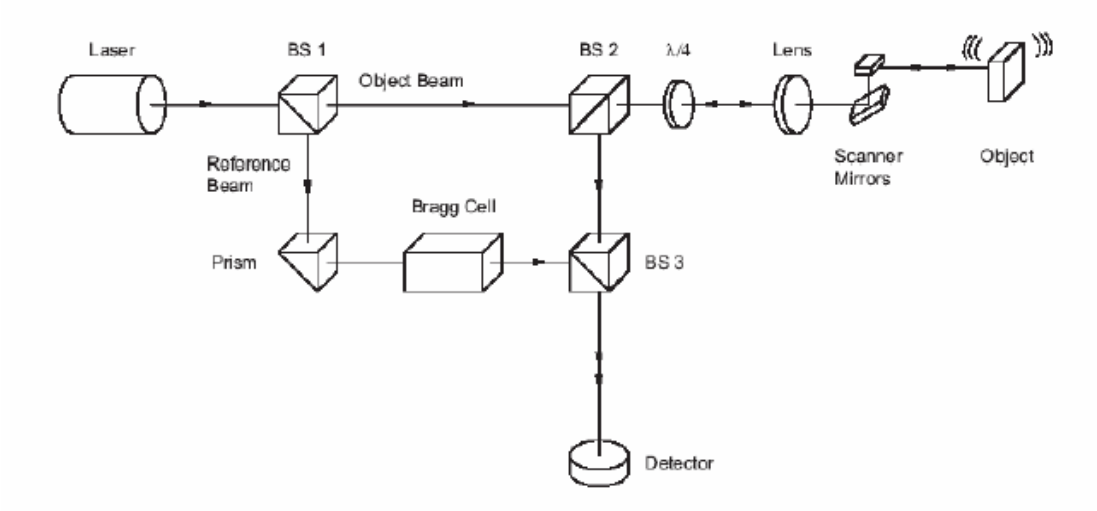

Figure 3.3 Laser Head Work Flow

3.3 Damage Detection Code

Theoretical development of Damage Detection Code is by Dr. A. F. Saleeb. For the current study features like Generation of Modal Displacement, Generation of Natural Frequencies, Damage Detection using Modal Displacements obtained from SLV and Damage Detection Code and Processing of damage parameter distribution were performed.

3.4 Initial Preparation

An Aluminum Plate, 12 inches wide, 24 inches long and 0.125 inches thick was purchased, which had yield strength of 17,000 psi and hardness of 32 Brinell. Lead Zirconate Titanate (PZT) was used as an Actuator, so 25mm long and 15mm wide PZT was arranged. Tape Copper was placed on one side of the Actuator and the connectivity was checked using a voltmeter. Epoxy and Core (hardener) was prepared and smeared on

the same side of the PZT where the copper tape was placed. Then the Actuator was glued to the Aluminum Plate, pressed with a heavy load and left for 24 hours.

After the period of attaching the Actuator with the Aluminum Plate, the connectivity was checked again using voltmeter. Using a soldering machine black copper wire was connected to the copper tape and red copper wire was connected to the surface of PZT. Border lines of 17 mm were drawn on all sides of Aluminum Plate. For the side, where Actuator was glued, two lines were drawn. First line, 2 inches from the edge of the plate was drawn to indicate the line for the clamp. Second line was drawn 1.5 inches from the first line as a border for that side as shown in Figure 3.4.

Figure 3.4 Aluminum Plate and Actuator

3.5 Polyvinylidene Fluoride (PVDF)

Polyvinylidene fluoride (PVDF) as a Piezo Film Element was used as a reference sensor. First of all, sensor head was glued on one side of a double coated tape. Small piece of paper was also glued on the top part of the tape for easy removal of the sensor if necessary. Then the sensor was placed on the exact opposite location of the Actuator. The face of the specimen with Actuator was so placed to face the laser from Scanning Laser Vibrometer as shown in Figure 3.5.

Figure 3.5 Piezo Film Element

3.6 Experiment Set Up

Experiment from general set up to data collection is reported in the following subheadings.

3.6.1 General

Line drawn on the Aluminum Plate for the clamp was used to align the Specimen. On a heavy cantilever type clamp, equipped with four tightening screws, the Specimen was clamped firmly. Level of the surface of the clamp, floor and the top of the Specimen

was checked to insure horizontal level. Edges of the Specimen were marked on the surface of the clamp for future repetitions.

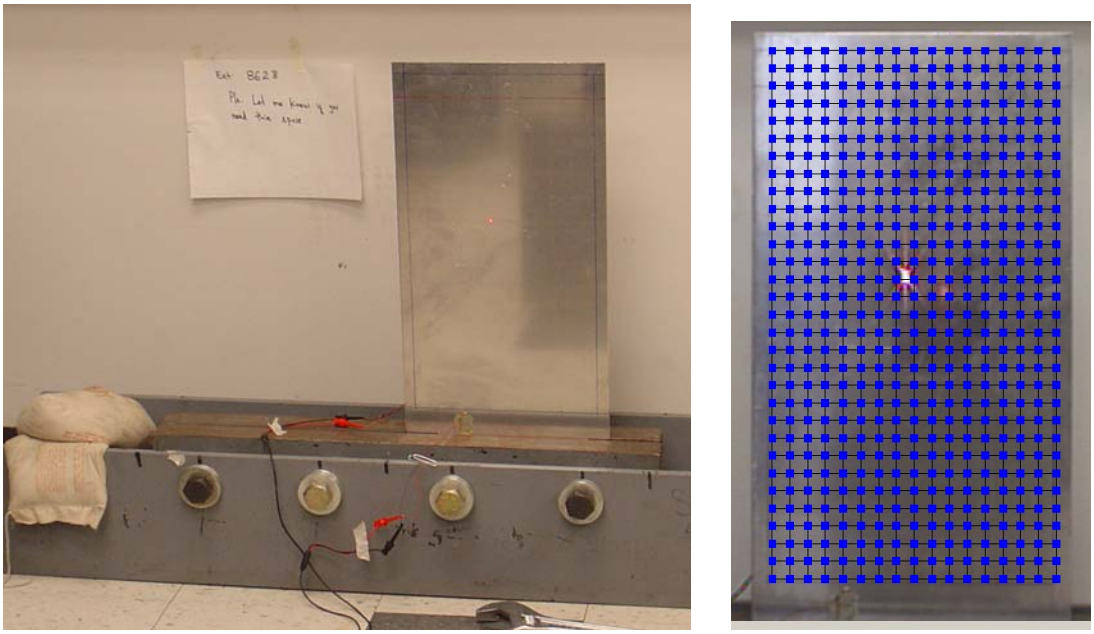

Figure 3.6 Specimen and Clamp (left) and video view from SLV (right)

3.6.2 Scanning Laser Vibrometer (SLV) Set Up

First of all, the connectivity of the controller of SLV was checked. PVDF was connected to Analog Input Ref 1. Actuator was connected to Generator Output Signal 1. Velocity in Analog Input was connected to Output of Velocity and Trigger In was connected to Sync. Then the Laser Head was connected to the controller.

3.6.3 Scan Head Optimal Distance Set Up

Scan Head Optimal Distance is the distance between specimen and the lens in the Laser Head of SLV. Scan Head Optimal Distance was obtained by using the following formula;

$$99mm + (N \times L)mm$$

Where,

N = 0, 1, 2, 3,…….

L = 204mm (plus or minus 1mm)

Using the above formula, Scan Head Optimal Distance was obtained which was recorded to be 1527mm when N was taken as seven.

After the distance was fixed, all the locations were marked including, four corners of Laser Head and four corners of Laser Head Stand.

Figure 3.7 SLV Laser Head and Specimen after the fixed Scan Head Optimal Distance

3.7 Scanning Laser Vibrometer Software Set Up

Experiment from general set up to data collection is reported in the following subheadings.

3.7.1 General

SLV has two major modes in its software, 1) Acquisition 2) Presentation, as described in Chapter II. Acquisition Mode allows us to input the experiment where as Presentation Mode is used for viewing the results.

3.7.2 Estimating Frequency Using SAP2000 and Defining Mode Clusters

SAP2000 was used to estimate few natural frequencies of the Specimen to begin with. It was obtained from SAP2000 that the frequency of first mode shape should be around 8 Hz and frequency of 10^{th} mode shape should be around 360 Hz. So, three clusters of mode shapes were decided. First Cluster starting from 125 mille Hz to 400 Hz would provide around 10 initial mode shapes. Second Cluster starting from 650 Hz to 1.8 KHz would provide around 15 intermediate mode shapes and third cluster starting from 2 KHz to 3.1 KHz would provide around 12 higher mode shapes. For each cluster, starting frequencies were taken lesser and ending frequencies were taken more than the estimated frequency obtained from SAP2000 to be in safer side. Table 3.1 shows the modal frequencies obtained from SAP2000.

Table 3.1 Modal Frequencies obtained from SAP2000

M O D A L P E R I O D S A N D F R E Q U E N C I E S

MODE	PERIOD (TIME)	FREQUENCY (CYC/TIME)	FREQUENCY (RAD/TIME)	EIGENVALUE (RAD/TIME)**2
1	0.120196	8.319734	52.274432	2732.616
2	0.031058	32.197718	202.304232	40927.002
3	0.019405	51.533552	323.794860	104843.111
4	0.009385	106.555517	669.508060	448241.042
5	0.006933	144.245969	906.324156	821423.476
6	0.005015	199.412252	1252.944	1.5699E+06
7	0.004766	209.808148	1318.263	1.7378E+06
8	0.003717	269.034564	1690.394	2.8574E+06
9	0.003401	294.053902	1847.595	3.4136E+06
10	0.002830	353.366119	2220.265	4.9296E+06
11	0.002532	394.902999	2481.249	6.1566E+06
12	0.002078	481.323412	3024.244	9.1461E+06
13	0.001924	519.646966	3265.038	1.0660E+07
14	0.001810	552.468172	3471.260	1.2050E+07
15	0.001794	557.516932	3502.982	1.2271E+07
16	0.001664	600.889797	3775.502	1.4254E+07
17	0.001391	719.079307	4518.109	2.0413E+07
18	0.001386	721.330742	4532.255	2.0541E+07
19	0.001316	759.918422	4774.708	2.2798E+07
20	0.001271	786.537056	4941.958	2.4423E+07
21	0.001117	895.459793	5626.340	3.1656E+07
22	0.001004	995.633199	6255.748	3.9134E+07
23	0.000997	1002.608	6299.570	3.9685E+07
24	0.000959	1042.496	6550.198	4.2905E+07
25	0.000936	1068.042	6710.705	4.5034E+07
26	0.000911	1098.088	6899.487	4.7603E+07
27	0.000900	1111.621	6984.524	4.8784E+07
28	0.000823	1215.581	7637.718	5.8335E+07
29	0.000770	1298.054	8155.915	6.6519E+07
30	0.000745	1341.672	8429.975	7.1064E+07
31	0.000733	1364.786	8575.206	7.3534E+07
32	0.000718	1392.258	8747.816	7.6524E+07
33	0.000713	1401.818	8807.881	7.7579E+07
34	0.000623	1604.702	10082.639	1.0166E+08
35	0.000610	1638.389	10294.304	1.0597E+08
36	0.000602	1660.448	10432.905	1.0885E+08
37	0.000589	1698.395	10671.331	1.1388E+08
38	0.000580	1724.926	10838.027	1.1746E+08
39	0.000569	1757.440	11042.324	1.2193E+08
40	0.000558	1792.474	11262.449	1.2684E+08
41	0.000534	1872.295	11763.978	1.3839E+08
42	0.000532	1880.565	11815.940	1.3962E+08
43	0.000498	2009.189	12624.107	1.5937E+08
44	0.000496	2017.809	12678.266	1.6074E+08
45	0.000488	2049.794	12879.236	1.6587E+08
46	0.000465	2151.230	13516.576	1.8270E+08
47	0.000459	2180.653	13701.450	1.8773E+08
48	0.000453	2209.587	13883.247	1.9274E+08
49	0.000441	2269.800	14261.575	2.0339E+08
50	0.000417	2398.526	15070.380	2.2712E+08

Program SAP2000 Nonlinear Version 7.40

3.7.3 Beginning the Experiment

Acquisition Mode was turned on by clicking the Acquisition button. The Beam Shutter in the laser head was opened manually. Red laser light was seen coming from the laser head. Any previous grid on the computer screen was deleted. On the computer screen only the live image of the specimen was present before the continuation to next step.

On the right bottom corner of the screen, auto focus for camera was clicked, to focus the specimen. On the top right corner of the screen, auto focus of DVF5000 was clicked to focus the beam. It was observed that the beam adjusted its size by growing larger in diameter first then reducing to a very small diameter until optimal diameter size was achieved.

To align the coordinate of the video camera and the laser, since the specimen was shinning bright, manual steps were taken. After clicking the Align coordinate button located at the top center part of the tool bar, auto align was disabled and all previous alignment were deleted. Nine buttons located on the mid right corner of the screen were used to drag the laser around the surface of the specimen. Using this, five points in differing locations were picked where the center and the left buttons of mouse were clicked. Then it was observed that the laser beam was following the click of the mouse right button inside the surface of the specimen. Throughout the experiment, every time the computer was turned off, this process of alignment was repeated.

The border line drawn on the specimen was used to Define Scan Points. Define Scan Points button located on the mid top of the screen on the tool bar was clicked. With the rectangular draw tool bar, a rectangle was drawn over the boarder line on the specimen. The X density and Y density values defines the mesh. So for the first cluster the values for X and Y densities were 40 and 40 respectively which would create a mesh with 527 total nodal points. For second and third clusters X and Y densities were 70 and 70 which would create a mesh with 1537 total nodal points.

Assign Focus Scan in Scan toolbar was selected and a success message was confirmed. Focus During Scan was also checked.

3.7.4 Acquisition Settings

Acquisition Setting consisted of eight parameter window pages. In General page measurement mode was taken as FFT, Averaging was takes as Magnitude with 5 and Remeasure was checked. In Channels page, for active, Vibrometer and Reference 1 were checked, for quantity, Displacement was selected for both Vibrometer and Reference 1. In Filters page, No Filter was selected for both Vibrometer and Reference 1. In Frequency page, for Band Width, 400 Hz, 2 KHz and 4KHz were placed for first, second and third clusters respectively. Similarly, for From block, 125mHz, 650 Hz and 2KHz , for To block, 400Hz, 1.8 KHz and 3.1KHz were placed. For FFT Lines block, 3200, 1600, 3200 were placed which provided a resolution of 125mHz, 1.25 Hz and 1.25 Hz respectively. In Windows page all rectangular windows were taken. In Trigger page, for Source, External (TTL) with Rising was taken. In Signal Enhancement (SE) page,

Vibrometer was selected and Speckle Tracking was checked in Fast position. In Vibrometer page, Velocity was selected to be 10mm/s/v and Filters were selected to be Off. In the Generator page, Active was checked and for Wave Form Burst Chrip with 20% start and 50% end was selected. The start and end frequency was provided according to the clusters. For the Amplitude block 3 volt was provided.

3.7.5 Summary of Acquisition Mode

For First Cluster: Total Nodal Points = 527

Averaging = 5

Band Width = 400 Hz

From = 125 mHz

To = 400 Hz

Resolution = 125 mHz

FFT = 3200

For Second Cluster: Total Nodal Points = 1537

Averaging = 5

Band Width = 2 KHz

From = 650 Hz

To = 1.8 KHz

Resolution = 1.25 Hz

FFT = 1600

For Third Cluster: Total Nodal Points = 1537

Averaging = 5

Band Width = 4 KHz

From = 2 KHz

To = 3.1 KHz

Resolution = 1.25 Hz

FFT = 3200

3.7.6 Presentation Mode

Presentation Mode is used for manipulation of the data. SLV was turned to Presentation Mode by clicking the button of Presentation Mode right next to the button of Acquisition. 3D Views was clicked to get the object in 3D. Analyzer window was obtained by clicking the arrow button on the left of the screen and Object and Analyzer was selected.

The Analyzer window allows selecting the peak of frequency. When all the peaks were checked, associated mode shape for each frequency appeared on the Object Window.

File – Save As ASCI was used to save the data and File – Save Graphics was used to save the Mode Shape.

3.8 Planning for the Experiment

Experiment from general set up to data collection is reported in the following subheadings.

3.8.1 Labeling the Experiments

Experiment for each cluster had to be repeated not only to check the results but also to build confidence in it. So, defining the name of each experiment played a vital role. Specimen before exposure to damage was named as “Healthy” and after damage was named “Damaged”. Both, Healthy and Damaged specimen had three clusters as explained before in 3.4.2, First cluster, Second cluster and Third cluster. Healthy Specimen was repeated three times. Two types of damage were introduced to the specimen and called Damage 1 and Damage 2, D1 and D2 in short, both D1 and D2 were repeated twice. Repeated experiment of Healthy specimen was called ‘A’ for first experiment, ‘B’ for second experiment and ‘C’ for third experiment. Repeated experiment of damaged experiment was called ‘E1’ for first experiment and ‘E2’ for second experiment.

So, A first cluster, A second cluster and A third cluster implied to Healthy specimen with first experiment containing lower, intermediate and higher mode shapes. B first cluster, B second cluster and B third cluster implied to Healthy specimen with second experiment containing lower, intermediate and higher mode shapes. C first cluster, C second cluster and C third cluster implied to Healthy specimen with third experiment containing lower, intermediate and higher mode shapes.

Similarly, for the damaged specimen, D1 E1 first cluster, D1 E1 second cluster and D1 E1 third cluster implied to first damage in the specimen with first experiment containing lower, intermediate and higher mode shapes. D2 E1 first cluster, D2 E1 second cluster and D2 E1 third cluster implied to second damage in the specimen with first experiment containing lower, intermediate and higher mode shapes. D1 E2 first cluster, D1 E2 second cluster and D1 E2 third cluster implied to first damage in the specimen with second experiment containing lower, intermediate and higher mode shapes. D2 E2 first cluster, D2 E2 second cluster and D2 E2 third cluster implied to second damage in the specimen with second experiment containing lower, intermediate and higher mode shapes.

3.8.2 Labeling the Mode Shapes

Mode Shapes were labeled according to their associated frequencies. During the experiment this way of naming the mode shapes helped tremendously. Since the frequency of damaged specimen should be less than that of the healthy specimen, the name of the mode shape itself was useful in determining the quality of the experiment.

So, D2 E2 2nd cluster 670 implied to the mode shape which was obtained from second experiment of second damaged specimen and was from intermediate cluster having natural frequency of 670Hz.

3.9 Damage Size Determination

Experiment from general set up to data collection is reported in the following subheadings.

3.9.1 Initial Steps

Damage is defined as changes in structures, which affects its performance. The mode shape and natural frequencies of a structure is affected by damage. As described in Chapter I, the natural frequency of damaged structure should reduce. So, as long as the natural frequency of the structure remains unchanged, the damage induced can be termed ineffective.

After the processing of data from all Healthy experiments, the obtained mode shapes and frequencies were studied. Frequency of damaged specimen should be less than the frequency of the healthy specimen. So, to obtain lesser frequency, numbers of initial damages were introduced in the specimen. After performing the experiment and studying the frequencies from each damage size, next size for the damage was determined. As shown in Figure 3.8.

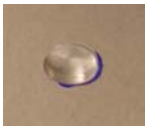

Single D

Three D

Eight D

Twenty-Eight D

Location of Single D

Location of Twenty-Eight D

Figure 3.8 Different Sizes and Location of Initial Damages

Single D was made using an End Mill with diameter of 0.25inch. All initial and final (D1 and D2) damages had depth of half the thickness of the specimen which was 0.0625 inches. Three D, Eight D and Twenty-Eight D were all created by dragging the same End Mill to the appropriate distance. For each damage size, experiments were performed twice to confirm the result. Along the line of drag, Three D had length of 0.75 inches, Eight D had length of 2 inches and Twenty Eight D had length of 7 inches. Widths of all these initial damages were 0.25 inches. Table 3.2 shows the frequencies of both healthy and damaged experiment.

Table 3.2 Frequencies tabulated to check the size of the damage Frequency (Hz)						
A	B	C	1 Hole	3 Holes	8 Holes	28 Holes
7.625	7.875	8	8	7.65	8	7.8
31.88	31.5	32.13	32.13	32	32	31.85
48.25	49	49.88	49.75	49.25	49.38	49
105.4	104.4	106.4	106	106	105.5	104.3
136	137.3	140.1	139.5	138.1	138.6	137
192	191.6	192.1	192	191.9	191.1	186.4
205.5	205.4	207.4	206.6	206.6	206	205.3
260.4	264	264.6	264.4	263.8	263.4	263.1
276.5	277.1	283	277.1	279.4	280	275.8
342.9	339.3	346.5	345.1	343.8	344.1	343.8
386	387.9	390.6	389.8	389	388.9	388.8
702.5	697.5	703.8	703.8	702.5	701.3	695
745	742.5	742.5	741.3	741.3	740.5	737.5
876.3	873.8	880	878.8	876.3	872.3	866.3
981.3	968.8	978.8	971.3	975	967.5	968.8
1000	1001	1006	1004	1003	997	993.8
1058	1058	1059	1058	1058	1056	1053
1088	1089	1095	1090	1090	1088	1085
1178	1178	1180	1178	1179	1176	1168
1304	1299	1313	1306	1311	1304	1291
1330	1343	1347	1341	1339	1338	1338
1354	1354	1357	1355	1356	1351	1350
1371	1373	1379	1375	1373	1370	1365
1569	1569	1575	1565	1571	1564	1558
1752	1755	1752	1740	1744	1741	1739
2085	2101	2080	2081	2090	2081	2078
2144	2146	2154	2150	2141	2141	2139
2353	2350	2364	2343	2353	2334	2337
2434	2430	2435	2434	2430	2425	2413
2547	2527	2566	2551	2545	2543	2534
2605	2606	2610	2609	2607	2603	2596
2991	2988	2996	2985	2993	2982	2978

From the Table 3.2 above it was noticed that the frequency of the specimen decreased as the damage size increased. It was also observed that the decrease in frequency was more noticeable in the higher frequency.

3.9.2 Final Damage Size

From Table 3.2, it was noticed, that the size of the damage was affecting the specimen. So, two types of final damages, bigger in size than that of 28 D damage were planned to be introduced in the specimen. As mentioned earlier, first damage D1 would be of same length as that of 28 D, which was 7 inches but the width would be doubled, which would now be 0.5 inches. It was anticipated that the frequencies obtained from this damage would be lesser that that of 28 D damage. Second final damage, D2, was also planned having almost double size than that of the first damage D1. Before D2 was introduced to the specimen, D1 was experimented twice as mention above. Figure 3.9 shows the two final damages.

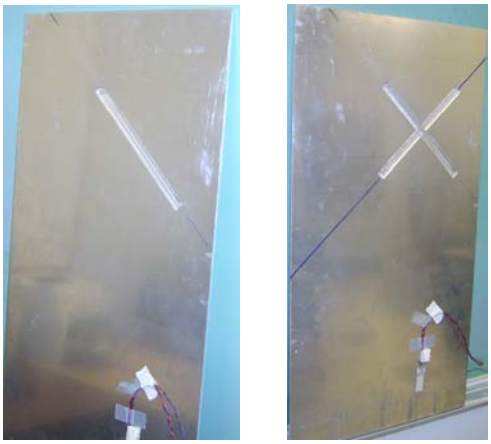

Figure 3.9 Final Damages D1 (left) and D2

3.10 Matching Mode Shapes and Frequencies

Experiment from general set up to data collection is reported in the following subheadings.

3.10.1 Obtaining Mode Shapes from SLV

Analyzer option was used to obtain the Mode Shapes. In the analyzer window, using a select curser, peak in the magnitude was selected. After SLV calculated the frequency and mode shape, if the shape did not appear like a mode shape, then it was discarded. Figure 3.10 shows the peak of magnitude of frequency.

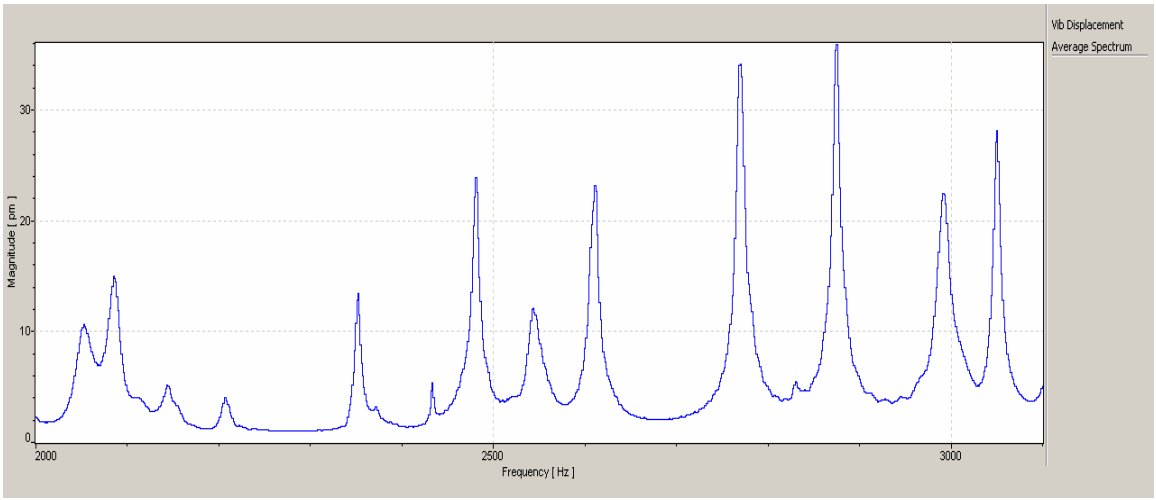

Figure 3.10 Analyzer window option of SLV for Mode Shape calculation

Obtained Mode Shapes presented collectively.

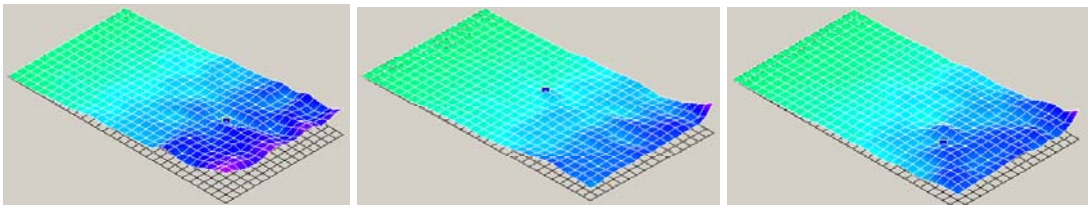

A-7.625 B-7.875 C-8

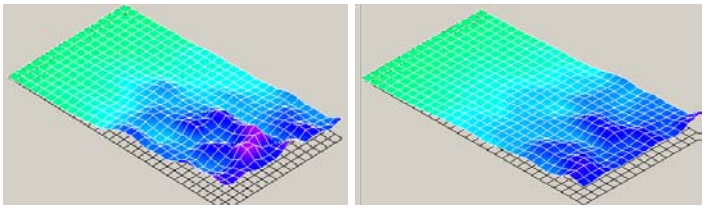

D1-E1-7.875 D1-E2-8

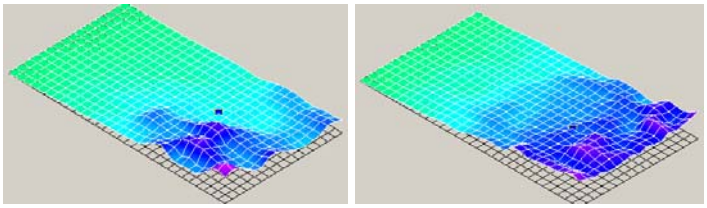

D2-E1-8 D2-E2-8

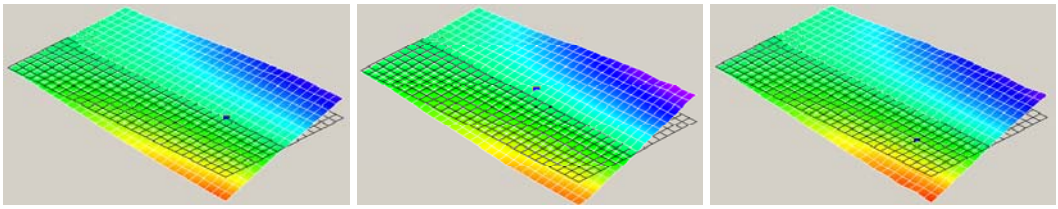

A-31.88 B-31.5 C-32.13

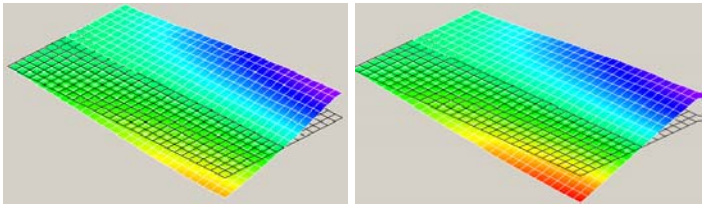

D1-E1-31.75 D1-E2-31.8

Figure 3.11 Mode Shapes and associated Frequencies with experiment label

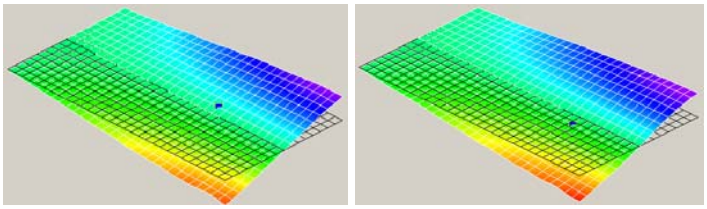

D2-E1-31.63 D2-E2-31.5

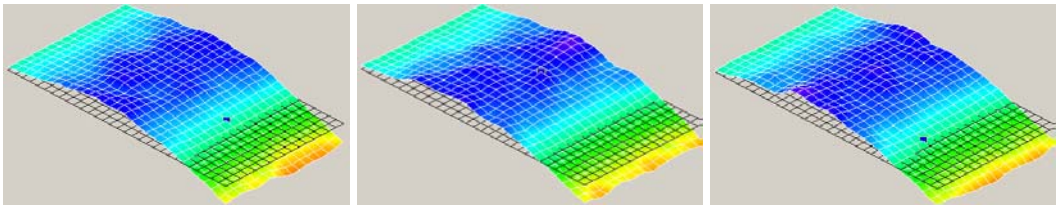

A-48.25 B-49 C-49.88

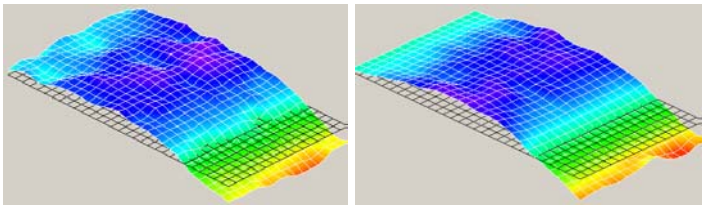

D1-E1-47.5 D1-E2-48.75

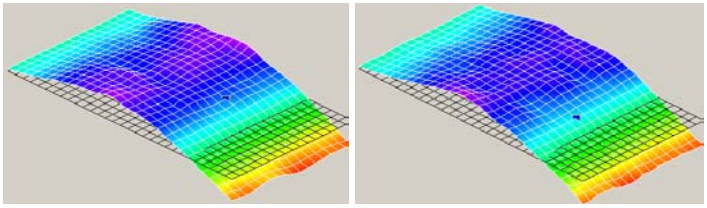

D2-E1-48.38 D2-E2-48.25

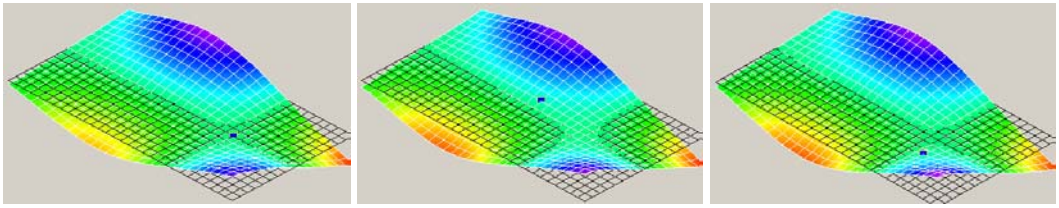

A-105.4 B-104.4 C-106.4

Figure 3.12 Mode Shapes and associated Frequencies with experiment label

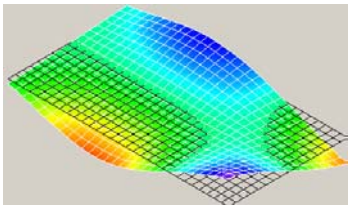

D1-E1-104.4

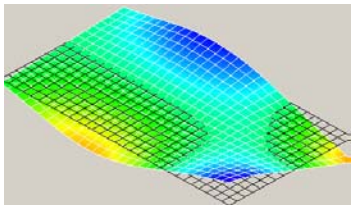

D1-E2-102.5

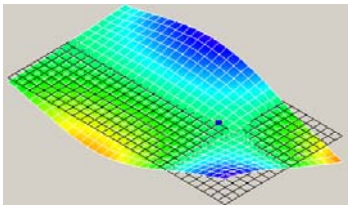

D2-E1-100.5

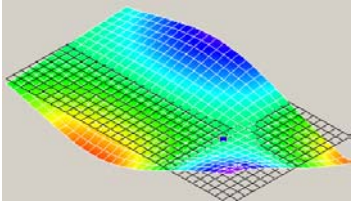

D2-E2-100.4

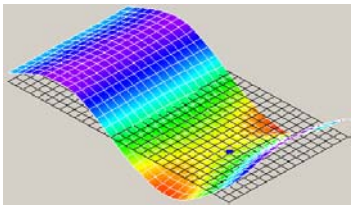

A-136

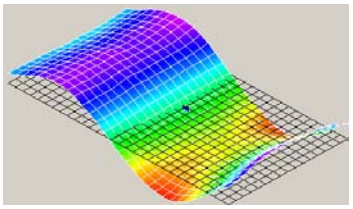

B-137.6

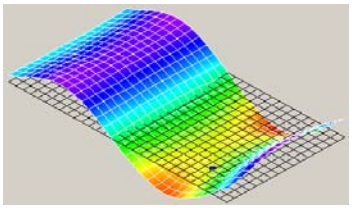

C-140.1

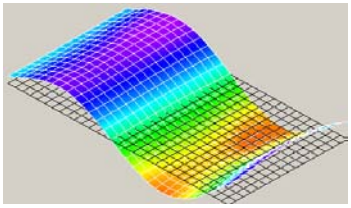

D1-E1-135

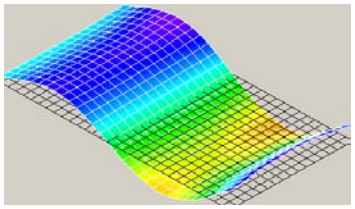

D1-E2-135.9

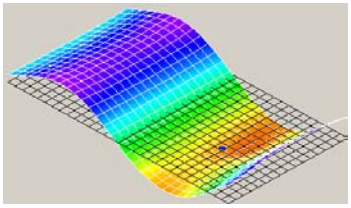

D2-E1-133.6

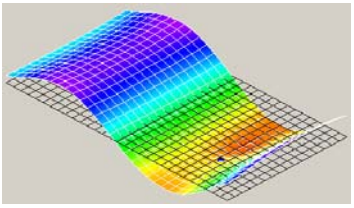

D2-E2-133.3

Figure 3.13 Mode Shapes and associated Frequencies with experiment label

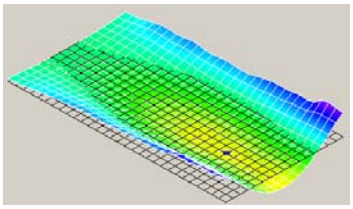

A-192

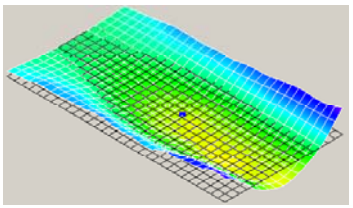

B-191.6

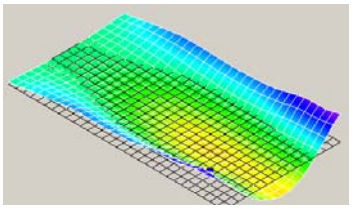

C-192.1

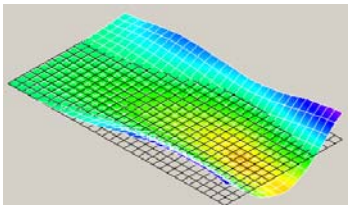

D1-E1-180.9

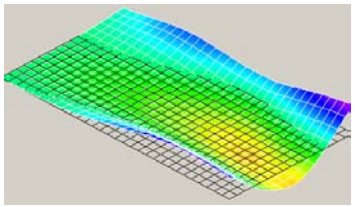

D1-E2-181

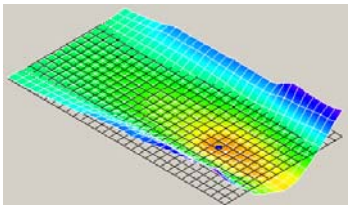

D2-E1-176.5

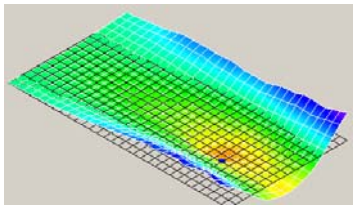

D2-E2-176.5

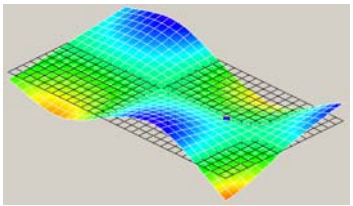

A-205.5

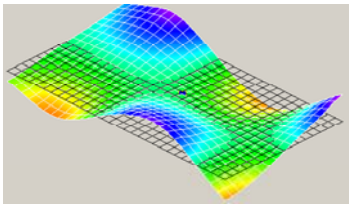

B-205.4

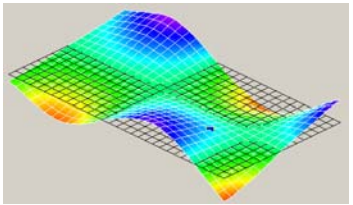

C-207.4

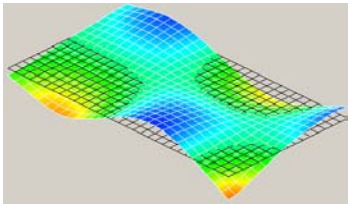

D1-E1-204.4

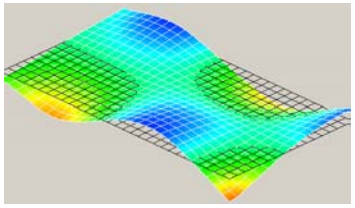

D1-E2-204.9

Figure 3.14 Mode Shapes and associated Frequencies with experiment label

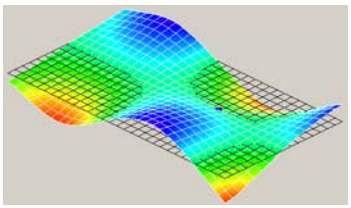

D2-E1-204.4

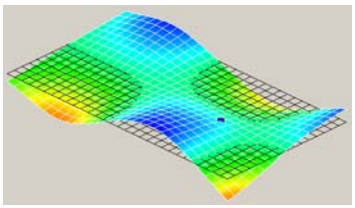

D2-E2-203.9

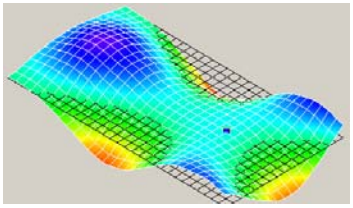

A-260.4

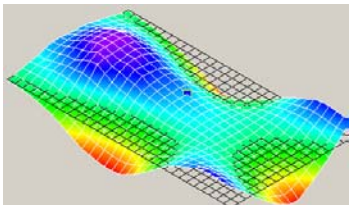

B-264

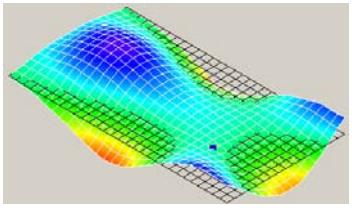

C-264.6

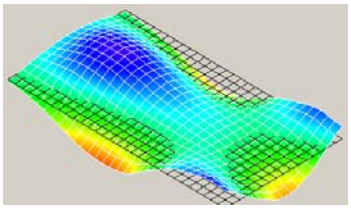

D1-E1-262.3

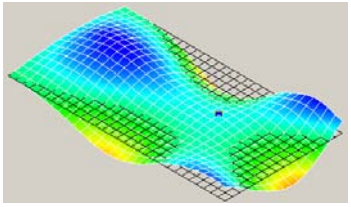

D2-E1-260

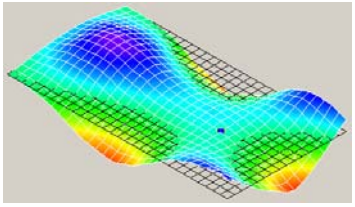

D2-E2-260.4

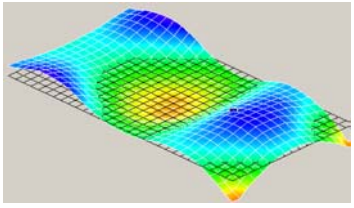

A-276.5

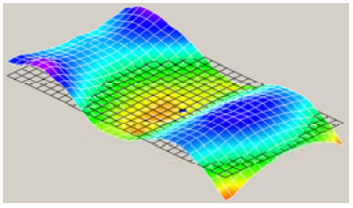

B-277.1

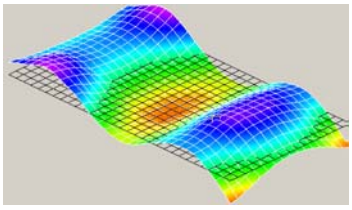

C-283

Figure 3.15 Mode Shapes and associated Frequencies with experiment label

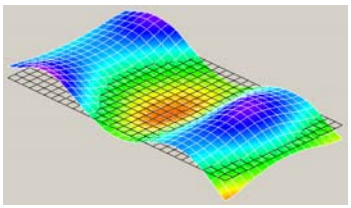

D1-E1-272.5

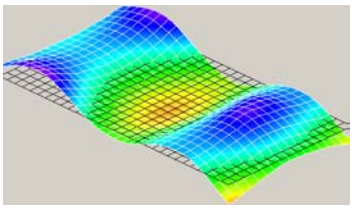

D1-E2-272.8

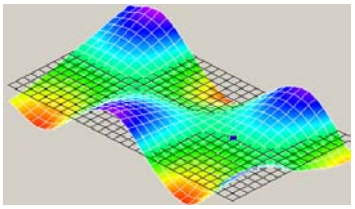

A-342.9

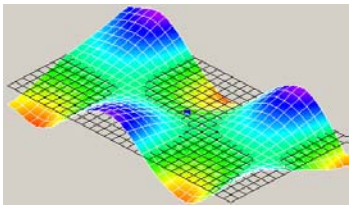

B-339.3

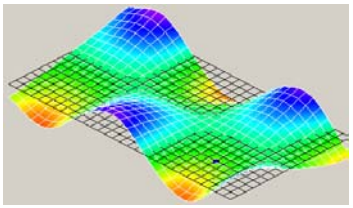

C-346.5

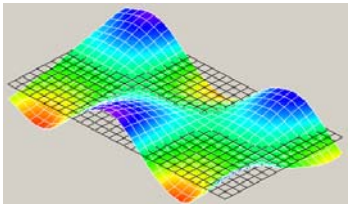

D1-E1-343.1

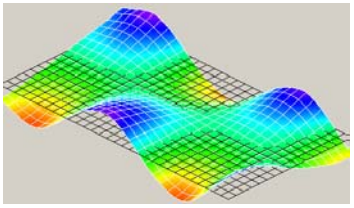

D1-E2-344.1

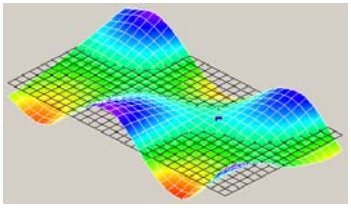

D2-E1-342.3

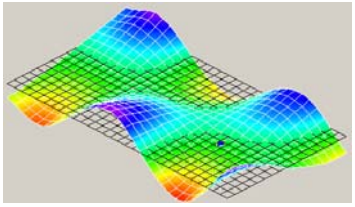

D2-E2-341.4

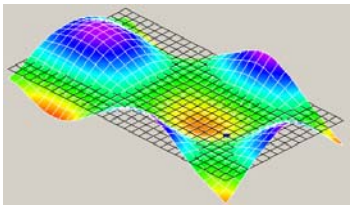

A-386

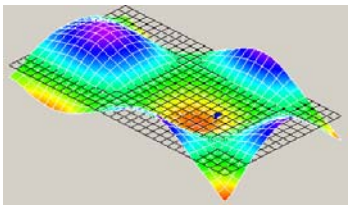

B387.9

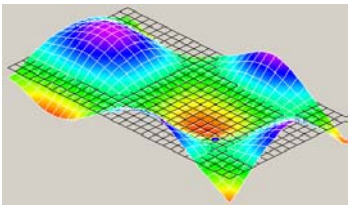

C-390.6

Figure 3.16 Mode Shapes and associated Frequencies with experiment label

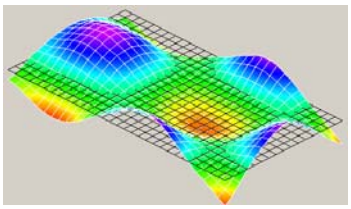

D1-E1-387.4

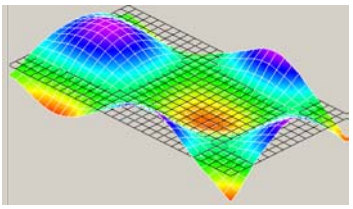

D1-E2-388.3

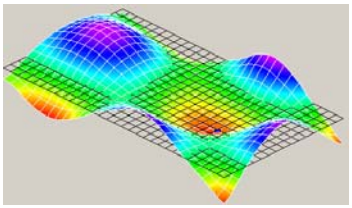

D2-E1-380.3

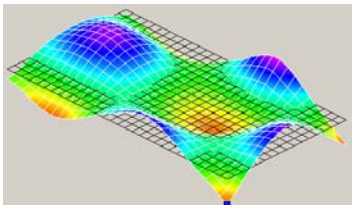

D2-E2-380.4

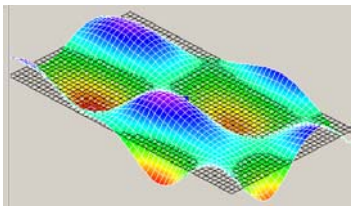

A-702

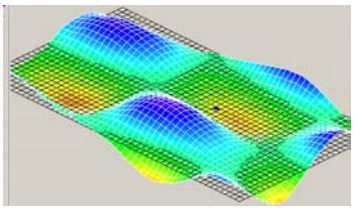

B-697.5

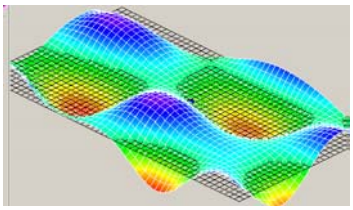

C-703.8

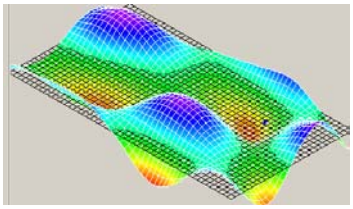

D1-E1-697.25

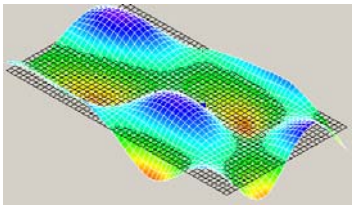

D1-E2-696.75

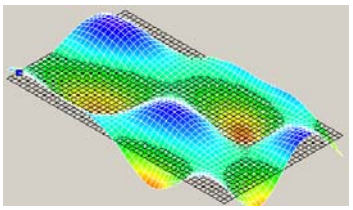

D2-E1-693.5

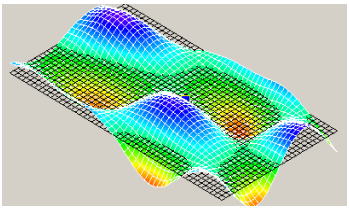

D2-E2-695

Figure 3.17 Mode Shapes and associated Frequencies with experiment label

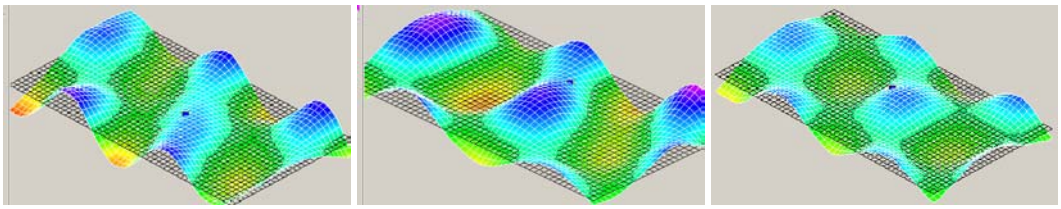

A-745 B-742.5 C-742.5

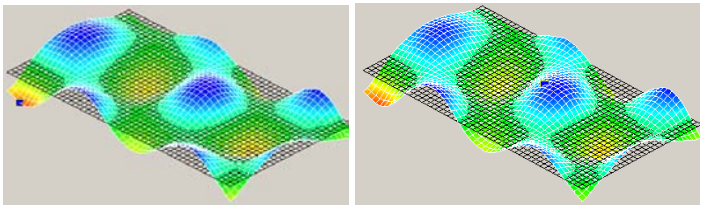

D2-E1-735.6 D2-E2-736.5

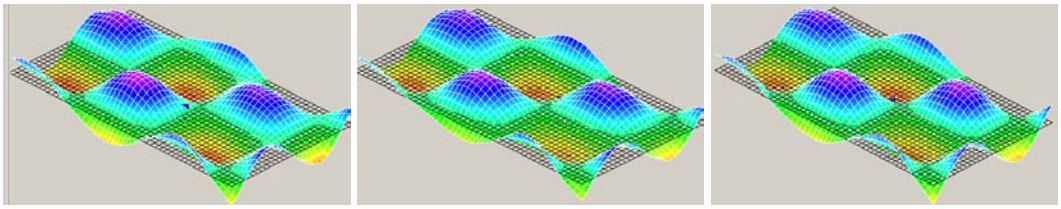

A-876.3 B873.8 C-880

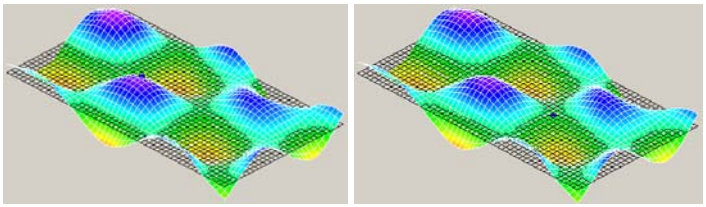

D1-E1-871 D1-E2-871

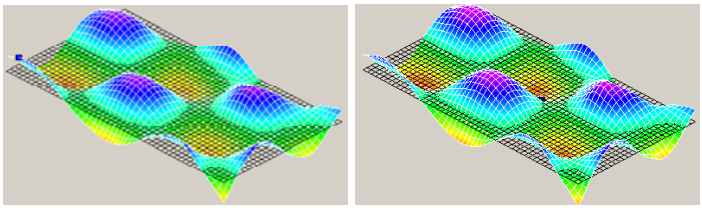

D2-E1-865 D2-E2-867

Figure 3.18 Mode Shapes and associated Frequencies with experiment label

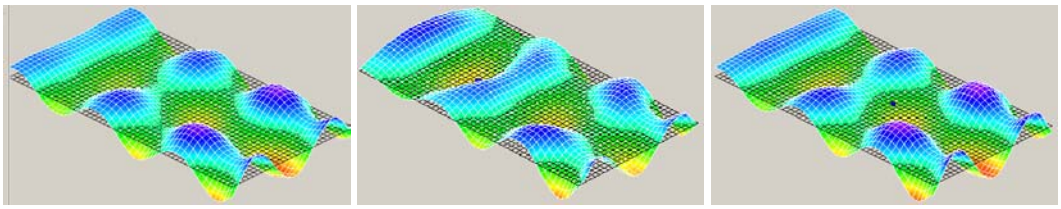

A-981.3 B-968.8 C-978.8

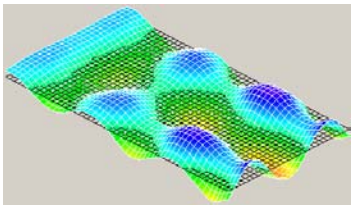

D1-E2-970

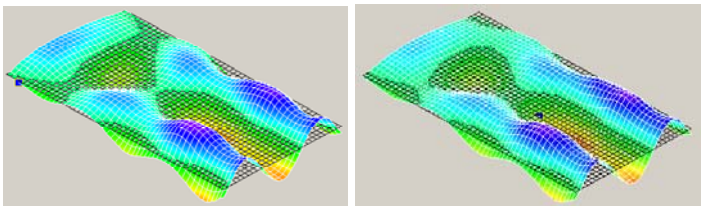

D2-E1-963 D2-E2-964

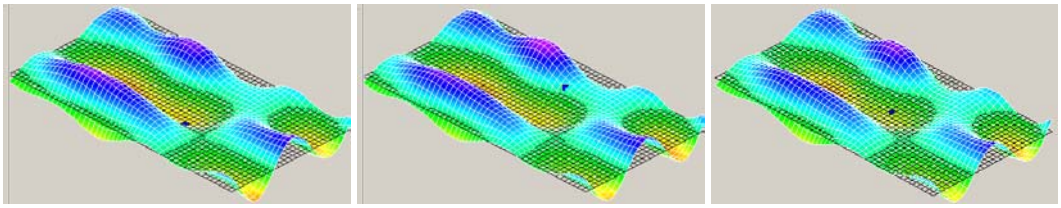

A-1058 B-1058 C-1059

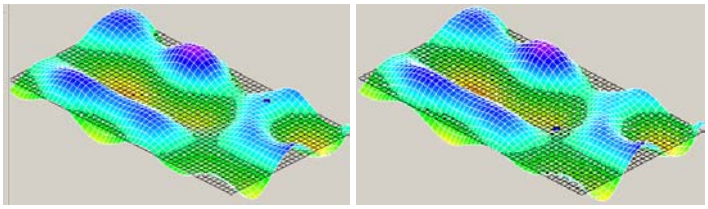

D1-E1-1050 D1-E2-1050

Figure 3.19 Mode Shapes and associated Frequencies with experiment label

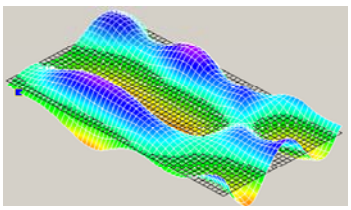

D2-E1-1043

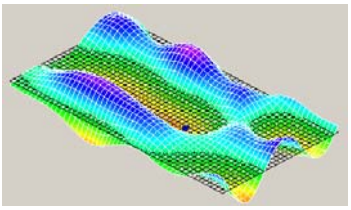

D2-E2-1042

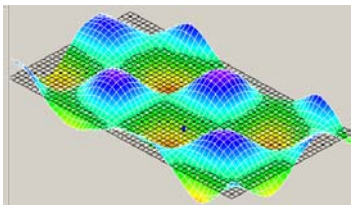

A-1088

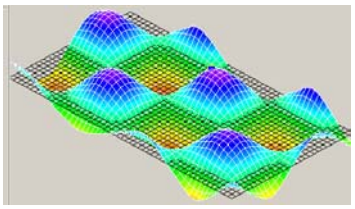

B-1089

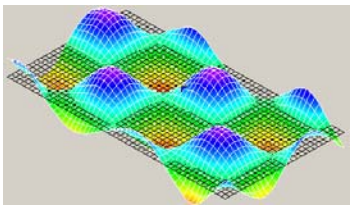

C-1095

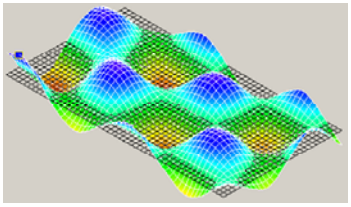

D2-E1-1075

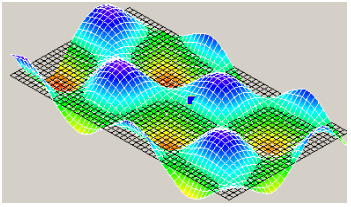

D2-E2-1074

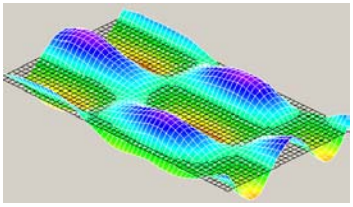

A-1178

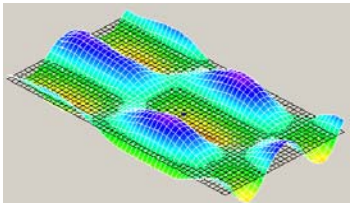

C-1180

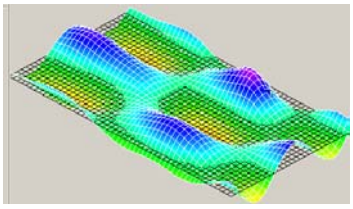

D1-E1-1163

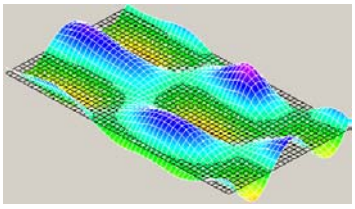

D1-E2-1163

Figure 3.20 Mode Shapes and associated Frequencies with experiment label

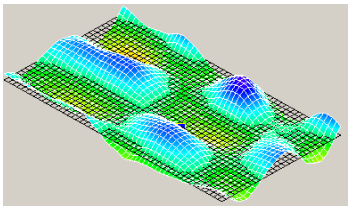

D2-E1-1145

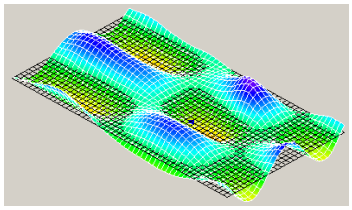

D2-E2-1148

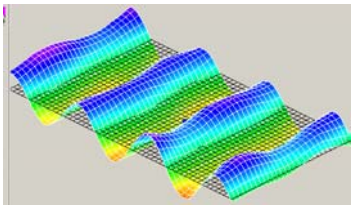

A-1304

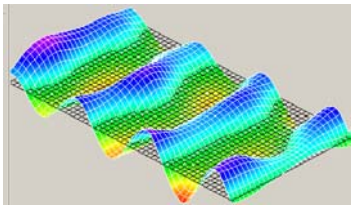

B-1299

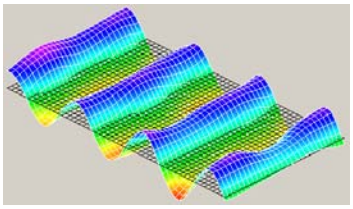

C-1313

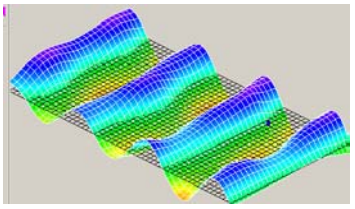

D1-E1-1294

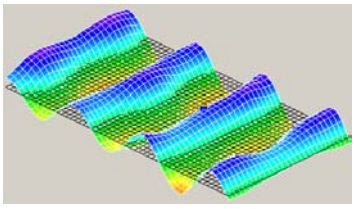

D1-E2-1294

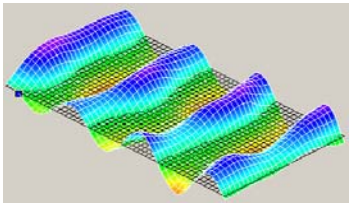

D2-E1-1283

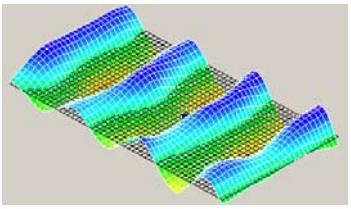

D2-E2-1283

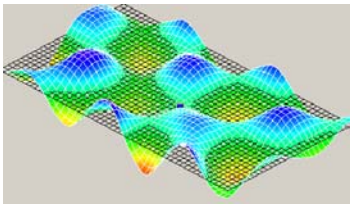

A-1330

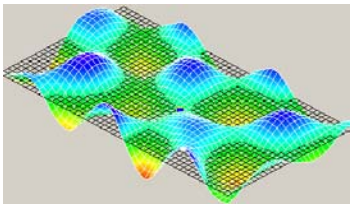

B-1343

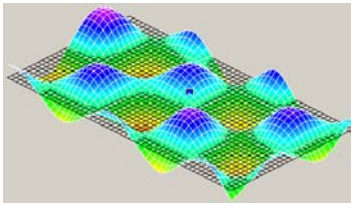

C-1347

Figure 3.21 Mode Shapes and associated Frequencies with experiment label

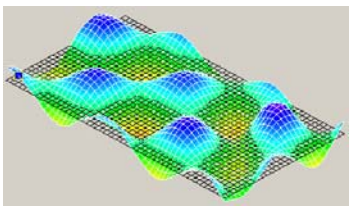

D2-E1-1317

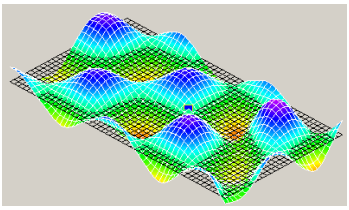

D2-E2-1316

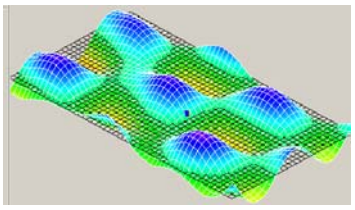

A-1354

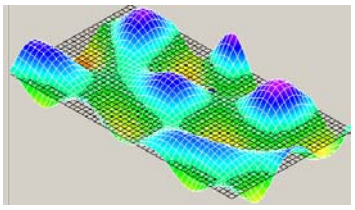

B-1354

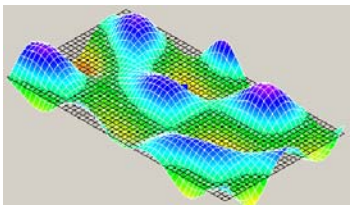

C-1357

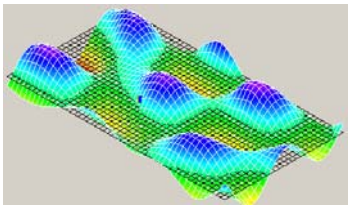

D1-E1-1341

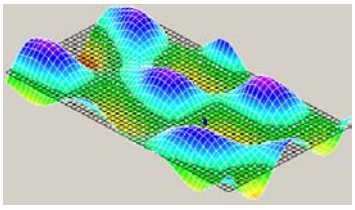

D1-E2-1345

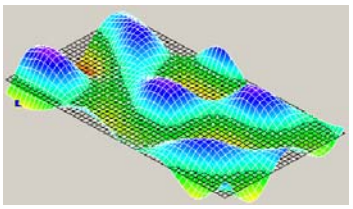

D2-E1-1332

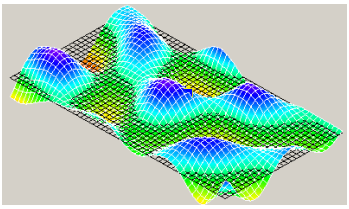

D2-E2-1330

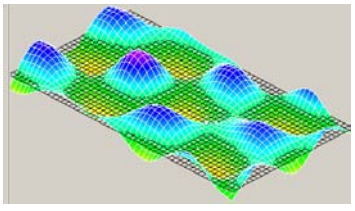

A-1569

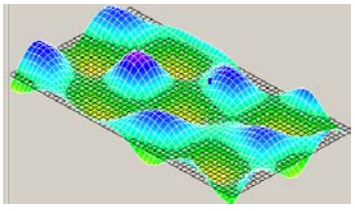

B-1569

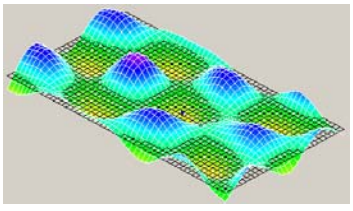

C-1575

Figure 3.22 Mode Shapes and associated Frequencies with experiment label

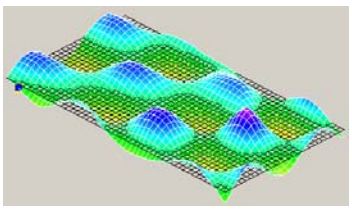

D2-E1-1540

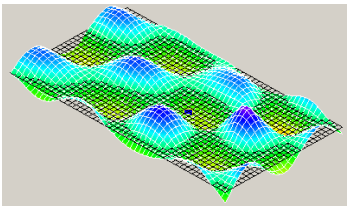

D2-E2-1540

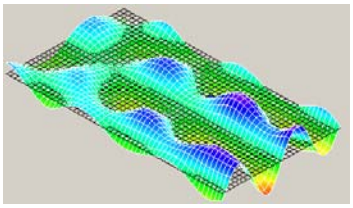

A-1626

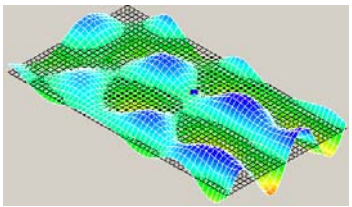

B-1625

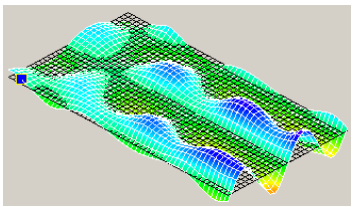

C-1627

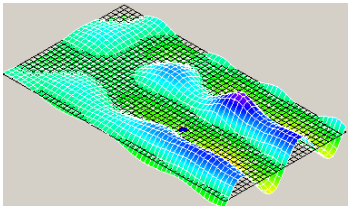

D2-E1-1593

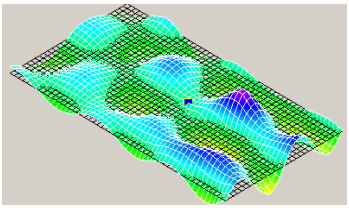

D2-E2-1588

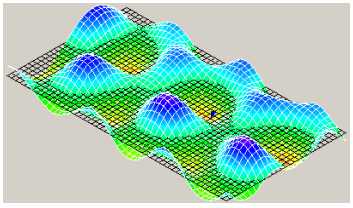

A-1646

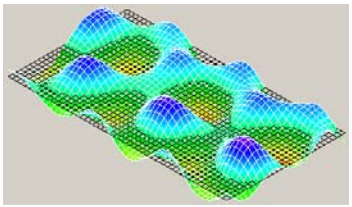

B-1645

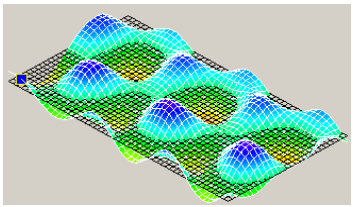

C-1654

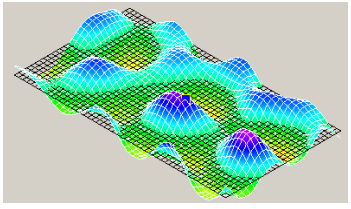

D2-E1-1613

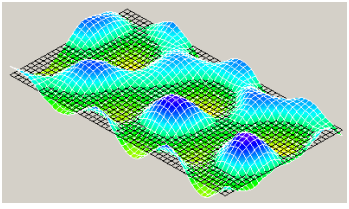

D2-E1-1623

Figure 3.23 Mode Shapes and associated Frequencies with experiment label

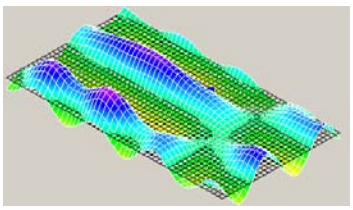

A-1690

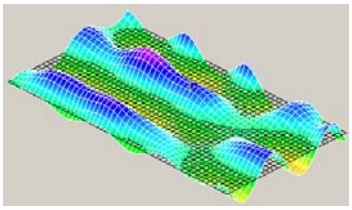

B-1691

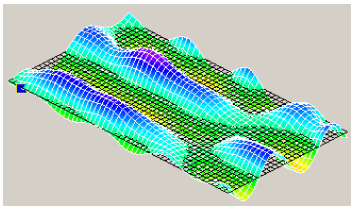

C1693

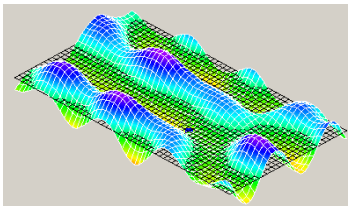

D2-E1-1684

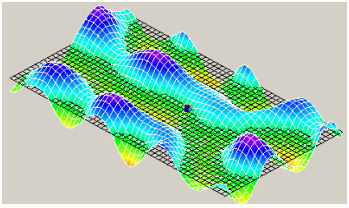

D2-E2-1683

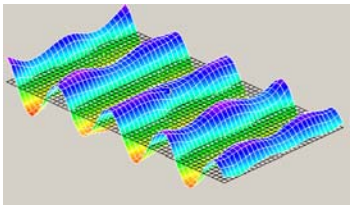

A-2085

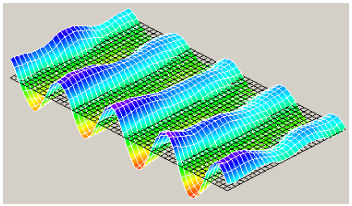

B-2070

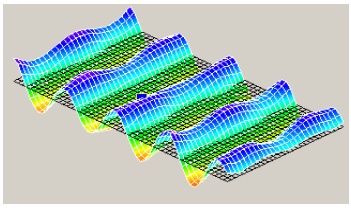

C-2101

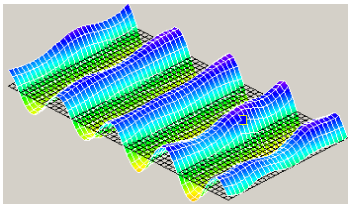

D1-E1-2066

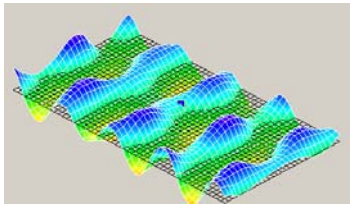

D1-E2-2060

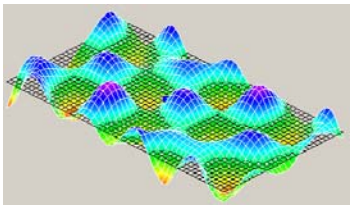

A-2144

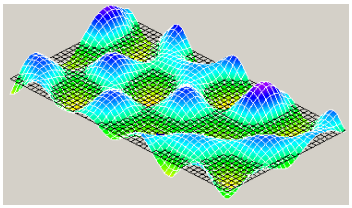

B-2146

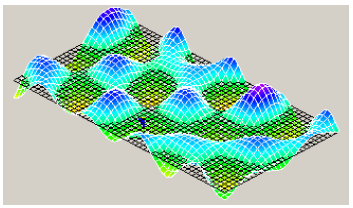

C-2154

Figure 3.24 Mode Shapes and associated Frequencies with experiment label

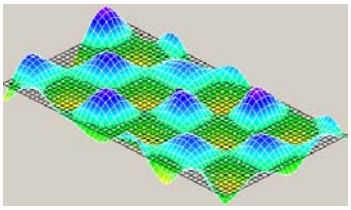

D1-E2-2122

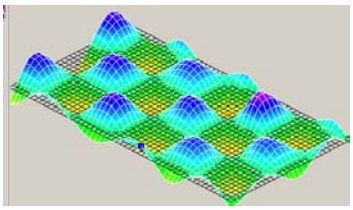

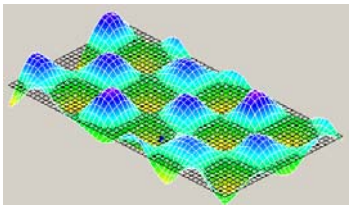

D2-E1-2097 D2-E2-2095

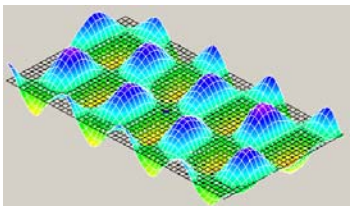

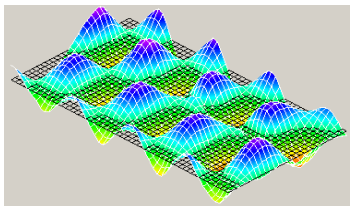

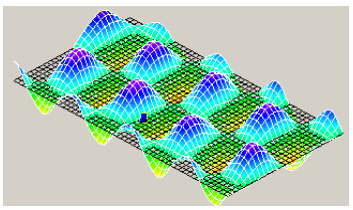

A-2353 B-2350 C-2364

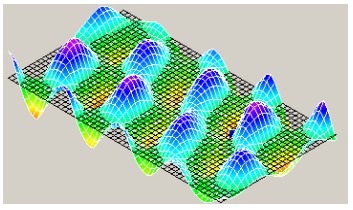

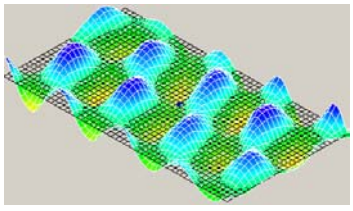

D1-E1-2328 D1-E2-2322

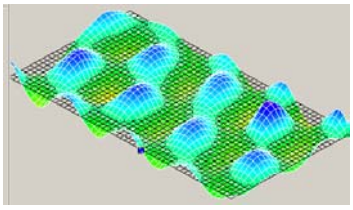

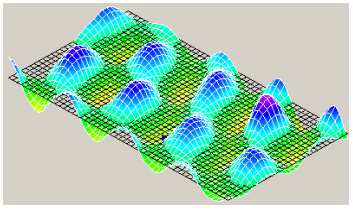

D2-E1-2293 D2-E2-2296

Figure 3.25 Mode Shapes and associated Frequencies with experiment label

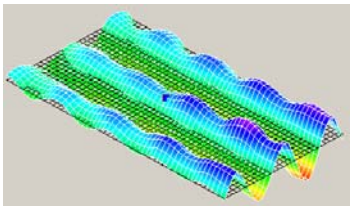

A-2434

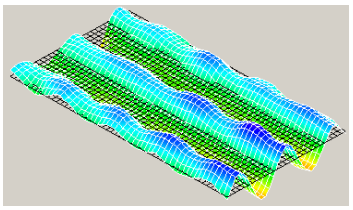

B-2430

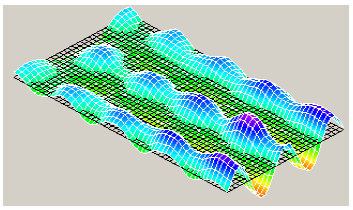

C-2435

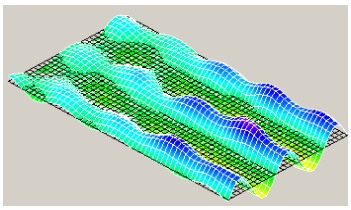

D1-E1-2410

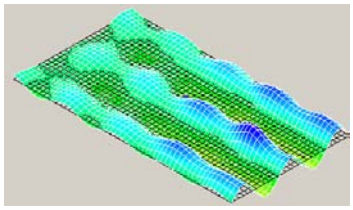

D1-E2-2392

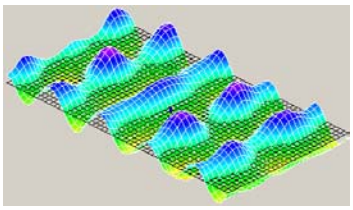

A-2547

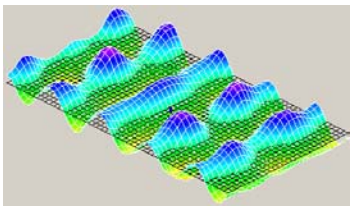

B-2527

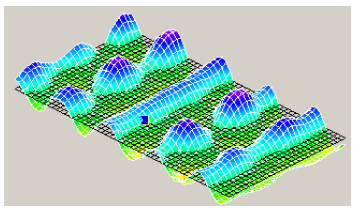

C-2566

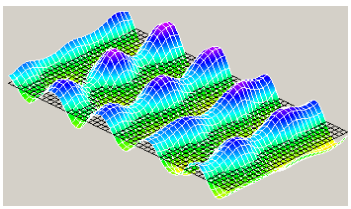

D1-E1-2517

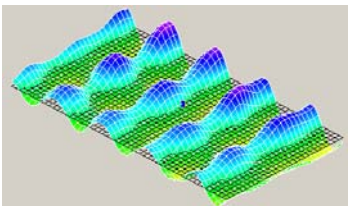

D1-E2-2515

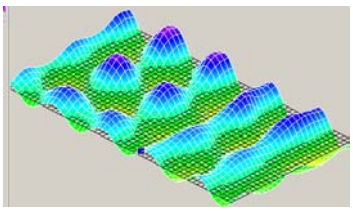

D2-E1-2473

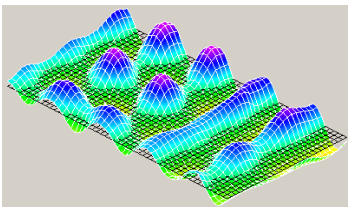

D2-E2-2478

Figure 3.26 Mode Shapes and associated Frequencies with experiment label

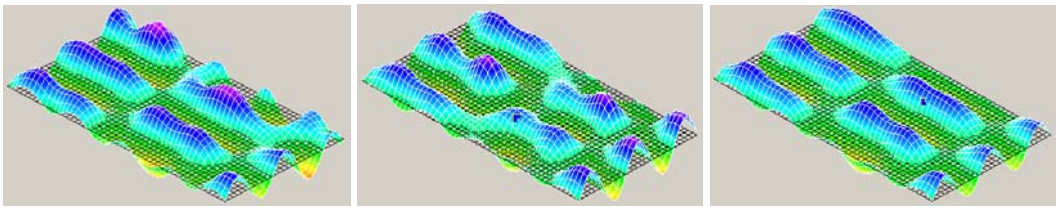

A-2605 B-2606 C-2610

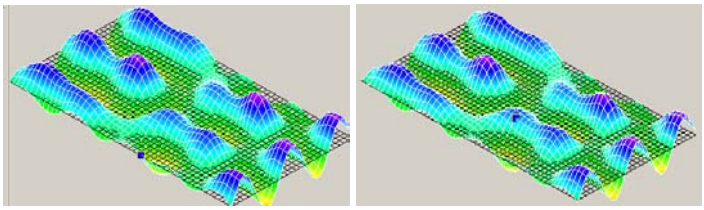

D2-E1-2530 D2-E2-2539

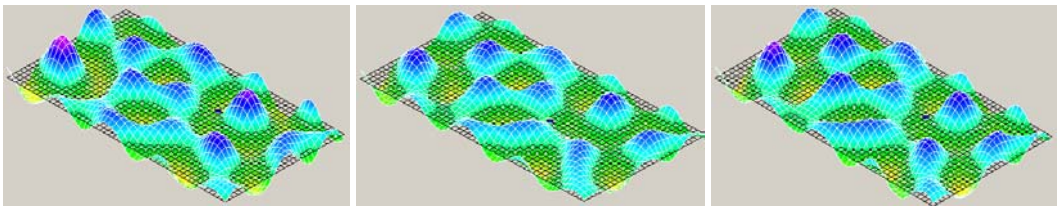

A-2771 B-2761 C-2780

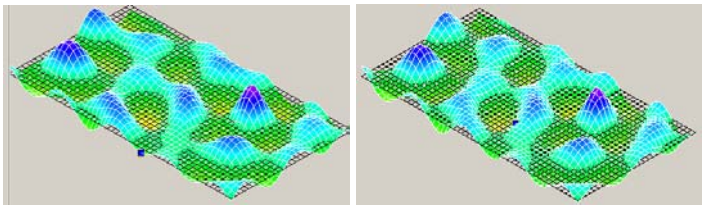

D2-E1-2724 D2-E2-2725

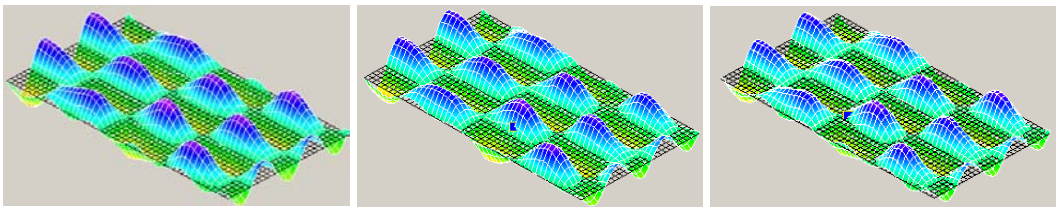

A-2991 B-2988 C-2996

Figure 3.27 Mode Shapes and associated Frequencies with experiment label

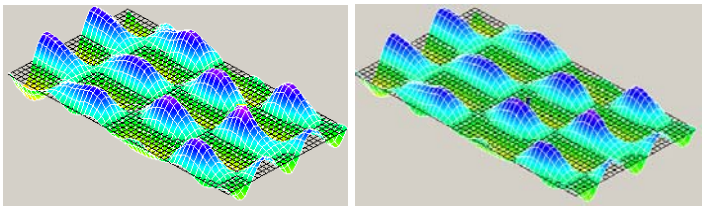

D1-E1-2944 D1-E2-2950

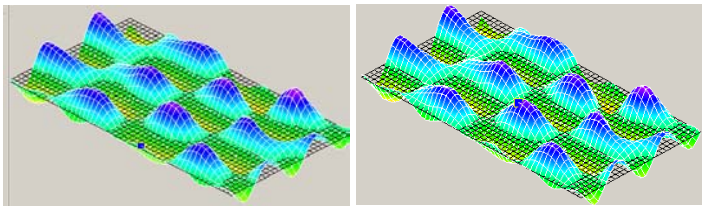

D2-E1-2899 D2-E2-2903

Figure 3.28 Mode Shapes and associated Frequencies with experiment label

3.10.2 Frequencies

Frequencies obtained from experiment is reported in the following subheadings.

Table 3.3 Frequencies in Hz with percentage decrease due to damage for labeled experiment.

Frequencies (Hz) and Percentage Decrease								
A	B	C	D1-E1	D1-E2	(%)	D2-E1	D2-E2	(%)
7.625	7.875	8	7.875	8	NA	8	8	NA
31.88	31.5	32.13	31.75	31.88	NA	31.63	31.5	NA
48.25	49	49.88	47.5	48.75	NA	48.38	48.25	NA
105.4	104.4	106.4	104.4	102.5	NA	100.5	100.4	NA
136	137.3	140.1	135	135.9	NA	133.6	133.3	NA
192	191.6	192.1	180.9	181	NA	176.5	176.5	NA
205.5	205.4	207.4	204.4	204.9	NA	204.4	203.9	NA
260.4	264	264.6	262.3	-	NA	260	260.4	NA
276.5	277.1	283	272.5	272.8	NA	-	-	NA
342.9	339.3	346.5	343.1	344.1	NA	342.3	341.4	NA
386	387.9	390.6	387.4	388.3	NA	380.3	380.4	NA
702.5	697.5	703.8	697.25	696.75	0.5	693.5	695	1
745	742.5	742.5	739	740	0.5	735.6	736.5	1
876.3	873.8	880	871	871	0.6	865	867	1.2
981.3	968.8	978.8	-	970	0.6	963	964	1.3
1000	1001	1006	-	-	NA	-	-	NA
1058	1058	1059	1050	1050	0.7	1043	1042	1.5
1088	1089	1095	-	-	NA	1075	1074	1.5
1178	-	1180	1163	1163	NA	1145	1148	NA
1304	1299	1313	1294	1294	0.8	1283	1283	1.7
1330	1343	1347	-	-	NA	1317	1316	1.7
1354	1354	1357	1341	1345	0.8	1332	1330	1.7
1371	1373	1379	1356	1365	0.9	1348	1350	1.8
1569	1569	1575	-	-	NA	1540	1540	2
1752	-	1752	1735	1738	NA	1729	1726	NA
2085	2101	2080	2066	2060	1.2	-	-	NA
2144	2146	2154	2122	-	NA	2097	2095	2.4
2353	2350	2364	2328	2322	1.3	2293	2296	2.6
2434	2430	2435	2410	2392	1.4	-	-	NA
2547	2527	2566	2517	2515	1.4	2473	2478	2.8
2605	2606	2610	-	-	NA	2530	2539	2.8
2991	2988	2996	2944	2950	1.5	2899	2903	3

3.11 Experiment Error Assessment

Difference in repeated healthy specimen was studied for the assessment of the accuracy of the Scanning Laser Vibrometer. It was observed that the modal displacement obtained from SLV was very small and the difference in repeated experiments was following a pattern which indicated that processing of the data by SLV had replaced noise. It was also observed that the order of magnitude of mode shape was very close to the order of magnitude of delta mode shape. The error of this type could have generated the increase in natural frequency of the specimen after damage. For lower frequency mode shape the order of magnitude for delta mode shape and mode shape itself was observed to be very close but for higher frequency the order in magnitude increased indicating the effect of damage.

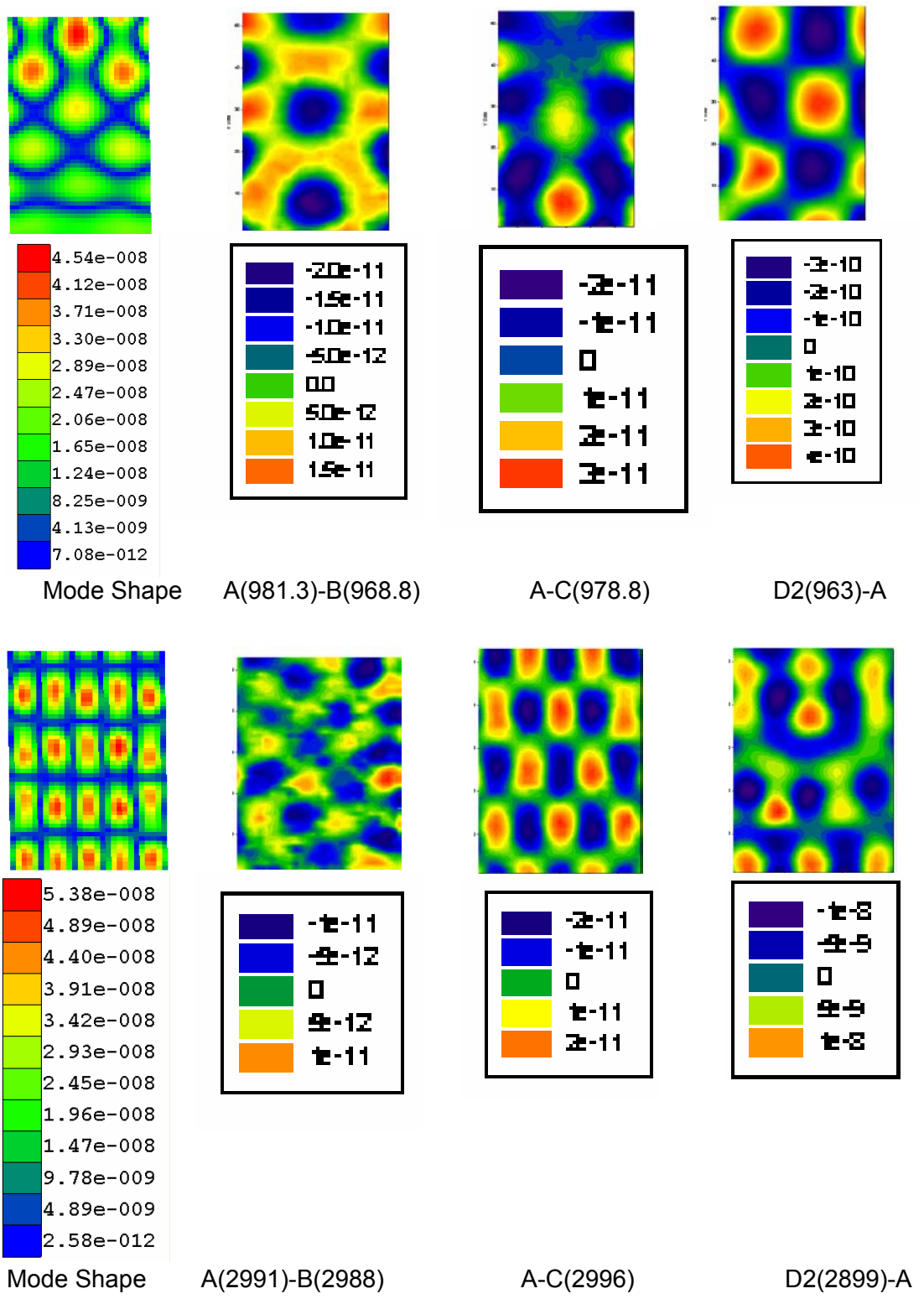

Figure 3.29 Order of Magnitude obtained from SLV for low and high frequency.

Figure 3.29 shows order of magnitude of mode shape, difference between first healthy experiment and first repetition, difference between first healthy experiment and second repetition and difference between first healthy experiment and first damage experiment. The gain in order of magnitude in the difference between first healthy experiment and first damage experiment indicates the potential for detection.

3.12 Summary

Frequency of the specimen was observed to have an immediate affect when damage sizes were increased. The pattern of reduction in frequency was observed to be more promising towards the higher frequencies and bigger damage sizes. From this chapter, it was possible to conclude that for detection proposes, mode shapes associated with the higher frequencies were more potential than the lower frequencies. Also, the bigger sizes of the damage were more potential for detection proposes than smaller damage sizes.

Error present in the experiment was also observed and it was concluded that the difference in magnitude drop created by the damage should be higher than the error for the detection of the damage.

CHAPTER IV

COMPARATIVE STUDY OF EXPERIMENTAL CASES AND DAMAGE DETECTION RESULTS

4.1 General

Processing of the data obtained from Scanning Laser Vibrometer (SLV) with different approaches was performed, which this Chapter tends to report. While viewing the mode shapes with naked eye, for both the healthy and damaged mode shapes, it becomes difficult even for an expert to observe the difference in them. So, Sigma Plot was used to obtain and plot the difference between the displacements of healthy and damaged mode shapes (Delta Mode Shape). A consisting pattern in the plot was anticipated since the difference between repeated experiment of healthy and damage specimen should provide similar results.

As explained in Chapter I, ASG Damage code was used to process the data for detection purposed and E-View was used for viewing.

4.2 Mode Shapes, Delta Mode Shapes and E-View plots for D1-E1

Mode shapes plotted using Eview and delta mode shape plotted using Sigma Plot.

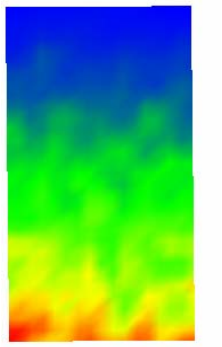

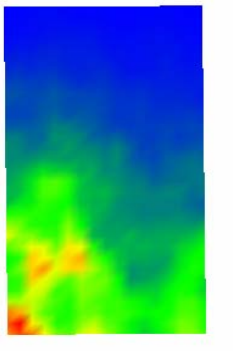

Healthy Mode Shape Damaged Mode Shape

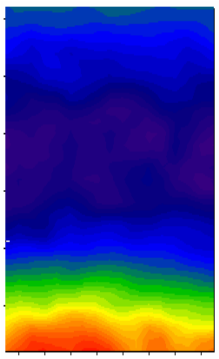

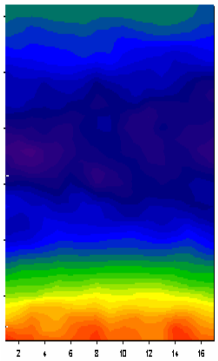

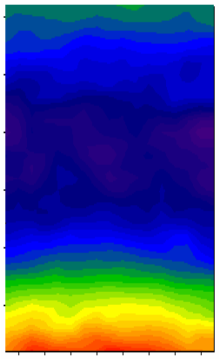

E1- D1(47.5)-A(48.25) D1-B(49) D1-C(49.88)

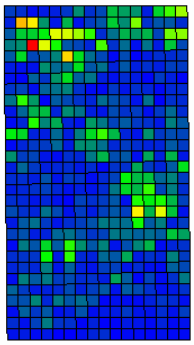

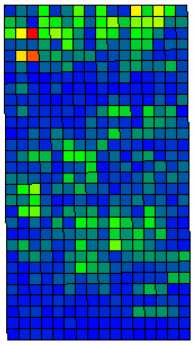

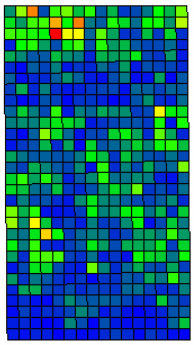

D1(48.15)-A(47.5) D1-B(49) D1-C(49.88)

Figure 4.1 Mode Shapes, Delta Mode Shapes and E-View plots for D1-E1 with associated frequencies

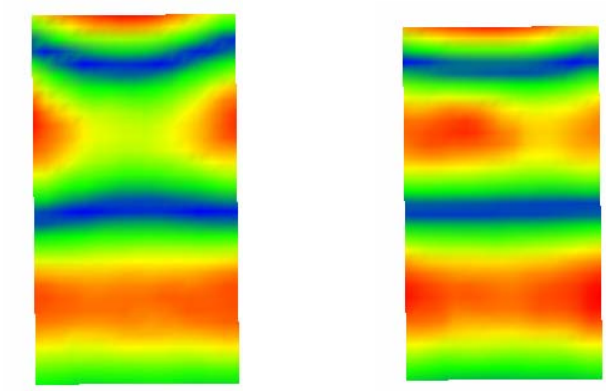

Healthy Mode Shape Damaged Mode Shape

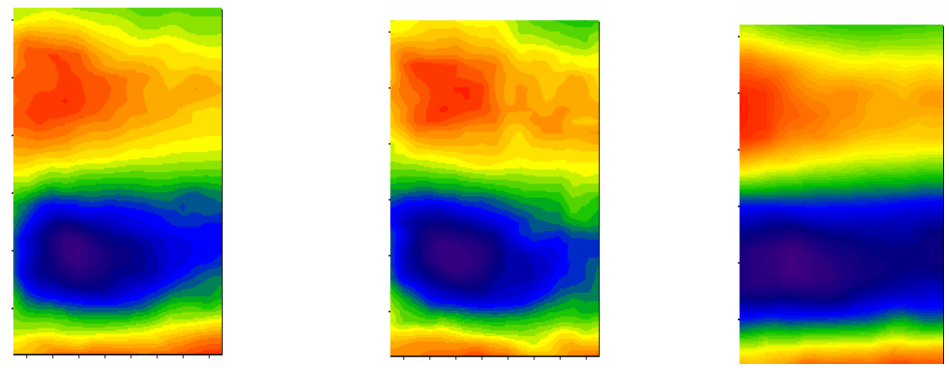

E1- D1(135)-A(136) D1-B(137.6) D1-C(140.1)

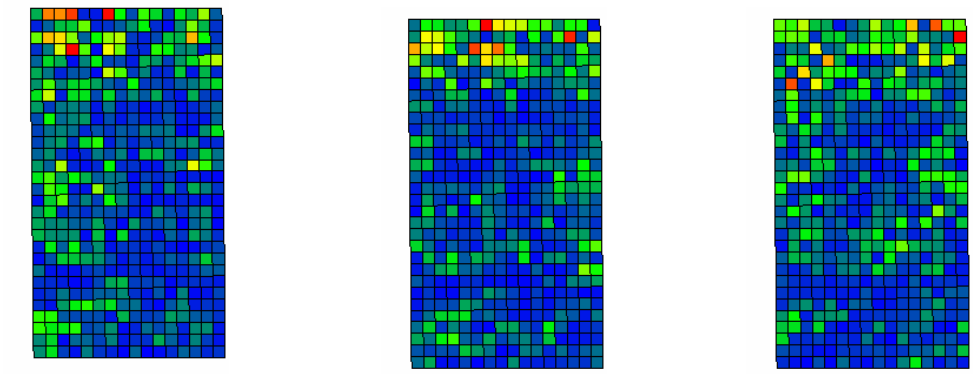

D1(135)-A(136) D1-B(137.6) D1-C(140.1)

Figure 4.2 Mode Shapes, Delta Mode Shapes and E-View plots for D1-E1 with associated frequencies

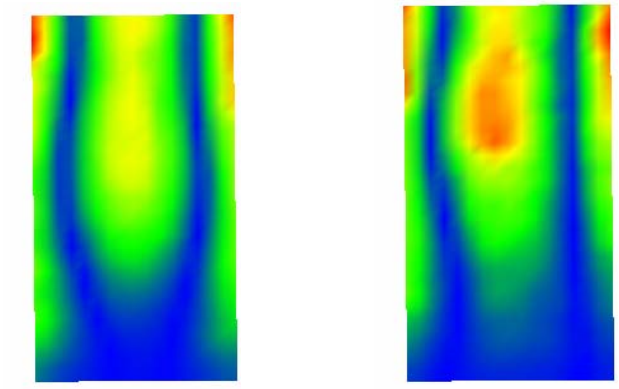

Healthy Mode Shape Damaged Mode Shape

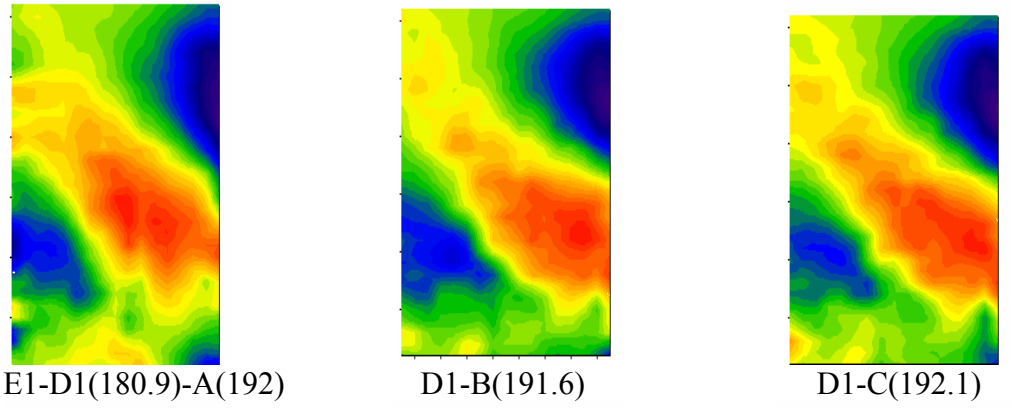

E1-D1(180.9)-A(192) D1-B(191.6) D1-C(192.1)

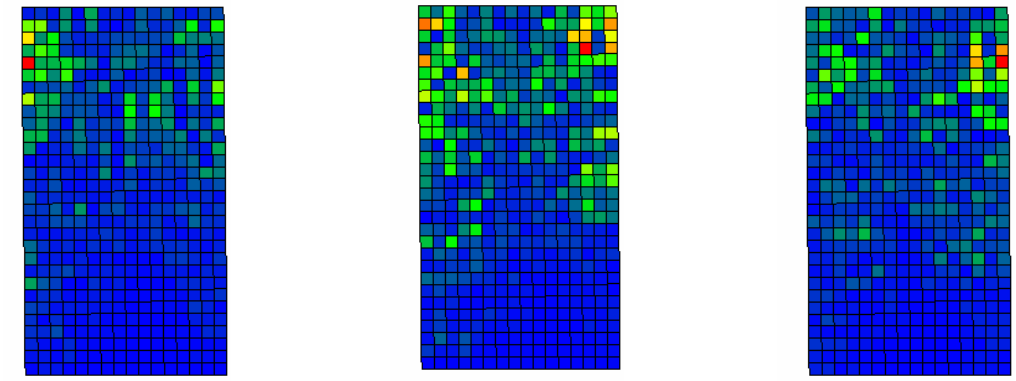

D1(180.9)-A(192) D1-B(191.6) D1-C(192.1)

Figure 4.3 Mode Shapes, Delta Mode Shapes and E-View plots for D1-E1 with associated frequencies

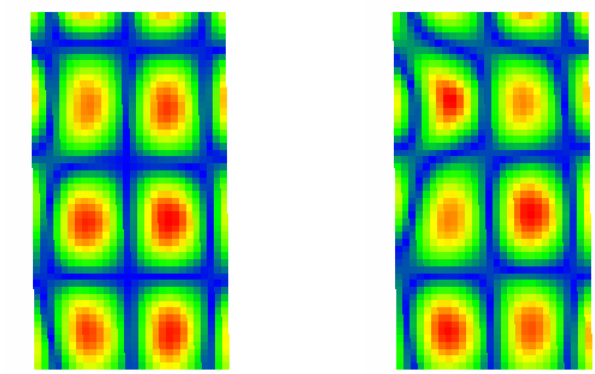

Healthy Mode Shape Damaged Mode Shape

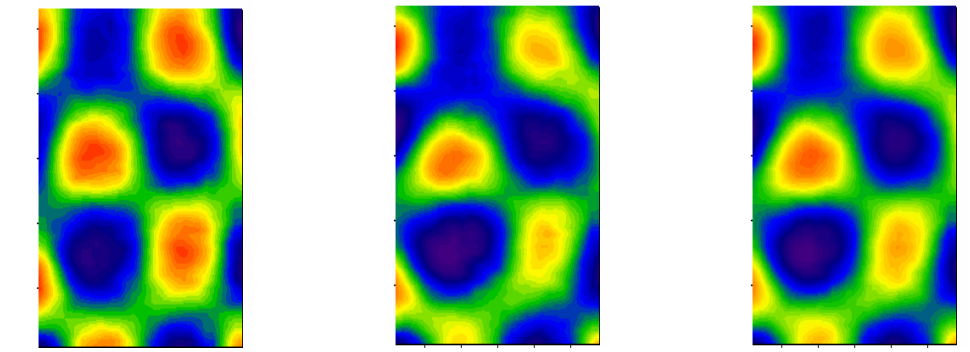

E1- D1(871)-A(876.3) D1-B(873.8) D1-C(880)

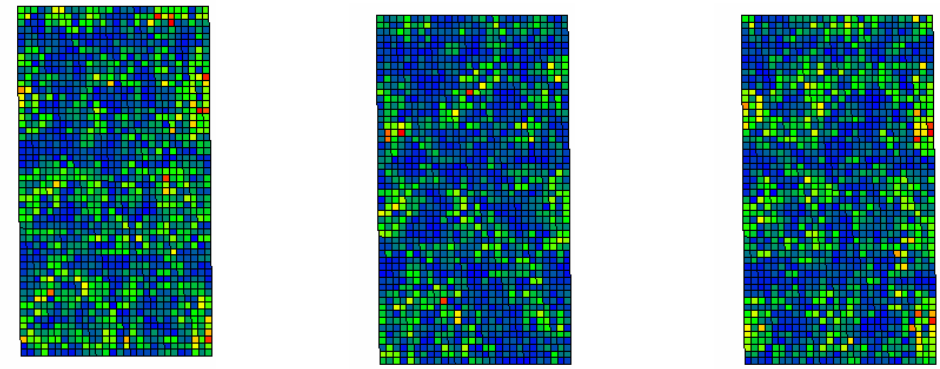

D1(871)-A(876.3) D1-B(873.3) D1-C(880)

Figure 4.4 Mode Shapes, Delta Mode Shapes and E-View plots for D1-E1 with associated frequencies

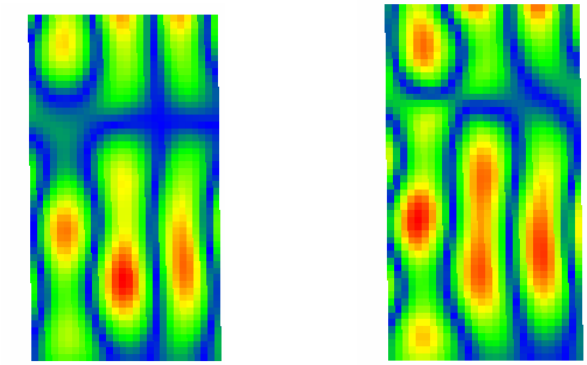

Healthy Mode Shape Damaged Mode Shape

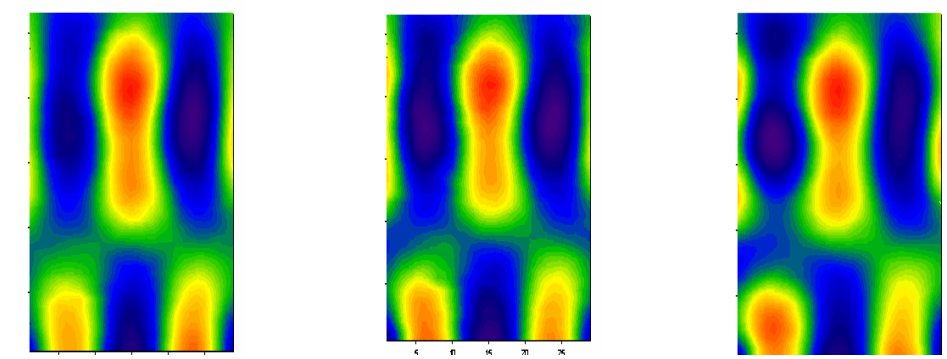

E1- D1(1050)-A(1058) D1-B(1058) D1-C(1059)

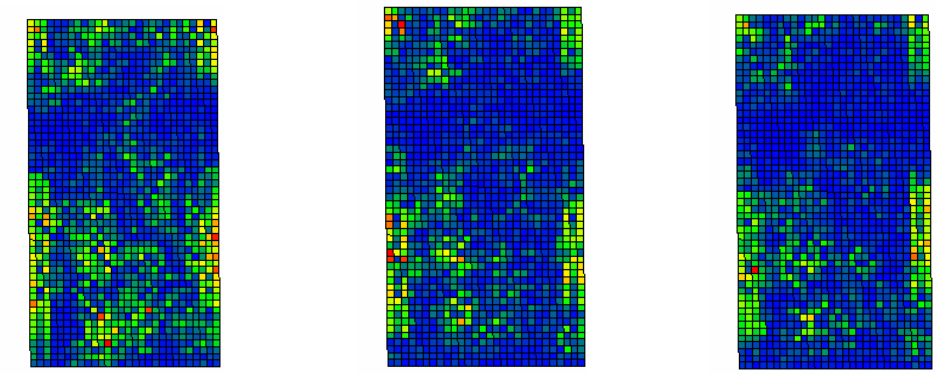

D1(1050)-A1058 D1-B(1058) D1-C(1059)

Figure 4.5 Mode Shapes, Delta Mode Shapes and E-View plots for D1-E1 with associated frequencies

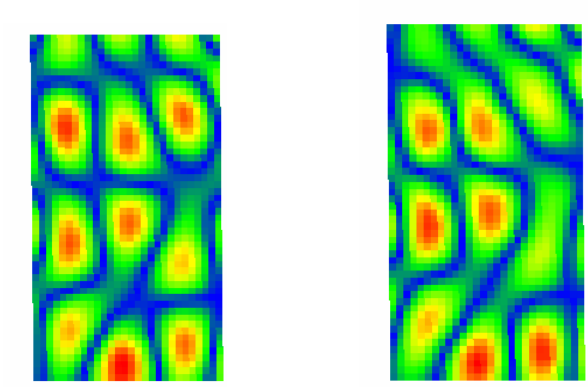

Healthy Mode Shape Damaged Mode Shape

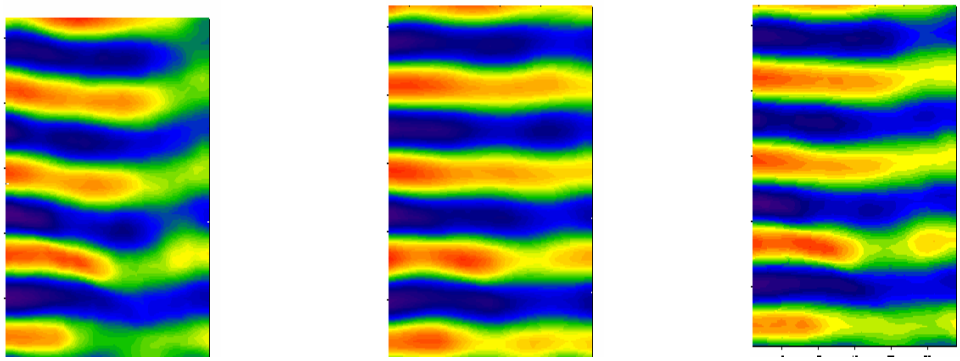

E1- D1(1341)-A(1354) D1-B(1354) D1-C(1357)

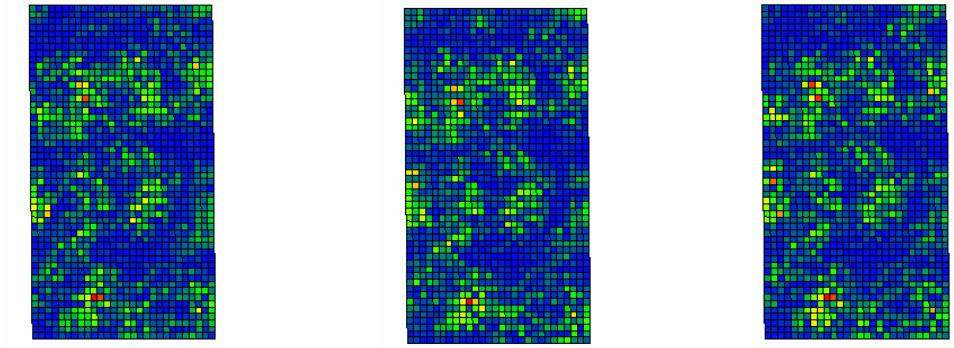

D1(1341)-A(1354) D1-B(1354) D1-C(1357)

Figure 4.6 Mode Shapes, Delta Mode Shapes and E-View plots for D1-E1 with associated frequencies

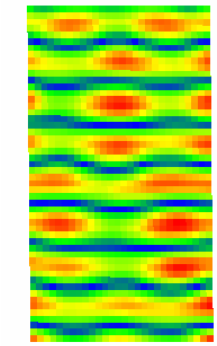

Healthy Mode Shape

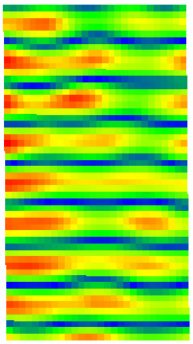

Damaged Mode Shape

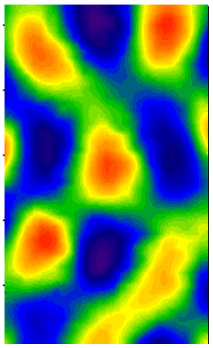

E1-D1(2066)-A(2085)

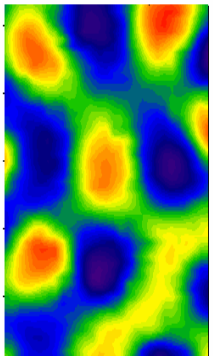

D1-B(2070)

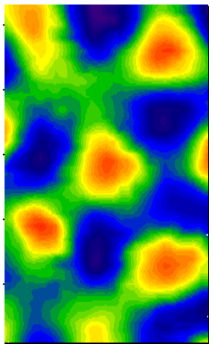

D1-C(2101)

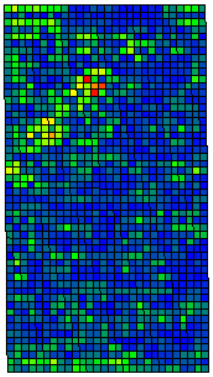

D1(2066)-A(2085)

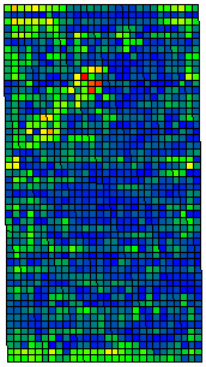

D1-B(2070)

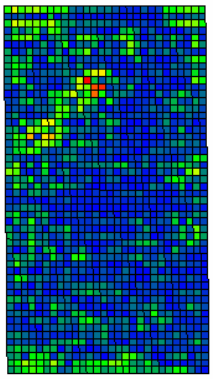

D1-C(2101)

Figure 4.7 Mode Shapes, Delta Mode Shapes and E-View plots for D1-E1 with associated frequencies

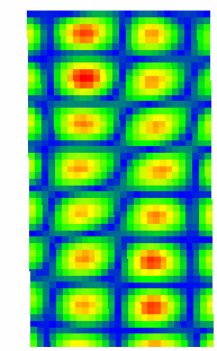

Healthy Mode Shape

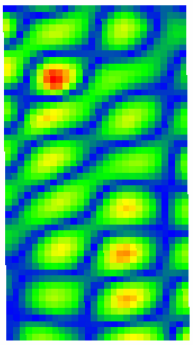

Damaged Mode Shape

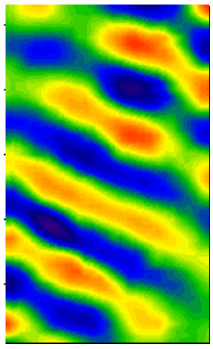

E1-D1(2328)-A(2353)

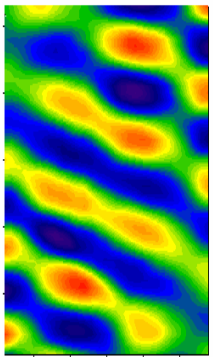

D1-B(2350)

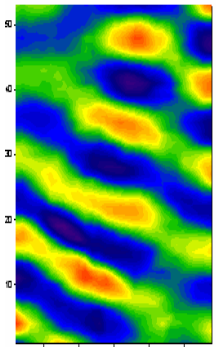

D1-C(2364)

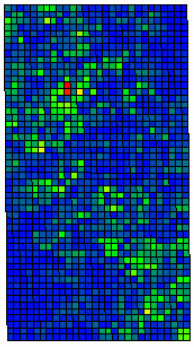

D1(2328)-A(2353)

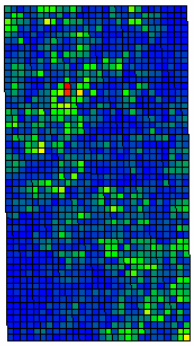

D1-B(2350)

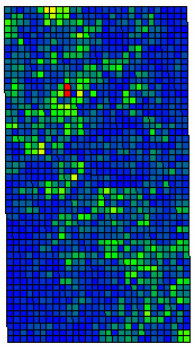

D1-C(2364)

Figure 4.8 Mode Shapes, Delta Mode Shapes and E-View plots for D1-E1 with associated frequencies

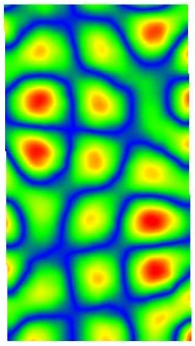

Healthy Mode Shape

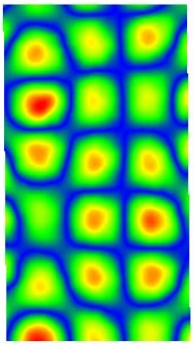

Damaged Mode Shape

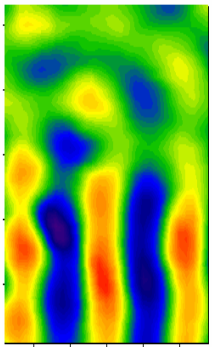

E1- D1(2410)-A(2434)

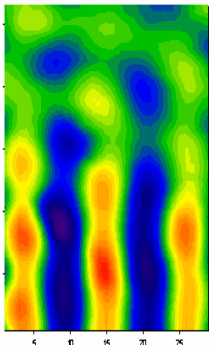

D1-B(2430)

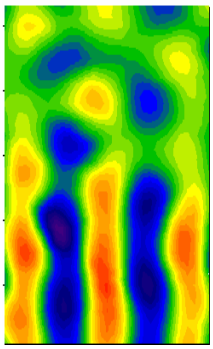

D1-C(2435)

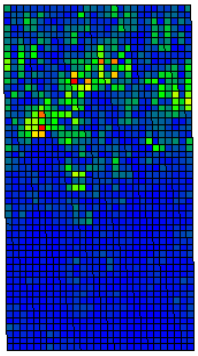

D1(2410)-A(2434)

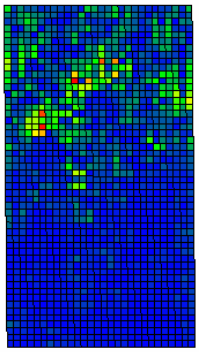

D1-B(2430)

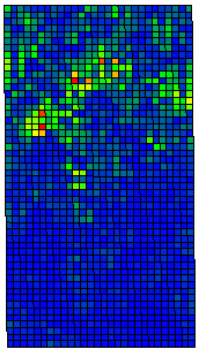

D1-C(2435)

Figure 4.9 Mode Shapes, Delta Mode Shapes and E-View plots for D1-E1 with associated frequencies

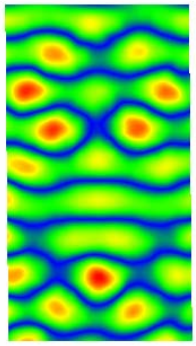

Healthy Mode Shape

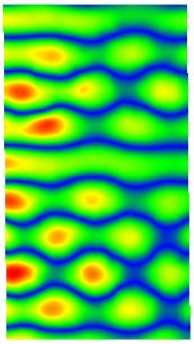

Damaged Mode Shape

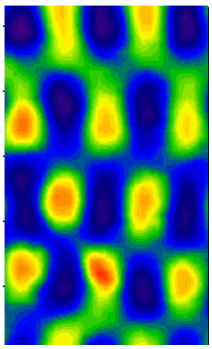

E1- D1(2517)-A(2547)

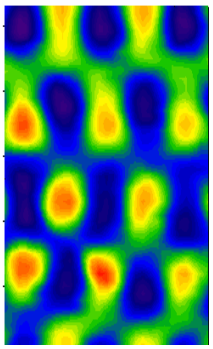

D1-B(2547)

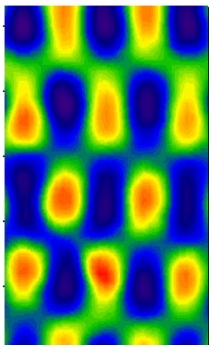

D1-C(2566)

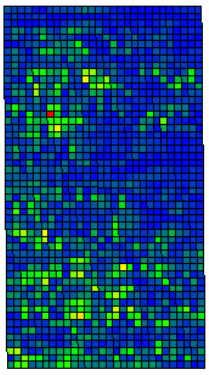

D1(2517)-A(2547)

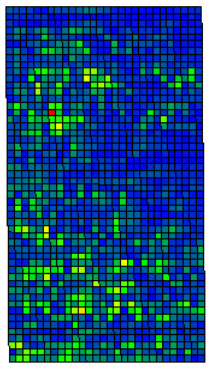

D1-B(2547)

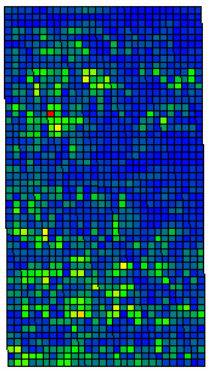

D1-C(2566)

Figure 4.10 Mode Shapes, Delta Mode Shapes and E-View plots for D1-E1 with associated frequencies

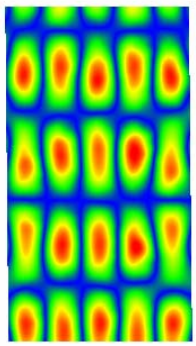

Healthy Mode Shape

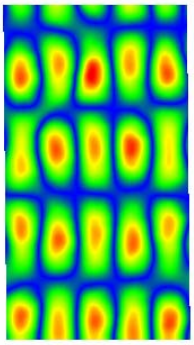

Damaged Mode Shape

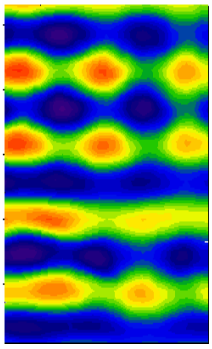

E1- D1(2944)-A(2991)

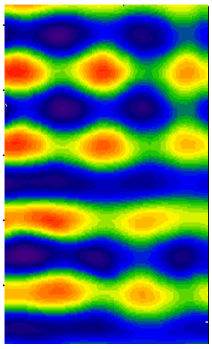

D1-B(2988)

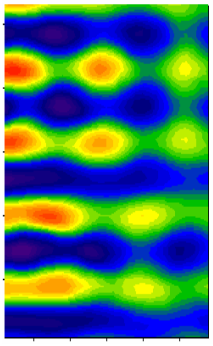

D1-C(2996)

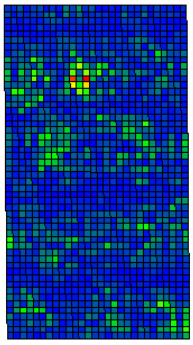

D1(2944)-A(2991)

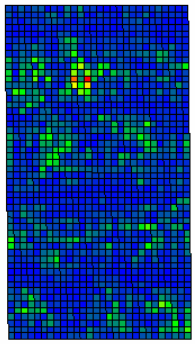

D1-B(2988)

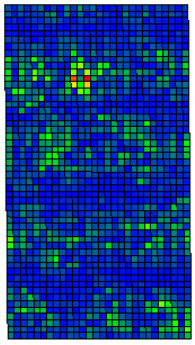

D1-C(2966)

Figure 4.11 Mode Shapes, Delta Mode Shapes and E-View plots for D1-E1 with associated frequencies

4.3 Mode Shape, Delta Mode Shapes and E-View plots for D1-E2

Mode shapes plotted using Eview and delta mode shape plotted using Sigma Plot.

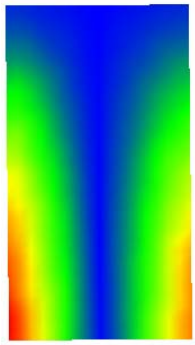

Healthy Mode Shape

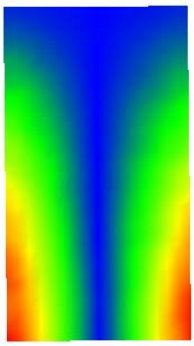

Damaged Mode Shape

E2-D1(31.88)-A(31.88)

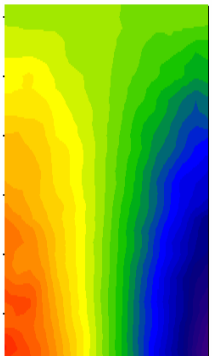

D1-B(31.5)

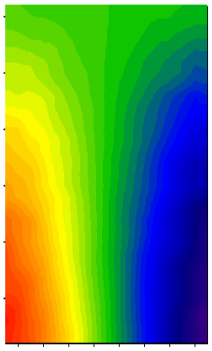

D1-C(32.13)

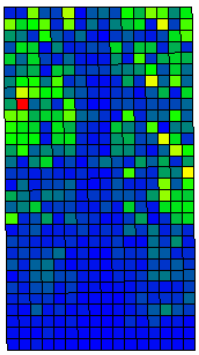

D1(31.88)-A(31.88)

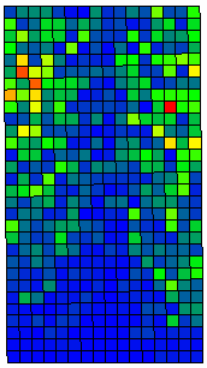

D1-B(31.5)

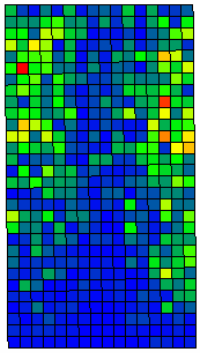

D1-C(32.13)

Figure 4.12 Mode Shapes, Delta Mode Shapes and E-View plots for D1-E2 with associated frequencies

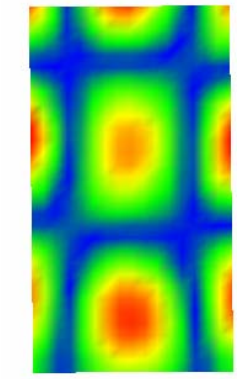

Healthy Mode Shape

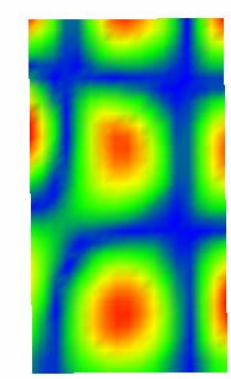

Damaged Mode Shape

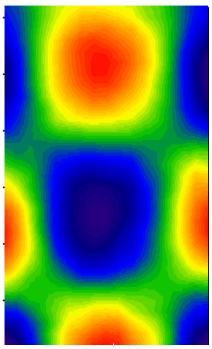

E2-D1(388.3)-A(386)

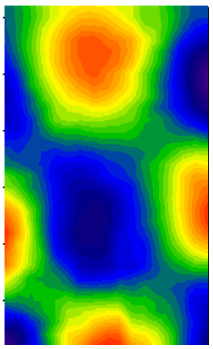

D1-B(387.9)

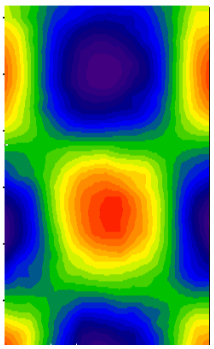

D1-C(390.6)

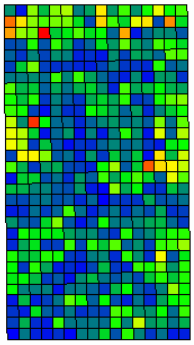

D1(388.3)-A(386)

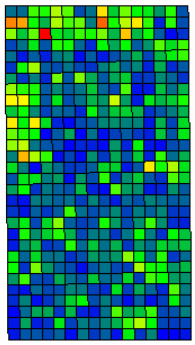

D1-B(387.9)

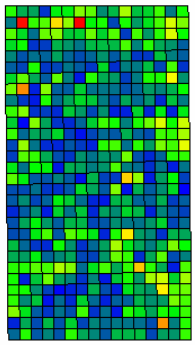

D1-C(390.6)

Figure 4.13 Mode Shapes, Delta Mode Shapes and E-View plots for D1-E2 with associated frequencies

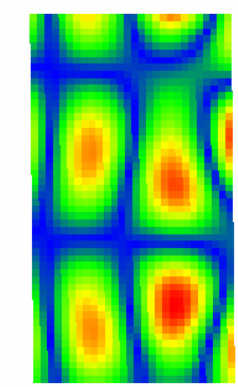

Healthy Mode Shape

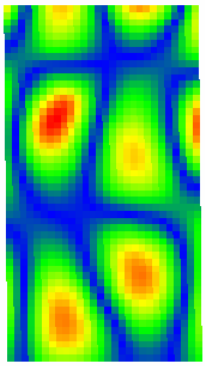

Damaged Mode Shape

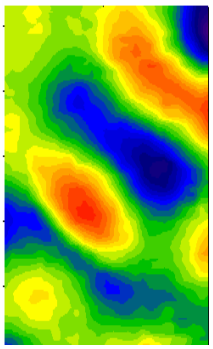

E2-D1(696.75)-A(702.5)

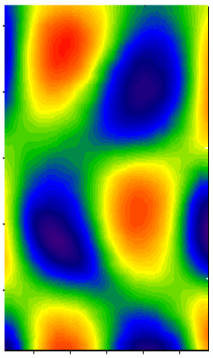

D1-B(697.5)

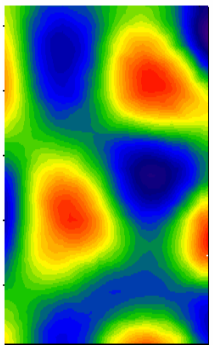

D1-C(703.8)

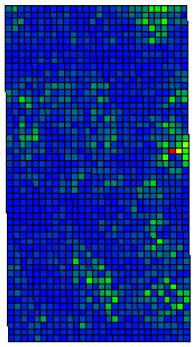

D1(696.75)-A(702.5)

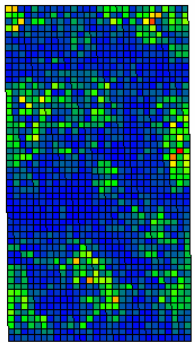

D1-B(697.5)

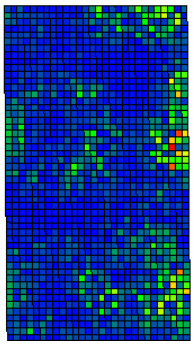

D1-C(703.8)

Figure 4.14 Mode Shapes, Delta Mode Shapes and E-View plots for D1-E2 with associated frequencies

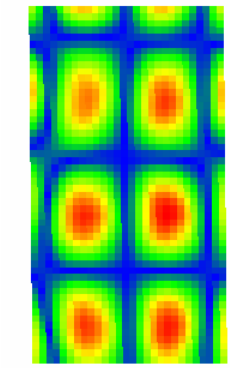

Healthy Mode Shape

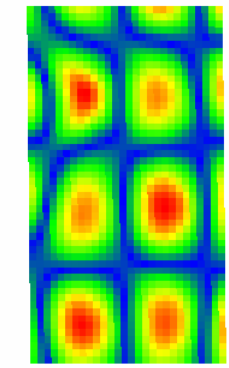

Damaged Mode Shape

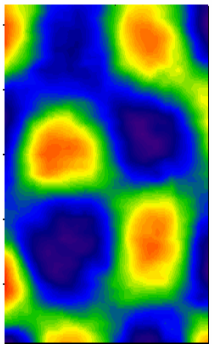

E1-D1(871)-A(876.3)

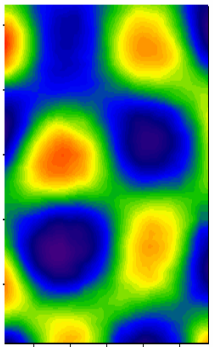

D1-B(873.8)

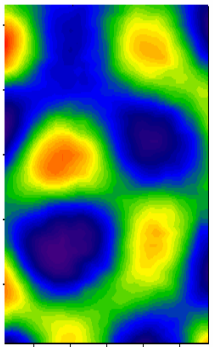

D1-C(880)

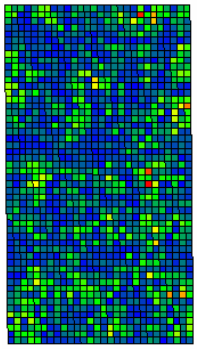

D1(871)-A(876.3)

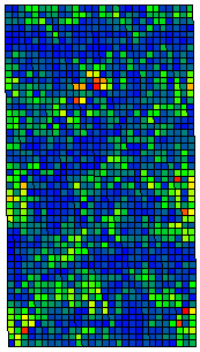

D1-B(873.8)

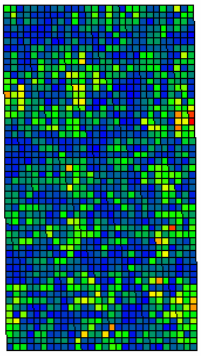

D1-C(880)

Figure 4.15 Mode Shapes, Delta Mode Shapes and E-View plots for D1-E2 with associated frequencies

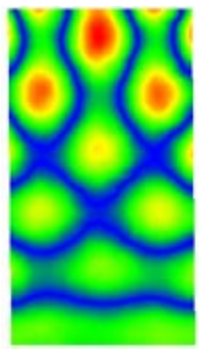

Healthy Mode Shape

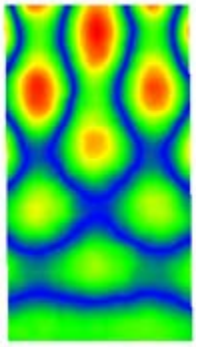

Damaged Mode Shape

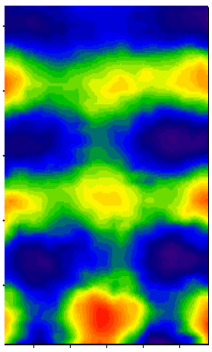

E2-D1(970)-A(981.3)

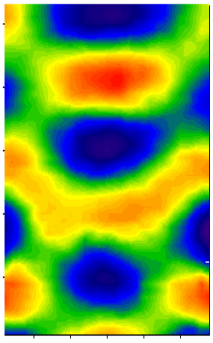

D1-B(968.8)

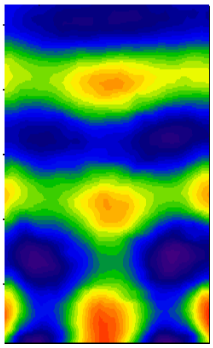

D1-C(978.8)

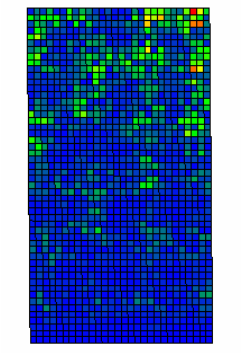

D1(970)-A(981.3)

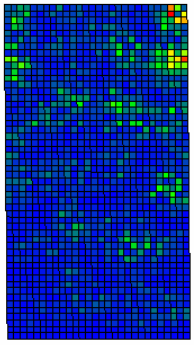

D1-B(968.8)

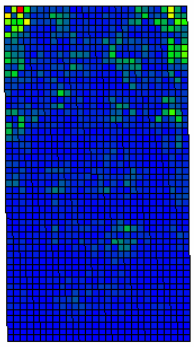

D1-C(978.8)

Figure 4.16 Mode Shapes, Delta Mode Shapes and E-View plots for D1-E2 with associated frequencies

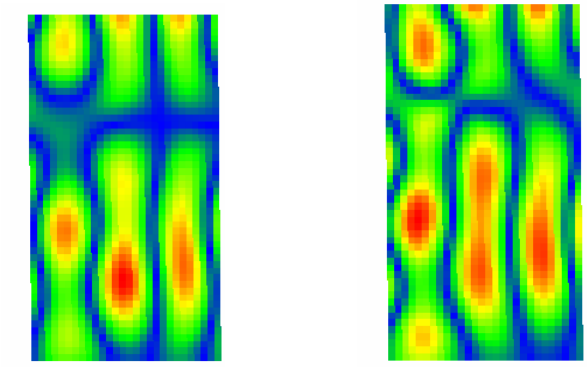

Healthy Mode Shape Damaged Mode Shape

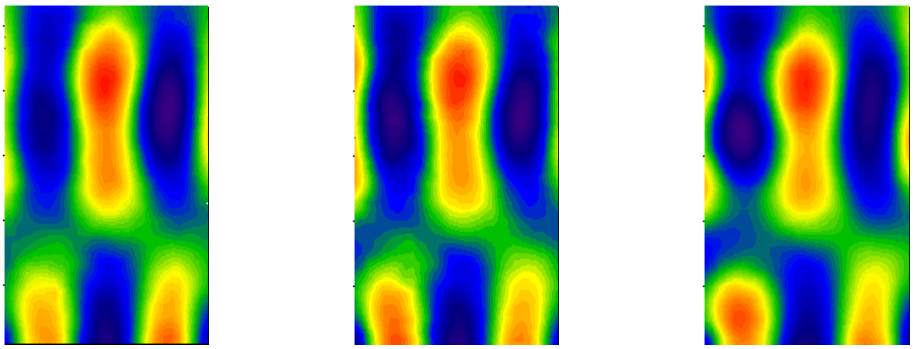

E2-D1(1050)-A(1058) D1-B(1058) D1-C(1059)

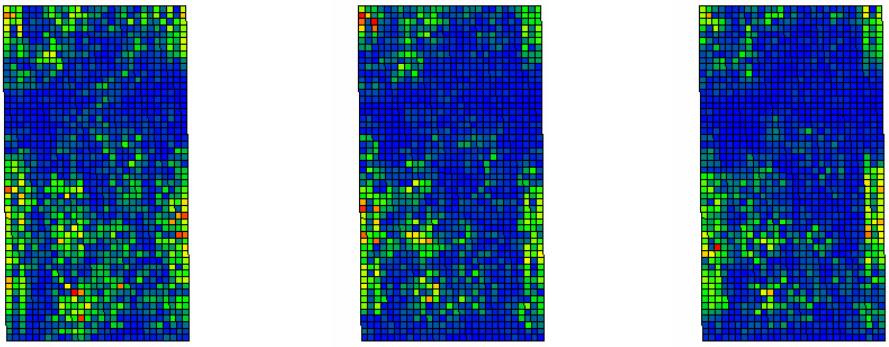

E2-D1(1050)-A(1058) D1-B(1058) D1-C(1059)

Figure 4.17 Mode Shapes, Delta Mode Shapes and E-View plots for D1-E2 with associated frequencies

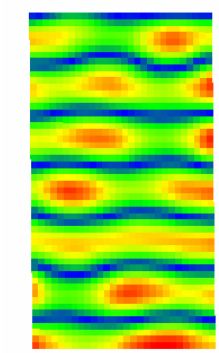

Healthy Mode Shape

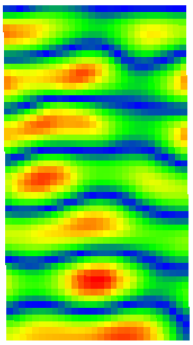

Damaged Mode Shape

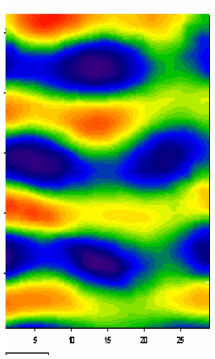

E2-D1(1294)-A(1304)

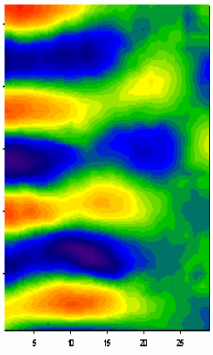

D1-B(1299)

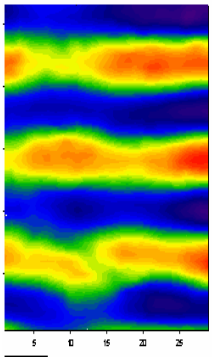

D1-C(1313)

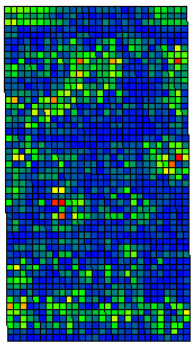

D1(1294)-A(1304)

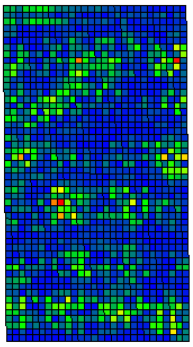

D1-B(1299)

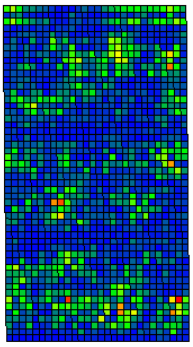

D1-C(1313)

Figure 4.18 Mode Shapes, Delta Mode Shapes and E-View plots for D1-E2 with associated frequencies

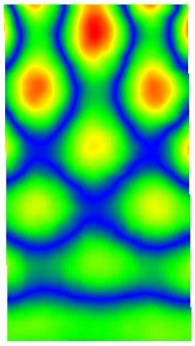

Healthy Mode Shape

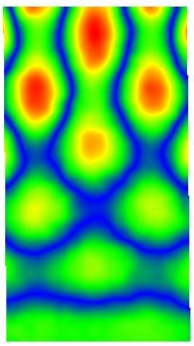

Damaged Mode Shape

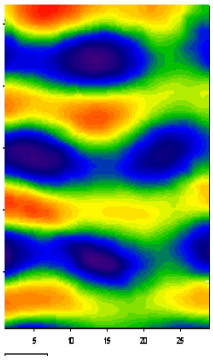

E2-D1(1345)-A(1354)

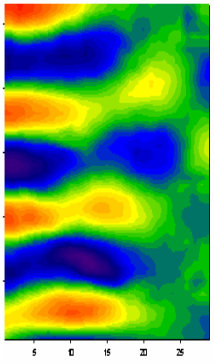

D1-B(1354)

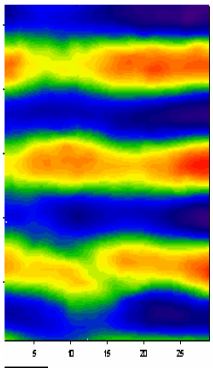

D1-C(1357)

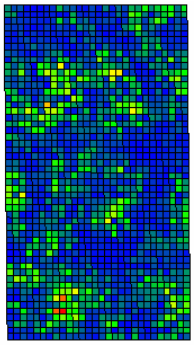

D1(1345)-A(1354)

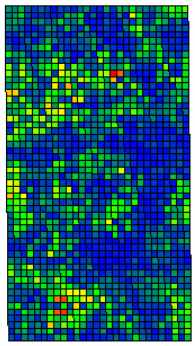

D1-B(1354)

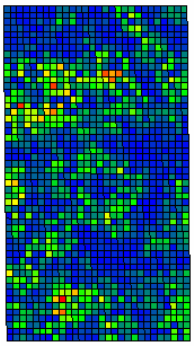

D1-C(1357)

Figure 4.19 Mode Shapes, Delta Mode Shapes and E-View plots for D1-E2 with associated frequencies

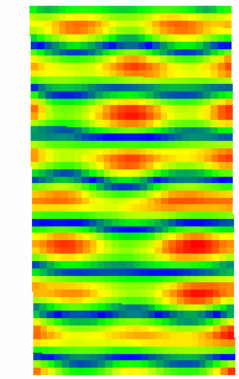

Healthy Mode Shape

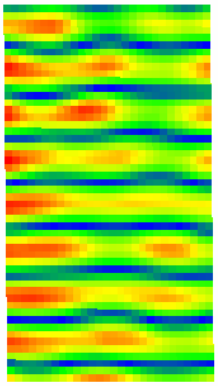

Damaged Mode Shape

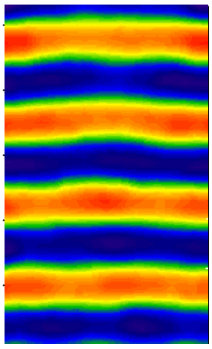

E2-D1(2060)-A(2085)

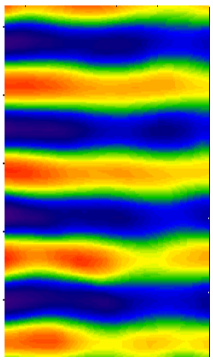

D1-B(2070)

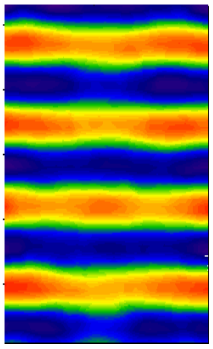

D1-C(2101)

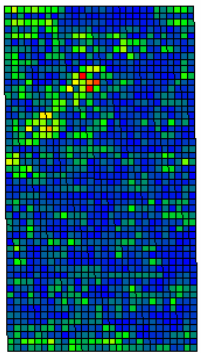

D1(2060)-A(2085)

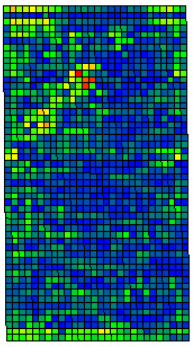

D1-B(2070)

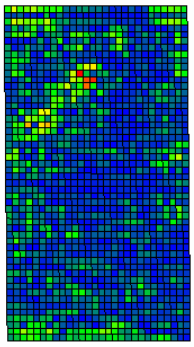

D1-C(2101)

Figure 4.20 Mode Shapes, Delta Mode Shapes and E-View plots for D1-E2 with associated frequencies

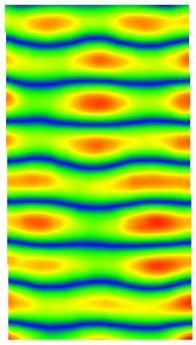

Healthy Mode Shape

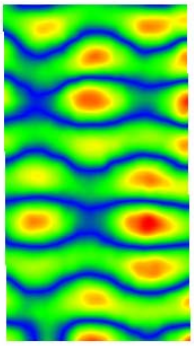

Damaged Mode Shape

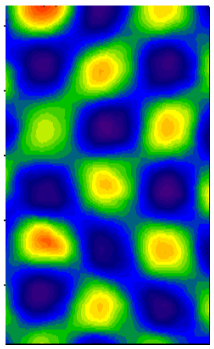

E2-D1(2122)-A(2144)

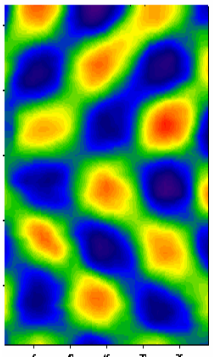

D1-B(2146)

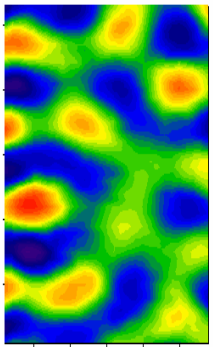

D1-C(2154)

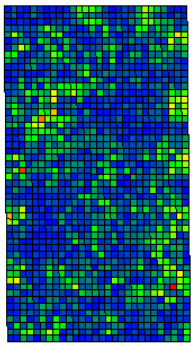

D1(2122)-A(2144)

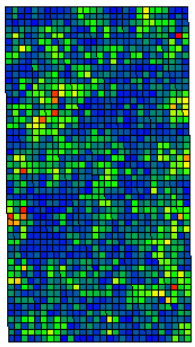

D1-B(2146)

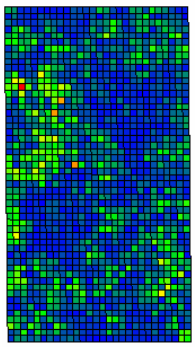

D1-C(2154)

Figure 4.21 Mode Shapes, Delta Mode Shapes and E-View plots for D1-E2 with associated frequencies

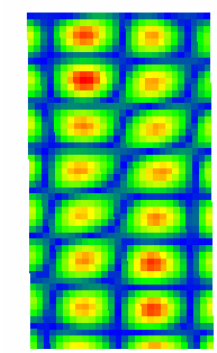

Healthy Mode Shape

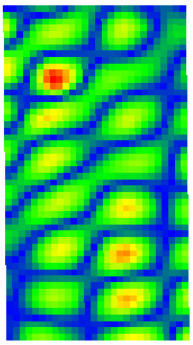

Damaged Mode Shape

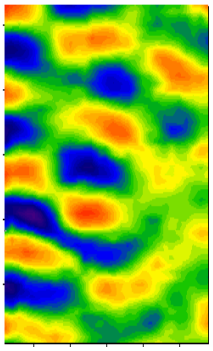

E2-D1(2322)-A(2353)

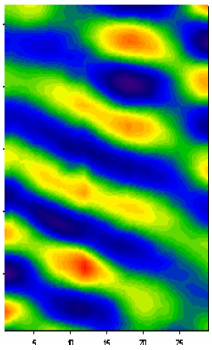

D1-B(2350)

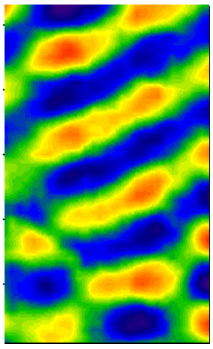

D1-C(2364)

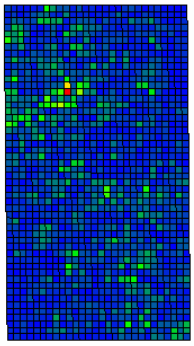

D1(2322)-A(2353)

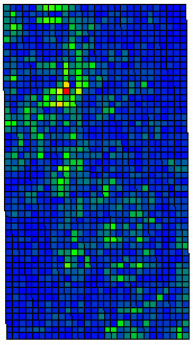

D1-B(2350)

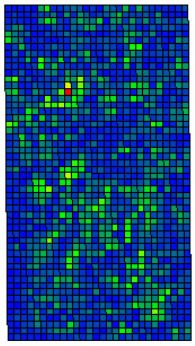

D1-C(2364)

Figure 4.22 Mode Shapes, Delta Mode Shapes and E-View plots for D1-E2 with associated frequencies

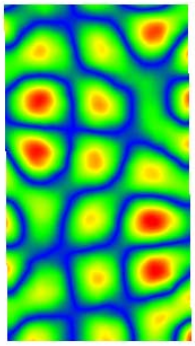

Healthy Mode Shape

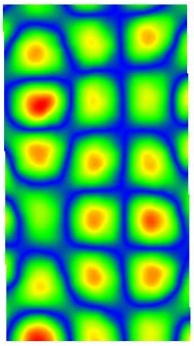

Damaged Mode Shape

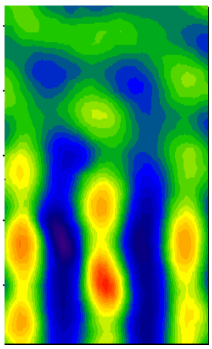

E2-D1(2392)-A(2434)

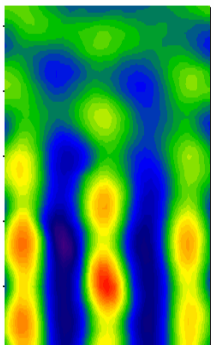

D1-B(2430)

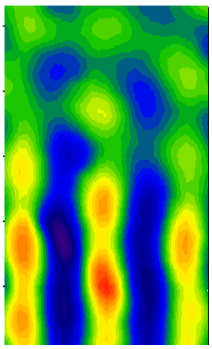

D1-C(2435)

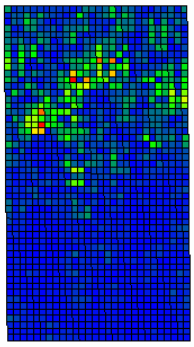

D1(2392)-A(2434)

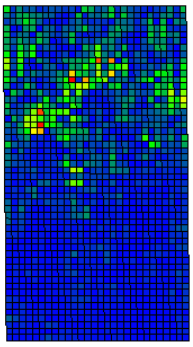

D1-B(2430)

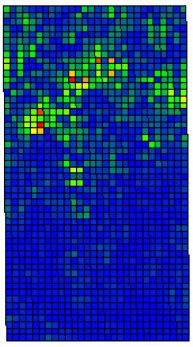

D1-C(2435)

Figure 4.23 Mode Shapes, Delta Mode Shapes and E-View plots for D1-E2 with associated frequencies

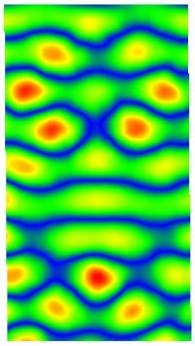

Healthy Mode Shape

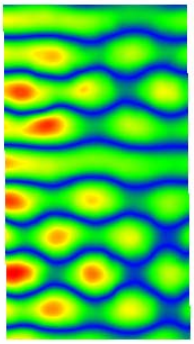

Damaged Mode Shape

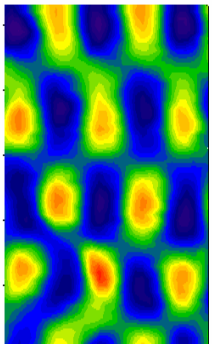

E2-D1(2515)-A(2547)

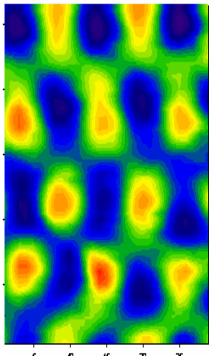

D1-B(2527)

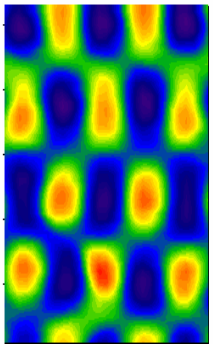

D1-C(2566)

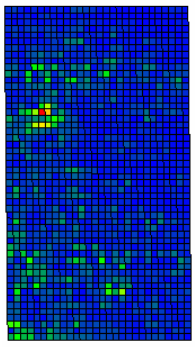

D1(2515)-A(2547)

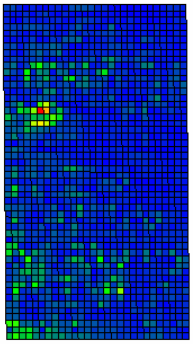

D1-B(2527)

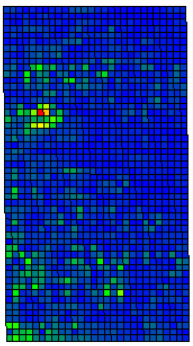

D1-C(2566)

Figure 4.24 Mode Shapes, Delta Mode Shapes and E-View plots for D1-E2 with associated frequencies

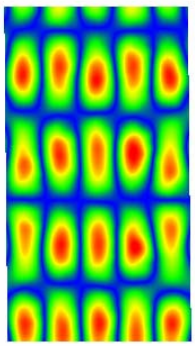

Healthy Mode Shape

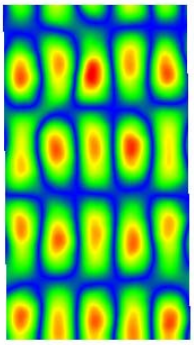

Damaged Mode Shape

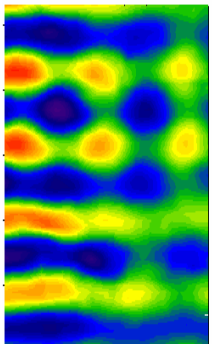

E2-D1(2950)-A(2991)

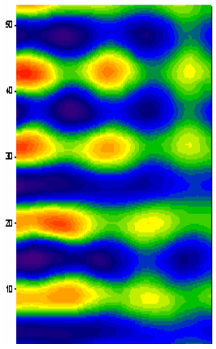

D1-B(2988)

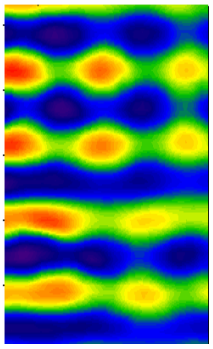

D1-C(2996)

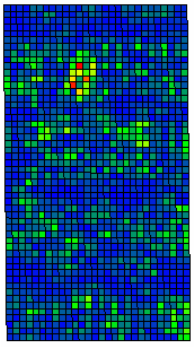

D1(2950)-A(2991)

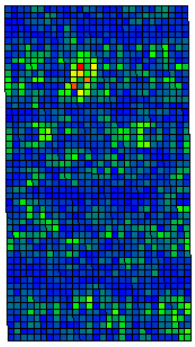

D1-B(2988)

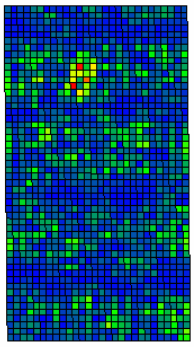

D1-C(2996)

Figure 4.25 Mode Shapes, Delta Mode Shapes and E-View plots for D1-E2 with associated frequencies

4.4 Delta Mode Shapes and E-View plots for D2-E1

Mode shapes plotted using Eview and delta mode shape plotted using Sigma Plot.

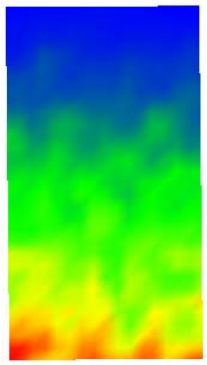

Healthy Mode Shape

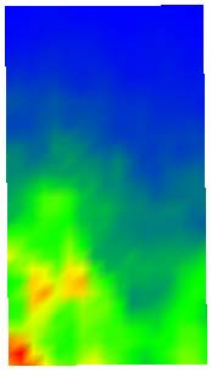

Damaged Mode Shape

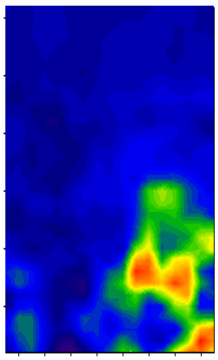

E1-D2(8)-A(7.625)

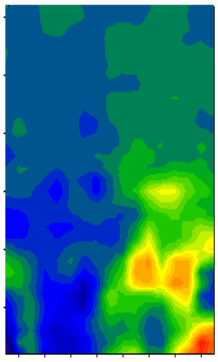

D2-B(7.875)

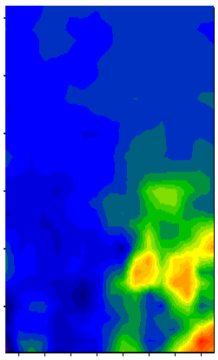

D2-C(8)

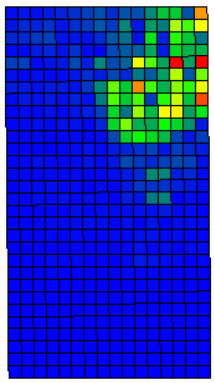

D2(8)-A(7.625)

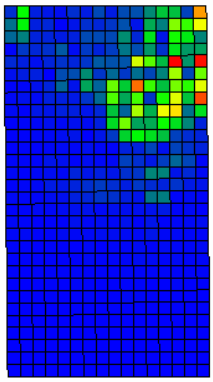

D2-B(7.875)

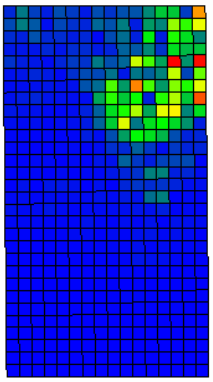

D2-C(8)

Figure 4.26 Mode Shapes, Delta Mode Shapes and E-View plots for D2-E1 with associated frequencies

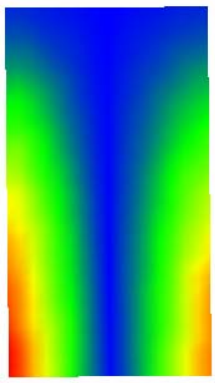

Healthy Mode Shape

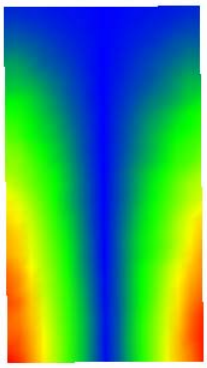

Damaged Mode Shape

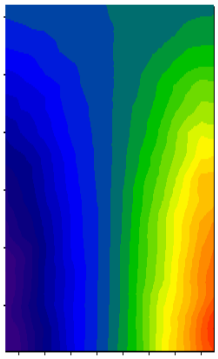

E1-D2(31.63)-A(31.88)

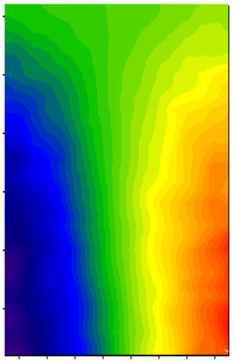

D2-B(31.5)

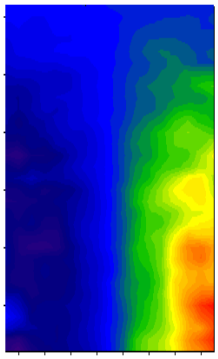

D2-C(32.12)

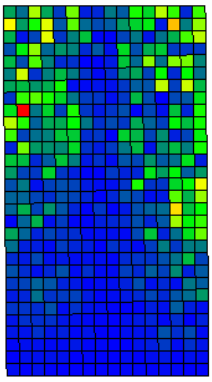

D2(31.63)-A(31.88)

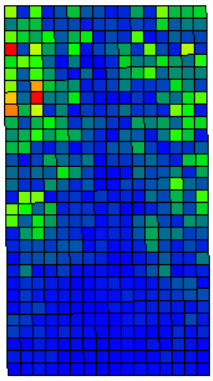

D2-B(31.5)

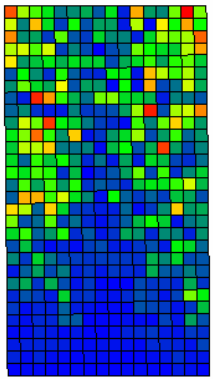

D2-C(32.12)

Figure 4.27 Mode Shapes, Delta Mode Shapes and E-View plots for D2-E1 with associated frequencies

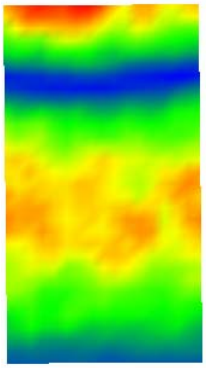

Healthy Mode Shape

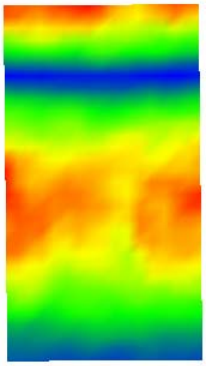

Damaged Mode Shape

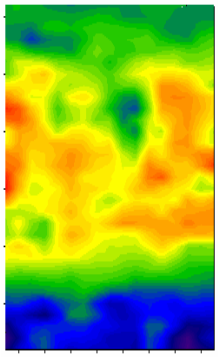

E1-D2(48.38)-A(48.25)

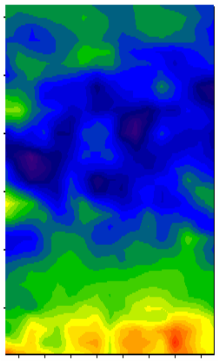

D2-B(49)

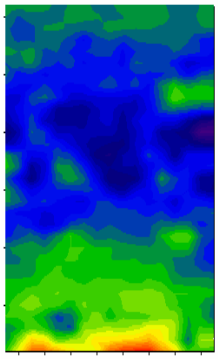

D2-C(49.88)

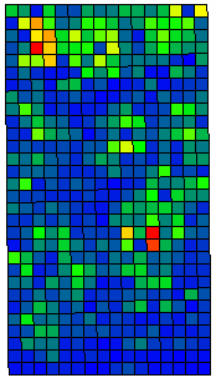

D2(48.38)-A(48.25)

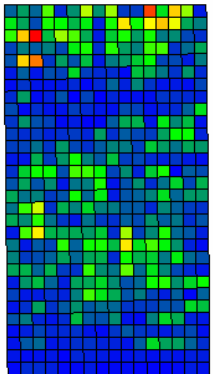

D2-B(49)

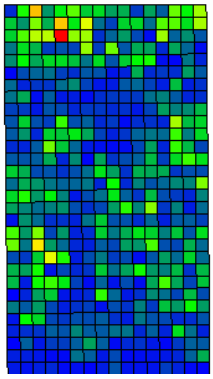

D2-C(49.88)

Figure 4.28 Mode Shapes, Delta Mode Shapes and E-View plots for D2-E1 with associated frequencies

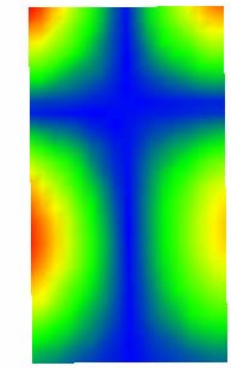

Healthy Mode Shape

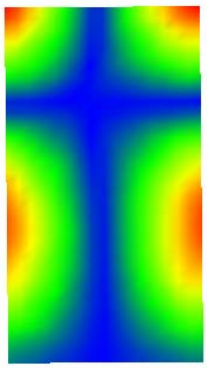

Damaged Mode Shape

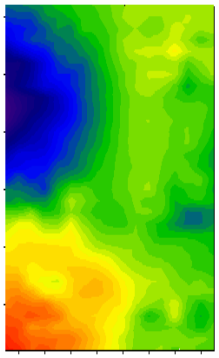

E1-D2(100.5)-A(105.4)

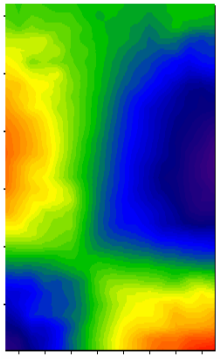

D2-B(104.4)

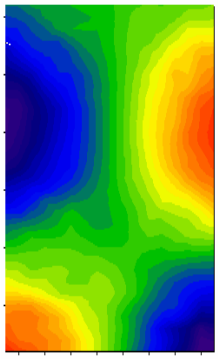

D2-C(106.4)

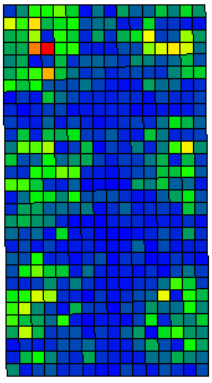

D2(100.5)-A(105.4)

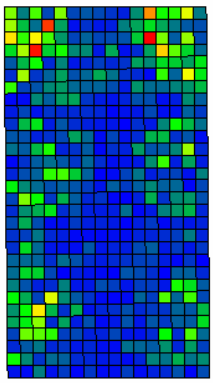

D2-B(104.4)

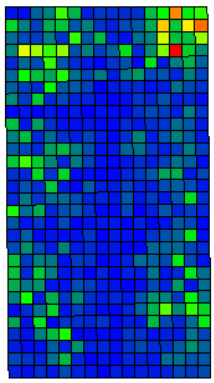

D2-C(106.4)

Figure 4.29 Mode Shapes, Delta Mode Shapes and E-View plots for D2-E1 with associated frequencies

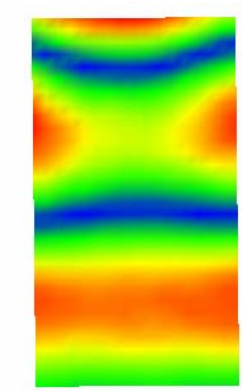

Healthy Mode Shape

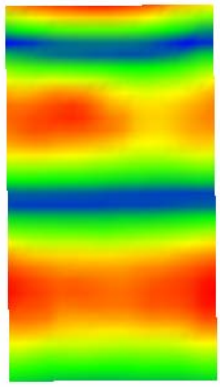

Damaged Mode Shape

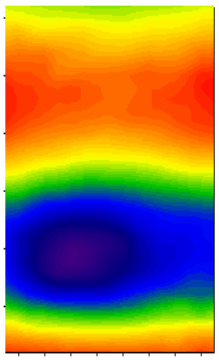

E1-D2(133.6)-A(136)

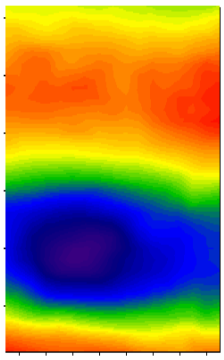

D2-B(137.6)

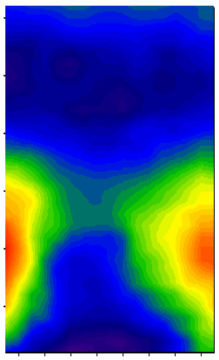

D2-C(140.1)

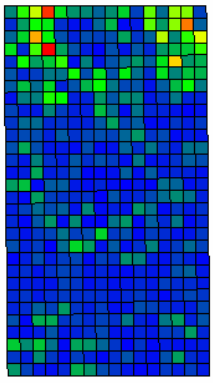

D2(133.6)-A(136)

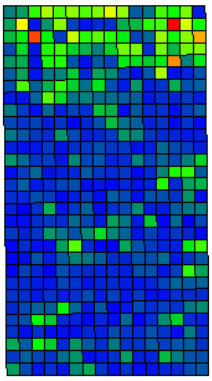

D2-B(137.6)

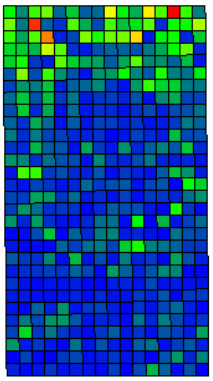

D2-C(140.1)

Figure 4.30 Mode Shapes, Delta Mode Shapes and E-View plots for D2-E1 with associated frequencies

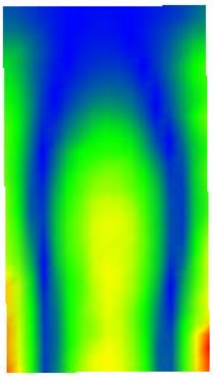

Healthy Mode Shape

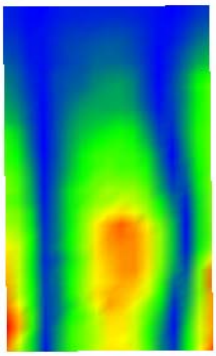

Damaged Mode Shape

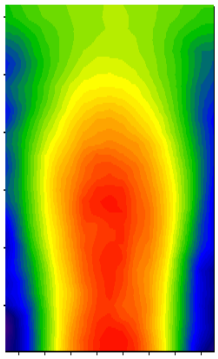

E1-D2(176.5)-A(192)

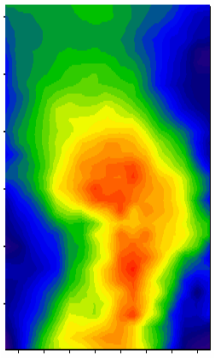

D2-B(191.6)

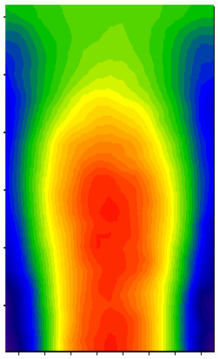

D2-C(192.1)

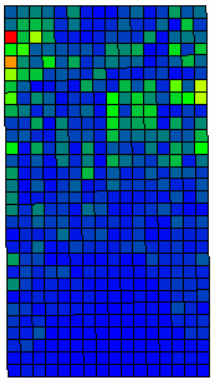

D2(176.5)-A(192)

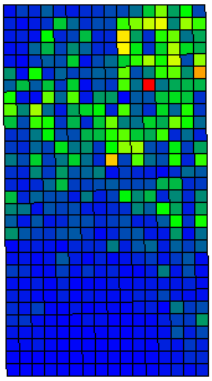

D2-B(191.6)

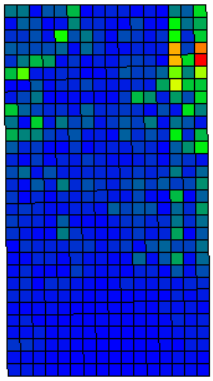

D2-C(192.1)

Figure 4.31 Mode Shapes, Delta Mode Shapes and E-View plots for D2-E1 with associated frequencies

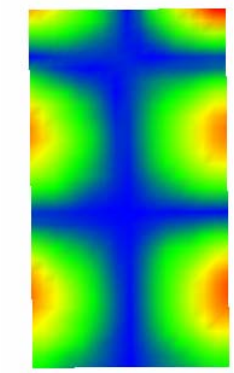

Healthy Mode Shape

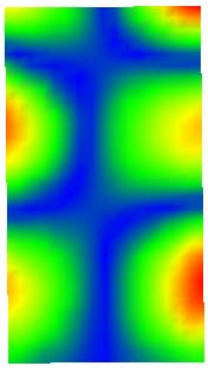

Damaged Mode Shape

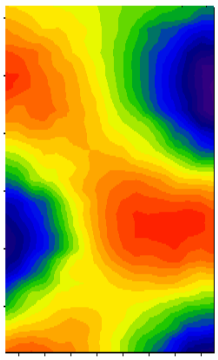

E1-D2(204.4)-A(205.4)

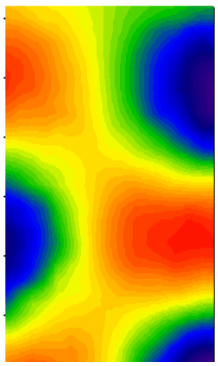

D2-B(205.4)

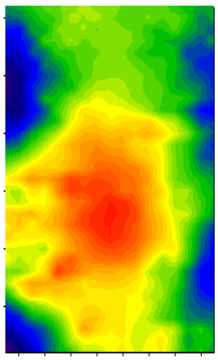

D2-C(207.4)

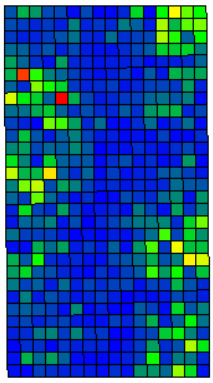

D2(204.4)-A(205.4)

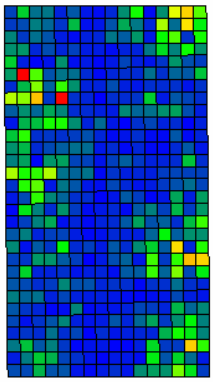

D2-B(205.4)

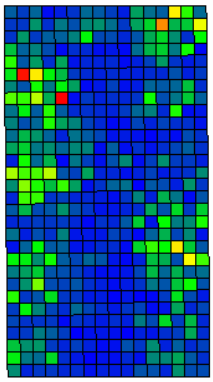

D2-C(207.4)

Figure 4.32 Mode Shapes, Delta Mode Shapes and E-View plots for D2-E1 with associated frequencies

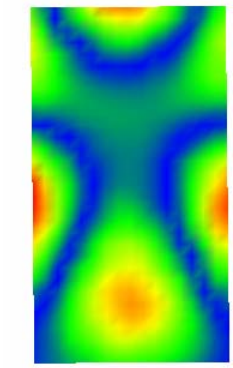

Healthy Mode Shape

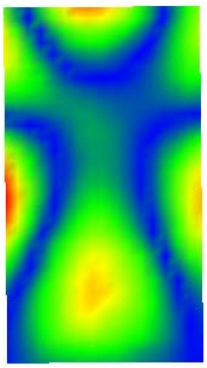

Damaged Mode Shape

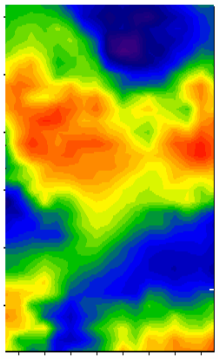

E1-D2(260)-A(260.4)

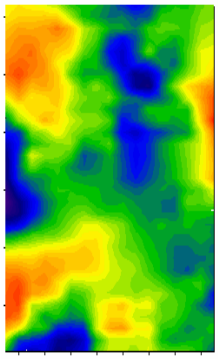

D2-B(264)

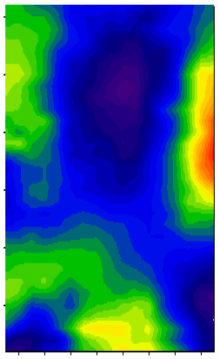

D2-C(264.6)

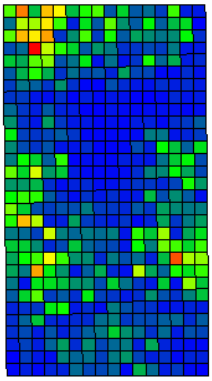

D2(260)-A(260.4)

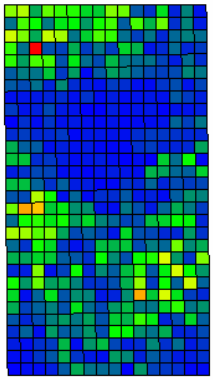

D2-B(264)

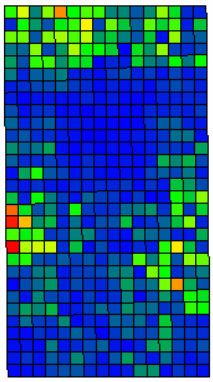

D2-C(264.6)

Figure 4.33 Mode Shapes, Delta Mode Shapes and E-View plots for D2-E1 with associated frequencies

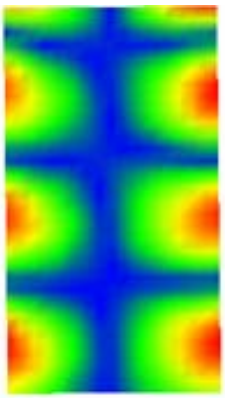

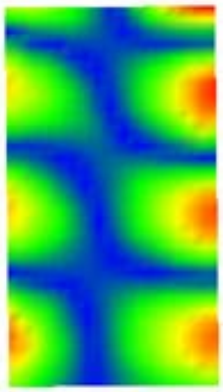

Healthy Mode Shape Damaged Mode Shape

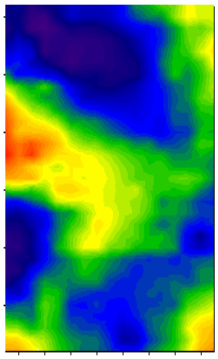

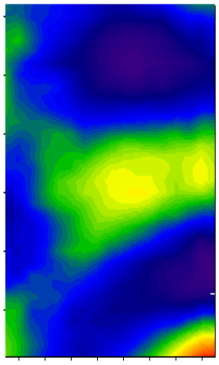

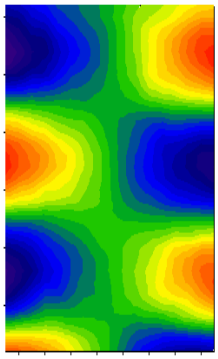

E1-D2(342.3)-A(342.9) D2-B(339.3) D2-C(346.5)

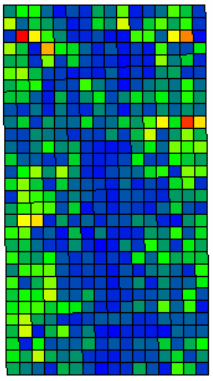

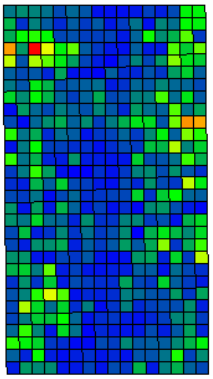

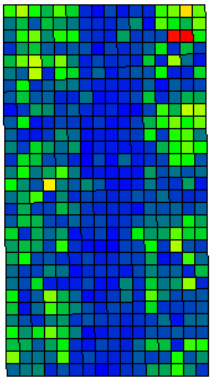

D2(342.3)-A(342.9) D2-B(339.3) D2-C(346.5)

Figure 4.34 Mode Shapes, Delta Mode Shapes and E-View plots for D2-E1 with associated frequencies

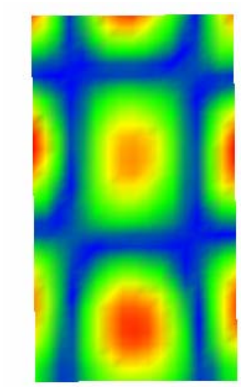

Healthy Mode Shape

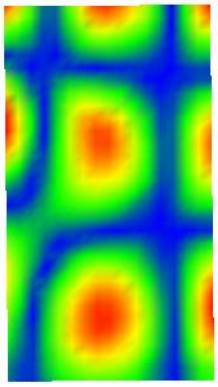

Damaged Mode Shape

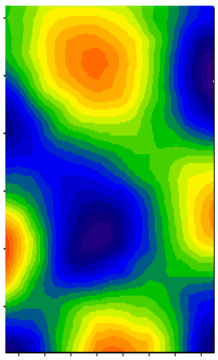

E1-D2(380.3)-A(386)

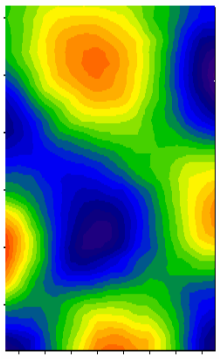

D2-B(387.9)

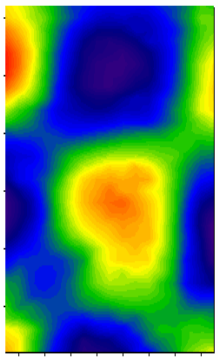

D2-C(390.6)

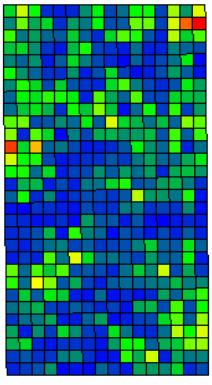

D2(380.3)-A(386)

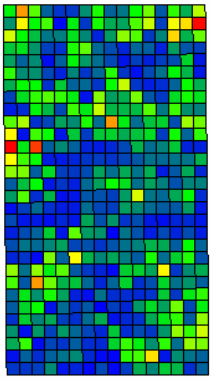

D2-B(387.9)

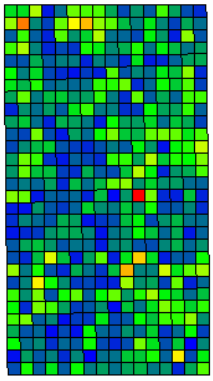

D2-C(390.6)

Figure 4.35 Mode Shapes, Delta Mode Shapes and E-View plots for D2-E1 with associated frequencies

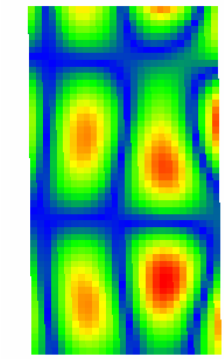

Healthy Mode Shape

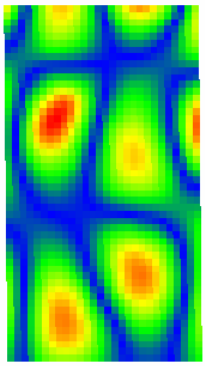

Damaged Mode Shape

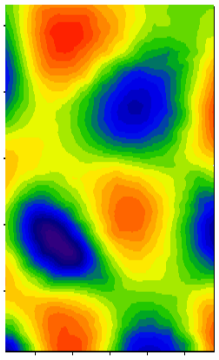

E1-D2(693.5)-A(702)

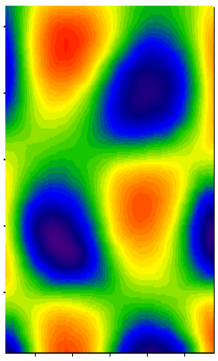

D2-B(697.5)

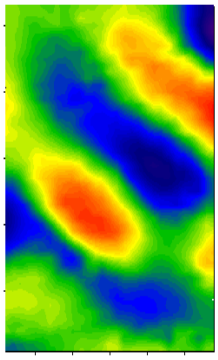

D2-C(703.8)

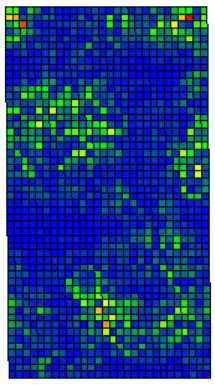

D2(693.5)-A(702)

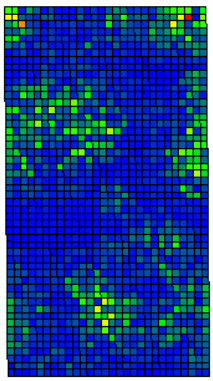

D2-B(697.5)

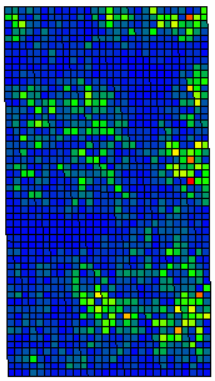

D2-C(703.8)

Figure 4.36 Mode Shapes, Delta Mode Shapes and E-View plots for D2-E1 with associated frequencies

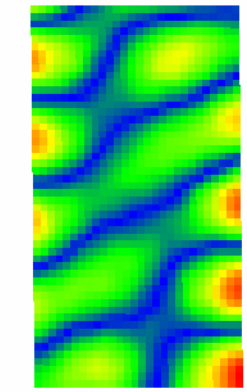

Healthy Mode Shape

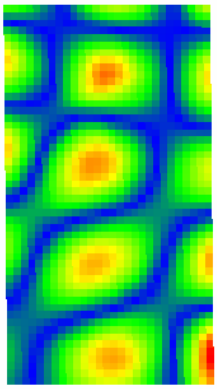

Damaged Mode Shape

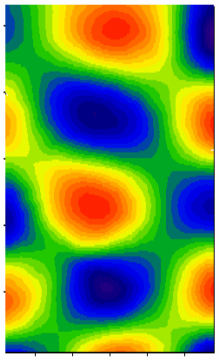

E1-D2(735.6)-A(745)

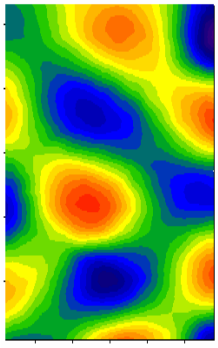

D2-B(742.5)

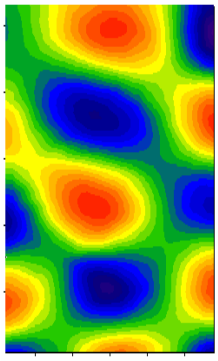

D2-C(742.5)

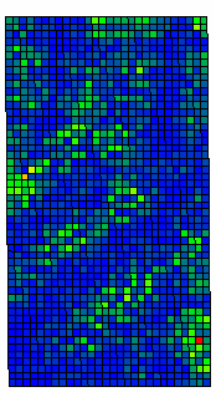

D2(735.6)-A(745)

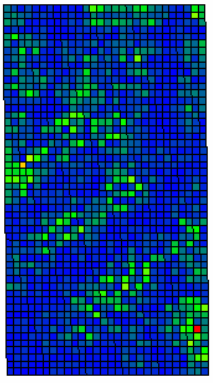

D2-B(742.5)

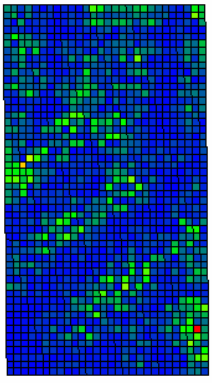

D2-C(742.5)

Figure 4.37 Mode Shapes, Delta Mode Shapes and E-View plots for D2-E1 with associated frequencies

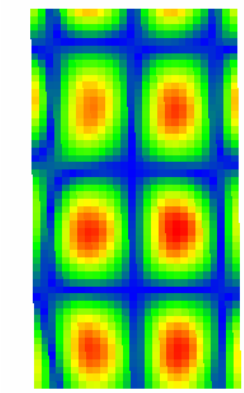

Healthy Mode Shape

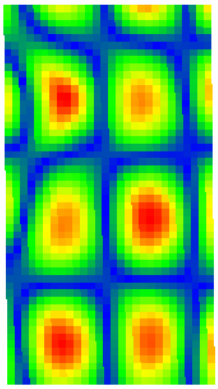

Damaged Mode Shape

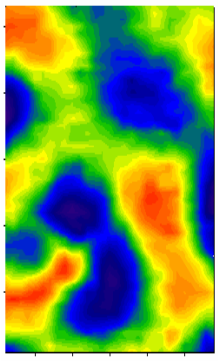

E1-D2(865)-A(876.3)

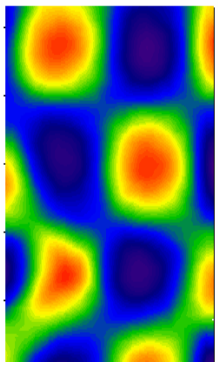

D2-B(873.8)

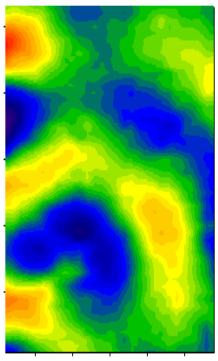

D2-C(880)

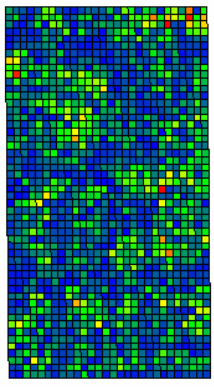

D2(865)-A(876.3)

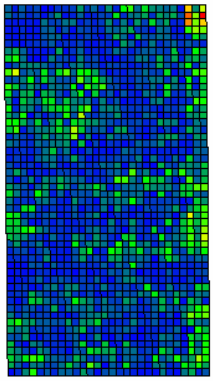

D2-B(873.8)

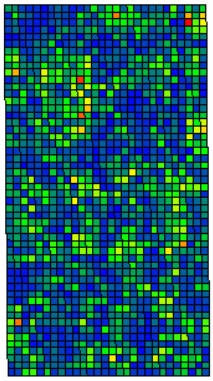

D2-C(880)

Figure 4.38 Mode Shapes, Delta Mode Shapes and E-View plots for D2-E1 with associated frequencies

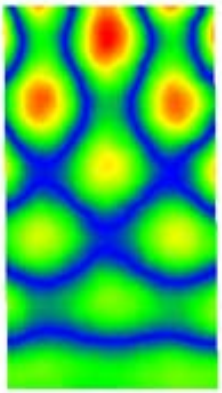

Healthy Mode Shape

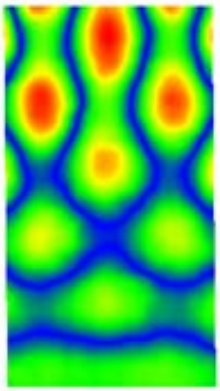

Damaged Mode Shape

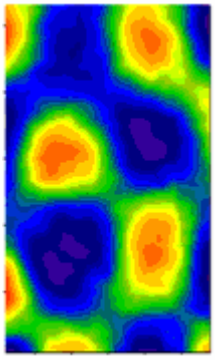

E1-D2(963)-A(981.3)

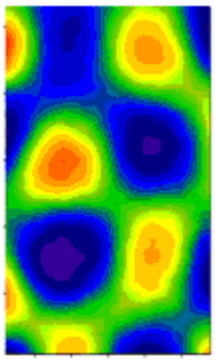

D2-B(968.8)

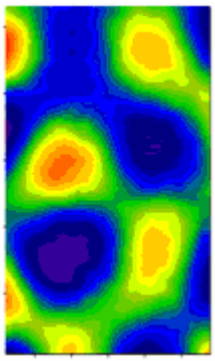

D2-C(978.8)

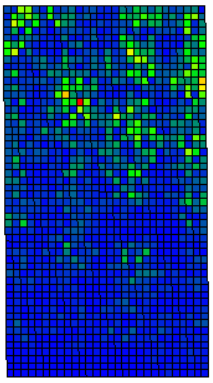

D2(963)-A(981.3)

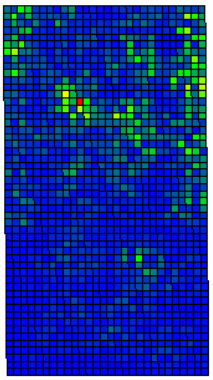

D2-B(968.8)

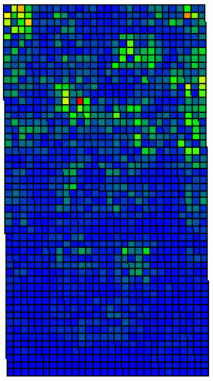

D2-C(978.8)

Figure 4.39 Mode Shapes, Delta Mode Shapes and E-View plots for D2-E1 with associated frequencies

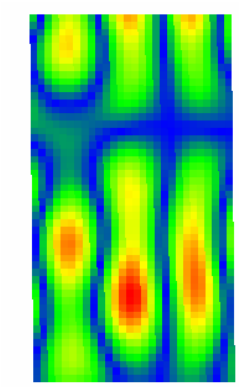

Healthy Mode Shape

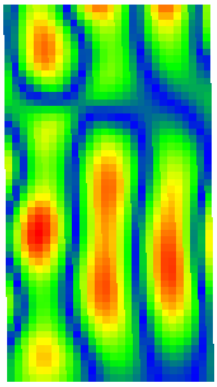

Damaged Mode Shape

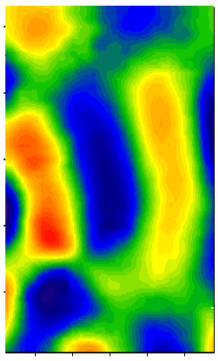

E1-D2(1043)-A(1058)

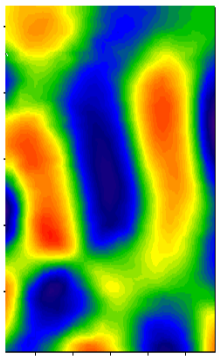

D2-B(1058)

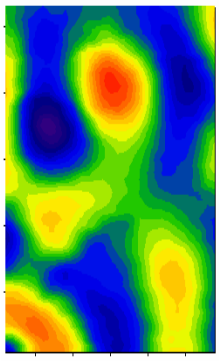

D2-C(1059)

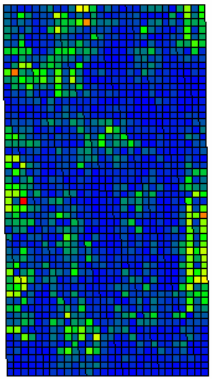

D2(1043)-A(1058)

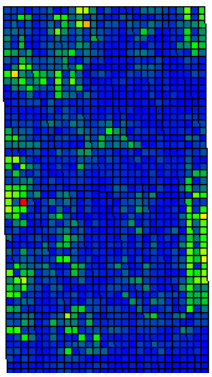

D2-B(1058)

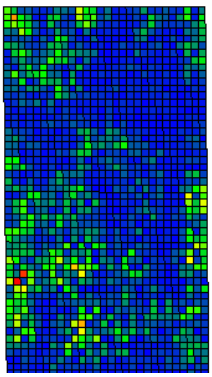

D2-C(1059)

Figure 4.40 Mode Shapes, Delta Mode Shapes and E-View plots for D2-E1 with associated frequencies

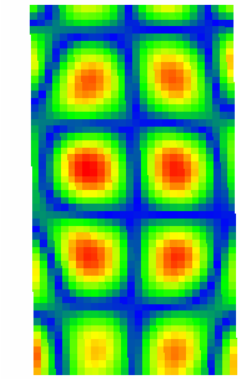

Healthy Mode Shape

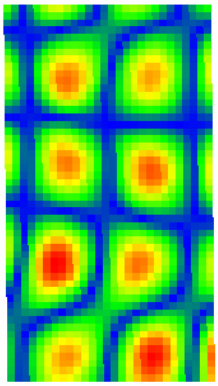

Damaged Mode Shape

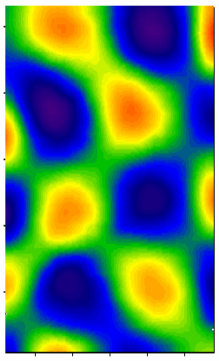

E1-D2(1075)-A(1088)

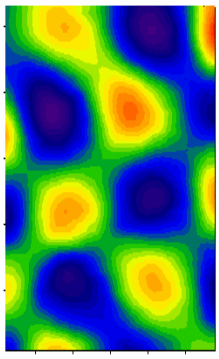

D2-B(1089)

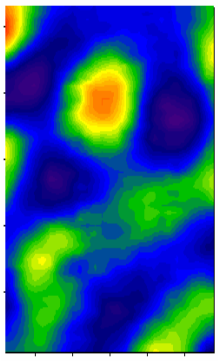

D2-C(1095)

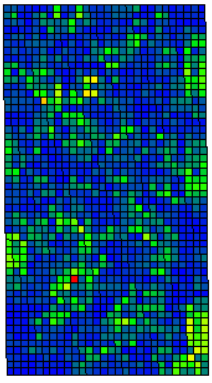

D2(1075)-A(1088)

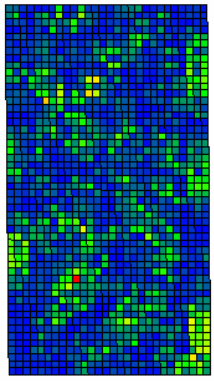

D2-B(1089)

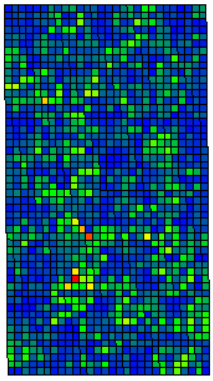

D2-C(1095)

Figure 4.41 Mode Shapes, Delta Mode Shapes and E-View plots for D2-E1 with associated frequencies

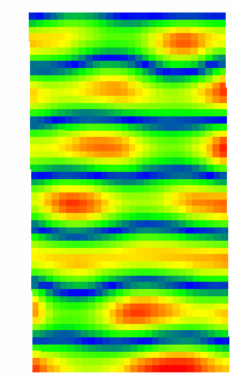

Healthy Mode Shape

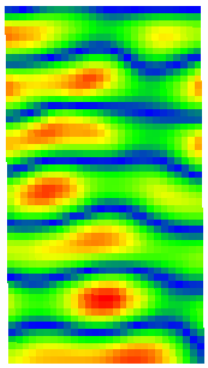

Damaged Mode Shape

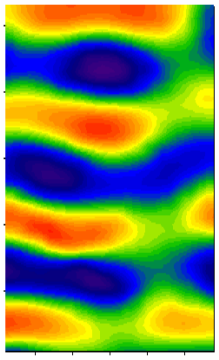

E1-D2(1283)-A(1304)

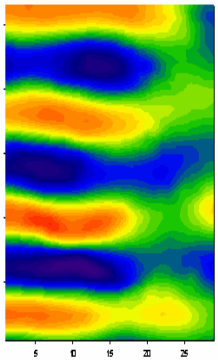

D2-B(1299)

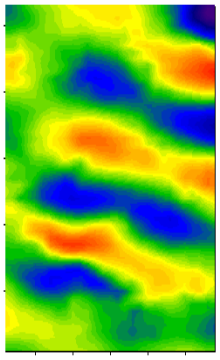

D2-C(1313)

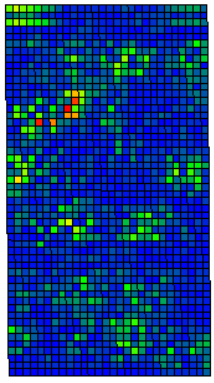

D2(1283)-A(1304)

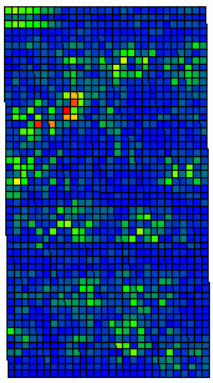

D2-B(1299)

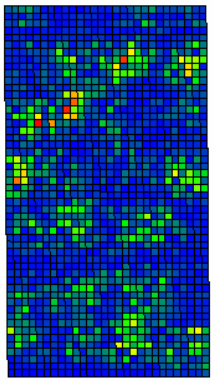

D2-C(1313)

Figure 4.42 Mode Shapes, Delta Mode Shapes and E-View plots for D2-E1 with associated frequencies

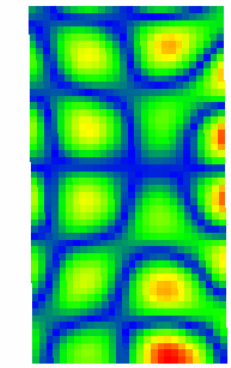

Healthy Mode Shape

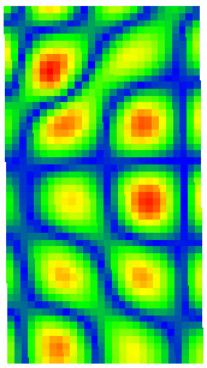

Damaged Mode Shape

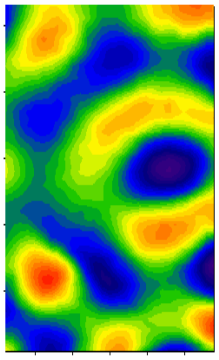

E1-D2(1317)-A(1330)

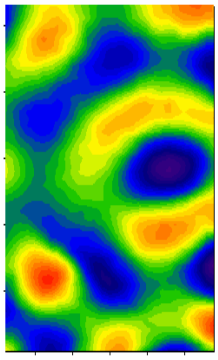

D2-B(1343)

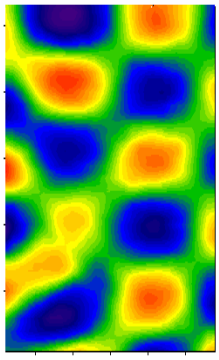

D2-C(1347)

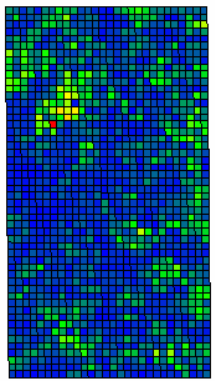

D2(1317)-A(1330)

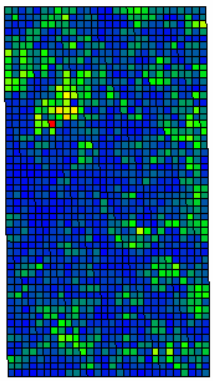

D2-B(1343)

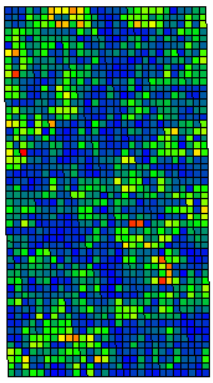

D2-C(1347)

Figure 4.43 Mode Shapes, Delta Mode Shapes and E-View plots for D2-E1 with associated frequencies

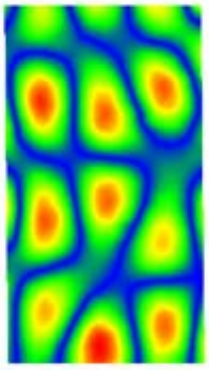

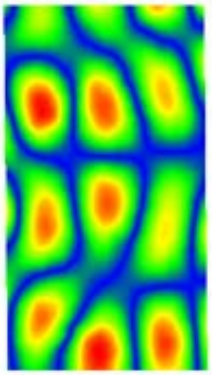

Healthy Mode Shape Damaged Mode Shape

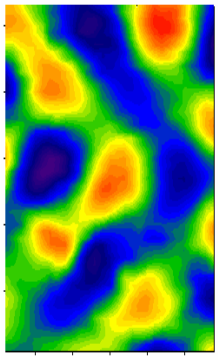

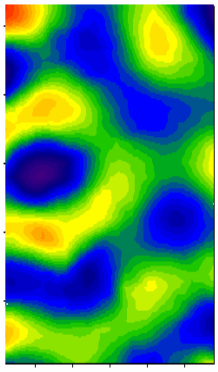

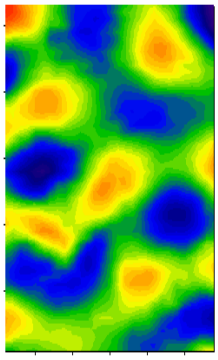

E1-D2(1332)-A(1354) D2-B(1354) D2-C(1357)

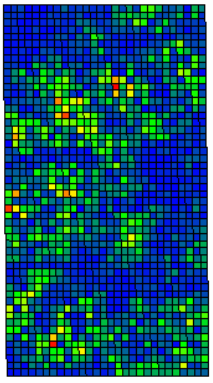

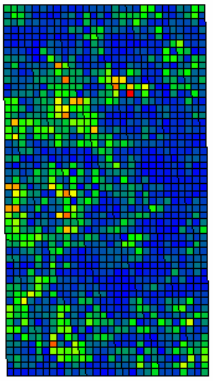

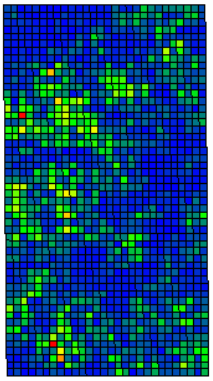

D2(1332)-A(1354) D2-B(1354) D2-C(1357)

Figure 4.44 Mode Shapes, Delta Mode Shapes and E-View plots for D2-E1 with associated frequencies

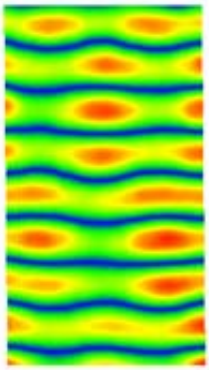

Healthy Mode Shape

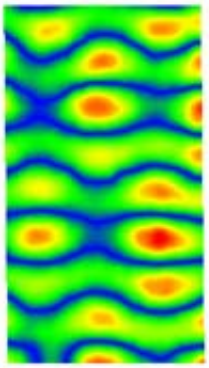

Damaged Mode Shape

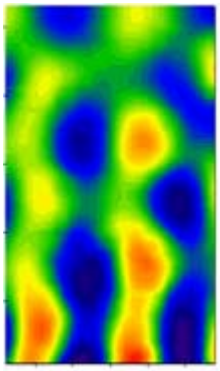

E1-D2(2097)-A(2144)

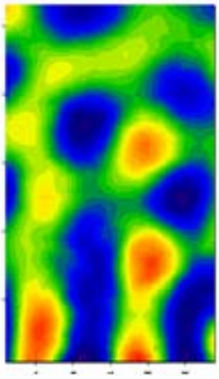

D2-B(2146)

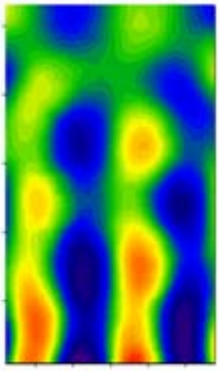

D2-C(2154)

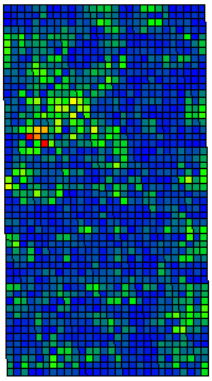

D2(2097)-A(2144)

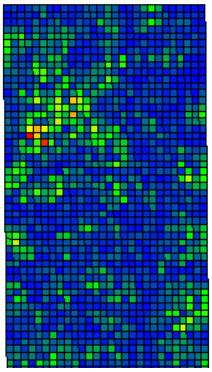

D2-B(2146)

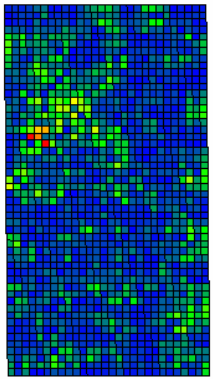

D2-C(2154)

Figure 4.45 Mode Shapes, Delta Mode Shapes and E-View plots for D2-E1 with associated frequencies

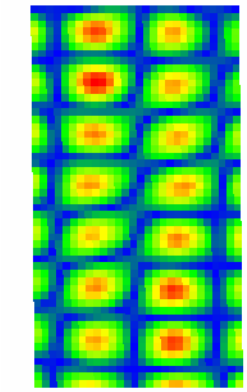

Healthy Mode Shape

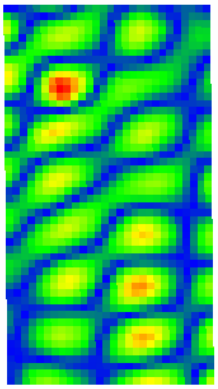

Damaged Mode Shape

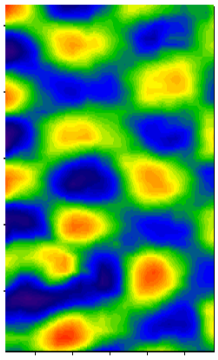

E1-D2(2293)-A(2353)

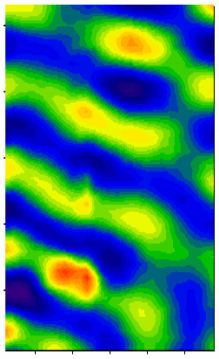

D2-B(2350)

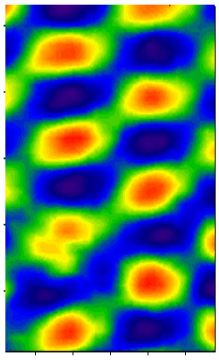

D2-C(2364)

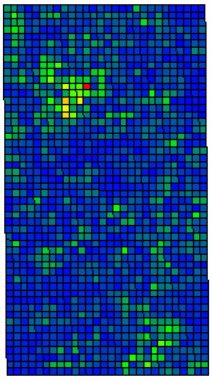

D2(2293)-A(2353)

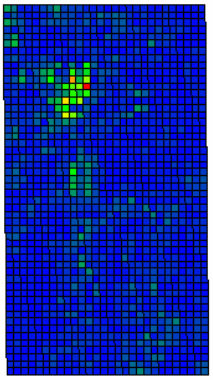

D2-B(2350)

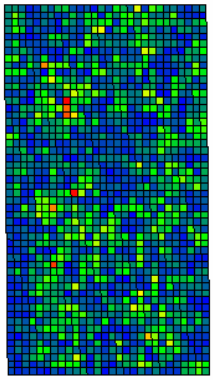

D2-C(2364)

Figure 4.46 Mode Shapes, Delta Mode Shapes and E-View plots for D2-E1 with associated frequencies

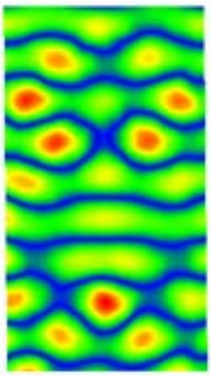

Healthy Mode Shape

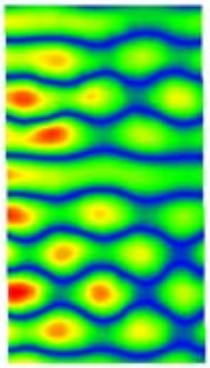

Damaged Mode Shape

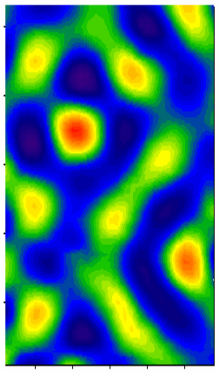

E1-D2(2473)-A(2547)

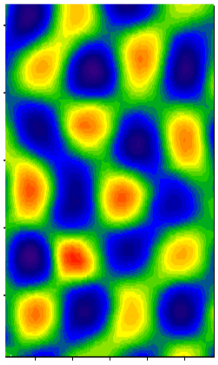

D2-B(2527)

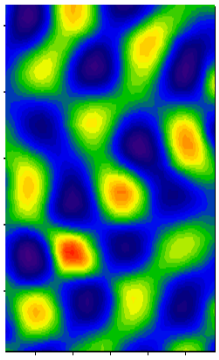

D2-C(2566)

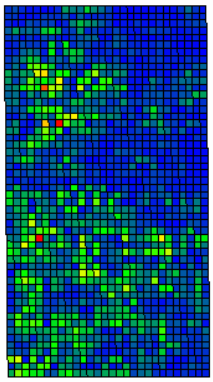

D2(2473)-A(2547)

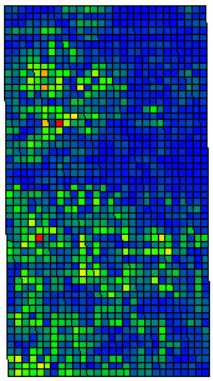

D2-B(2527)

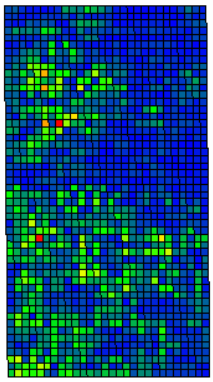

D2-C(2566)

Figure 4.47 Mode Shapes, Delta Mode Shapes and E-View plots for D2-E1 with associated frequencies

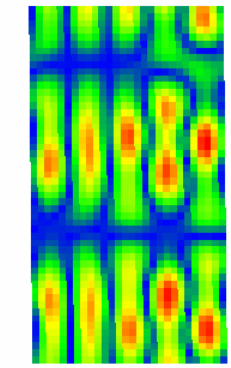

Healthy Mode Shape

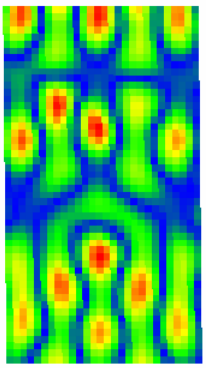

Damaged Mode Shape

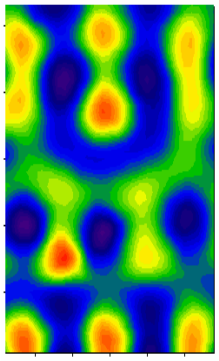

E1-D2(2530)-A(2605)

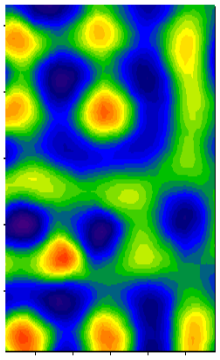

D2-B(2606)

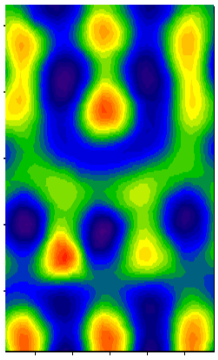

D2-C(2610)

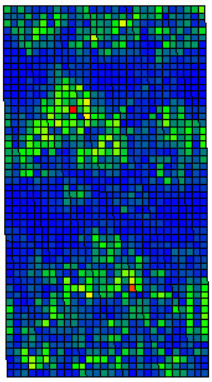

D2(2530)-A(2605)

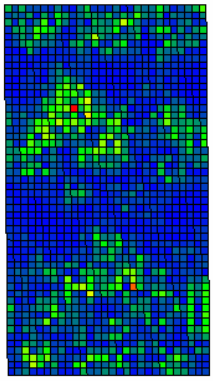

D2-B(2606)

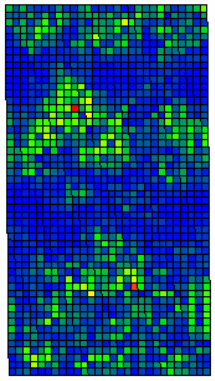

D2-C(2610)

Figure 4.48 Mode Shapes, Delta Mode Shapes and E-View plots for D2-E1 with associated frequencies

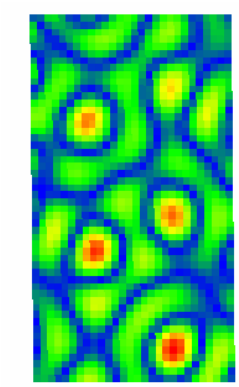

Healthy Mode Shape

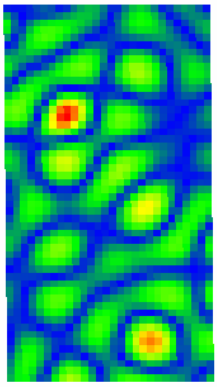

Damaged Mode Shape

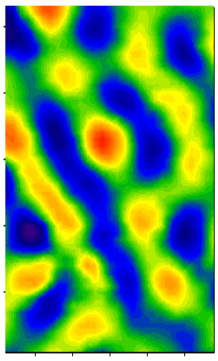

E1-D2(2724)-A(2771)

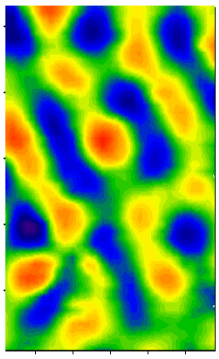

D2-B(2761)

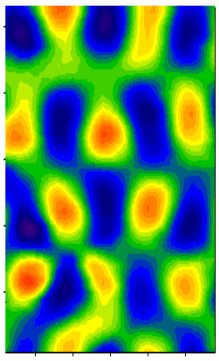

D2-C(2780)

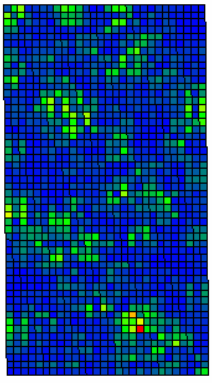

D2(2724)-A(2771)

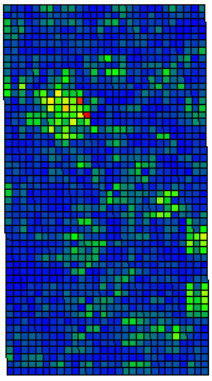

D2-B(2761)

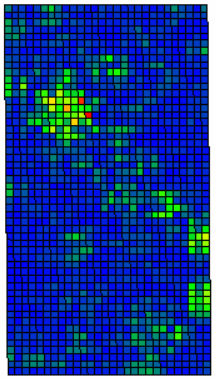

D2-C(2780)

Figure 4.49 Mode Shapes, Delta Mode Shapes and E-View plots for D2-E1 with associated frequencies

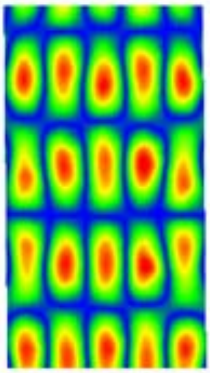

Healthy Mode Shape

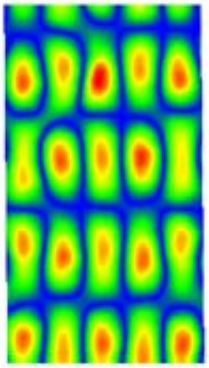

Damaged Mode Shape

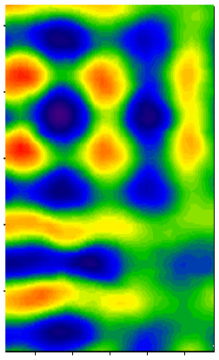

E1-D2(2899)-A(2991)

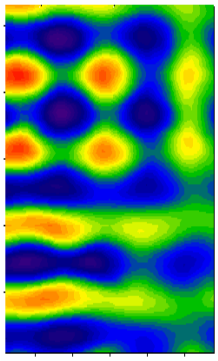

D2-B(2988)

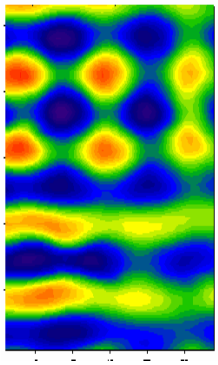

D2-C(2996)

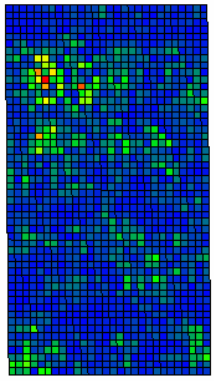

D2(2899)-A(2991)

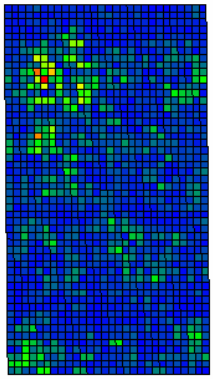

D2-B(2988)

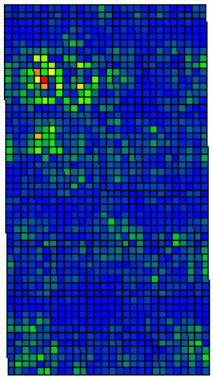

D2-C(2996)

Figure 4.50 Mode Shapes, Delta Mode Shapes and E-View plots for D2-E1 with associated frequencies

4.5 Mode Shape, Delta Mode Shapes and E-View plots for D2-E2

Mode shapes plotted using Eview and delta mode shape plotted using Sigma Plot.

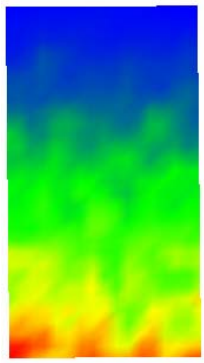

Healthy Mode Shape

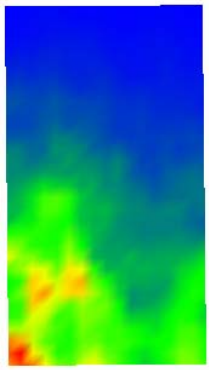

Damaged Mode Shape

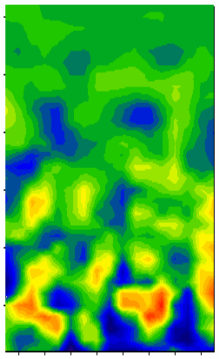

E2-D2(8)-A(7.625)

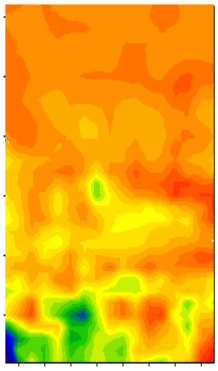

D2-B(7.875)

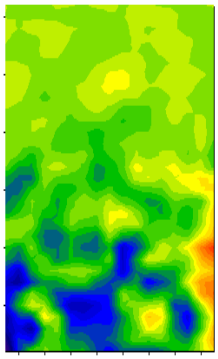

D2-C(8)

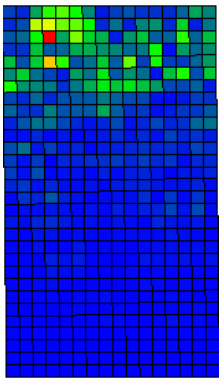

D2(8)-A(7.625)

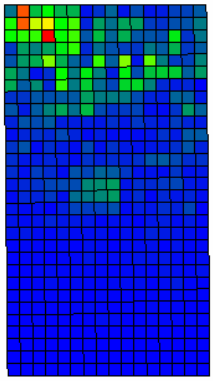

D2-B(7.875)

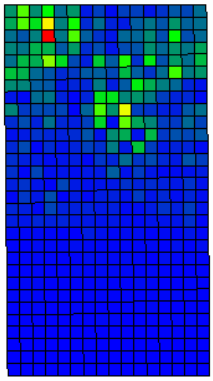

D2-C(8)

Figure 4.51 Mode Shapes, Delta Mode Shapes and E-View plots for D2-E2 with associated frequencies

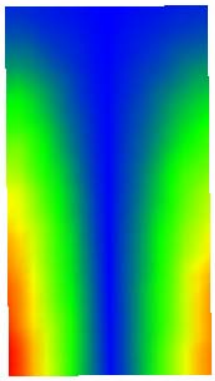

Healthy Mode Shape

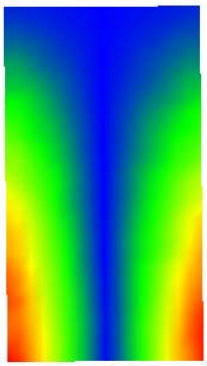

Damaged Mode Shape

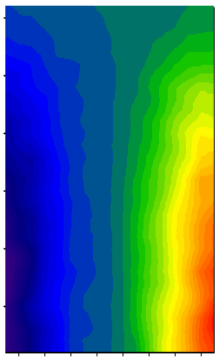

E2-D2(31.5)-A(31.88)

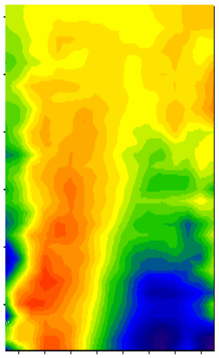

D2-B(31.5)

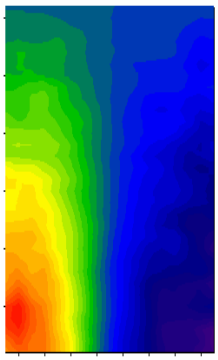

D2-C(32.12)

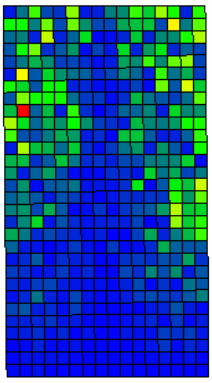

D2(31.5)-A(31.88)

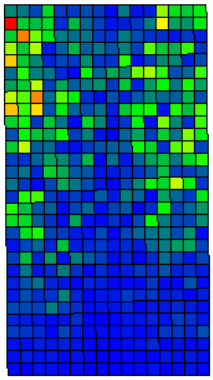

D2-B(31.5)

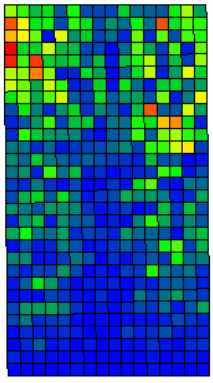

D2-C(32.12)

Figure 4.52 Mode Shapes, Delta Mode Shapes and E-View plots for D2-E2 with associated frequencies

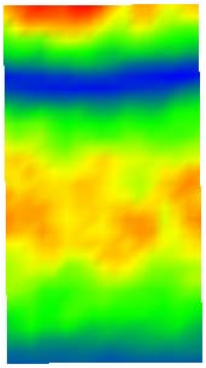

Healthy Mode Shape

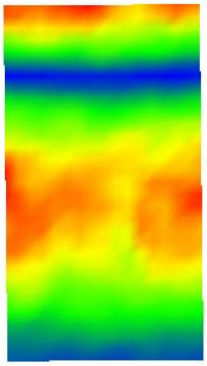

Damaged Mode Shape

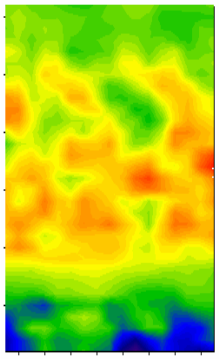

E2-D2(48.25)-A(48.25)

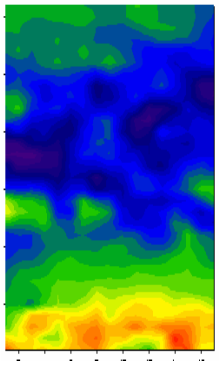

D2-B(49)

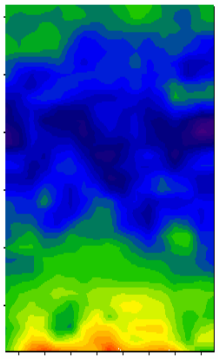

D2-C(49.88)

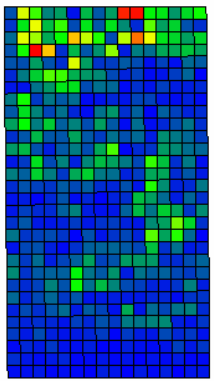

D2(48.25)-A(48.25)

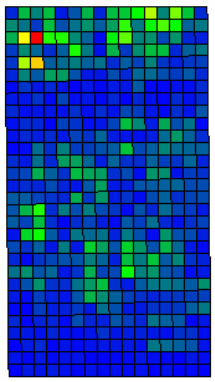

D2-B(49)

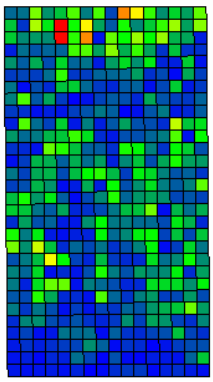

D2-C(49.88)

Figure 4.53 Mode Shapes, Delta Mode Shapes and E-View plots for D2-E2 with associated frequencies

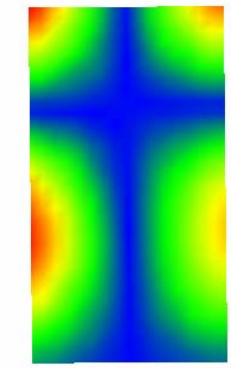

Healthy Mode Shape

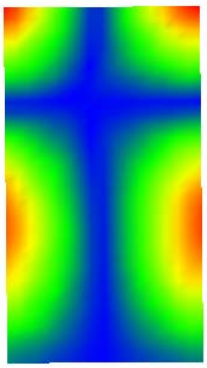

Damaged Mode Shape

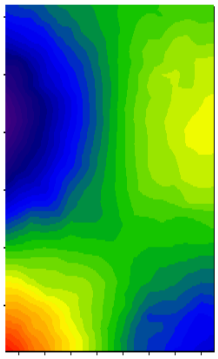

E2-D2(100.4)-A(105.4)

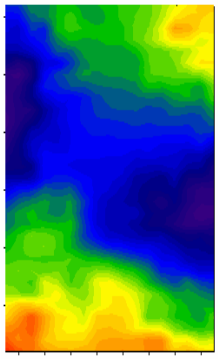

D2-B(104.4)

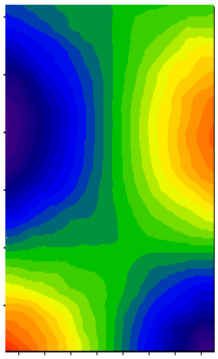

D2-C(106.4)

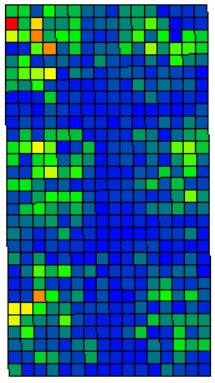

D2(100.4)-A(105.4)

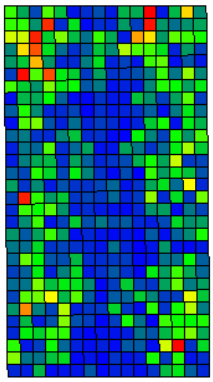

D2-B(104.4)

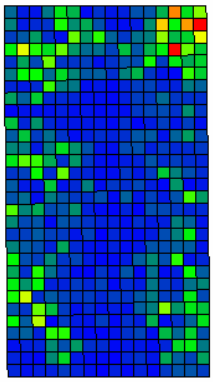

D2-C(106.4)

Figure 4.54 Mode Shapes, Delta Mode Shapes and E-View plots for D2-E2 with associated frequencies

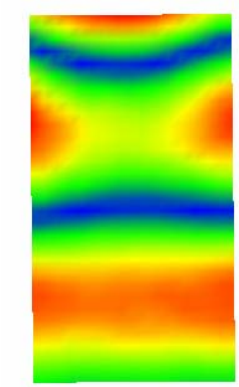

Healthy Mode Shape

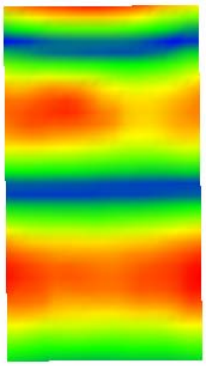

Damaged Mode Shape

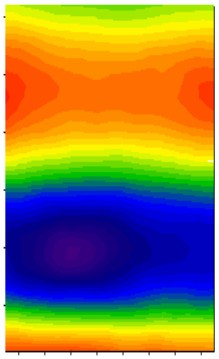

E2-D2(133.3)-A(136)

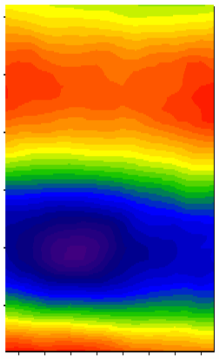

D2-B(137.6)

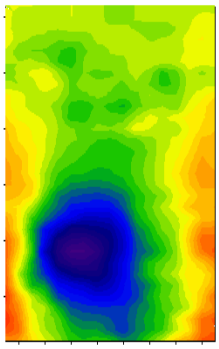

D2-C(140.1)

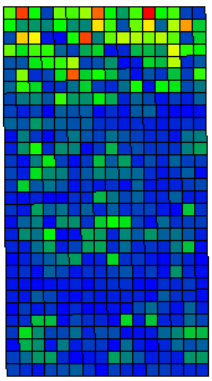

D2(133.3)-A(136)

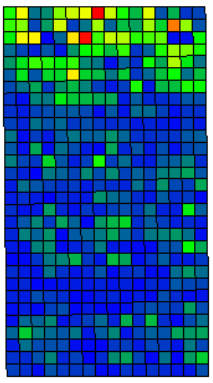

D2-B(137.6)

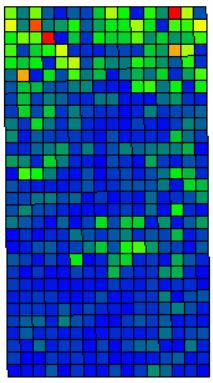

D2-C(140.1)

Figure 4.55 Mode Shapes, Delta Mode Shapes and E-View plots for D2-E2 with associated frequencies

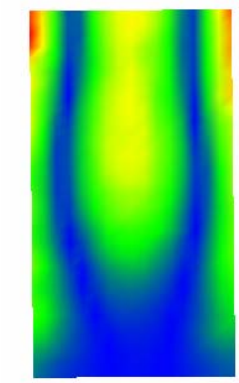

Healthy Mode Shape

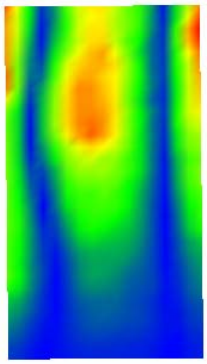

Damaged Mode Shape

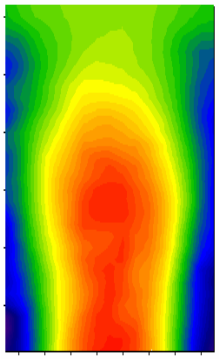

E2-D2(176.5)-A(192)

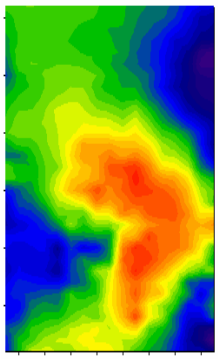

D2-B(191.6)

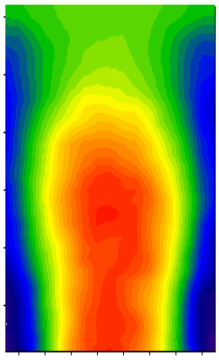

D2-C(192.1)

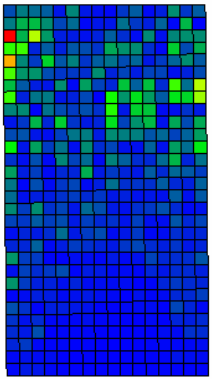

D2(176.5)-A(192)

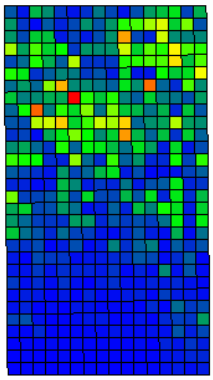

D2-B(191.6)

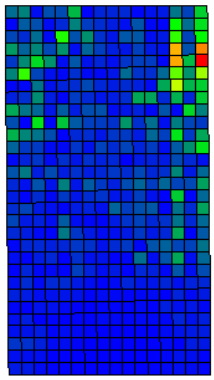

D2-C(192.1)

Figure 4.56 Mode Shapes, Delta Mode Shapes and E-View plots for D2-E2 with associated frequencies

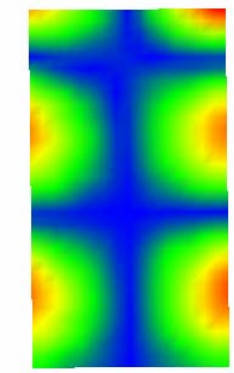

Healthy Mode Shape

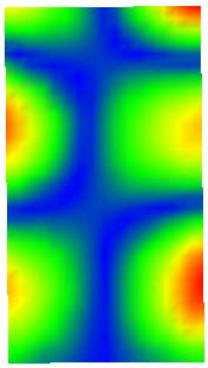

Damaged Mode Shape

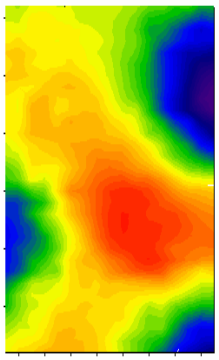

E2-D2(203.9)-A(205)

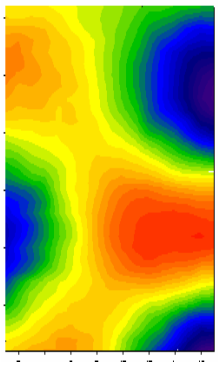

D2-B(203.4)

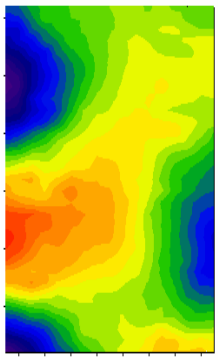

D2-C(207.4)

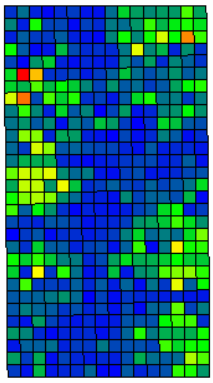

D2(203.9)-A(205)

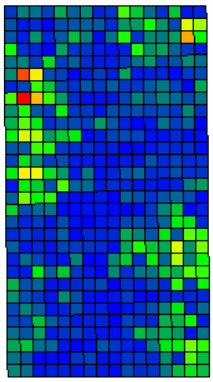

D2-B(203.4)

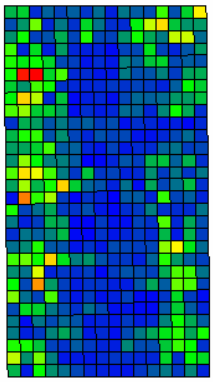

D2-C(207.4)

Figure 4.57 Mode Shapes, Delta Mode Shapes and E-View plots for D2-E2 with associated frequencies

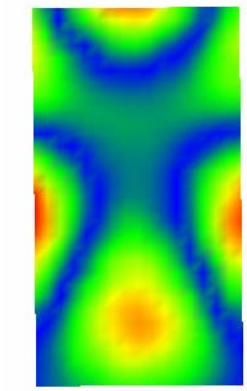

Healthy Mode Shape

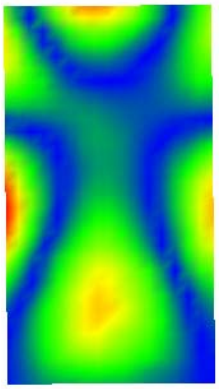

Damaged Mode Shape

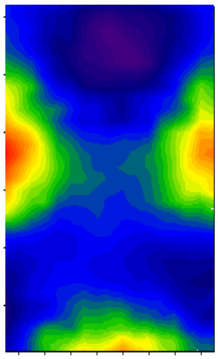

E2-D2(260.4)-A(260.4)

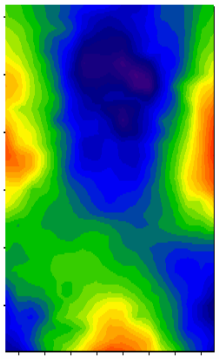

D2-B(264)

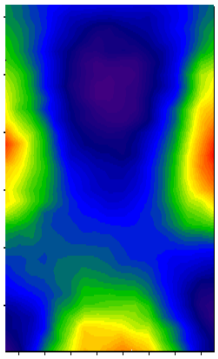

D2-C(264.6)

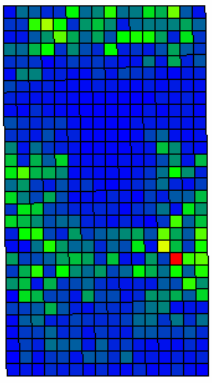

D2(260.4)-A(260.4)

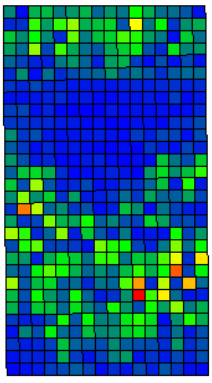

D2-B(264)

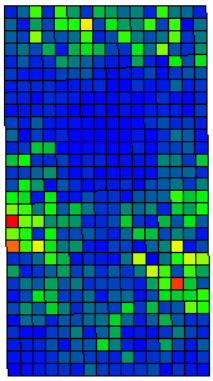

D2-C(264.6)

Figure 4.58 Mode Shapes, Delta Mode Shapes and E-View plots for D2-E2 with associated frequencies

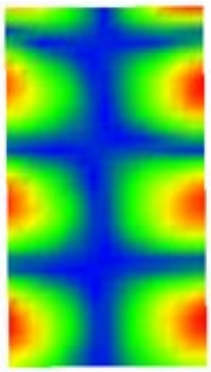

Healthy Mode Shape

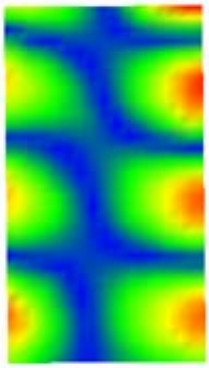

Damaged Mode Shape

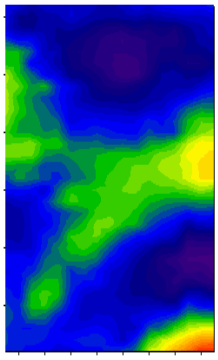

E2-D2(341.4)-A(342.9)

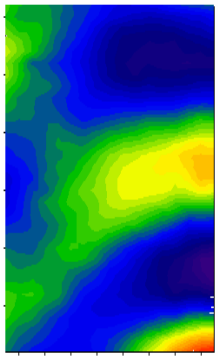

D2-B(339.3)

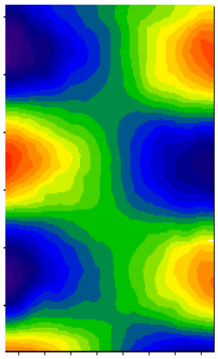

D2-C(346.5)

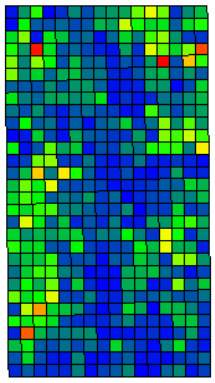

D2(341.4)-A(342.9)

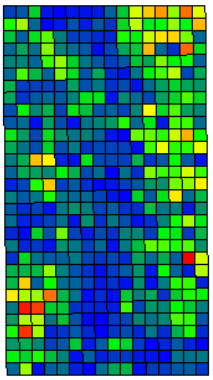

D2-B(339.3)

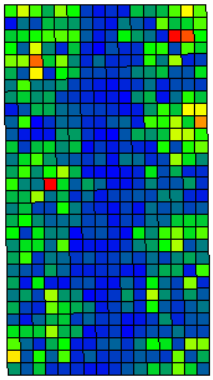

D2-C(346.5)

Figure 4.59 Mode Shapes, Delta Mode Shapes and E-View plots for D2-E2 with associated frequencies

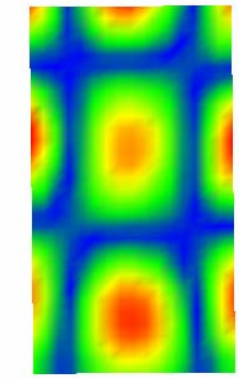

Healthy Mode Shape

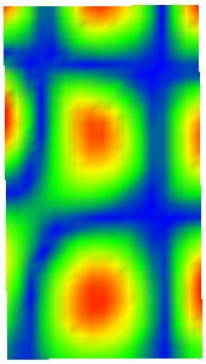

Damaged Mode Shape

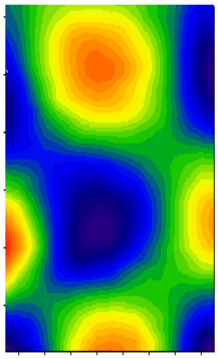

E2-D2(380.4)-A(386)

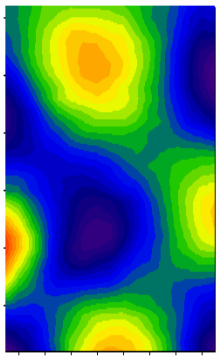

D2-B(387.9)

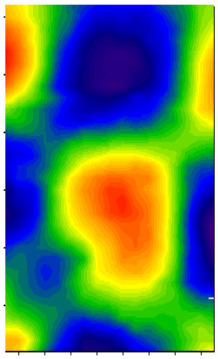

D2-C(390.6)

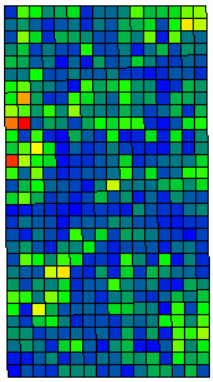

D2(380.4)-A(386)

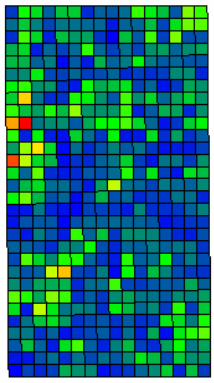

D2-B(387.9)

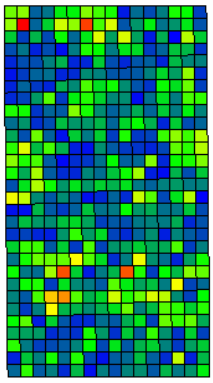

D2-C(390.6)

Figure 4.60 Mode Shapes, Delta Mode Shapes and E-View plots for D2-E2 with associated frequencies

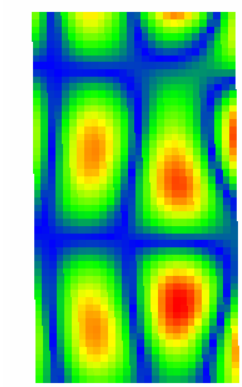

Healthy Mode Shape

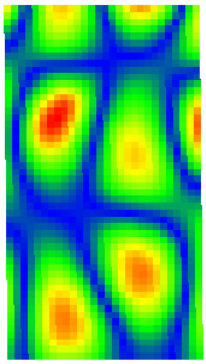

Damaged Mode Shape

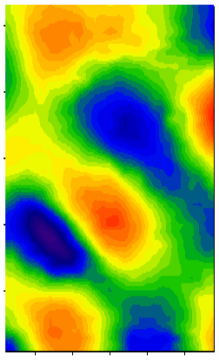

E2-D2(695)-A(702)

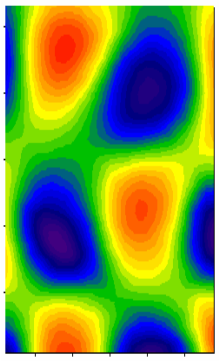

D2-B(697.5)

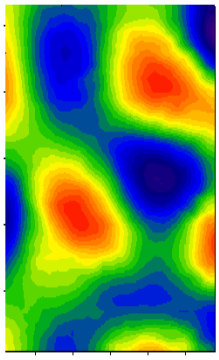

D2-C(703.8)

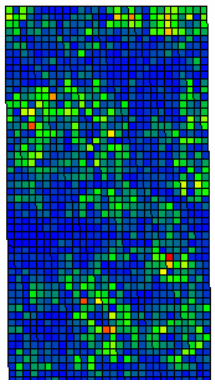

D2(695)-A(702)

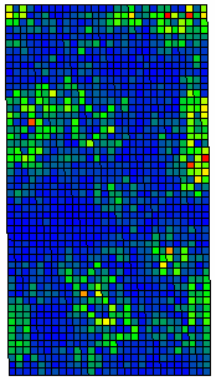

D2-B(697.5)

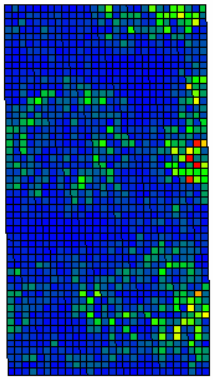

D2-C(703.8)

Figure 4.61 Mode Shapes, Delta Mode Shapes and E-View plots for D2-E2 with associated frequencies

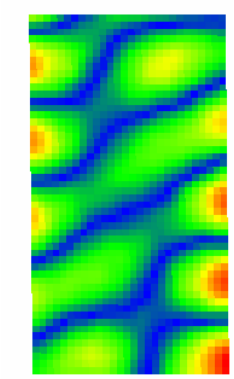

Healthy Mode Shape

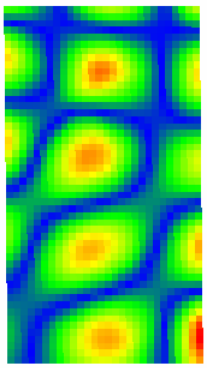

Damaged Mode Shape

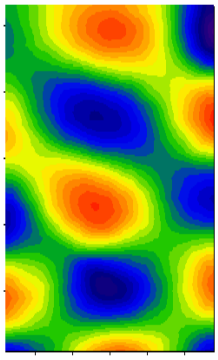

E2-D2(736.5)-A(745)

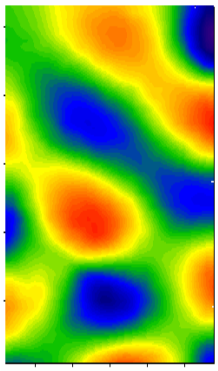

D2-B(742.5)

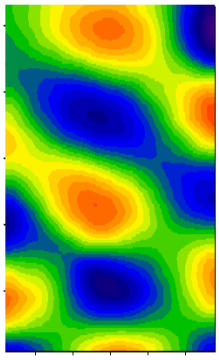

D2-C(742.5)

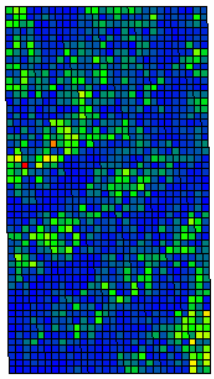

D2(736.5)-A(745)

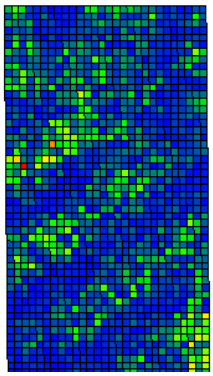

D2-B(742.5)

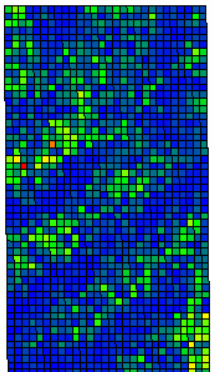

D2-C(742.5)

Figure 4.62 Mode Shapes, Delta Mode Shapes and E-View plots for D2-E2 with associated frequencies

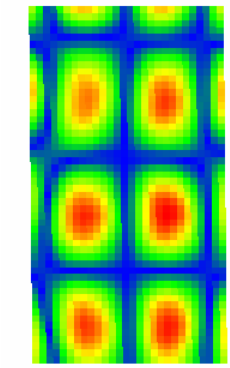

Healthy Mode Shape

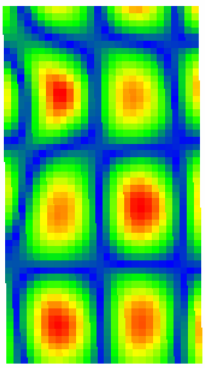

Damaged Mode Shape

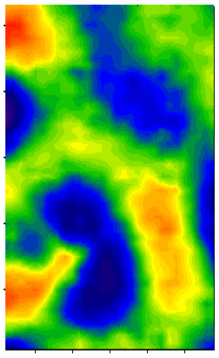

E2-D2(867)-A(876.3)

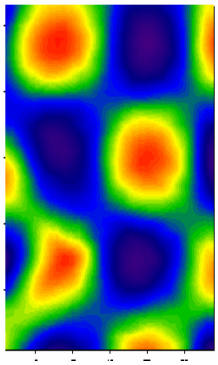

D2-B(873.8)

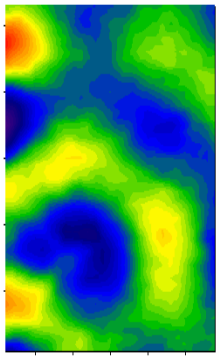

D2-C(880)

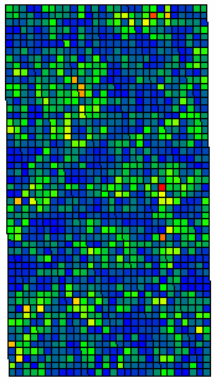

D2(867)-A(876.3)

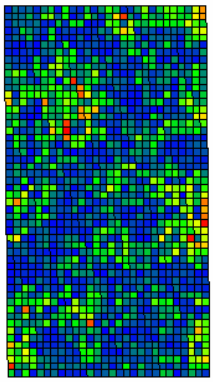

D2-B(873.8)

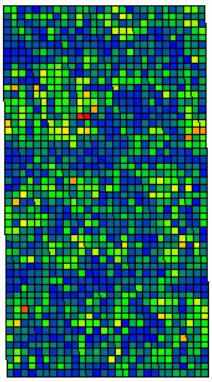

D2-C(880)

Figure 4.63 Mode Shapes, Delta Mode Shapes and E-View plots for D2-E2 with associated frequencies

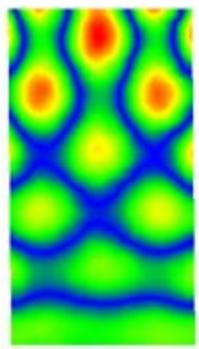

Healthy Mode Shape

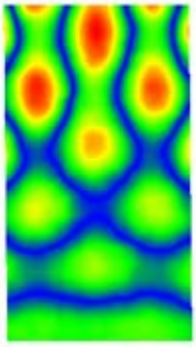

Damaged Mode Shape

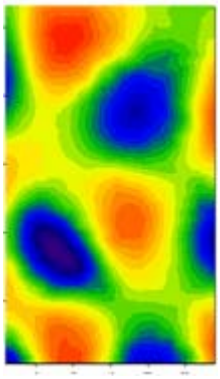

E2-D2(964)-A(981.3)

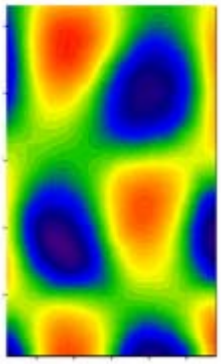

D2-B(968.8)

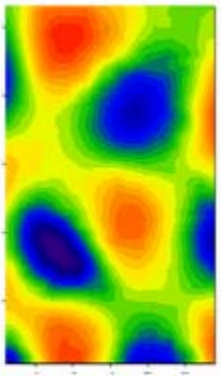

D2-C(978.8)

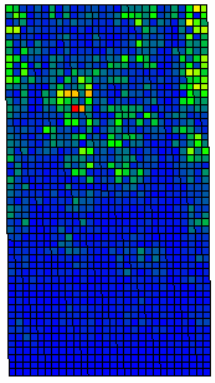

D2(964)-A(981.3)

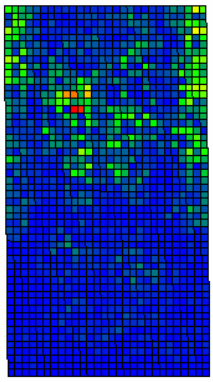

D2-B(968.8)

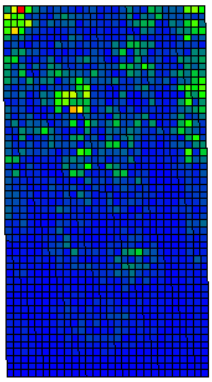

D2-C(978.8)

Figure 4.64 Mode Shapes, Delta Mode Shapes and E-View plots for D2-E2 with associated frequencies

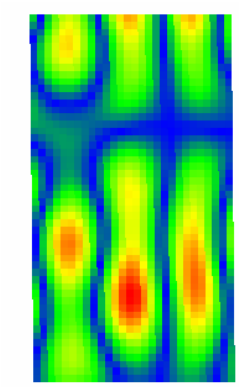

Healthy Mode Shape

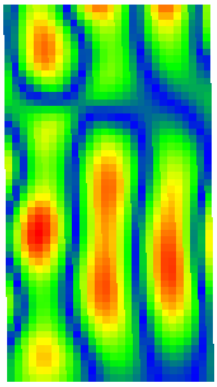

Damaged Mode Shape

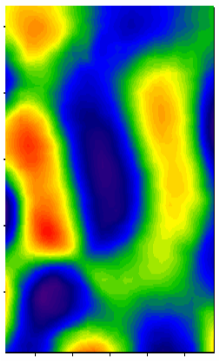

E2-D2(1042)-A(1058)

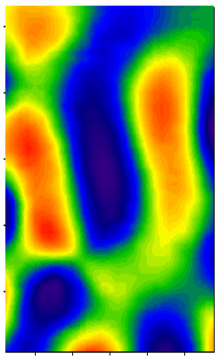

D2-B(1058)

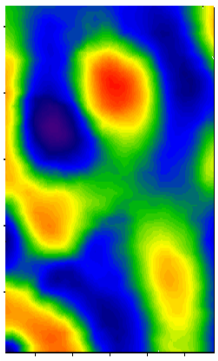

D2-C(1059)

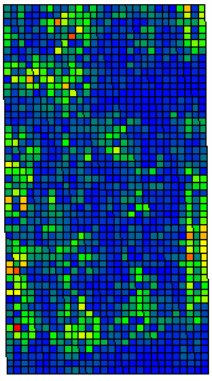

D2(1042)-A(1058)

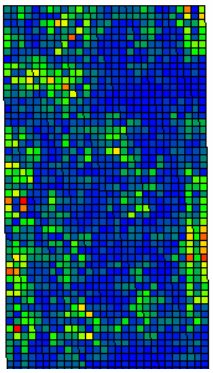

D2-B(1058)

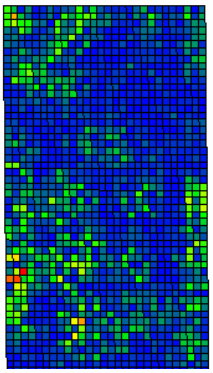

D2-C(1059)

Figure 4.65 Mode Shapes, Delta Mode Shapes and E-View plots for D2-E2 with associated frequencies

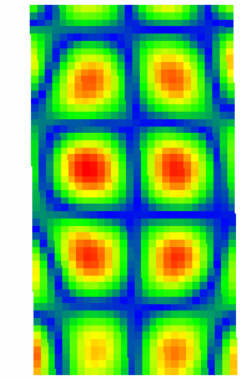

Healthy Mode Shape

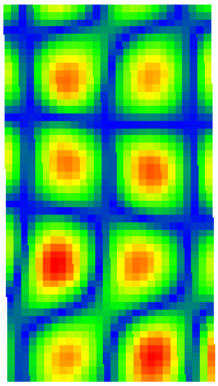

Damaged Mode Shape

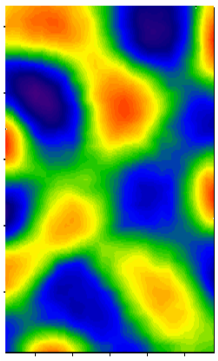

E2-D2(1074)-A(1088)

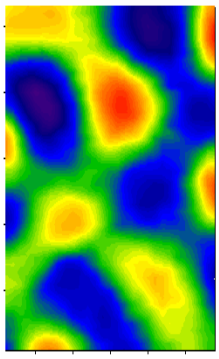

D2-B(1089)

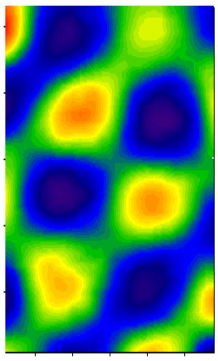

D2-C(1095)

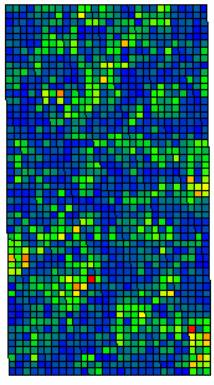

D2(1074)-A(1088)

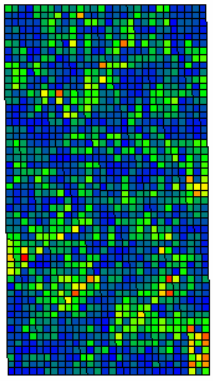

D2-B(1089)

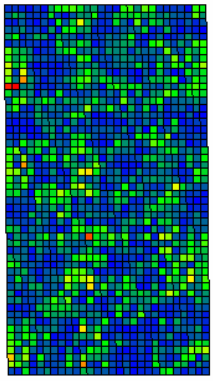

D2-C(1095)

Figure 4.66 Mode Shapes, Delta Mode Shapes and E-View plots for D2-E2 with associated frequencies

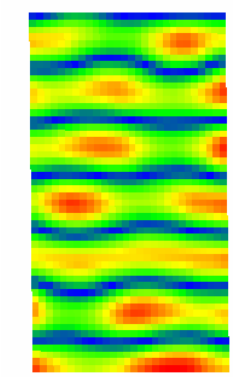

Healthy Mode Shape

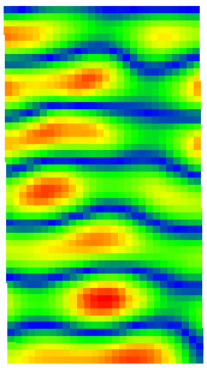

Damaged Mode Shape

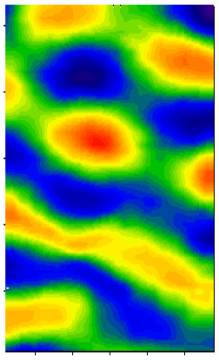

E2-D2(1283)-A(1304)

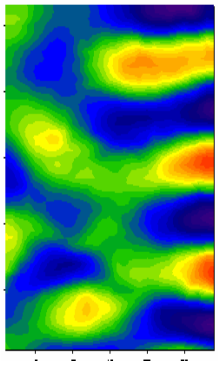

D2-B(1299)

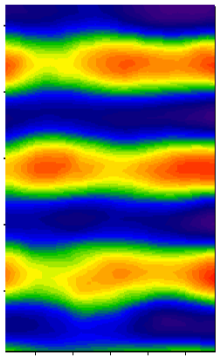

D2-C(1313)

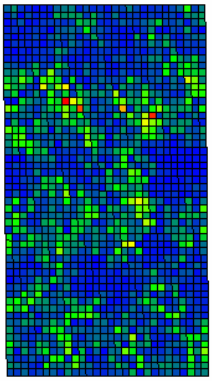

D2(1283)-A(1304)

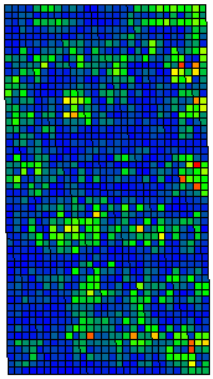

D2-B(1299)

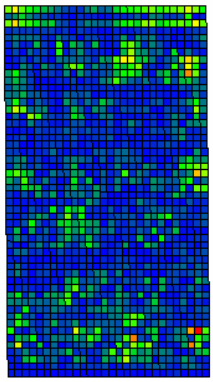

D2-C(1313)

Figure 4.67 Mode Shapes, Delta Mode Shapes and E-View plots for D2-E2 with associated frequencies

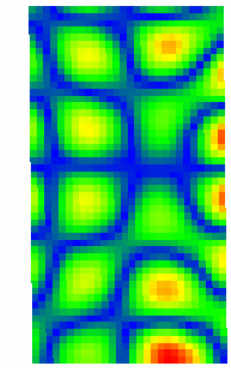

Healthy Mode Shape

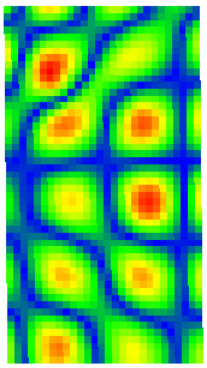

Damaged Mode Shape

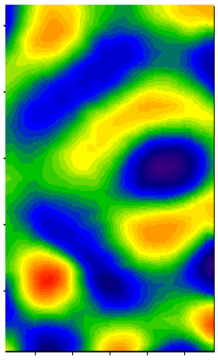

E2-D2(1316)-A(1330)

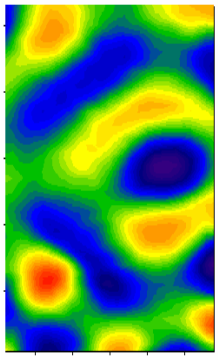

D2-B(1343)

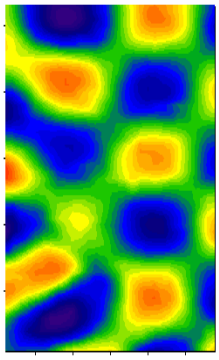

D2-C(1347)

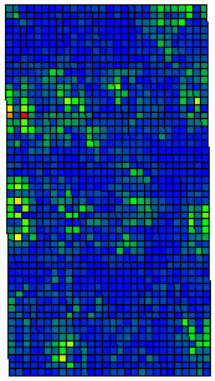

D2(1316)-A(1330)

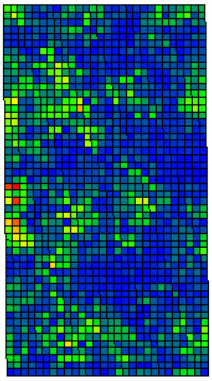

D2-B(1343)

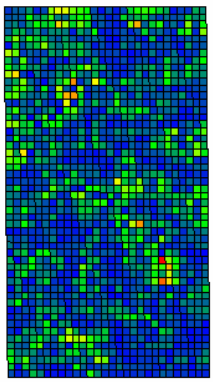

D2-C(1347)

Figure 4.68 Mode Shapes, Delta Mode Shapes and E-View plots for D2-E2 with associated frequencies

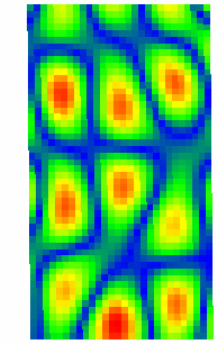

Healthy Mode Shape

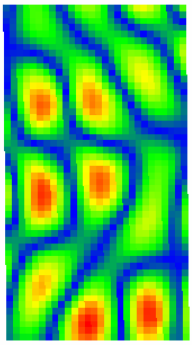

Damaged Mode Shape

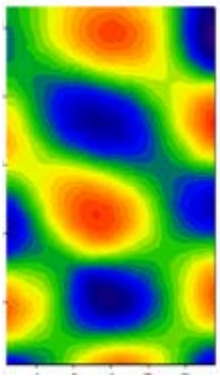

E2-D2(1330)-A(1354)

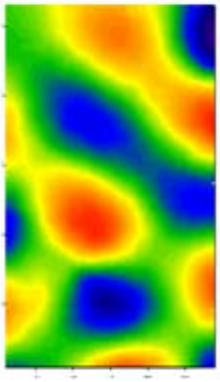

D2-B(1354)

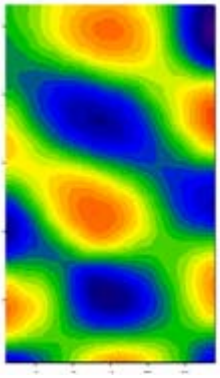

D2-C(1357)

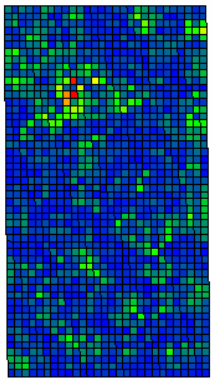

D2(1330)-A(1354)

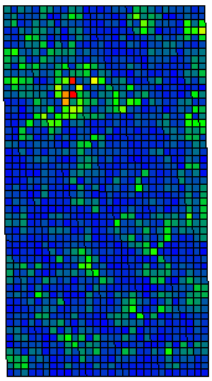

D2-B(1354)

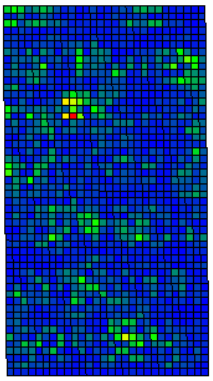

D2-C(1357)

Figure 4.69 Mode Shapes, Delta Mode Shapes and E-View plots for D2-E2 with associated frequencies

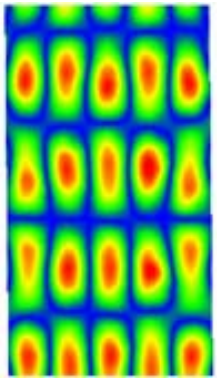

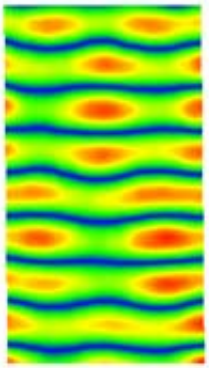

Healthy Mode Shape Damaged Mode Shape

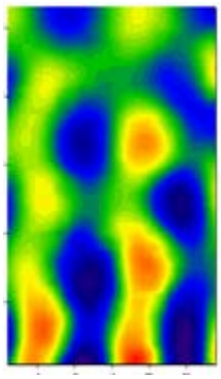

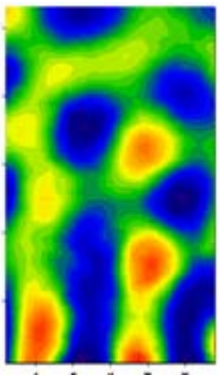

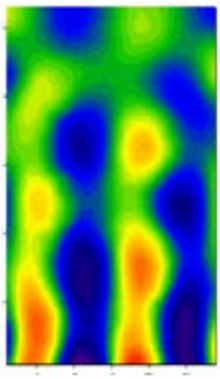

E2-D2(2095)-A(2144) D2-B(2146) D2-C(2154)

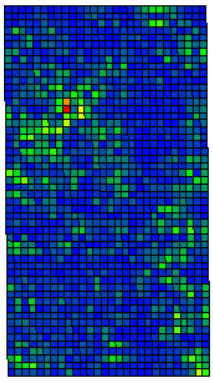

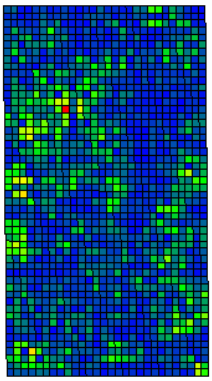

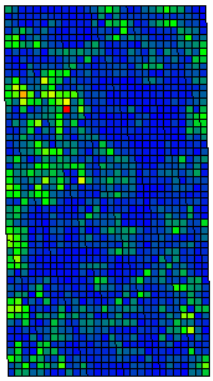

D2(2095)-A(2144) D2-B(2146) D2-C(2154)

Figure 4.70 Mode Shapes, Delta Mode Shapes and E-View plots for D2-E2 with associated frequencies

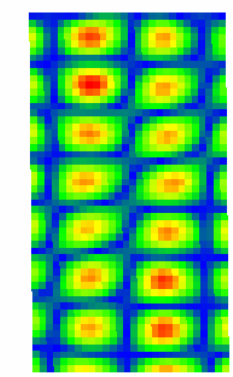

Healthy Mode Shape

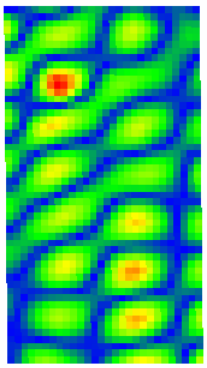

Damaged Mode Shape

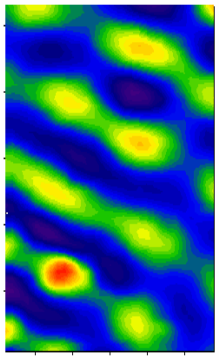

E2-D2(2296)-A(2353)

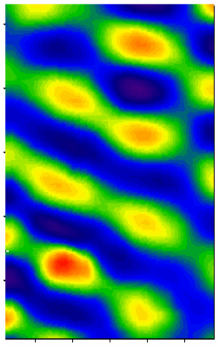

D2-B(2350)

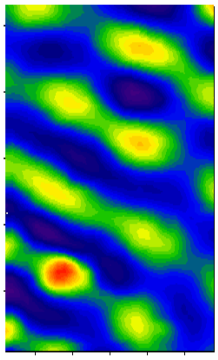

D2-C(2364)

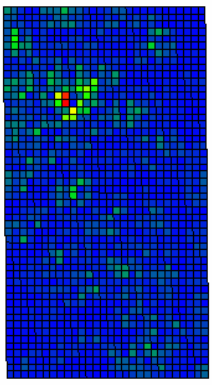

D2(2296)-A(2353)

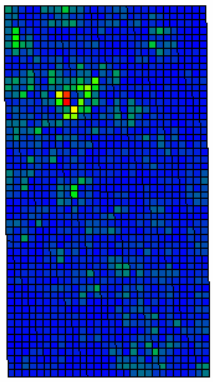

D2-B(2350)

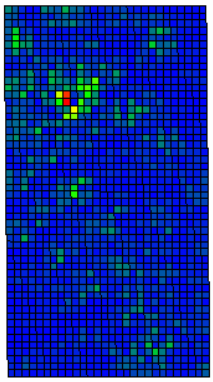

D2-C(2364)

Figure 4.71 Mode Shapes, Delta Mode Shapes and E-View plots for D2-E2 with associated frequencies

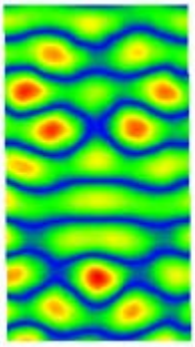

Healthy Mode Shape

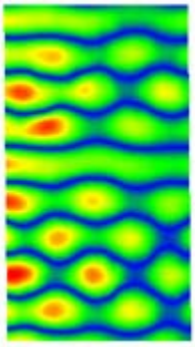

Damaged Mode Shape

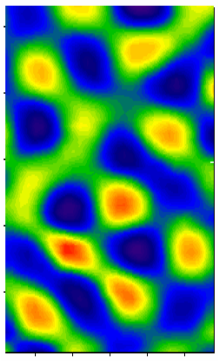

E2-D2(2478)-A(2547)

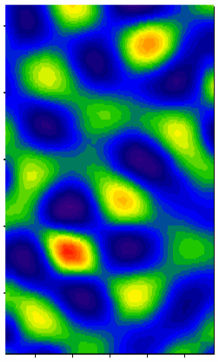

D2-B(2527)

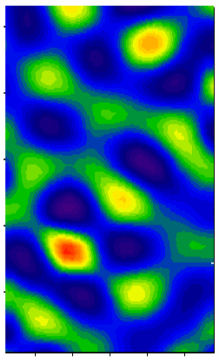

D2-C(2566)

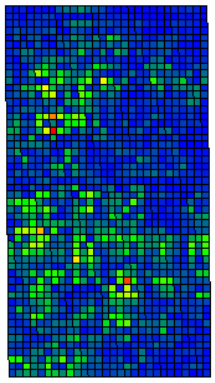

D2(2478)-A(2547)

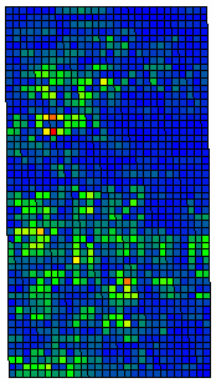

D2-B(2527)

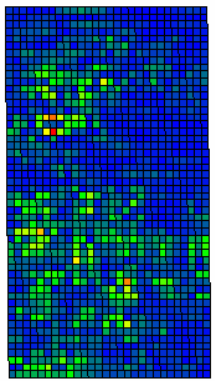

D2-C(2566)

Figure 4.72 Mode Shapes, Delta Mode Shapes and E-View plots for D2-E2 with associated frequencies

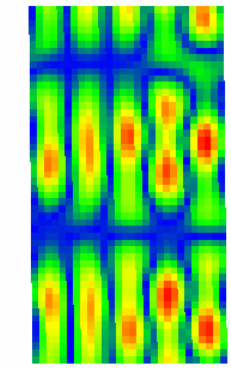

Healthy Mode Shape

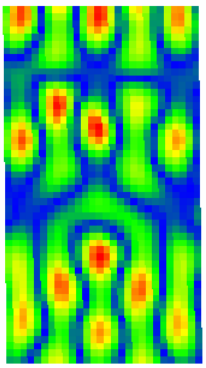

Damaged Mode Shape

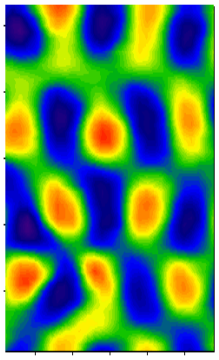

E2-D2(2539)-A(2605)

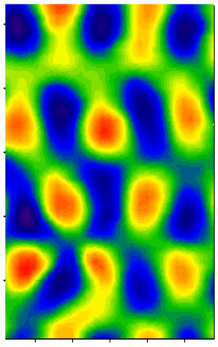

D2-B(2606)

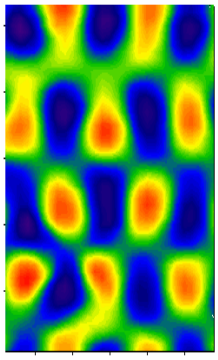

D2-C(2610)

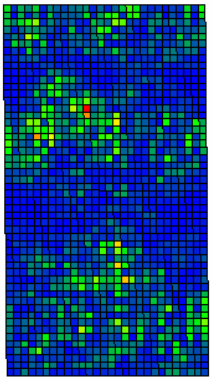

D2(2539)-A(2605)

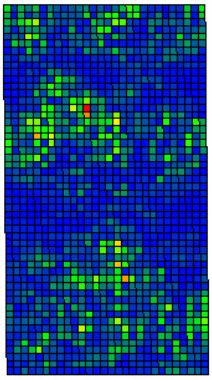

D2-B(2606)

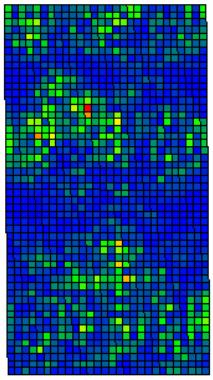

D2-C(2610)

Figure 4.73 Mode Shapes, Delta Mode Shapes and E-View plots for D2-E2 with associated frequencies

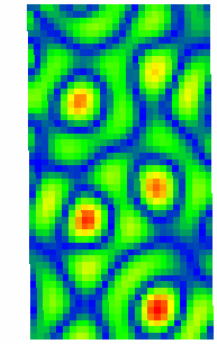

Healthy Mode Shape

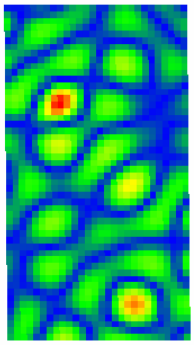

Damaged Mode Shape

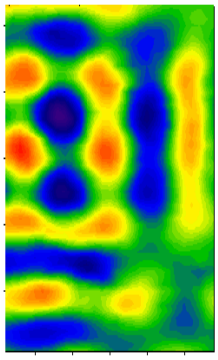

E2-D2(2725)-A(2771)

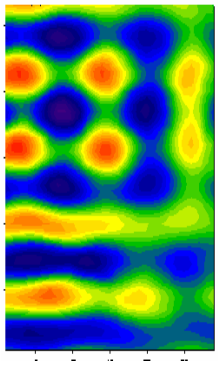

D2-B(2761)

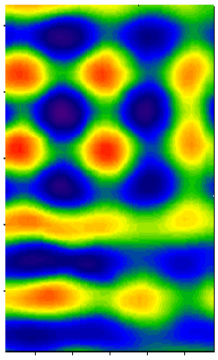

D2-C(2780)

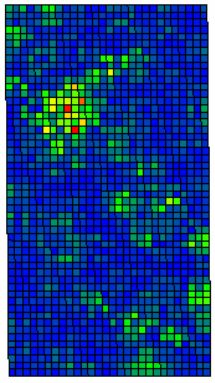

D2(2725)-A(2771)

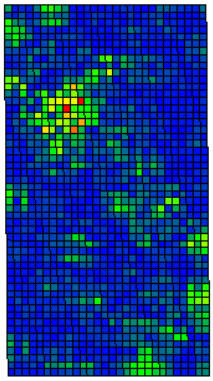

D2-B(2761)

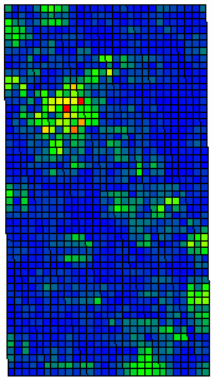

D2-C(2780)

Figure 4.74 Mode Shapes, Delta Mode Shapes and E-View plots for D2-E2 with associated frequencies

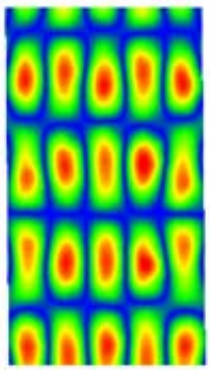

Healthy Mode Shape

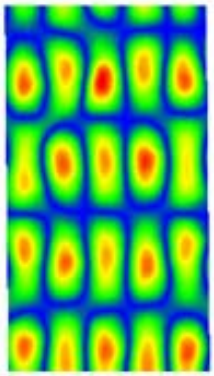

Damaged Mode Shape

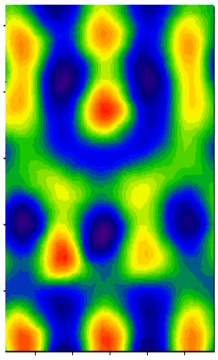

E2-D2(2903)-A(2991)

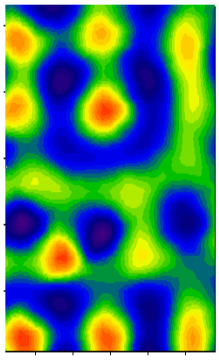

D2-B(2988)

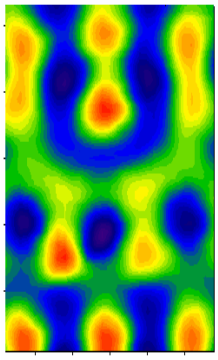

D2-C(2996)

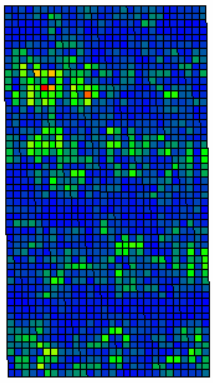

D2(2903)-A(2991)

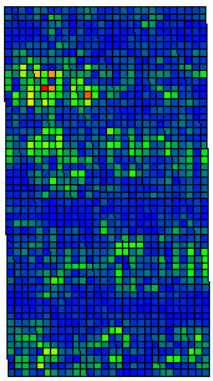

D2-B(2988)

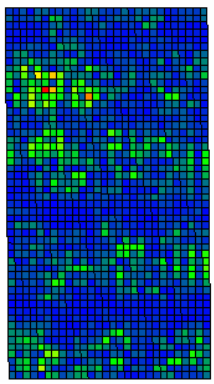

D2-C(2996)

Figure 4.75 Mode Shapes, Delta Mode Shapes and E-View plots for D2-E2 with associated frequencies

4.6 Observation of Delta Mode Shapes and Corresponding E-View Results

From the plots of delta mode shapes for repeated experiments, it was observed that the similar mode shapes of healthy and damaged specimen followed a pattern. The pattern was noticed to be obtained for lower, intermediate and higher mode shapes. The repeated pattern of delta mode shape signified similarity in the healthy and damaged mode shapes.

For the lower cluster of mode shapes, the slightest difference in the plots of delta mode shapes, among the repeated plots was observed to produce large difference in the e-view plots. For intermediate clusters this tendency was noticed to reduce. The difference in e-view plots were observed to be less and for the higher cluster, even a major difference in delta plot was not able to make a major difference in e-view results.

It was also observed that Delta Mode Shape itself was not potential for detection. For all of the cases, Delta Mode Shape was not capable to locate damage. The repeated pattern in Delta Mode Shape, could only conclude, the difference in displacement of Healthy and Damaged Mode Shapes to be significant hence larger in magnitude than noise. Both D1 and D2 damage configuration were detected when the repeated pattern in Delta Mode Shape was observed.

Delta Mode Shape not following similar pattern in repeated experiments signified that the experiment was not being able to capture the differences in the property of the specimen produced by damage. The noise in the experiment was able to cover the result

of the experiment hence similar result in repeated experiment was not observed. Since the difference was not observed from the experiment it was not also detected.

4.7 Computer Experiment of Damages and Formation of Six Different Cases

Using feature from Damage Detection Code, computer experiment for both D1 and D2 damage configuration were performed. Due to the large number of data files, six different cases were taken for observation.

Table 4.1 Six cases with their natural frequencies obtained from experiments

Clusters	Cases	Physical Experiment (Hz)	Computer Experiment (Hz)
Intermediate	First Case	963 – 981	976 – 1019
Intermediate	Second Case	1330 – 1357	1308 – 1341
Higher	Third Case	2095 – 2154	2049 – 2100
Higher	Fourth Case	2392 – 2435	2416 – 2480
Higher	Fifth Case	2473 - 2566	2457 – 2544
Higher	Sixth Case	2899 – 2996	2874 – 2933

The complexity of the Mode Shapes obtained from both physical and computer experiments were observed to be similar. Delta Mode Shape of computer experiment, which can be categorized as ideal experiment, was not locating the damage itself and was observed to be orthogonal to both healthy and damage mode shapes.

4.7.1 First Case (D1)

Sigma Plot and Eview used for plotting.

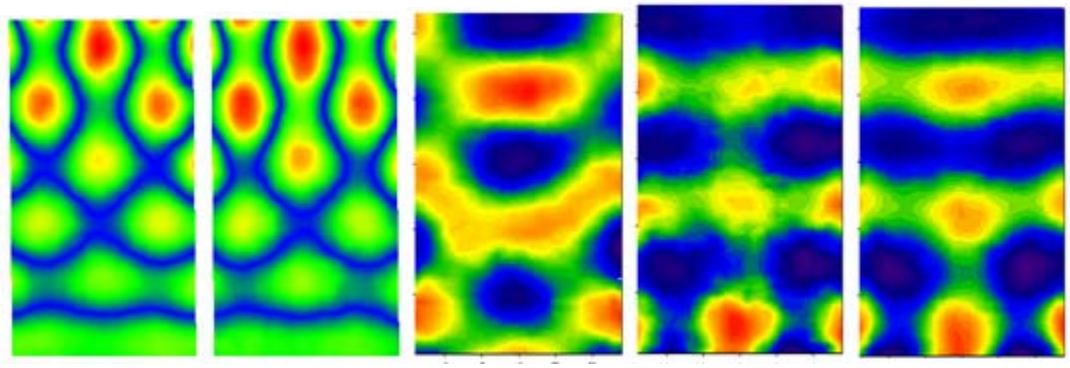

(i) (ii) (iii) (iv) (v)

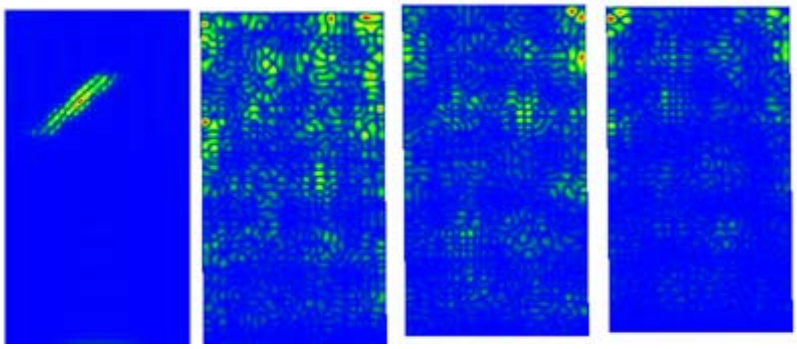

(vi) (vii) (viii) (ix)

Figure 4.76 First case, (i)Healthy Mode Shape, (ii)Damaged Mode Shape, (iii)(iv)(v)Delta Mode Shapes, (vi)Computer Experiment Result, (vii)(viii)(ix)Damage parameter distribution.

Delta mode shapes were not observed with similar pattern hence not useable for detection.

4.7.2 Second Case (D1)

Sigma Plot and Eview used for plotting.

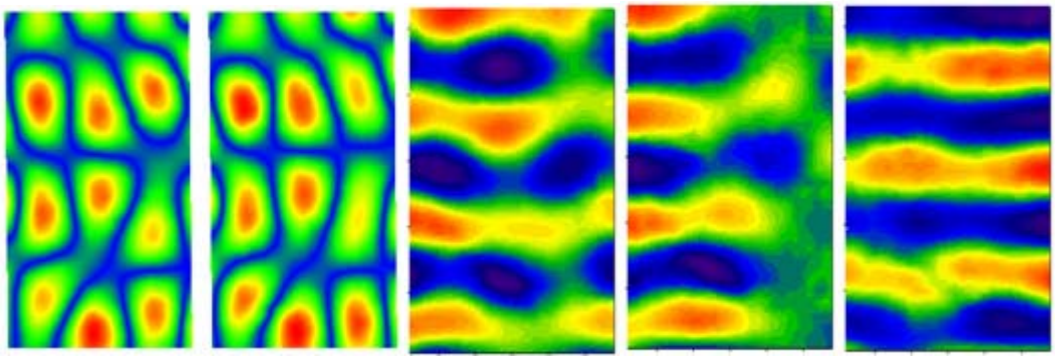

(i) (ii) (iii) (iv) (v)

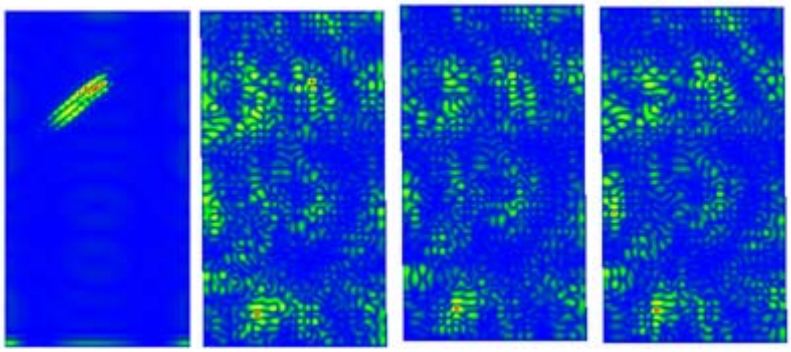

(vi) (vii) (viii) (ix)

Figure 4.77 Second case, (i)Healthy Mode Shape, (ii)Damaged Mode Shape, (iii)(iv)(v)Delta Mode Shapes, (vi)Computer Experiment Result, (vii)(viii)(ix)Damage parameter distribution.

Delta mode shapes were not observed with similar pattern hence not useable for detection.

4.7.3 Third Case (D1)

Sigma Plot and Eview used for plotting.

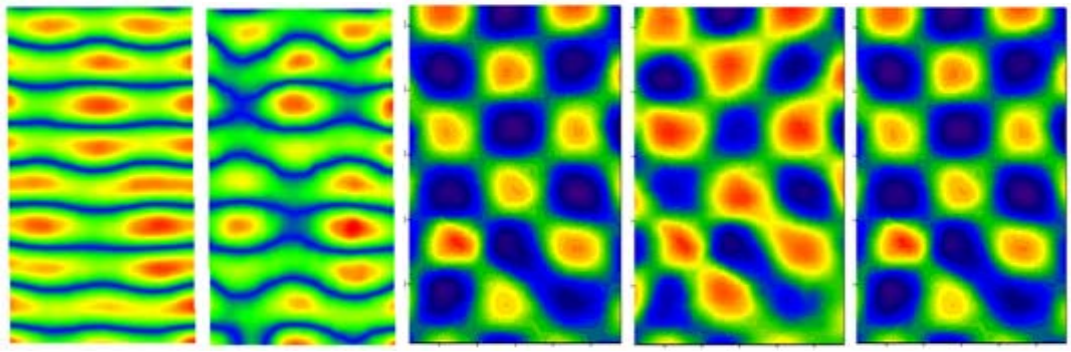

(i) (ii) (iii) (iv) (v)

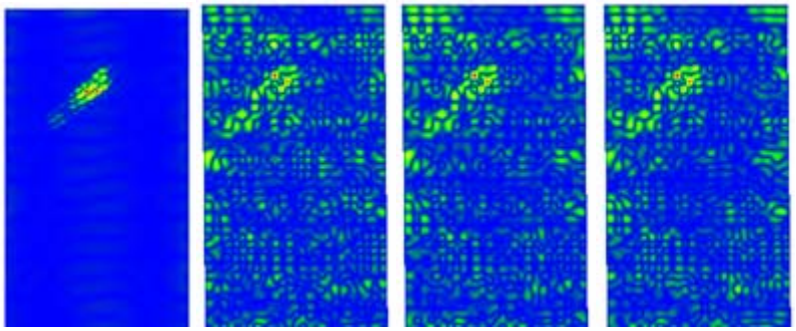

(vi) (vii) (viii) (ix)

Figure 4.78 Third case, (i)Healthy Mode Shape, (ii)Damaged Mode Shape, (iii)(iv)(v)Delta Mode Shapes, (vi)Computer Experiment Result, (vii)(viii)(ix)Damage parameter distribution.

Delta Mode Shapes were observed with similar pattern hence the result obtained from experiment has the potential for detection. Red spot in the damage parameter distribution lies on the damaged area indicating successful detection.

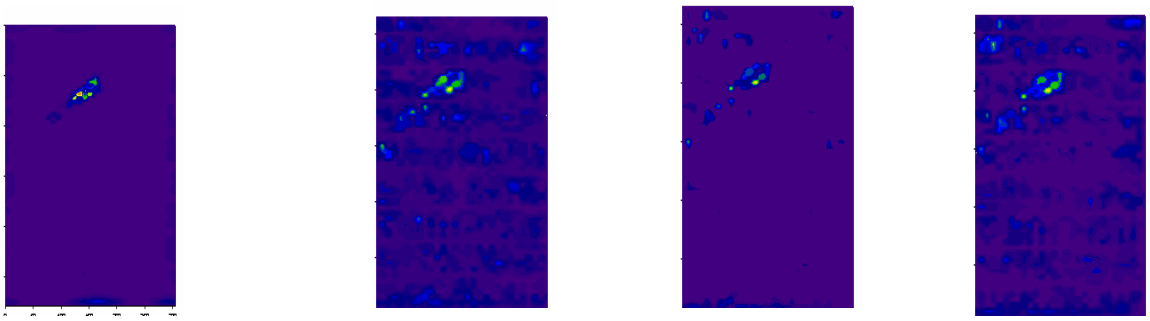

Figure 4.79 Sigma plot used to enhance the damage parameter distribution. Computer Experiment (left), three repetition of Physical Experiment (right).

Sigma Plot was used to enhance the damage parameter distribution for better detection. It was observed that even an ideal case like computer experiment was having difficulty in detection. It was also observed that all three repeated experiments were detecting the damage.

4.7.4 Fourth Case (D1)

Sigma Plot and Eview used for plotting.

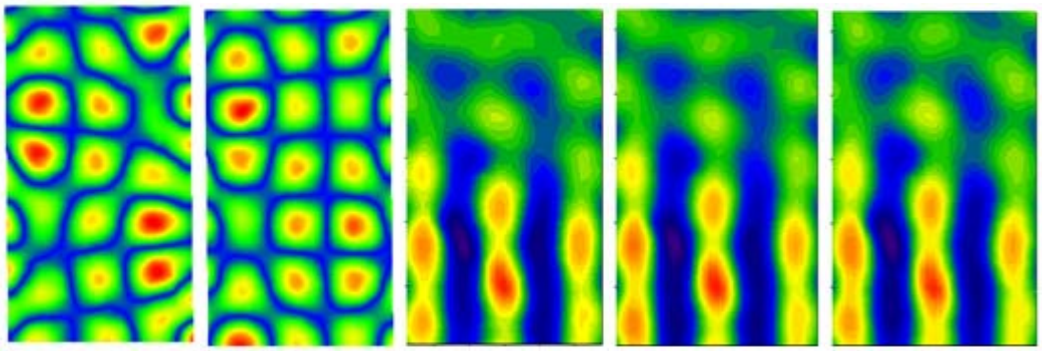

(i) (ii) (iii) (iv) (v)

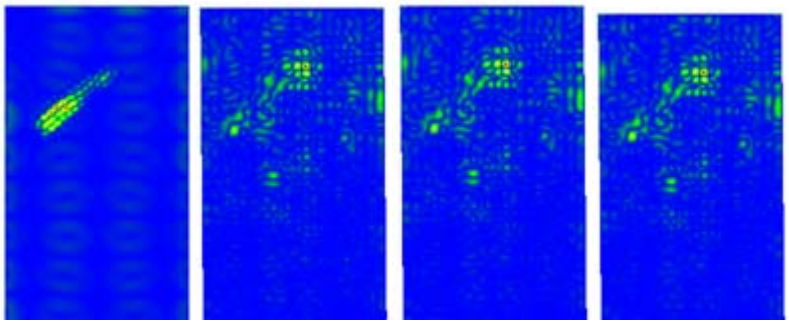

(vi) (vii) (viii) (ix)

Figure 4.80 Fourth case, (i)Healthy Mode Shape, (ii)Damaged Mode Shape, (iii)(iv)(v)Delta Mode Shapes, (vi)Computer Experiment Result, (vii)(viii)(ix)Damage parameter distribution.

Delta Mode Shapes were observed with similar pattern hence the result obtained from experiment has the potential for detection. Red spot in the damage parameter distribution lies on the damaged area indicating successful detection.

4.7.5 Fifth Case (D1)

Sigma Plot and Eview used for plotting.

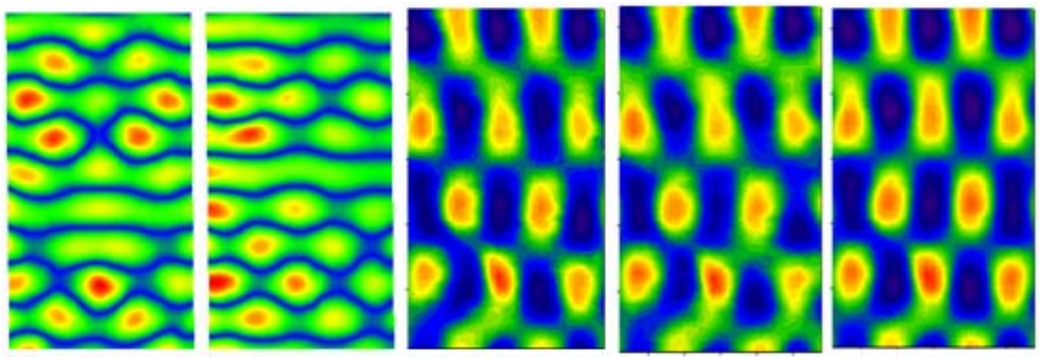

(i) (ii) (iii) (iv) (v)

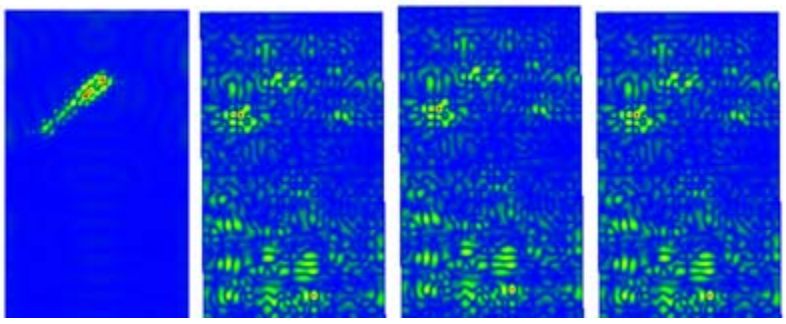

(vi) (vii) (viii) (ix)

Figure 4.81 Fifth case, (i)Healthy Mode Shape, (ii)Damaged Mode Shape, (iii)(iv)(v)Delta Mode Shapes, (vi)Computer Experiment Result, (vii)(viii)(ix)Damage parameter distribution.

Delta Mode Shape were observed to be following the pattern but similarity was observed to be less than that of the above cases hence damage parameter distribution was also observed with less accuracy.

4.7.6 Sixth Case (D1)

Sigma Plot and Eview used for plotting.

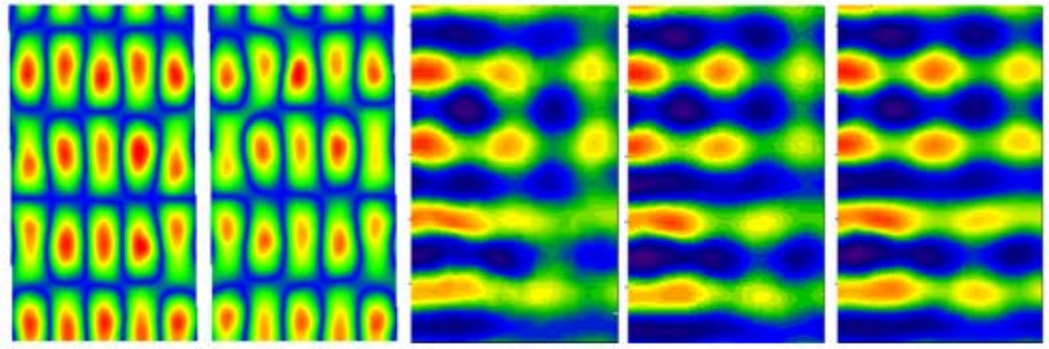

(i) (ii) (iii) (iv) (v)

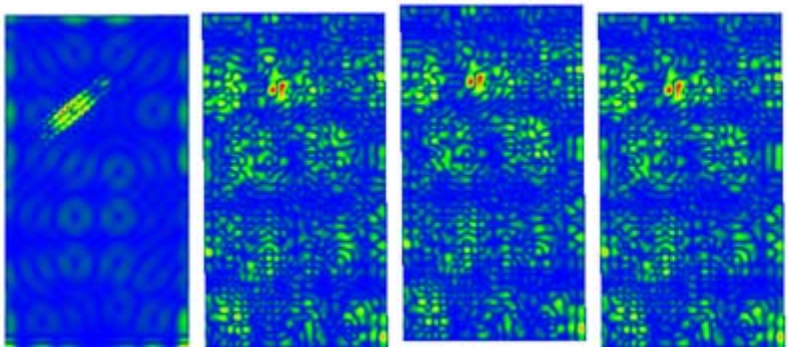

(vi) (vii) (viii) (ix)

Figure 4.82 Sixth case, (i)Healthy Mode Shape, (ii)Damaged Mode Shape, (iii)(iv)(v)Delta Mode Shapes, (vi)Computer Experiment Result, (vii)(viii)(ix)Damage parameter distribution.

Delta Mode Shape were observed to be following the pattern but similarity was observed to be less than that of the above cases hence damage parameter distribution was also observed with less accuracy.

Figure 4.83 Sigma plot used to enhance the damage parameter distribution. Computer Experiment (left), three repetition of Physical Experiment (right).

Sigma Plot was used to enhance the damage parameter distribution for better detection. It was observed that even an ideal case like computer experiment was having difficulty in detection. It was also observed that all three repeated experiments were detecting the damage.

4.7.7 First Case (D2)

Since damage configuration D2 was bigger than D1, it was detected even in intermediate clusters.

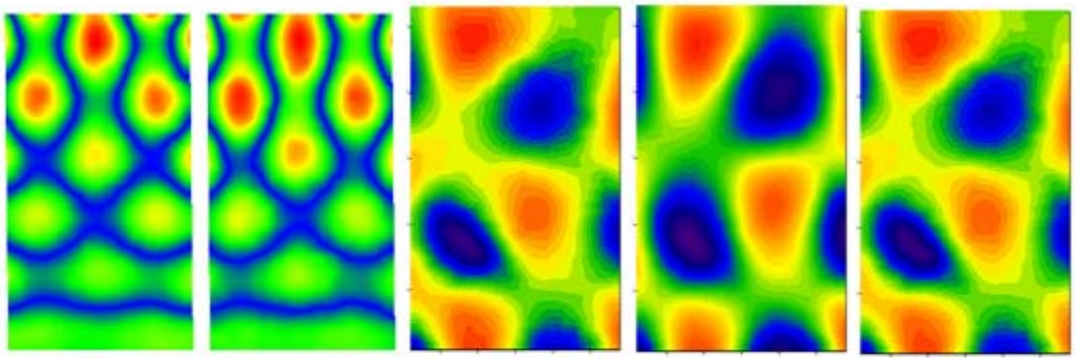

(i) (ii) (iii) (iv) (v)

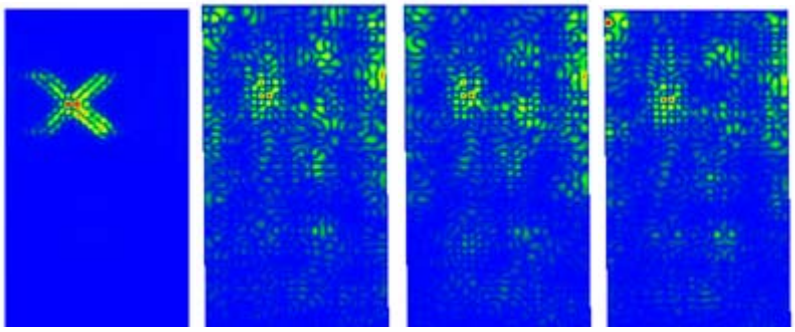

(vi) (vii) (viii) (ix)

Figure 4.84 First case, (i)Healthy Mode Shape, (ii)Damaged Mode Shape, (iii)(iv)(v)Delta Mode Shapes, (vi)Computer Experiment Result, (vii)(viii)(ix)Damage parameter distribution.

Delta Mode Shape were observed to be following the pattern but similarity was observed to be less than that of the above cases hence damage parameter distribution was also observed with less accuracy.

4.7.8 Second Case (D2)

Sigma Plot and Eview used for plotting.

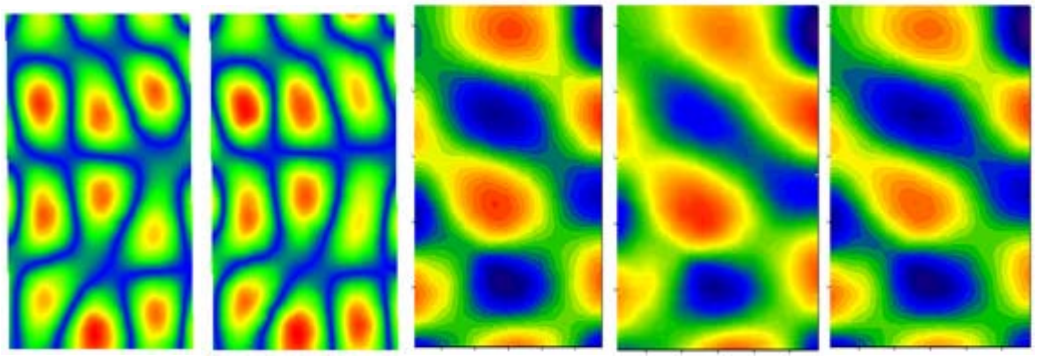

(i) (ii) (iii) (iv) (v)

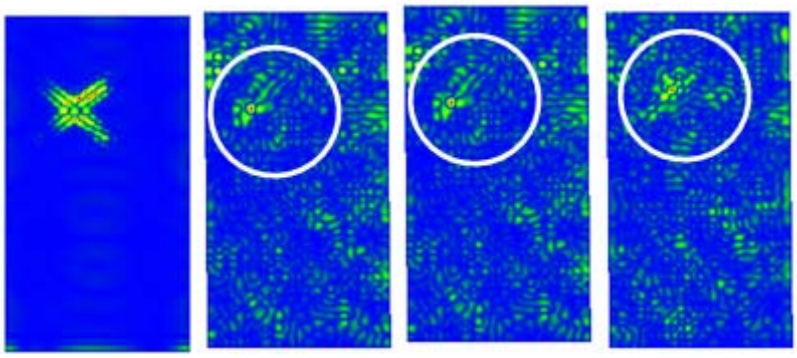

(vi) (vii) (viii) (ix)

Figure 4.85 Second case, (i)Healthy Mode Shape, (ii)Damaged Mode Shape, (iii)(iv)(v)Delta Mode Shapes, (vi)Computer Experiment Result, (vii)(viii)(ix)Damage parameter distribution.

Delta Mode Shapes were observed with similar pattern hence the result obtained from experiment has the potential for detection. Red spot in the damage parameter distribution lies on the damaged area indicating successful detection.

4.7.9 Third Case (D2)

Sigma Plot and Eview used for plotting.

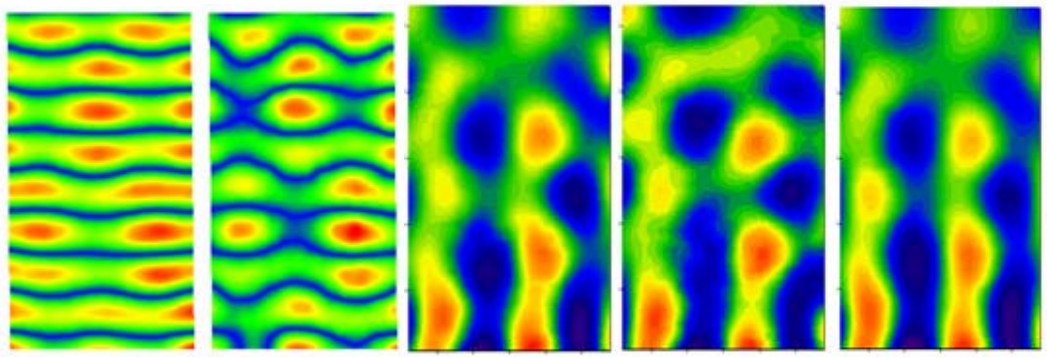

(i) (ii) (iii) (iv) (v)

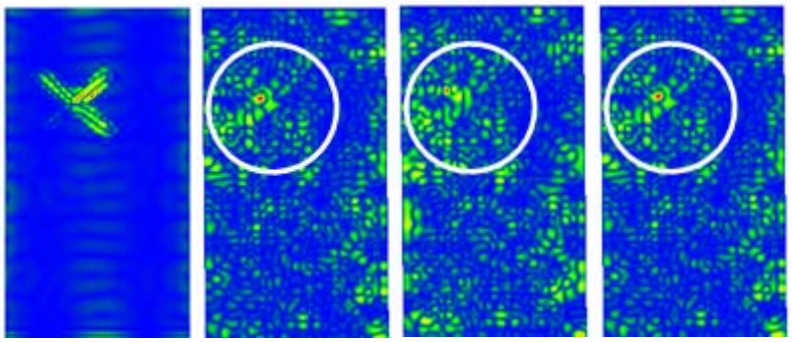

(vi) (vii) (viii) (ix)

Figure 4.86 Third case, (i)Healthy Mode Shape, (ii)Damaged Mode Shape, (iii)(iv)(v)Delta Mode Shapes, (vi)Computer Experiment Result, (vii)(viii)(ix)Damage parameter distribution.

Delta Mode Shapes were observed with similar pattern hence the result obtained from experiment has the potential for detection. Red spot in the damage parameter distribution lies on the damaged area indicating successful detection.

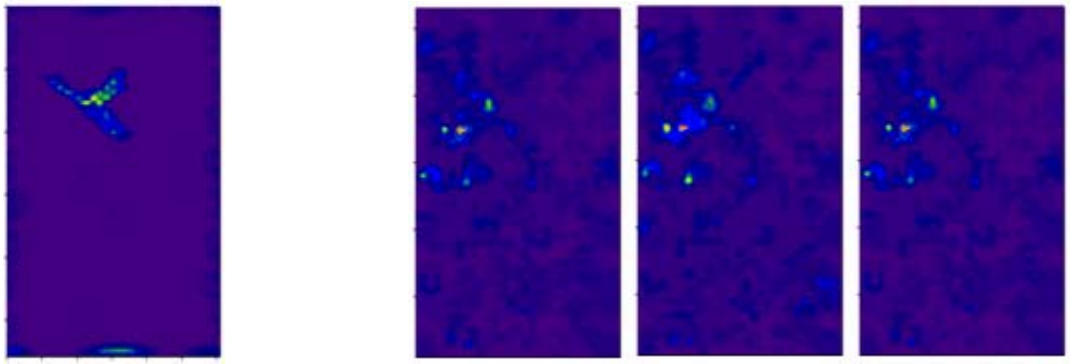

Figure 4.87 Sigma plot used to enhance the damage parameter distribution. Computer Experiment (left), three repetition of Physical Experiment (right).

4.7.10 Fourth Case (D2)

Sigma Plot and Eview used for plotting.

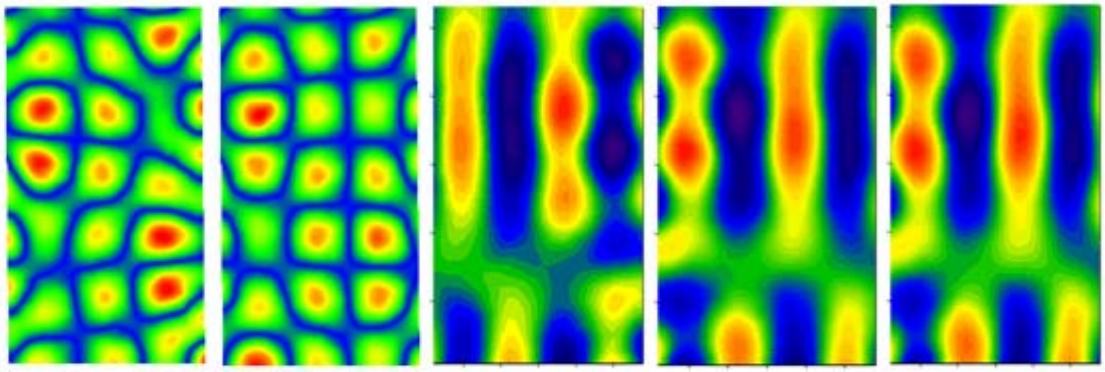

(i) (ii) (iii) (iv) (v)

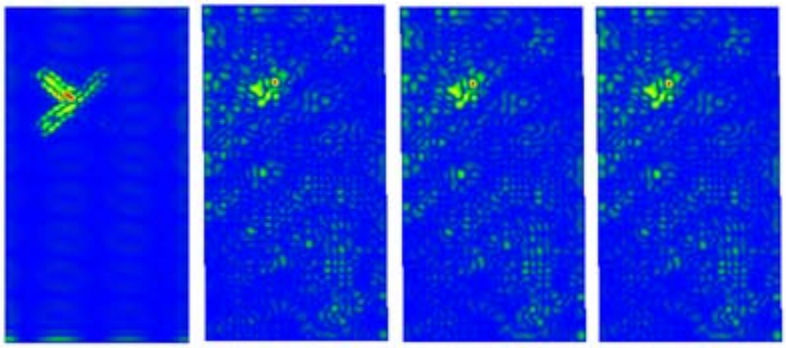

(vi) (vii) (viii) (ix)

Figure 4.88 Third case, (i)Healthy Mode Shape, (ii)Damaged Mode Shape, (iii)(iv)(v)Delta Mode Shapes, (vi)Computer Experiment Result, (vii)(viii)(ix)Damage parameter distribution.

Delta Mode Shapes were observed with similar pattern hence the result obtained from experiment has the potential for detection. Red spot in the damage parameter distribution lies on the damaged area indicating successful detection.

4.7.11 Fifth Case (D2)

Sigma Plot and Eview used for plotting.

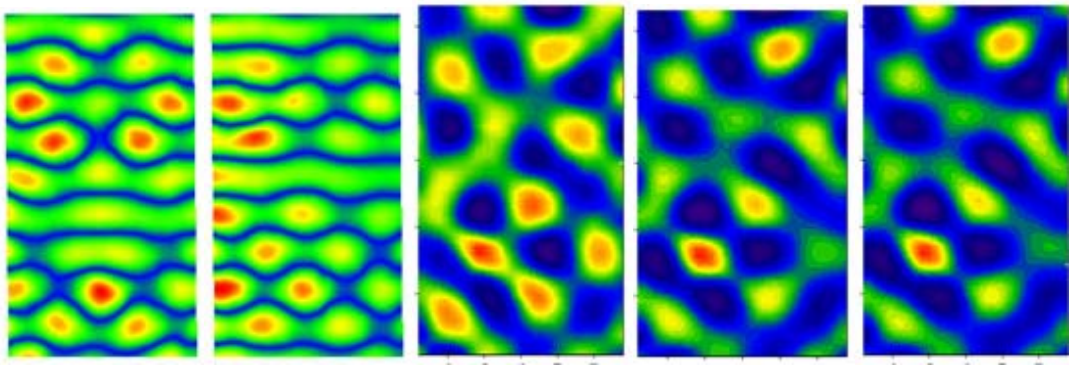

(i) (ii) (iii) (iv) (v)

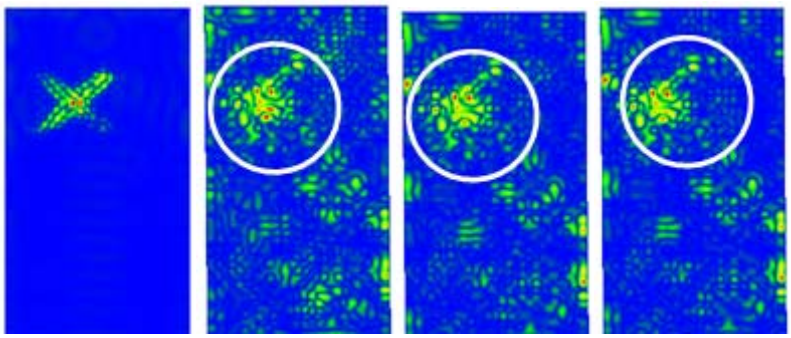

(vi) (vii) (viii) (ix)

Figure 4.89 Third case, (i)Healthy Mode Shape, (ii)Damaged Mode Shape, (iii)(iv)(v)Delta Mode Shapes, (vi)Computer Experiment Result, (vii)(viii)(ix)Damage parameter distribution.

Delta Mode Shape were observed to be following the pattern but similarity was observed to be less than that of the above cases hence damage parameter distribution was also observed with less accuracy.

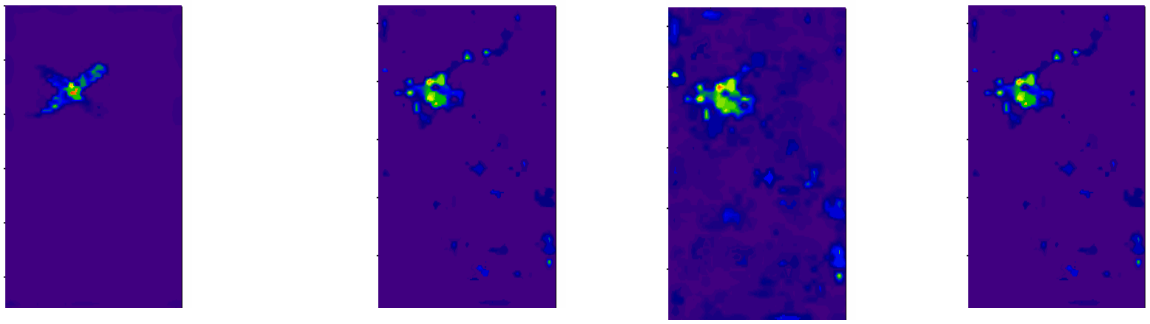

Figure 4.90 Sigma plot used to enhance the damage parameter distribution. Computer Experiment (left), three repetition of Physical Experiment (right).

4.7.12 Sixth Case (D2)

Sigma Plot and Eview used for plotting.

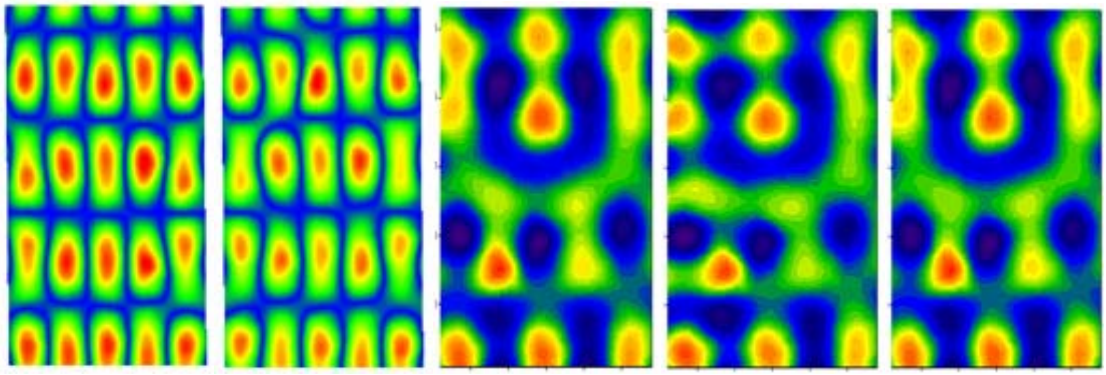

(i) (ii) (iii) (iv) (v)

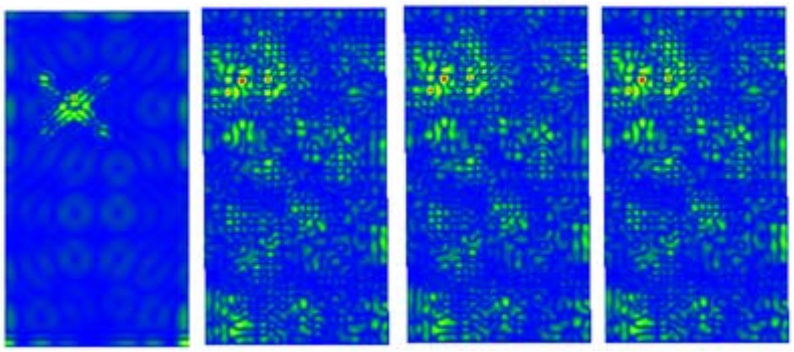

(vi) (vii) (viii) (ix)

Figure 4.91 Third case, (i)Healthy Mode Shape, (ii)Damaged Mode Shape, (iii)(iv)(v)Delta Mode Shapes, (vi)Computer Experiment Result, (vii)(viii)(ix)Damage parameter distribution.

Delta Mode Shapes were observed with similar pattern hence the result obtained from experiment has the potential for detection. Red spot in the damage parameter distribution lies on the damaged area indicating successful detection.

4.8 Comparative Study of Damage Sizes and Damage Detection Results

As explained in Chapter III, different trial sizes of damage were experimented before concluding two final damage sizes. First, Single D damage was introduced and the damage size was increased to 28 D damage. For comparison, Single D, 28 D, D1 and D2 were studied.

It was observed that bigger size damage was detected more often than smaller size damage. D2 being the biggest damage studied was detected at an intermediate cluster with natural frequency of 980 Hz. D1 was detected in higher cluster with frequency of 2114 Hz. 28 D was detected in higher cluster of 2996 Hz. Single D was not detected. The delta modes obtained from all the mode shapes of Single D were not following pattern. Hence it was concluded that SLV was not able to capture the difference brought by the damage. Single D damage was too small to make any significant changes for SLV to capture.

4.8.1 Example for Violation of Orthogonality

Nature of delta mode shape is to appear different than its mode shape. Delta mode shape should be orthogonal to both its healthy and damaged mode shapes so it should look different. In the experiment for lower clusters and few higher clusters delta mode shape was observed to appear similar to its healthy and / or damaged mode shapes. These kind of experimental results are not very potential for detection purposes. For a successful detection scheme Orthogonality should also be checked and verified before approaching to any detection process.

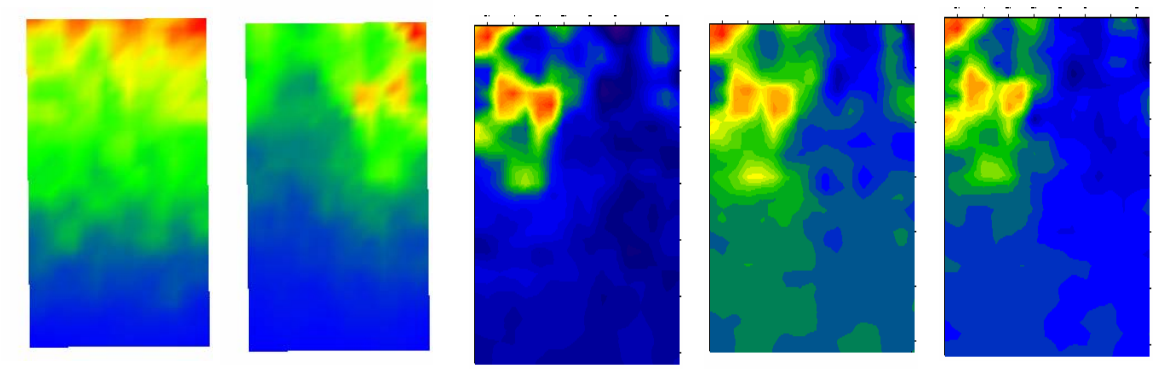

Figure 4.92 From left to right, Healthy Mode Shape (7.625 Hz), Damaged Mode Shape (8 Hz), three repeated Delta Mode Shapes

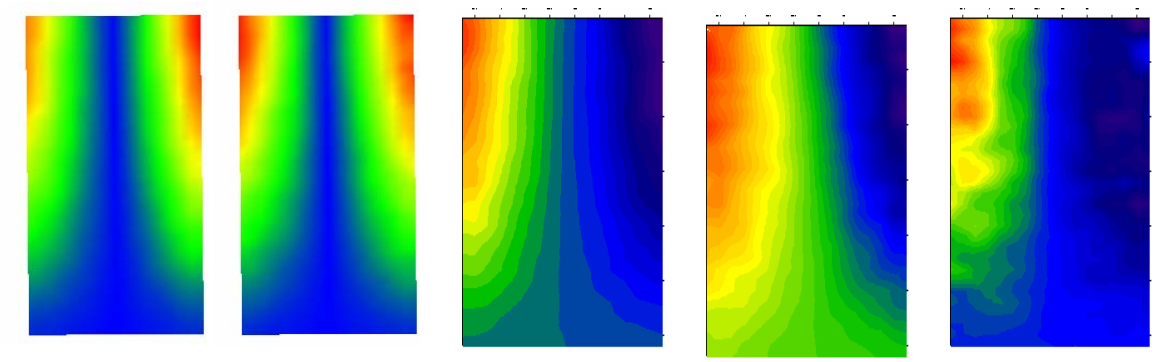

Figure 4.93 From left to right, Healthy Mode Shape (31.88 Hz), Damaged Mode Shape (31.63 Hz), three repeated Delta Mode Shapes

In Figure 4.92 and Figure 4.93, Delta Mode Shape looks similar to the Mode Shape. This indicates the Violation of Orthogonality.

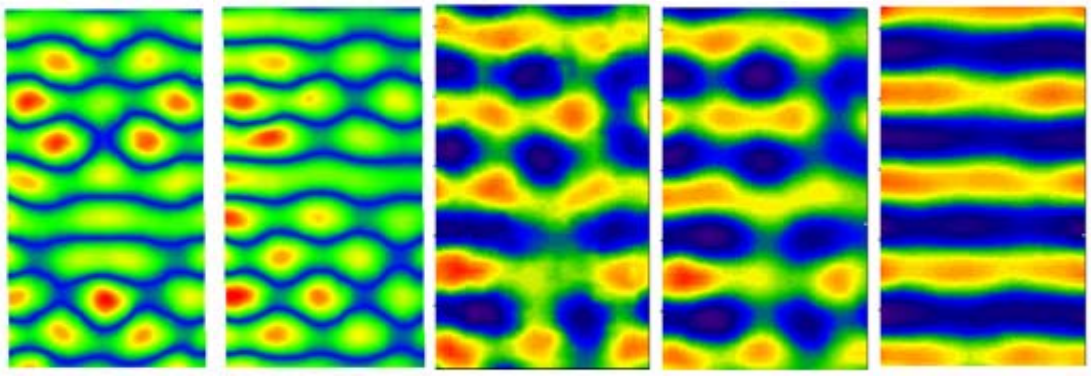

(i) (ii) (iii) (iv) (v)

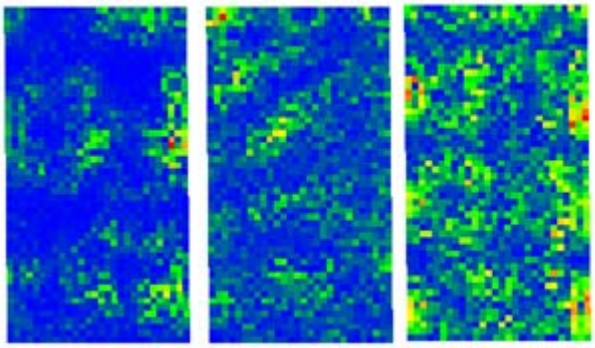

(vi) (vii) (viii)

Figure 4.94 Single D, Fifth Case (i)Healthy Mode Shape, (ii)Damaged Mode Shape, (iii)(iv)(v)Delta Mode Shapes, (vi)(vii)(viii)Damage parameter distribution.

Figure 4.94 shows a case where the detection was not successful. Delta Mode Shape was not following pattern which indicated that the damage was not being felt by SLV. Delta Mode was also observed to have similar bending as that of Mode Shapes which would indicate the Violation of Orthogonality.

4.8.2 Damage Sizes and Damage Detection Results

Sigma Plot and Eview used for plotting.

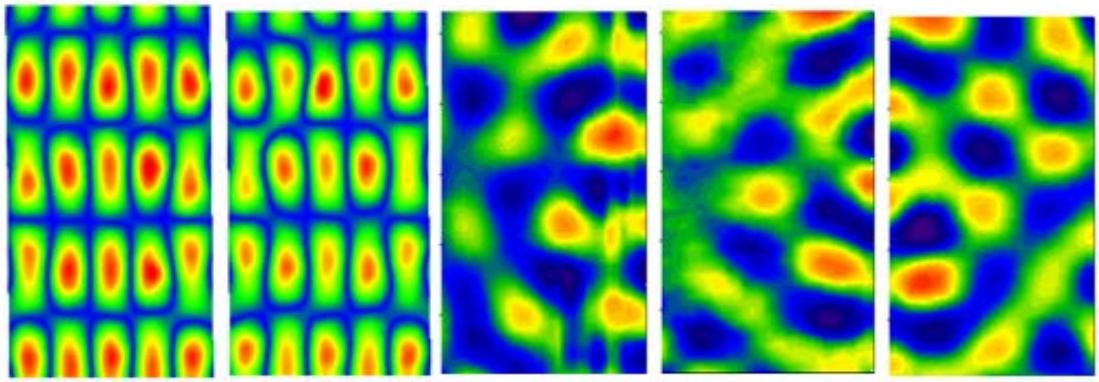

(i) (ii) (iii) (iv) (v)

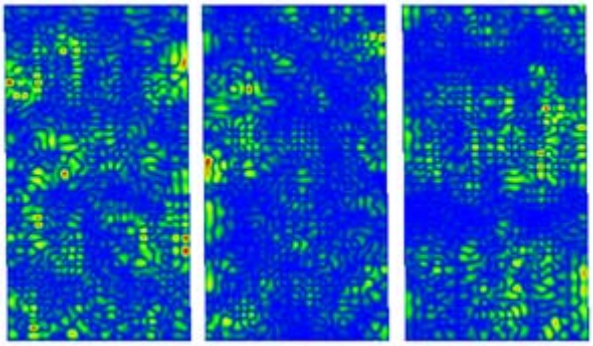

(vi) (vii) (viii)

Figure 4.95 Single D, Sixth Case (i)Healthy Mode Shape, (ii)Damaged Mode Shape, (iii)(iv)(v)Delta Mode Shapes, (vi)(vii)(viii)Damage parameter distribution.

In Figure 4.95 traces of violation of Orthogonality is observed. Delta Mode is not observed to follow pattern, hence the change introduced to the specimen was not observed by SLV and not detected.

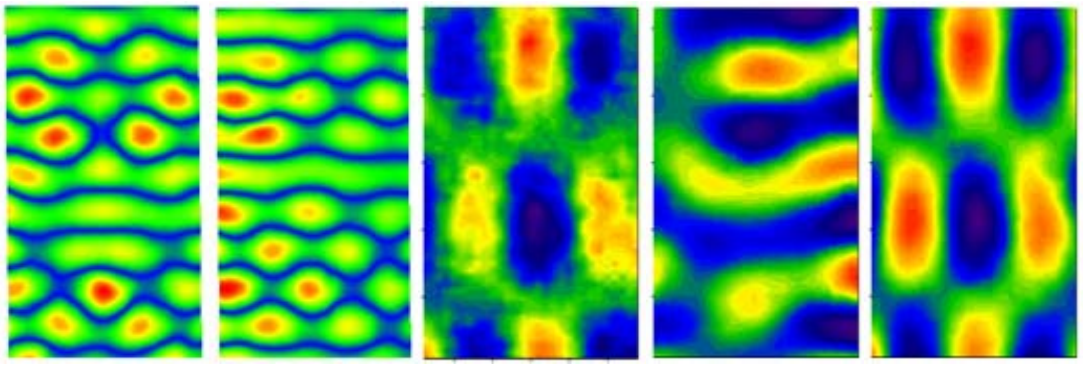

(i) (ii) (iii) (iv) (v)

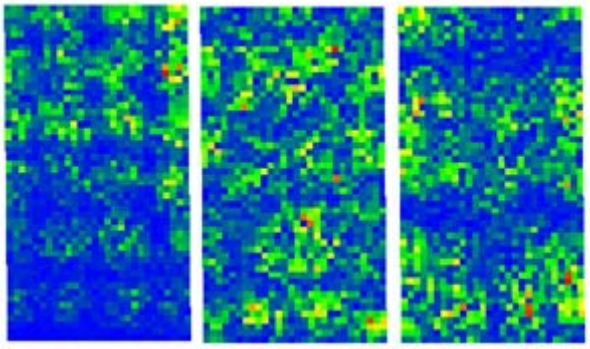

(vi) (vii) (viii)

Figure 4.96 28 D, Fifth Case (i)Healthy Mode Shape, (ii)Damaged Mode Shape, (iii)(iv)(v)Delta Mode Shapes, (vi)(vii)(viii)Damage parameter distribution.

In Figure 4.96 traces of Orthogonality has reduced but the pattern in Delta Mode Shape has not been observed so the detection was not successful.

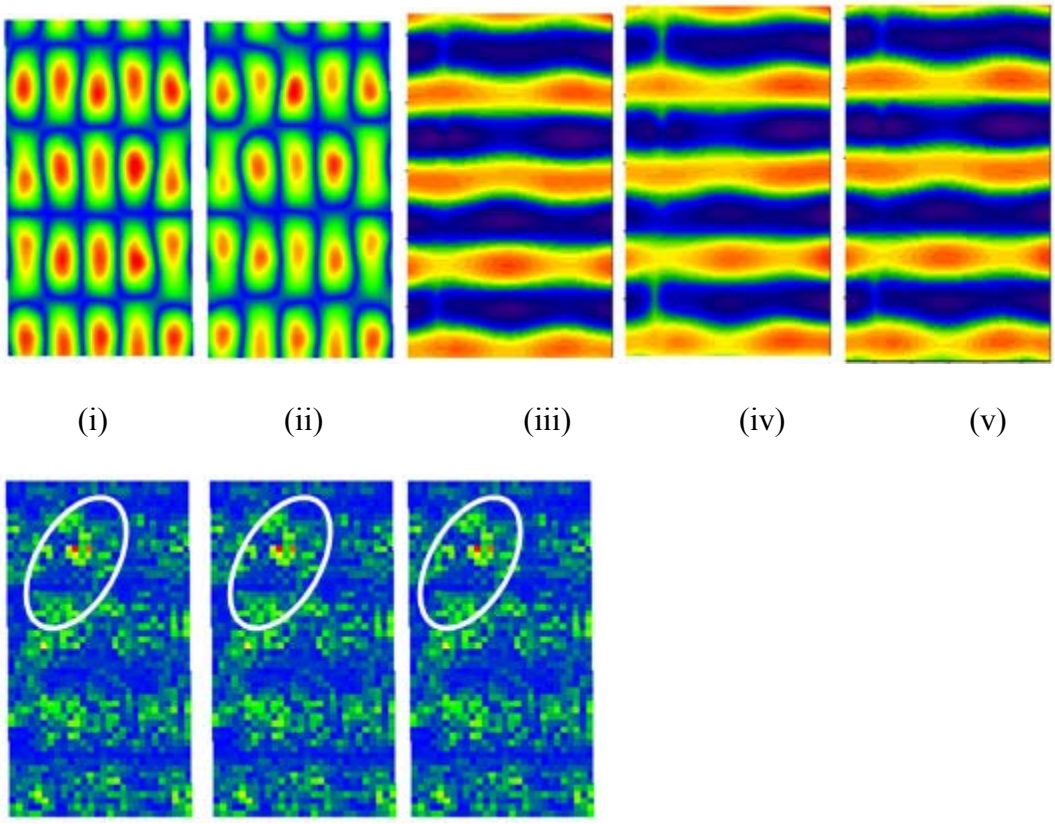

Figure 4.97 28 D, Sixth Case (i)Healthy Mode Shape, (ii)Damaged Mode Shape, (iii)(iv)(v)Delta Mode Shapes, (vi)(vii)(viii)Damage parameter distribution.

In Figure 4.97 it was observed that Delta Mode Shape appeared different than Mode Shapes. Similar pattern in Delta Mode Shape was also observed. Hence detection was successful.

It was also observed that for smaller size of damage only higher frequency mode shapes was able to detect. For larger size damage even lower frequencies mode shapes were able to detect.

4.9 Computer Experiment Case Study

In few Mode Shapes, it took eight hours for SLV to perform experiment, in the specimen with 12 x 21 inches surface area. So, for a civil engineering structure with large dimensions, it would take unrealistic and impractical amount of time. New techniques with faster scanning capabilities has to be invented which reduces experiment time. It was also observed that SLV can operate faster with less scanning points. If a detection scheme is powerful enough to detect with comparatively less number of scanning points, practical application of those schemes could be feasible.

It should also be noted that a small area of damage might not be in contact with scanning points. Damage being small in size, in most of the cases, would be well inside the scanning points. The scenario where the scanning points not intersecting or touching the damage was performed and studied to emulate practical situations.

The computer experiment having 2479 scanning points was performed. Geometry, Properties and Boundary Condition of the specimen were same as the previous experiment. Having 2376 elements damage was introduced into the specimen by reducing modulus of elasticity by eight percent. Termed as Fine Mesh, Damage Detection code was used to obtain six Mode Shapes and associated natural frequencies. The specified displacements obtained from Fine mesh were used into another Coarser Mesh having 84 scanning points with 66 elements. It was noted that the data points in coarser mesh was not intersecting or touching the damage.

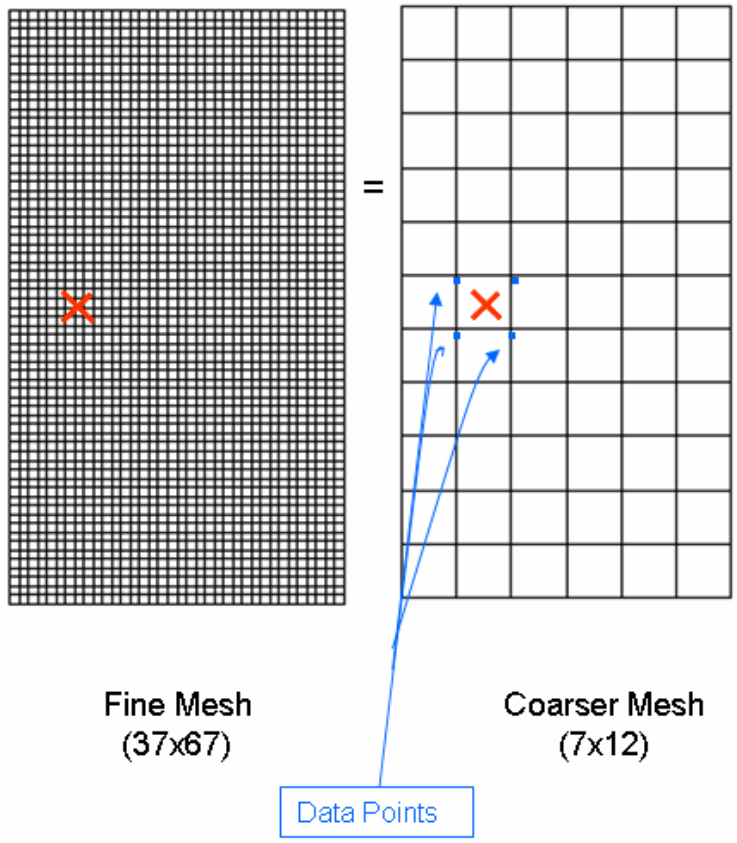

Figure 4.98 Damage and Scanning Points configuration of Fine Mesh (left) and Damage and Scanning Points configuration of Coarser Mesh

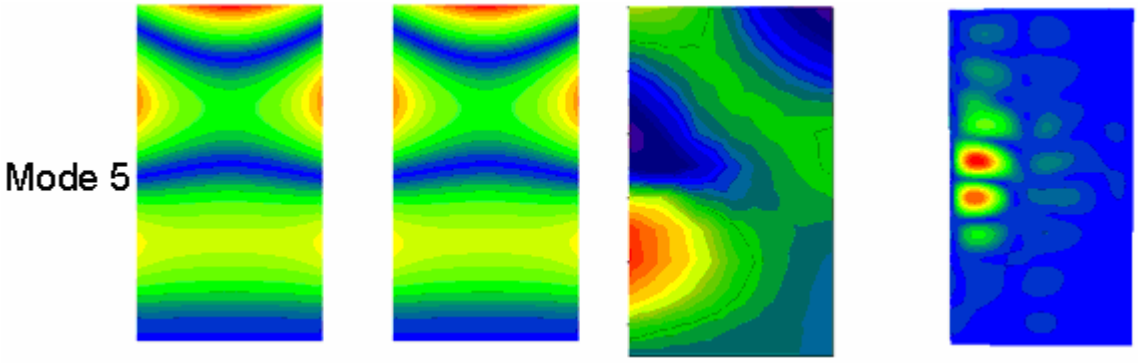

Figure 4.99 Left to Right, Healthy Mode Shape (149.44 Hz), Damaged Mode Shape (149.38 Hz), Delta Mode Shape, Damage Parameter Distribution.

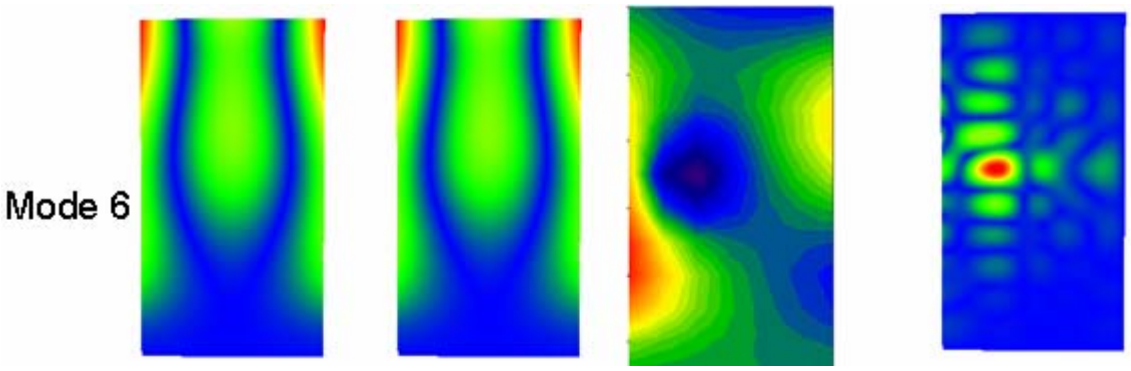

Figure 4.100 Left to Right, Healthy Mode Shape (200.28 Hz), Damaged Mode Shape (199.7 Hz), Delta Mode Shape, Damage Parameter Distribution.

It was observed that the detection technique used in Damage Code was capable for detection even for scanning points thirty times less than the original mesh size. Again coarser scanning points of 48 with 33 elements were studied. With 52 times less scanning points than the original 2479 scanning points and for mode-1 damage was successfully detected.

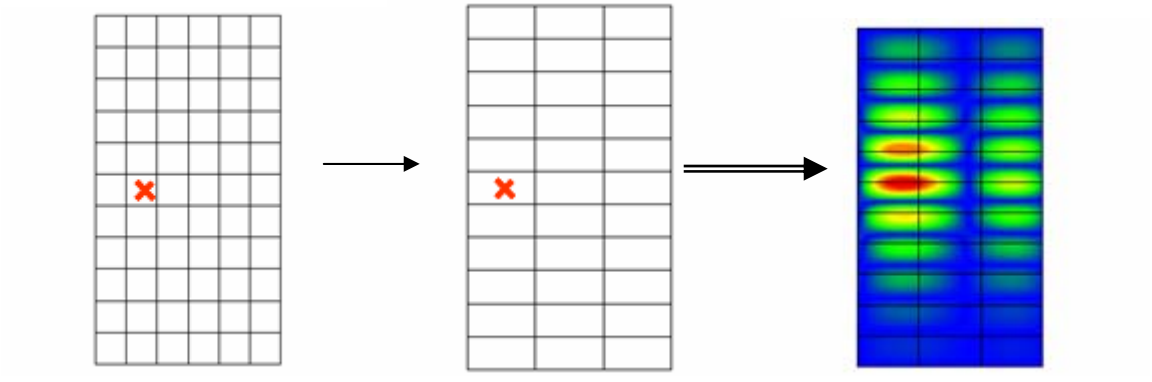

Figure 4.101 From left to right, Damage Configuration of 84 scanning points, Damage Configuration of 48 scanning points, Damage parameter distribution.

Figure 4.102 Mode-3, 48 Scanning Points, from left to right, Healthy Mode Shape, Damage Mode Shape.

It was observed that damage detection code has the capability to detect damage even in practical conditions where damage lies well inside the scanning points and the area of the damage is not scanned. This feature of damage detection code provides economical and practical applications in detection process.

4.10 Static Loading Case

SAP2000 was used for static loading analysis for the cantilever specimen. 22 x 12 x 0.125 inches specimen was modeled with 1326 nodes containing 1250 elements. Double Winged damage was introduced to the structure by reducing the young's modulus by 10^{th}. Various locations of loadings were applied and the specified displacements (few cases with displacements plus rotations) obtained from SAP2000 analysis of healthy specimen and damaged specimens were analyzed using the damage code.

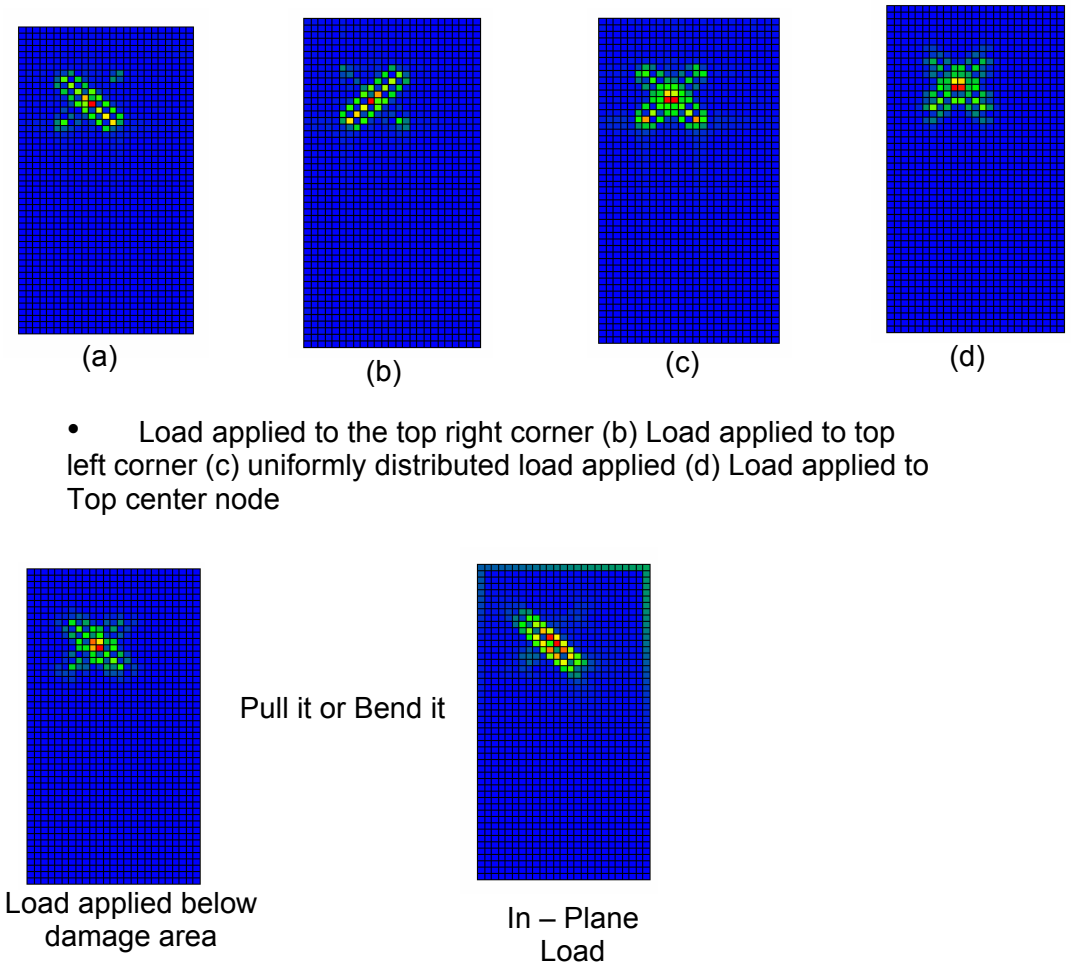

Figure 4.103 Damage Parameter distribution from various Static Loading Cases

Figure 4.103 Shows the Static Loading Cases studied for damage detection. For case (a) above static load was applied on the top right corner node. The direction of the load was out of the shown plane. The damage parameter distribution plot shows that the damage was detected successfully. For case (b) above static load was applied on the top left corner node. The direction of the load was out of the shown plane. The damage parameter distribution plot shows that the damage was detected successfully. For case (c) above static load was applied uniformly on the entire shell element. The direction of the

load was out of the shown plane. The damage parameter distribution plot shows that the damage was detected successfully. For case (d) above static load was applied on the top center node. The direction of the load was out of the shown plane. The damage parameter distribution plot shows that the damage was detected successfully.

To further explore the static loading case few more cases were studied. Static load, out of plane was applied on the specimen below the area of the damage. The exact center node which was towards the fixed end of the cantilever specimen and also was below all the nodes representing damage was applied with out of plane load. The damage parameter distribution plot shows that the damage was detected successfully. Case with in plane load was also studied. Top right corner node was applied with in plane load and damage parameter distribution verified the damage as being located.

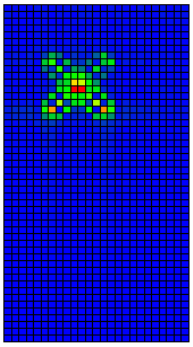

Figure 4.104 Damage Parameter Distribution, in plane load applied to all top nodes.

4.11 Static Vs. Dynamic Loading Case

It was observed from the study of the static loading cases that load could be applied in various ways for the detection. Pull it or Bend it concept was observed. Damage code was able to detect damage in all types and locations of the load. Various

location of loads was observed to increase the detection. It was also observed that various mode shapes had to be studied in dynamic case loading to increase the accuracy of the detection. When comparing the static loading case with dynamic loading case it was observed that the detection from static loading case was better than dynamic loading case. Figure 4.104 shows damage parameter distribution obtained from three different static loading cases compared with damage parameter distribution obtained from three different modes shapes of dynamic loading cases.

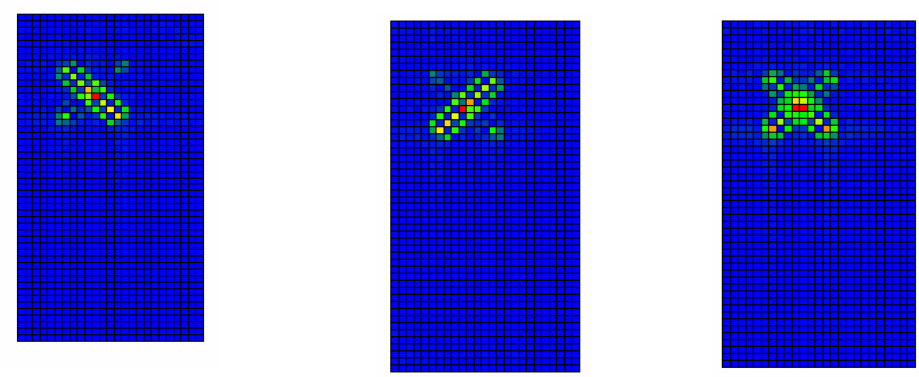

Damage Parameter Distribution Obtained from Various Load Locations for Static Loading Case

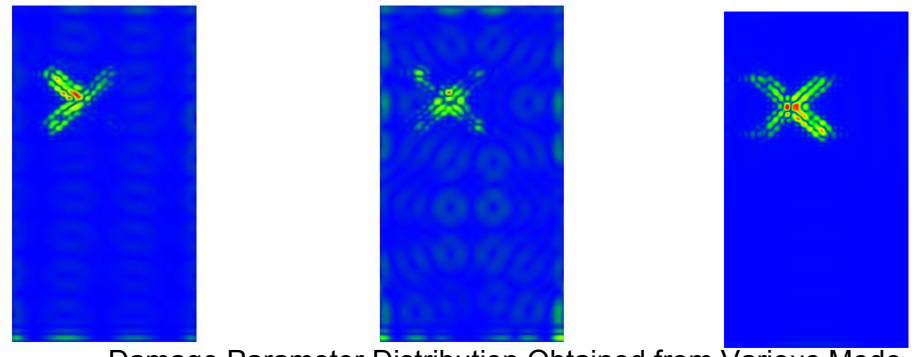

Damage Parameter Distribution Obtained from Various Mode Number for Dynamic Loading Case

Figure 4.105 Static Loading Vs. Dynamic Loading

From the above figure it could be concluded that the static loading cases were more potential for detection that dynamic loading cases. Both of the cases indicated the damage detection experiment for accurate detection to contain multiple locations of loads for static loading case and multiple mode shape for dynamic load case. Since the static loading experiment can be performed with less time and the instrument used in static loading cases are cheaper compared to dynamic loading instruments, one should choose static loading case for a successful and economical damage detection scheme.

CHAPTER V

SUMMARY, CONCLUSIONS AND FUTURE WORK

5.1 Summary

The presented study was conducted in conjunction with an ongoing research program dealing with the development of an integrated analytical/experimental nondestructive evaluation (NDE) methodology for global damage detection. The important ingredient is the use of a damage energy parameter. It provides the required sensitivity measure for detection of the damage on the basis of measured structural response. Scanning Laser Vibrometer was used as an experimental tool and Damage Detection Code (Detector) was used as an analytical post processing tool.

From the viewpoint of practical utilization in structures, extensive testing for a valid assessment of any NDE technique becomes necessary. Especially in view of the many complicating factors and the variety of damage scenarios that are likely to be encountered, assessment of the scheme becomes a necessary requirement. An investigation is performed keeping various methods of loadings in a real environment in mind.

5.2 Conclusions

Based on the presented results, a number of conclusions are made below. All of these should be viewed in the context of the rather limited scope of the experiments conducted here; i.e., limitations in voltage/signal strength, the type of PZT actuators, etc.

1. Comparison with reference of Healthy Mode Shapes and investigation of Delta Mode Shapes, alone are not sufficient for damage detection. Even for an ideal case (Computer Experiment) with varying natural frequencies, it was observed that the delta mode shape alone was not sufficient for detection
2. Frequency decreases due to damage and repeatability in the obtained Delta Mode Shapes are good indication for the quality of experiments, and hence their potential for detection. Decrease in frequency indicated that the magnitude of out of plane displacement has sufficient signal – noise ratio.
3. As anticipated and observed by many others, higher frequency / mode shapes provides more potential for a successful detection. From the experiment, it was observed that the order of magnitude in the delta mode shape compared to mode shape itself was observed to increase indicating a better potential for detection.
4. For the present experiment work, bigger damage size was observed with more potential for detection.
5. For the detection technique presently used, size of measurement grid was not observed to pause any practical difficulty in detection. Various mesh size considered was able to detect the damage accurately.
6. Static Loading Case shows great potential in detection compared to Dynamic Loading Case. It was also observed that the location (single or multiple) and

direction (in plane or out of plane) of the applied load for the static loading case was not pausing detection.

5.3 Future Work

Collectively, the results obtained from the work performed to date will provide guidance in forming proposals for possible future work areas and extensions of the use of integrated damage parameter – SLV techniques for health monitoring of structures. These include:

(i) Faster scanning time, lower frequencies with better accuracy and features to compare repeated experiments could be the areas of study for better Scanning Laser Vibrometer.

(ii) Research on different types of damages involving complex structures and boundary conditions.

(iii) Development of a powerful Graphical User Interface for the complete automated procedure for enhancement of feature extraction, feature-reconstruction and detection for 2D and 3D viewing.

(iv) Development of accurate measurement technique using static loading case for damage detection.

REFERENCES

1. W H Leong, W J Staszewski, B C Lee and F Scarpa, 2005, "Structural health monitoring using scanning laser vibrometry: III. Lamb waves for fatigue crack detection," Smart Mater. Struct. 14 (2005) 1387-1395.

2. B J Halkon, S R Frizzel and S J Rothberg, 2003, "Vibration measurements using continuous scanning laser vibrometry: velocity sensitivity model experimental validation," Meas. Sci. Technol. 14 (2003) 773–783.

3. P. F. Pai, BY-S Kim And J. H. Chung, 2004, "Dynamics-based Damage Inspection of an Aircraft Wing Panel," Journal Of Intelligent Material Systems And Structures, Vol. 15 803–19.

4. P. F. Pai and S. Jin, 1999, "Locating Structural Damage By Detecting Boundary Effects," Journal of Sound and vibration (2000) 231(4), 1079-1110.

5. A.Z. Khan, A.B. Stanbridge, D.J. Ewins, 2000, "Detecting damage in vibrating structures with a scanning LDV," Optics and Lasers in Engineering 32 (2000) 583-592.

6. P. F. Pai and L G Young, 2000, "Damage Detection in Beams Using Operational Deflection Shape," 2000, International Journal of Solid and Structure 38 2001 3161-3192.

7. P. F. Pai and L G Young, 2004, "Dynamics-based Damage Inspection of an Aircraft Wing Panel," Journal of Intelligent Material Systems and Structures, Vol. 15, No. 11, 803-821.
8. S Choi, S. Park and N. Stubbs, 2005, "Nondestructive damage detection in structures using changes in compliance," International Journal of Solids and Structures 42 (2005) 4494–4513.

9. A. S. J. Swami Das And Y. Chen, 1994, "Monitoring Crack Growth Through Change Of Modal Parameters," Journal of Sound and Vibration, 186-2, 214-232.

10. B. Titurus, M. I. Friswell, L. Starek, 2003, "Damage detection using generic elements: Part II. Damage detection," Computers and Structures 81, 2287–2299.

11. S. Vanlanduit, P. Guillaume, J. Schoukens and E. Parloo, 2002, "Linear and Nonlinear Damage Detection Using a Scanning Laser Vibrometer," Shock and Vibration, 9, 43-56.

12. G. A. Gordon and T. Douglas Mast, 1999, "Wide-Area Imaging of Ultrasonic Lamb Wave Fields by Electronic Speckle Pattern Interferometry," SPIE, 3586, 297-309.

13. Zimmerman, D. C., Kaouk, M., and Simmermacher, T., 1995, "Structural Damage Detection Using Frequency Response Functions," in Proc. of the 13th International Modal Analysis Conf., 179-184.

14. Kaouk, M., and Zimmerman, D. C., 1994, "Assessment of Damage Affecting All Structural Properties," in Proc. of the 9th VPI &SU Symposium on Dynamics and Control of Large Structures, 445-455.

15. Chen, J.-C., and garba, J. A., 1988, "On-Orbit Damage Assessment for Large Space Structures," AIAA Journal, Vol. 26, No. 9, 1119-1126.

16. McGowan, P. E., Smith, S. W., and Javeed, M., 1990, "Experiments for Locating Damage Members in a Truss Structures," Proc. 2nd USAF/NASA Workshop on system Identification and Health Monitoring of Precision Space Structures, 571-615.

17. Ricles, J. M., 1991, "Nondestructive Structural Damage Detection in Flexible Space Structures Using Vibration Characterization," NASA report CR-185670.

18. Sanayei, M., and Onipede. O., 1991, "Damage Assessment of Structures Using Static Test Data," AIAA Journal, Vol. 29, No. 7, 1174-1179.

19. Zimmerman, D.C., and Kaouk, M., 1992 “Eigenstructure Assignment Approach for Structural Damage Detection,” AIAA Journal, Vol. 30, No. 7, 1848-1855.

20. Schulz, M. J., Pai, P. F., and Abdelnaser, A. S., 1996, “Frequency Response Function Assignment Technique for Structural Damage Identification,” in *Proc.* Of the 14th International Modal Analysis Conference*,* 105-111.

21. Stubbs, N., and Osegueda, R., 1990, “Global Non-Destructive Damage Evaluation in Solids,” The International Journal of Analytical and Experimental Modal Analysis, Vol. 5, No. 2, 67-79.

22. West, W. M., 1984, “Illustration of The Use of Modal Assurance Criterion to Detect Structural Changes in an Orbiter Test Specimen,” in Proc. Air Force Conference on Aircraft Structural Integrity, 1-6.

23. Stubbs, N., Kim, J.-T., Topole, K., 1992, “An Efficient and Robust Algorithm for Damage Localization in Offshore Platforms,” in Proc. ASCE Tenth Structures Congress, 543-546.

24. Topole, K. G., and Stubbs, N., 1995, “Nondestructive Damage Evaluation of a Structure from Limited Modal Parameters,” Earthquake Engineering and Structural Dynamics, Vol. 24, No. 11, 1427-1436.

25. Saleeb, A. F., Tseng, S. M., and Gendy, A.S., 1997, “Development and Evaluation Studies on New NDE Techniques for Damage Detection in Structures.” Reprint.

26. Saleeb, A.F., and Gendy, A.S., 2000, “Nonlinear Dynamics for Mixed Shells with Large Rotation and Elasto-Plasticity,” International Journal of Computational Engineering Science, Vol. 1, No. 1, 1-31.

27. Saleeb, A.F., and Chang, T.Y., 1987, “An Efficient Quadrilateral Element for Plate Bending Analysis,” International Journal for Numerical Methods in Engineering, Vol. 24, 1123-1155.
28. Saleeb, A.F., Chang, T.Y., and Graf, W., 1987, “A Quadrilateral Shell Element using a Mixed Formulation,” Journal of Computer and Structures, Vol. 26, No. 5, 787-803.

29. Milind, L. Prabhu, 2002, “Defect Localization Capabilities of a Global Damage Detection Scheme: Spatial Pattern Recognition using Full-Field Vibration Test Data in Plates,” The University of Akron, Masters Thesis.

30. G. K. Ponnaluru, 2005, “Enhancement Of The Feature Extraction Capability In Global Damade Detection Using Wavelet Theory,” The University of Akron, Masters Thesis.

31. M. S. Shohel, 2001, “Study Of A New Global Damage Detection Scheme For Disk-Type Structures,” The University of Akron, Masters Thesis.

32. Polytec Scanning Vibrometer, PSV 400, Hardware Manual.

33. Polytec Scanning Vibrometer, Software 8.2, Software Manual.

34. Polytec Scanning Vibrometer, Theory Manual, As of Software 8.2.

APPENDIX

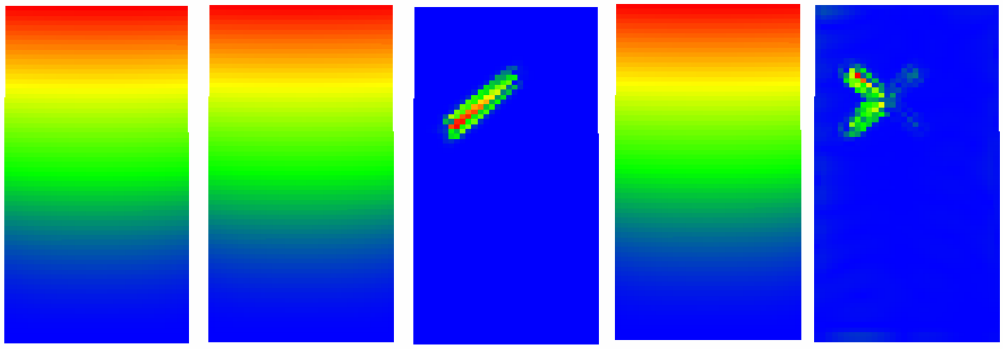

Healthy MS D1 MS Detector D2 MS Detector 1

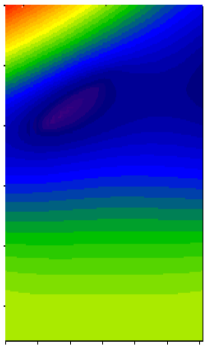

Delta Mode (D1)

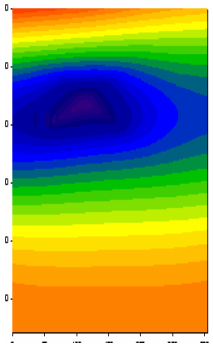

Delta Mode (D2)

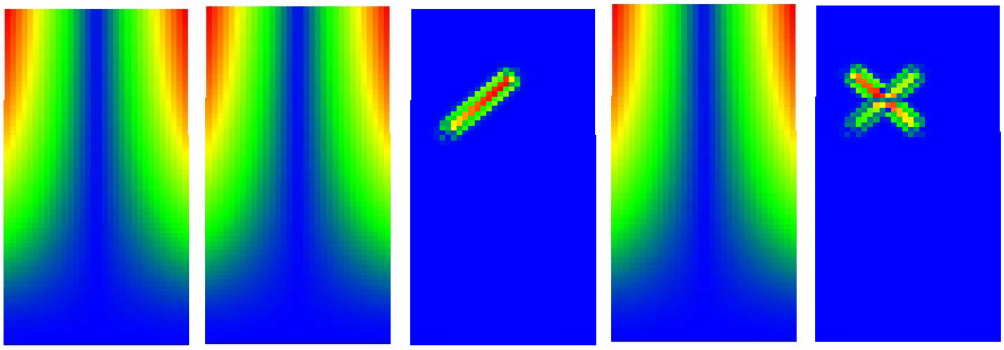

Healthy MS D1 MS Detector D2 MS Detector 2

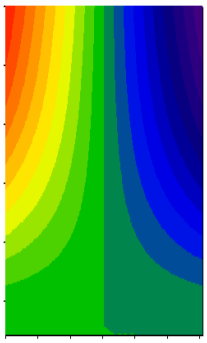

Delta Mode (D1)

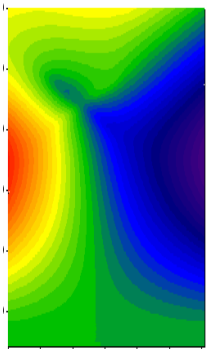

Delta Mode (D2)

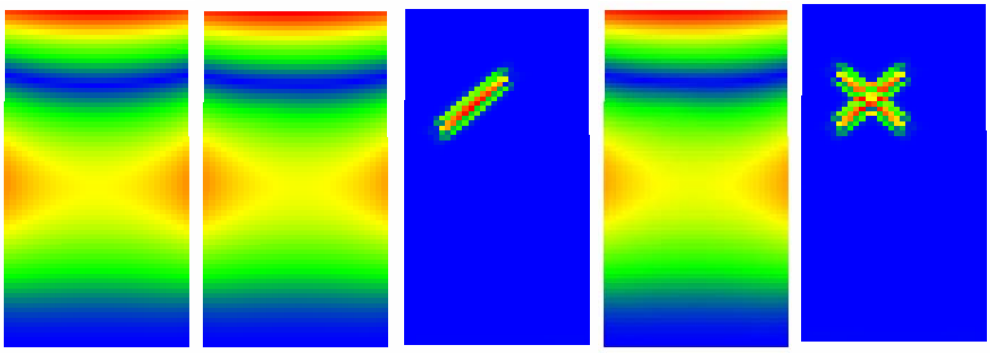

3

Healthy MS D1 MS Detector D2 MS Detector

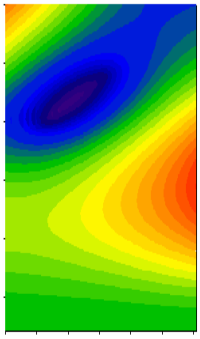

Delta Mode (D1)

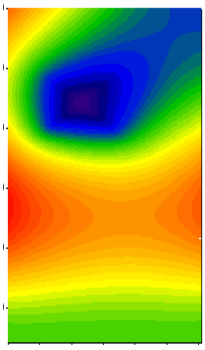

Delta Mode (D2)

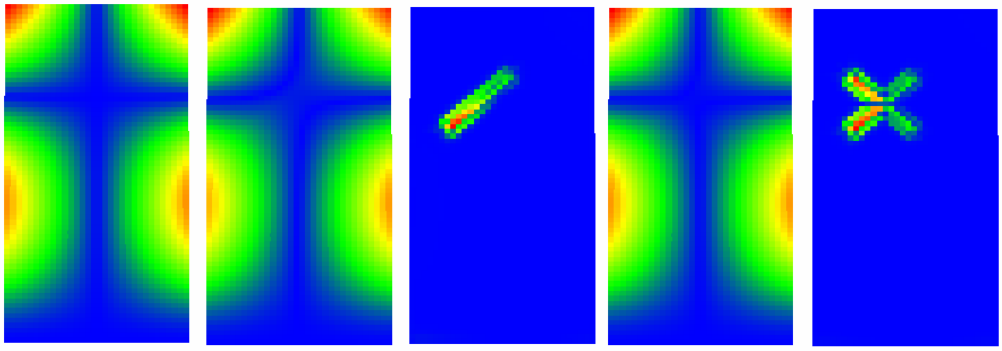

4

Healthy MS D1 MS Detector D2 MS Detector

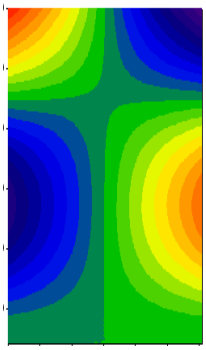

Delta Mode (D1)

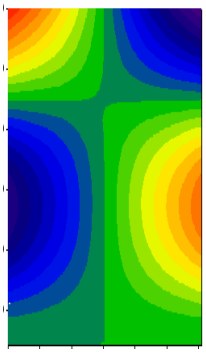

Delta Mode (D2)

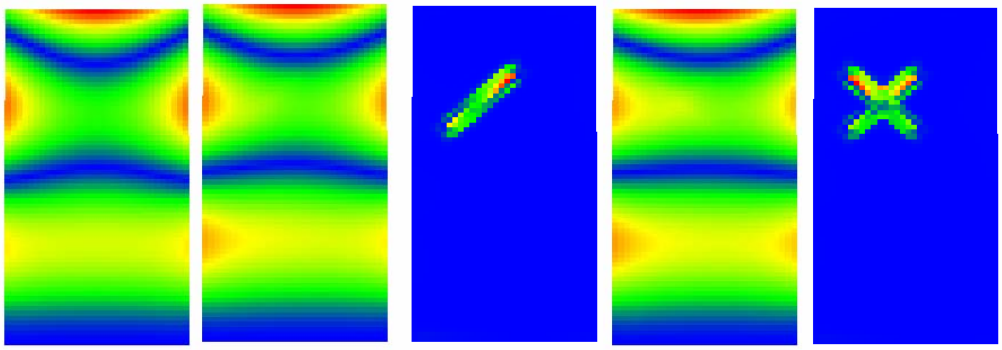

Healthy MS D1 MS Detector D2 MS Detector

5

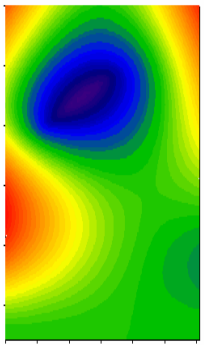

Delta Mode (D1)

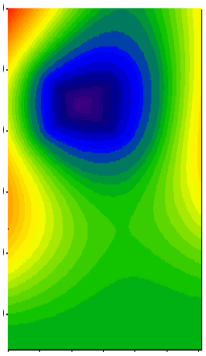

Delta Mode (D2)

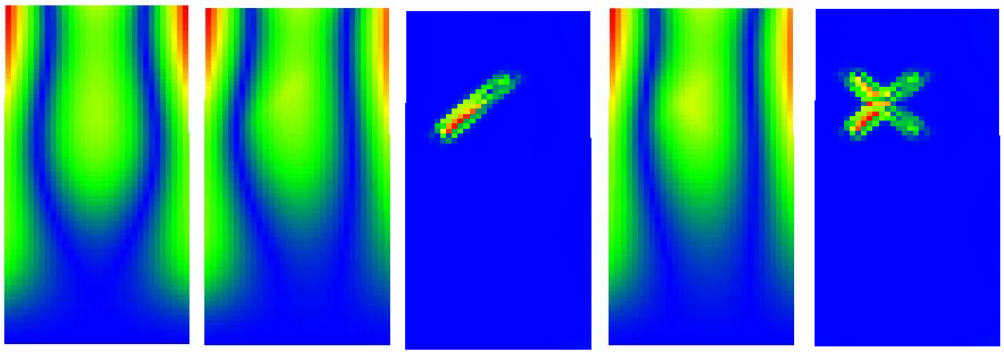

6

Healthy MS D1 MS Detector D2 MS Detector

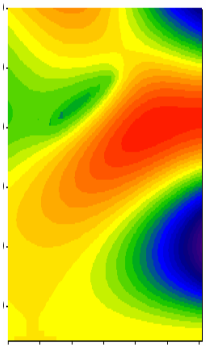

Delta Mode (D1)

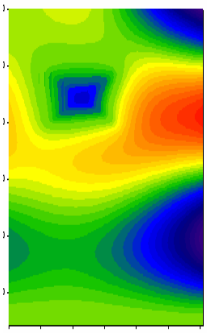

Delta Mode (D2)

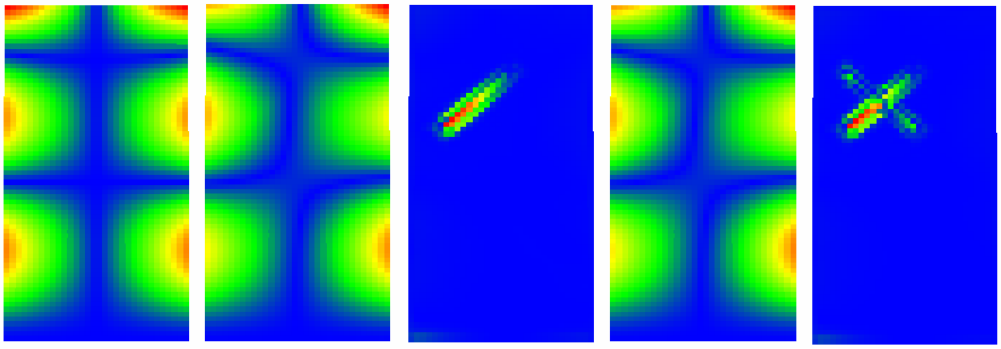

7

Healthy MS D1 MS Detector D2 MS Detector

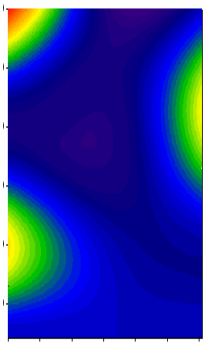

Delta Mode (D1)

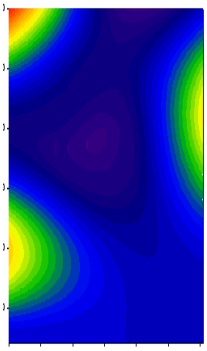

Delta Mode (D2)

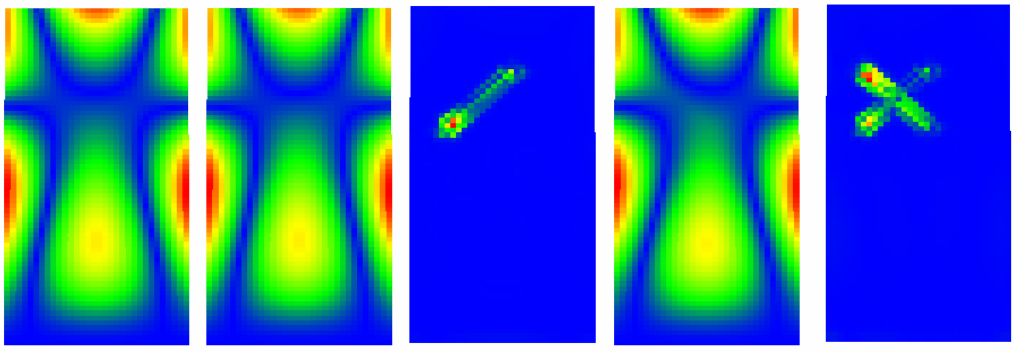

8

Healthy MS D1 MS Detector D2 MS Detector

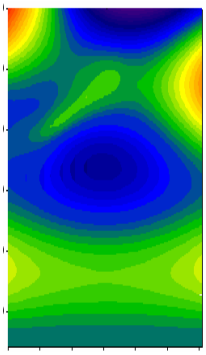

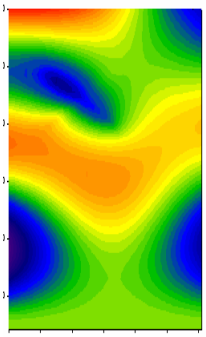

Delta Mode (D1) Delta Mode (D2)

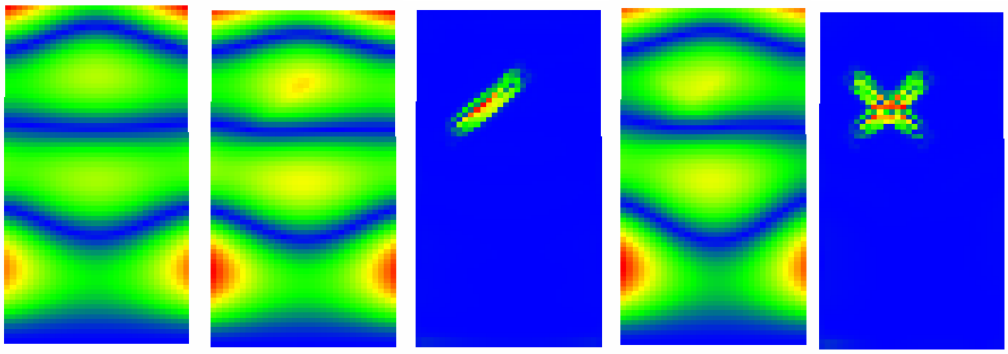

9

Healthy MS D1 MS Detector D2 MS Detector

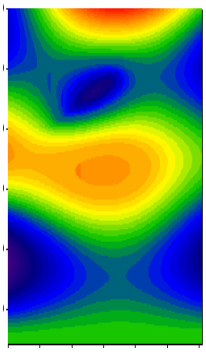

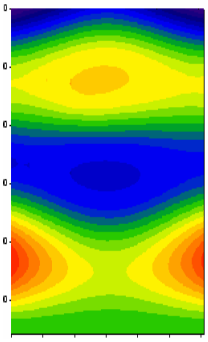

Delta Mode (D1) Delta Mode (D2)

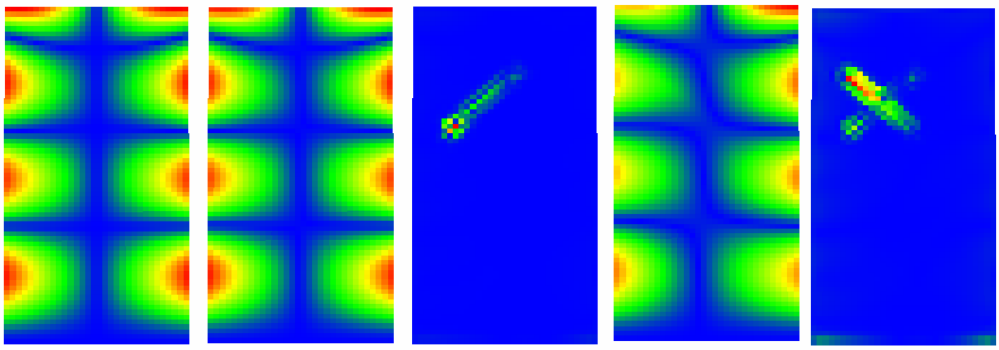

Healthy MS D1 MS Detector D2 MS Detector

10

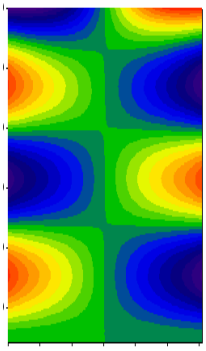

Delta Mode (D1)

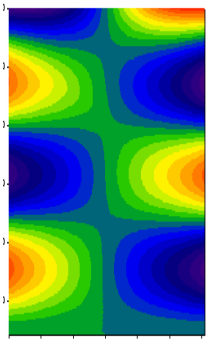

Delta Mode (D2)

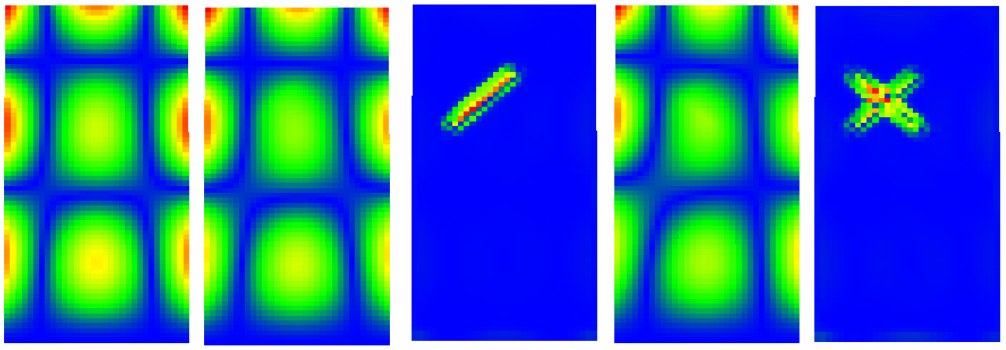

Healthy MS D1 MS Detector D2 MS Detector

11

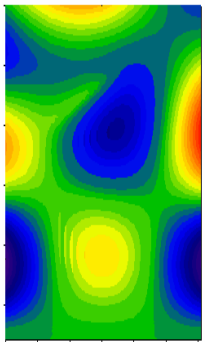

Delta Mode (D1)

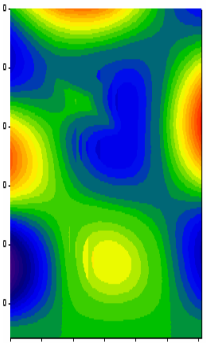

Delta Mode (D2)

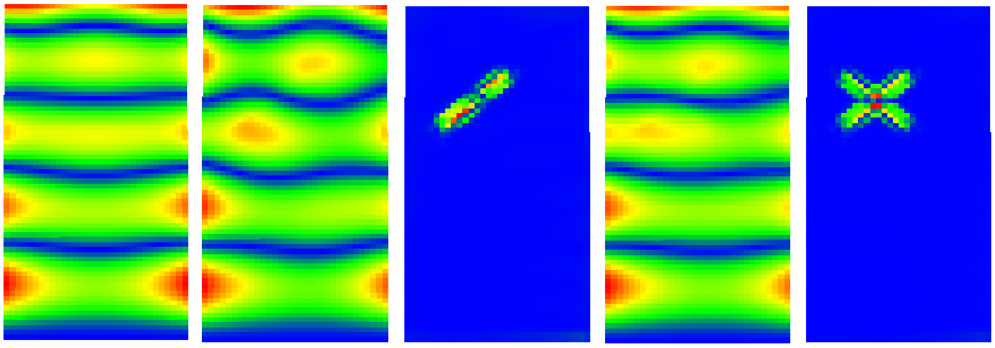

Healthy MS D1 MS Detector D2 MS Detector 12

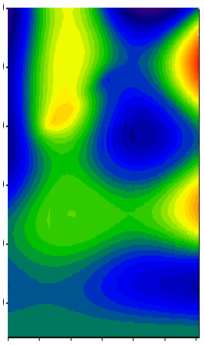

Delta Mode (D1)

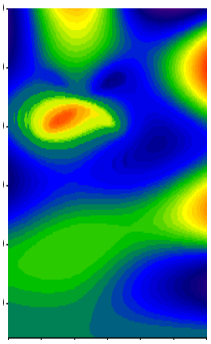

Delta Mode (D2)

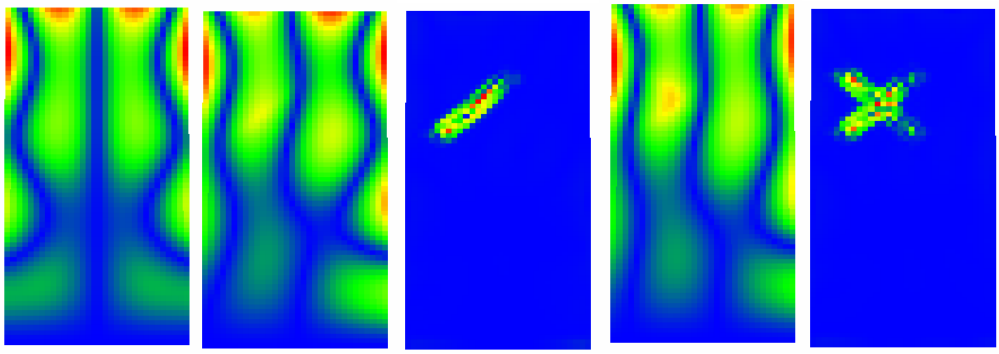

Healthy MS D1 MS Detector D2 MS Detector 13

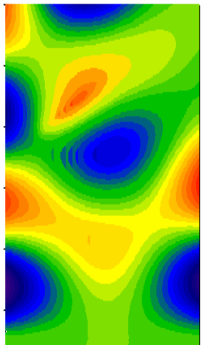

Delta Mode (D1)

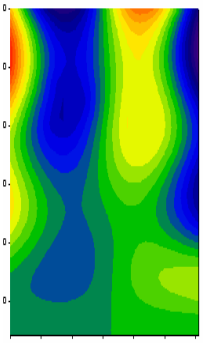

Delta Mode (D2)

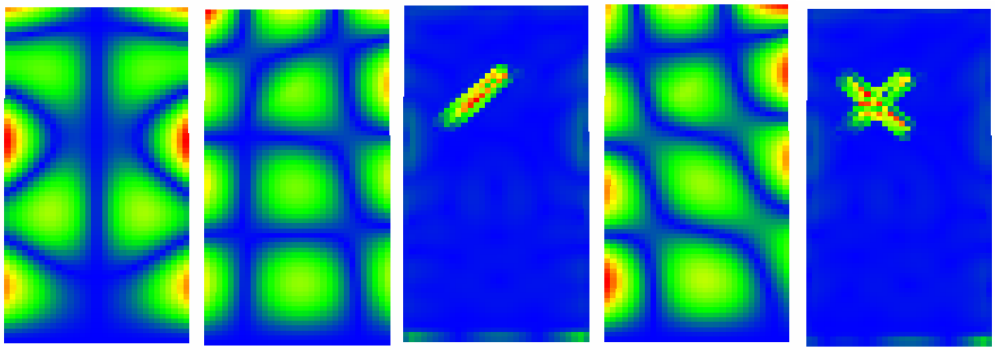

Healthy MS D1 MS Detector D2 MS Detector

14

Delta Mode (D1) Delta Mode (D2)

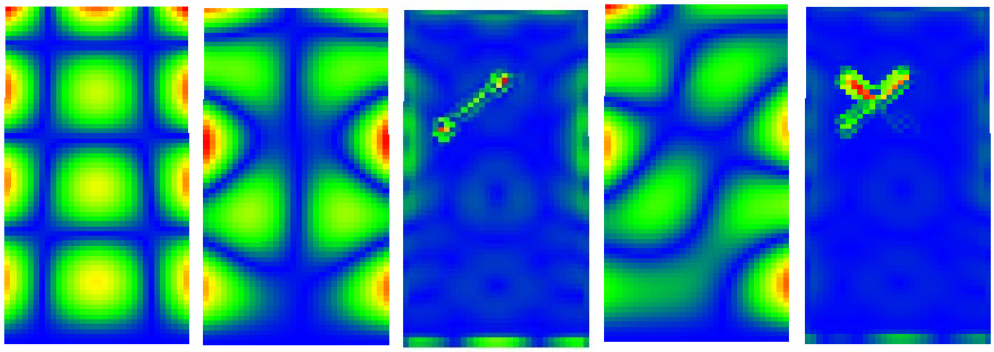

Healthy MS D1 MS Detector D2 MS Detector

15

Delta Mode (D1) Delta Mode (D2)

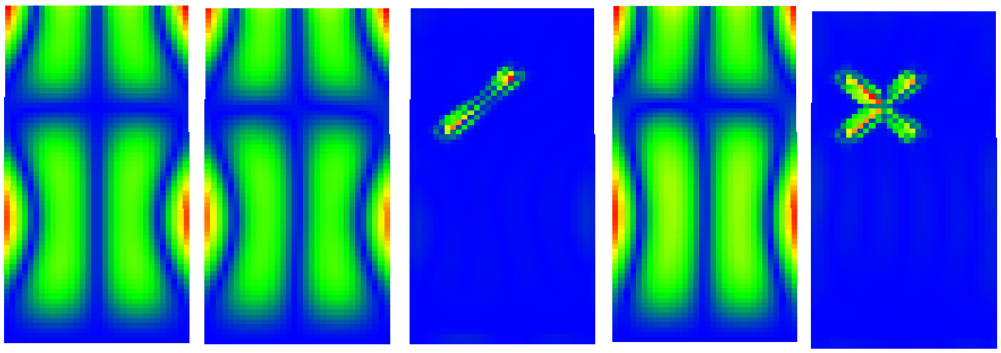

Healthy MS D1 MS Detector D2 MS Detector

16

Delta Mode (D1) Delta Mode (D2)

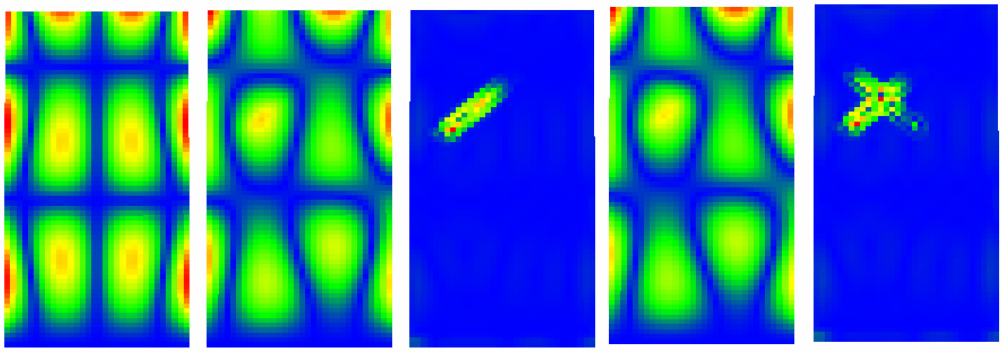

Healthy MS D1 MS Detector D2 MS Detector

17

Delta Mode (D1) Delta Mode (D2)

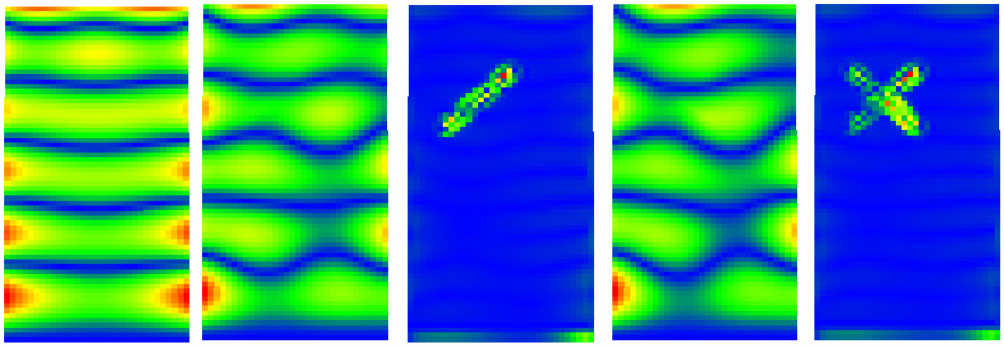

Healthy MS D1 MS Detector D2 MS Detector

18

Delta Mode (D1) Delta Mode (D2)

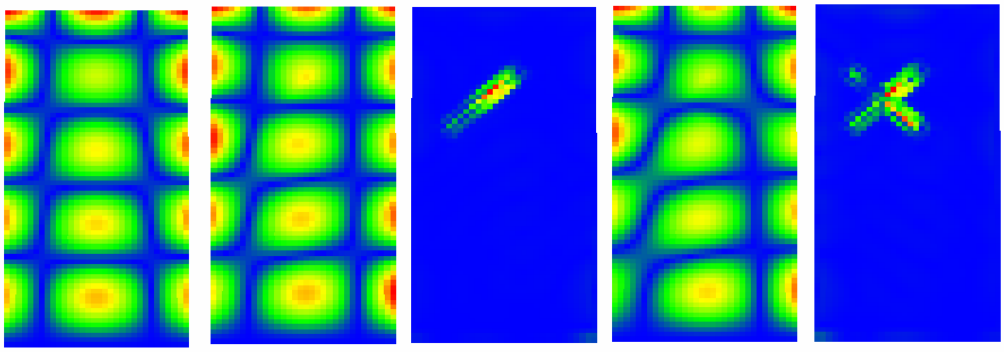

Healthy MS D1 MS Detector D2 MS Detector

19

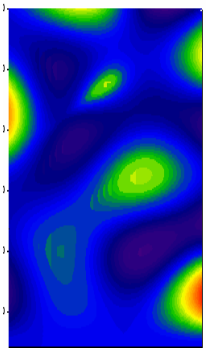

Delta Mode (D1)

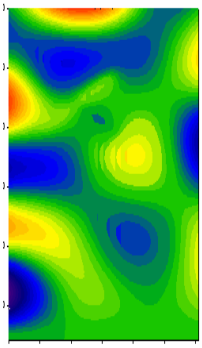

Delta Mode (D2)

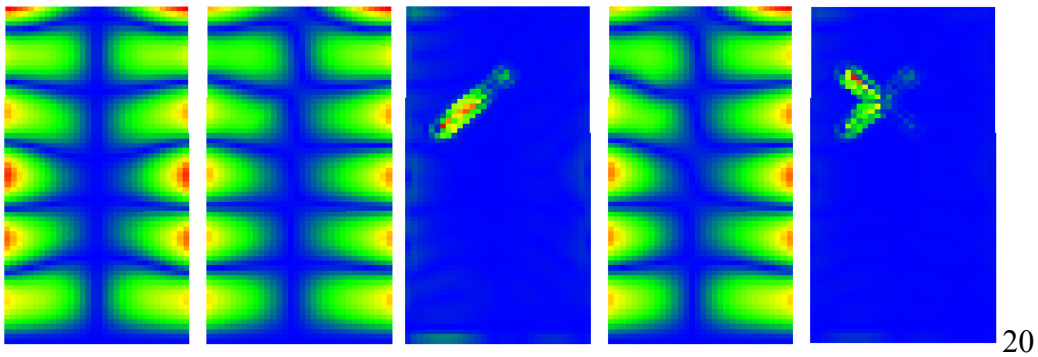

Healthy MS D1 MS Detector D2 MS Detector

20

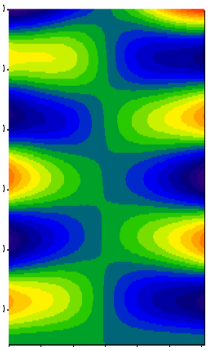

Delta Mode (D1)

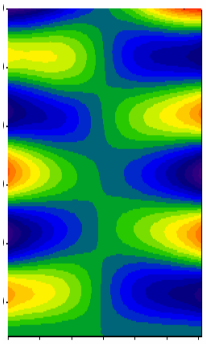

Delta Mode (D2)

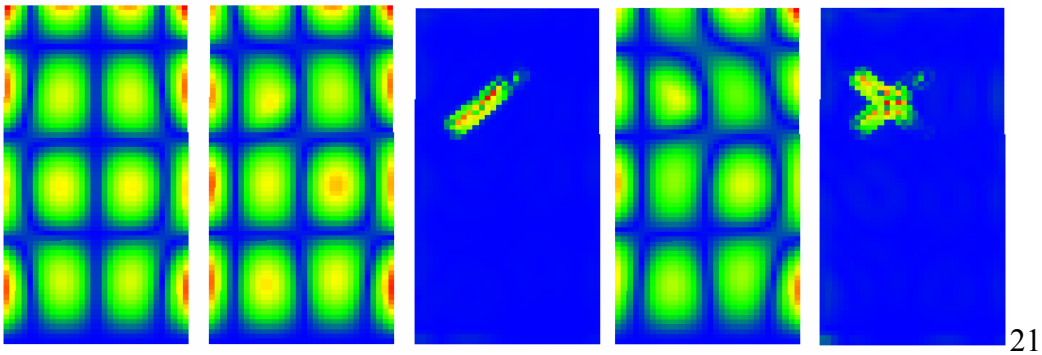

21

Healthy MS D1 MS Detector D2 MS Detector

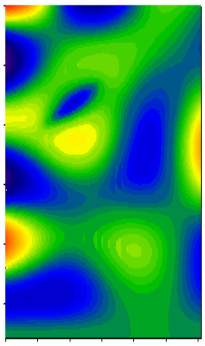

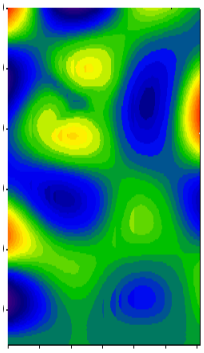

Delta Mode (D1) Delta Mode (D2)

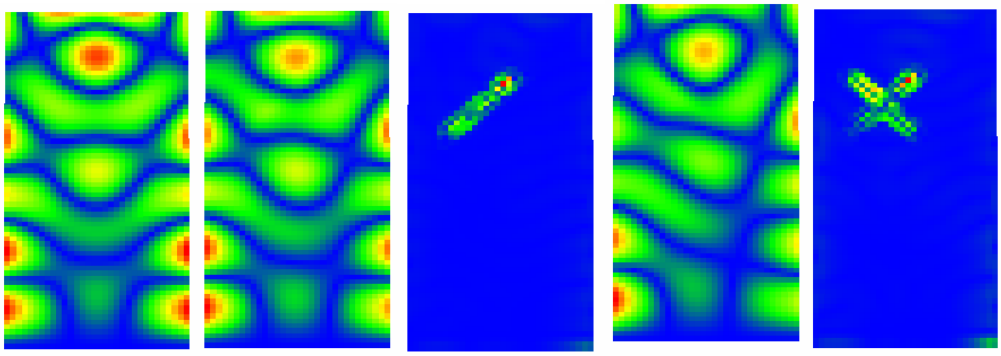

23

Healthy MS D1 MS Detector D2 MS Detector

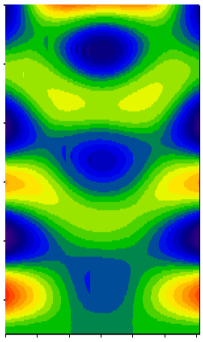

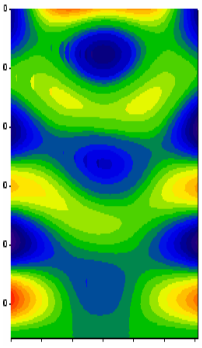

Delta Mode (D1) Delta Mode (D2)

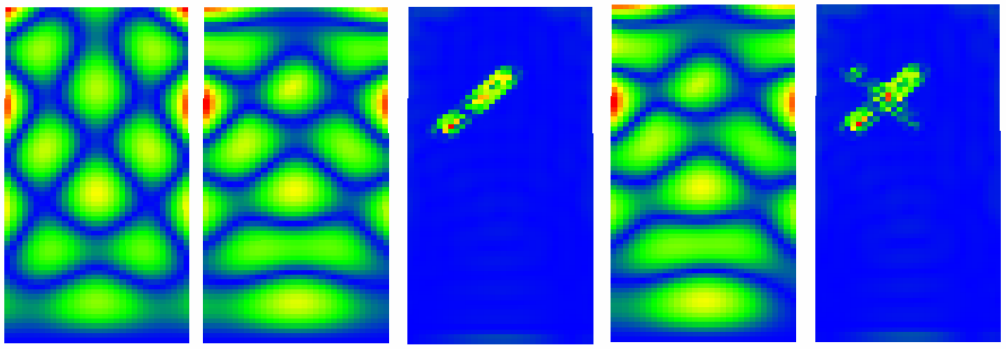

Healthy MS D1 MS Detector D2 MS Detector

24

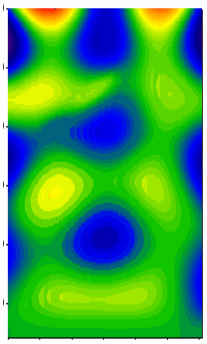

Delta Mode (D1)

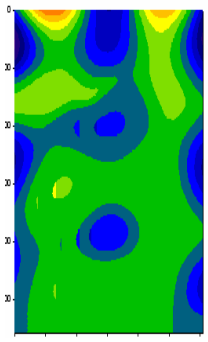

Delta Mode (D2)

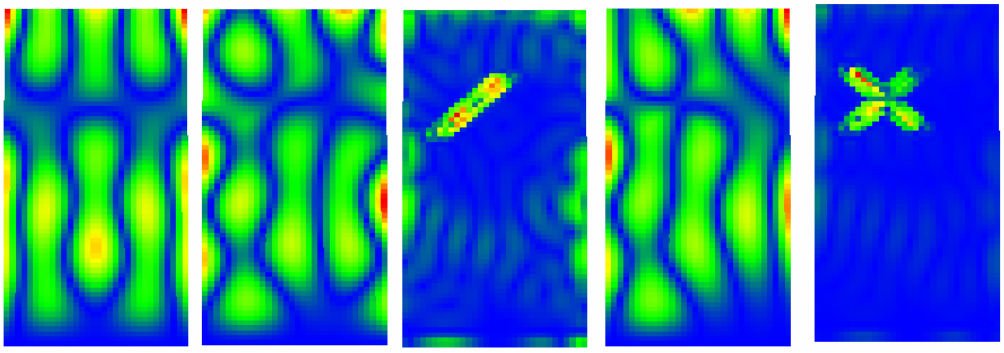

Healthy MS D1 MS Detector D2 MS Detector

25

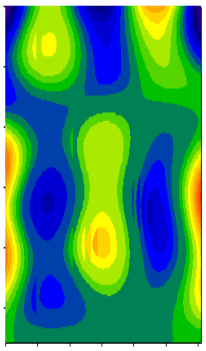

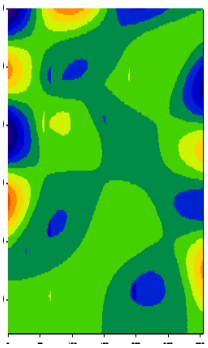

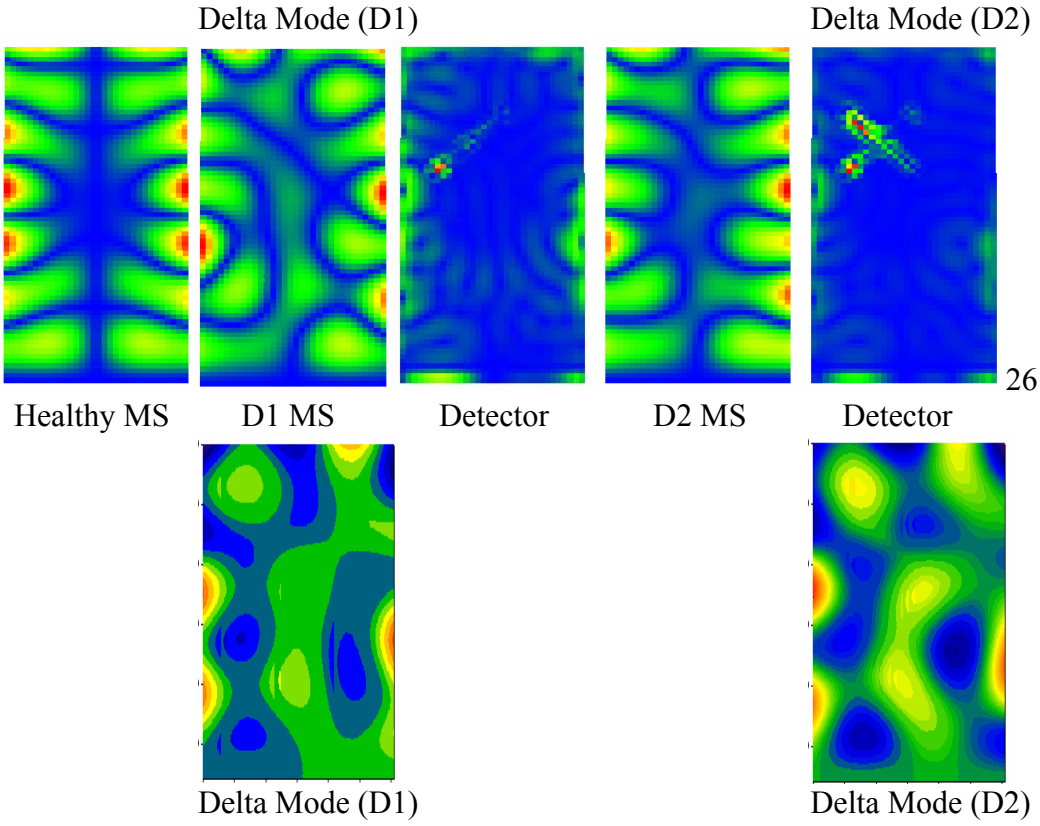
Delta Mode (D1)
Delta Mode (D2)
Healthy MS
D1 MS
Detector
D2 MS
Detector
Delta Mode (D1)
Delta Mode (D2)

26

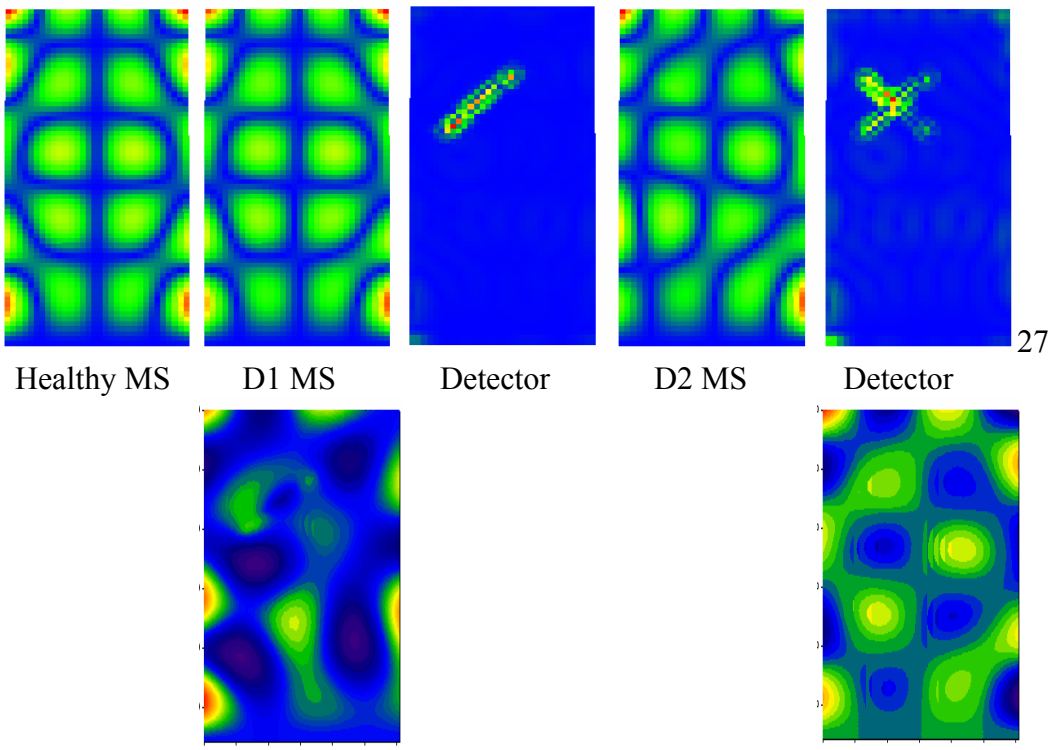
Healthy MS
D1 MS
Detector
D2 MS
Detector

27

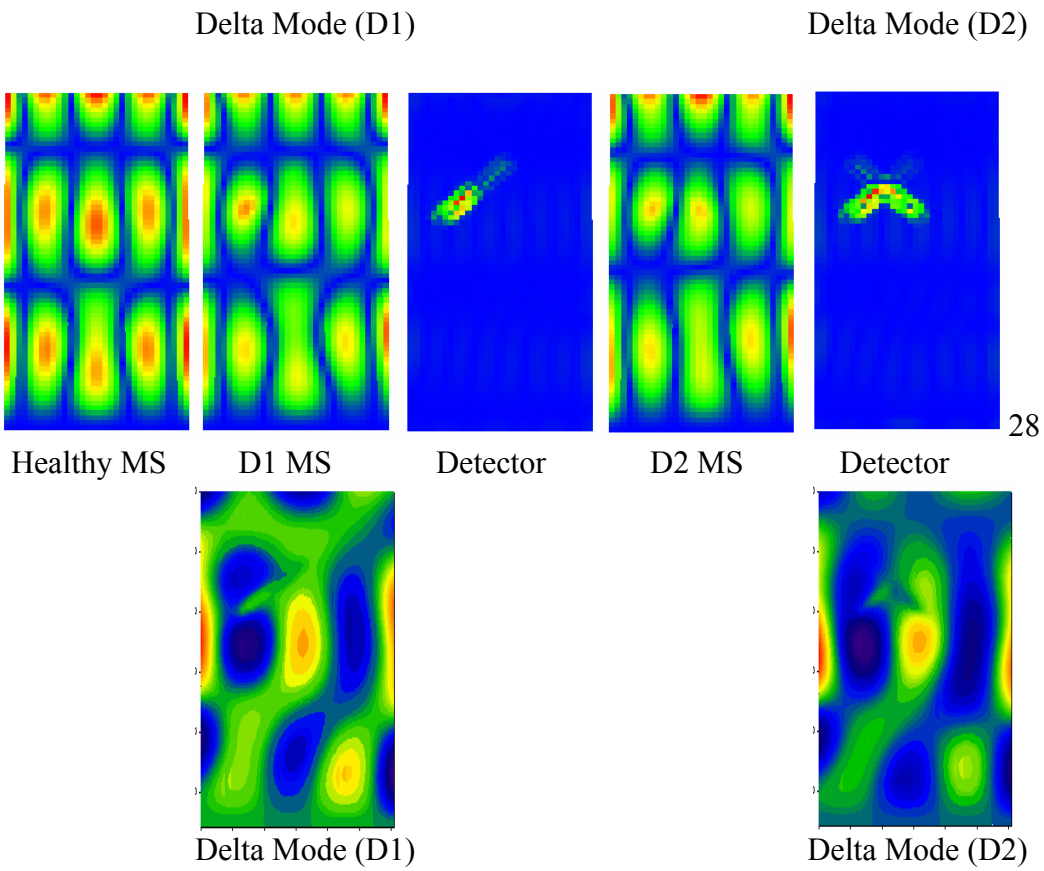
Delta Mode (D1)
Delta Mode (D2)
Healthy MS
D1 MS
Detector
D2 MS
Detector
28
Delta Mode (D1)
Delta Mode (D2)

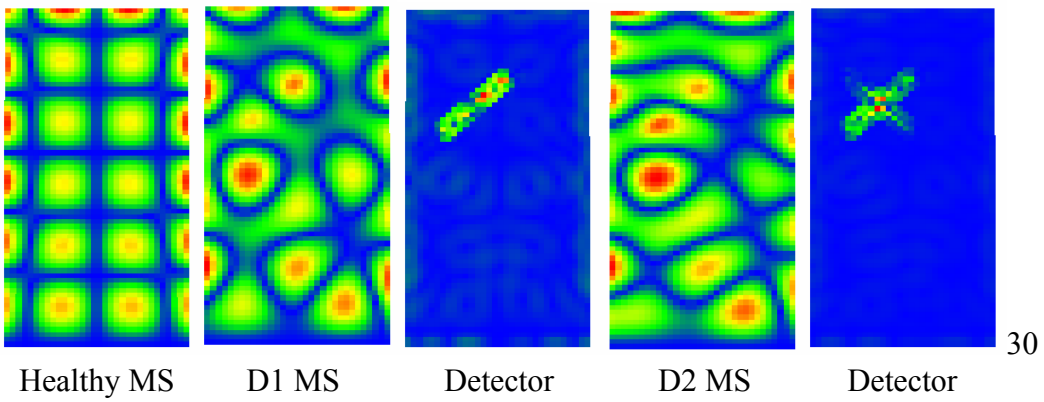
Healthy MS
D1 MS
Detector
D2 MS
Detector
30

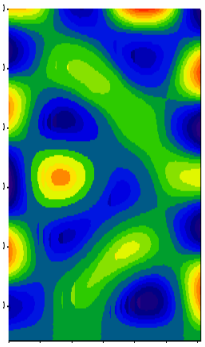

Delta Mode (D1)

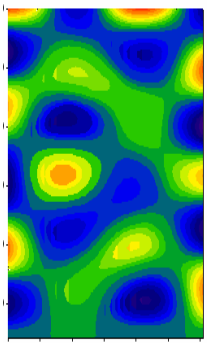

Delta Mode (D2)

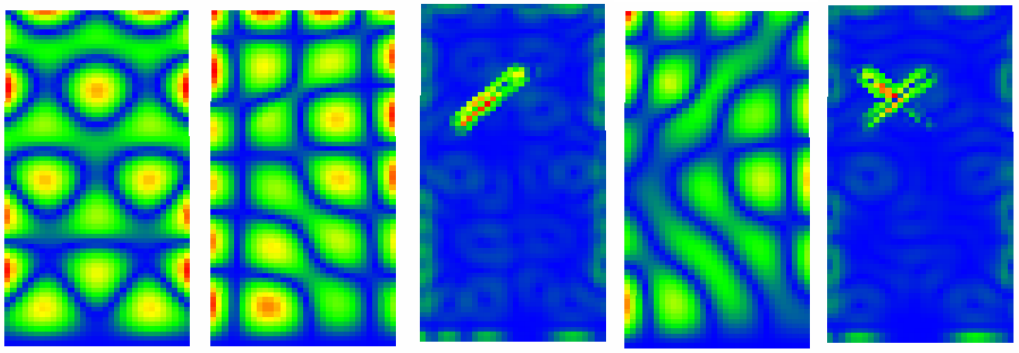

Healthy MS D1 MS Detector D2 MS Detector

31

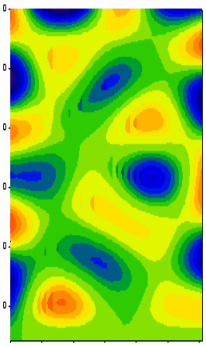

Delta Mode (D1)

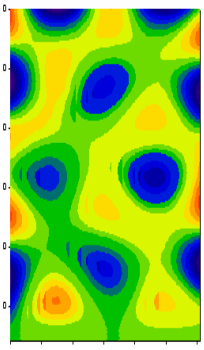

Delta Mode (D2)

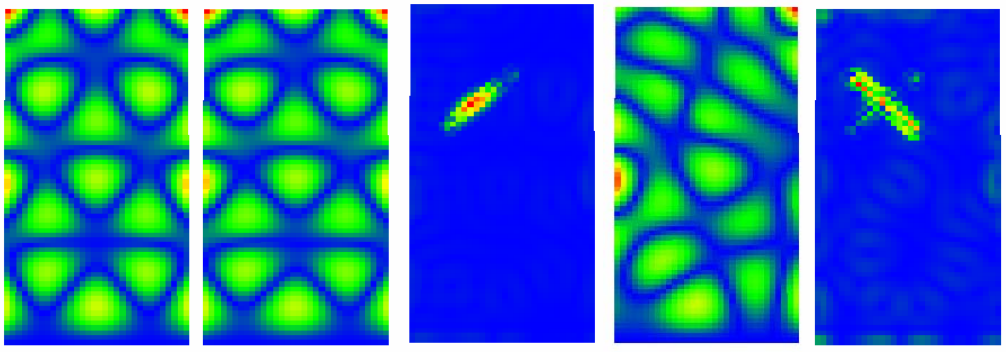

32

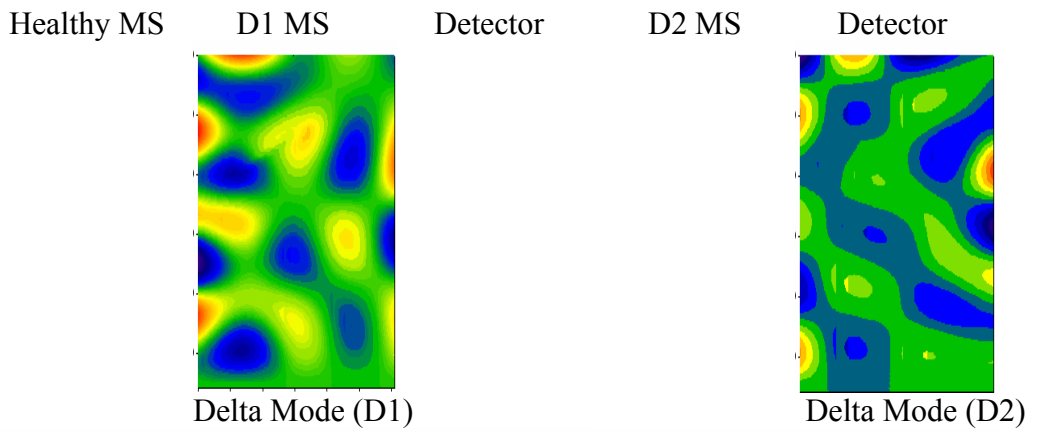
Healthy MS
D1 MS
Detector
D2 MS
Detector
Delta Mode (D1)
Delta Mode (D2)

33

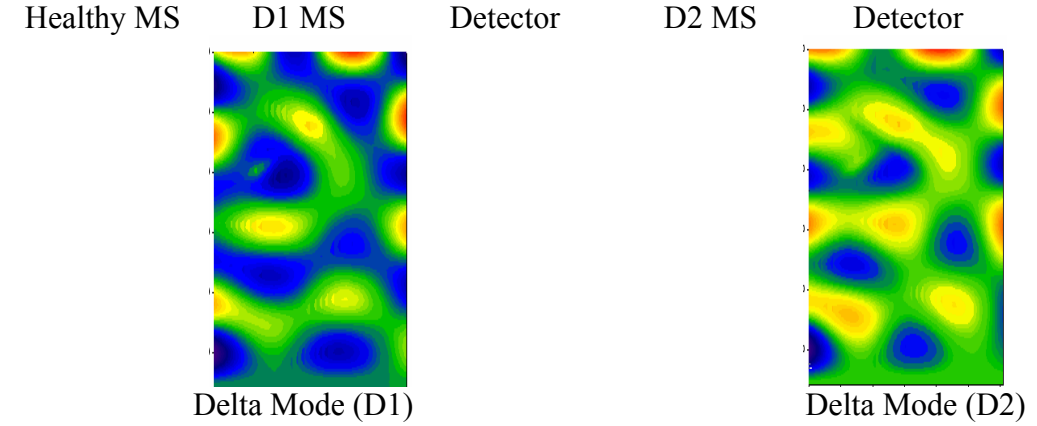
Healthy MS
D1 MS
Detector
D2 MS
Detector
Delta Mode (D1)
Delta Mode (D2)

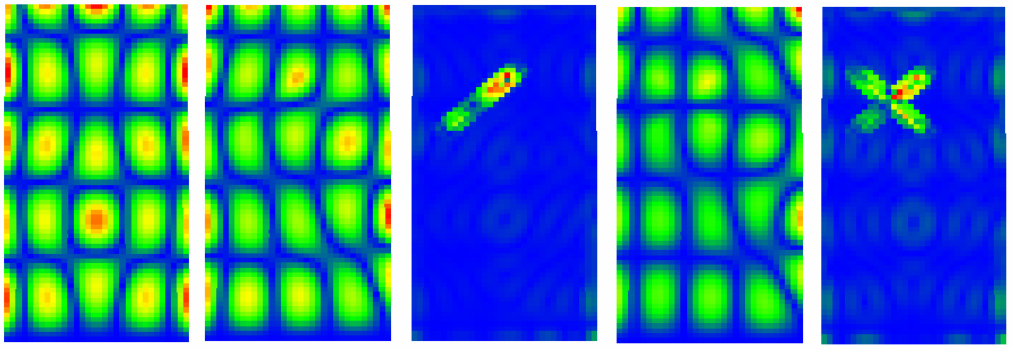

Healthy MS D1 MS Detector D2 MS Detector

34

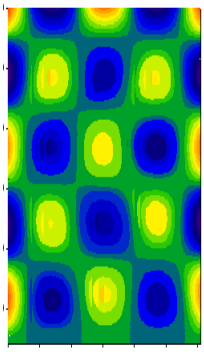

Delta Mode (D1)

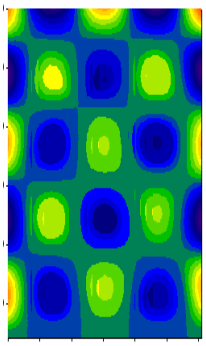

Delta Mode (D2)

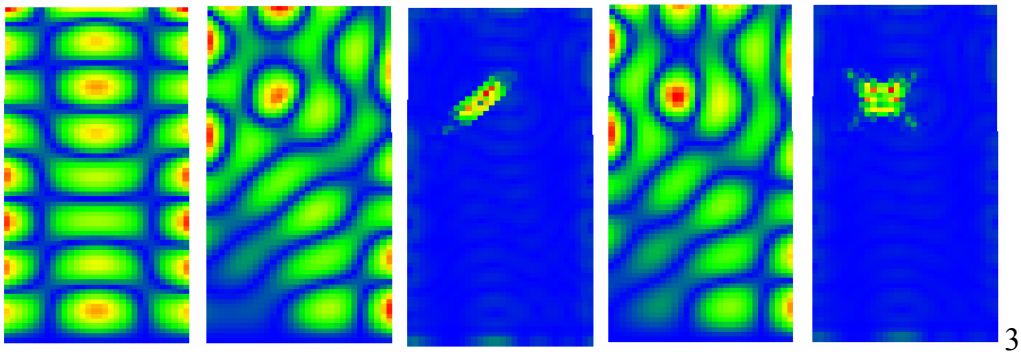

Healthy MS D1 MS Detector D2 MS Detector

35

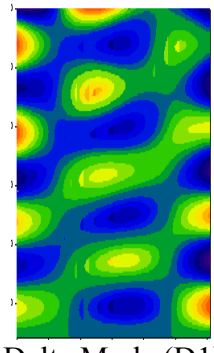

Delta Mode (D1)

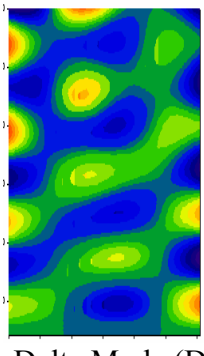

Delta Mode (D2)

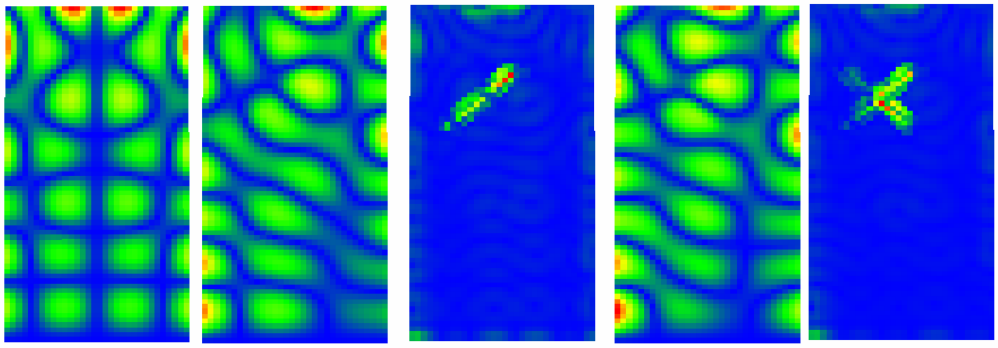

Healthy MS D1 MS Detector D2 MS Detector

36

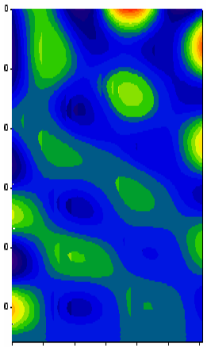

Delta Mode (D1)

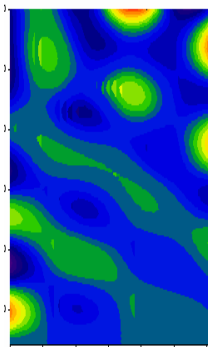

Delta Mode (D2)

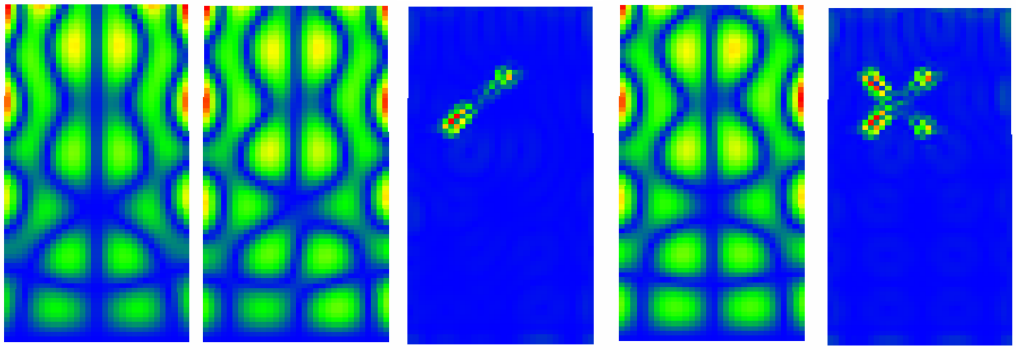

Healthy MS D1 MS Detector D2 MS Detector

37

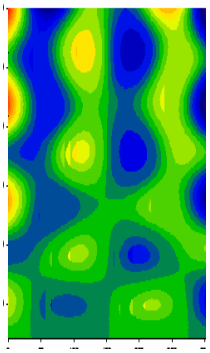

Delta Mode (D1)

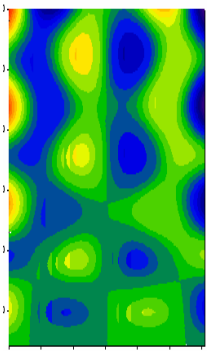

Delta Mode (D2)

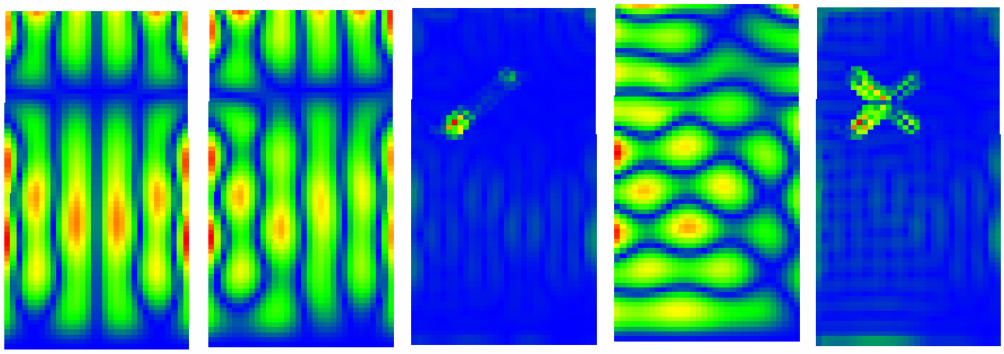

Healthy MS D1 MS Detector D2 MS Detector

38

Delta Mode (D1) Delta Mode (D2)

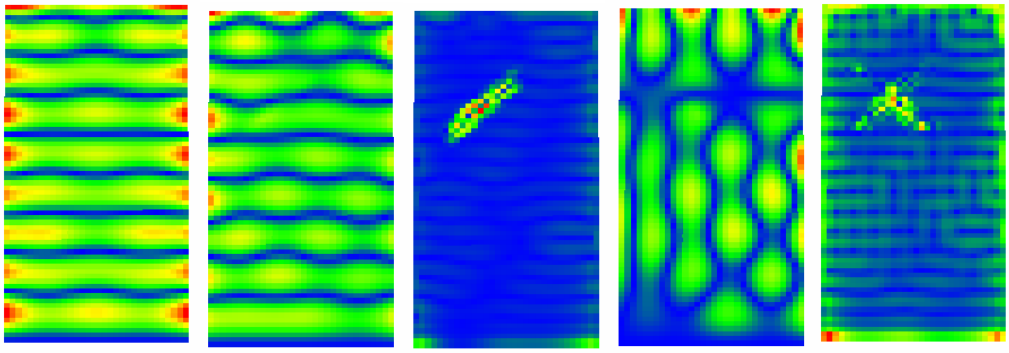

Healthy MS D1 MS Detector D2 MS Detector

39

Delta Mode (D1) Delta Mode (D2)

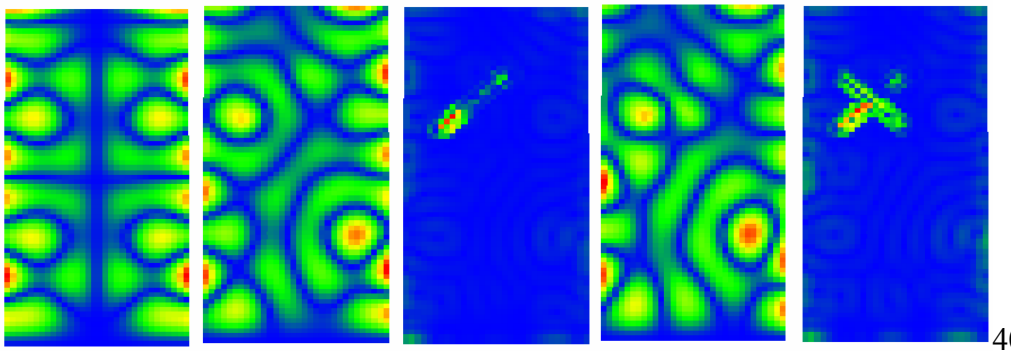

Healthy MS D1 MS Detector D2 MS Detector

40

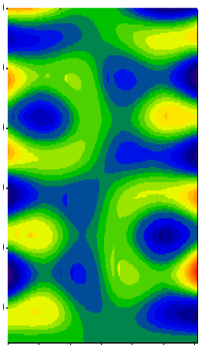

Delta Mode (D1)

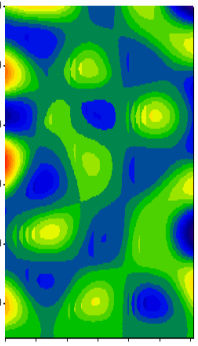

Delta Mode (D2)

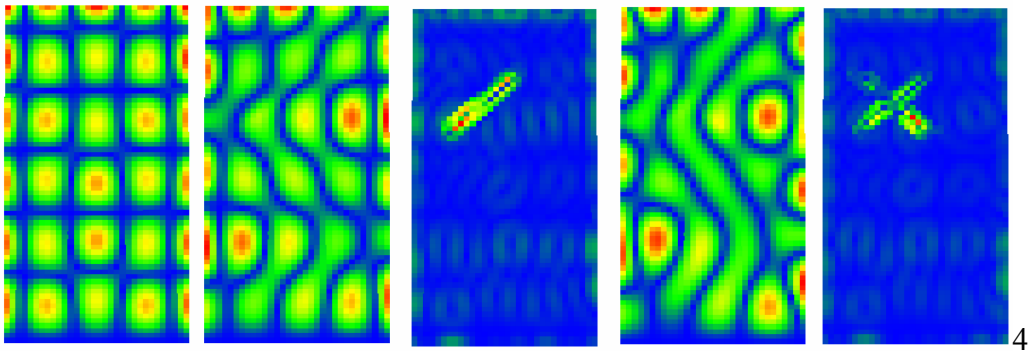

Healthy MS D1 MS Detector D2 MS Detector

41

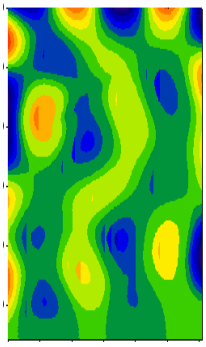

Delta Mode (D1)

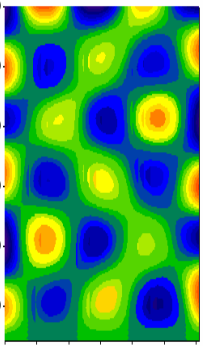

Delta Mode (D2)

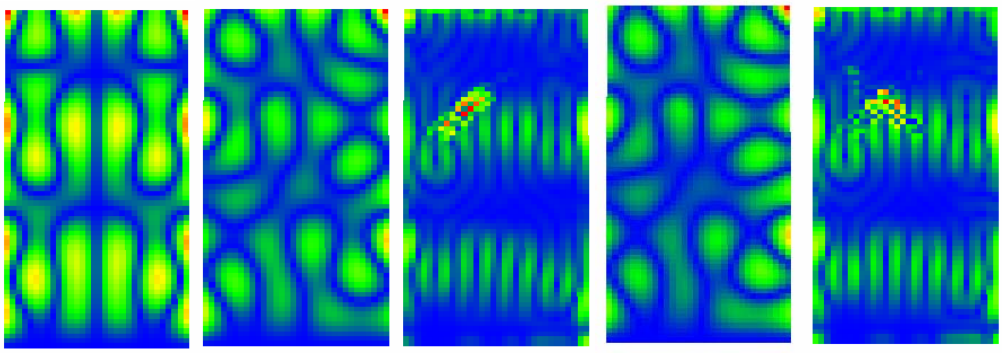

Healthy MS D1 MS Detector D2 MS Detector

42

Delta Mode (D1) Delta Mode (D2)

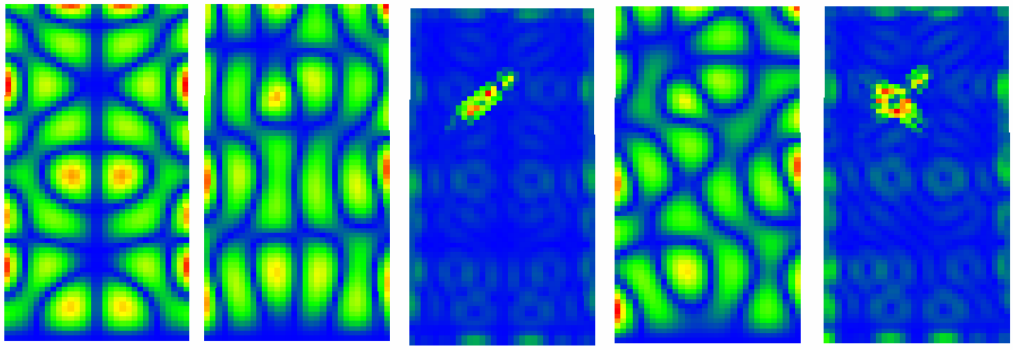

Healthy MS D1 MS Detector D2 MS Detector

43

Delta Mode (D1) Delta Mode (D2)

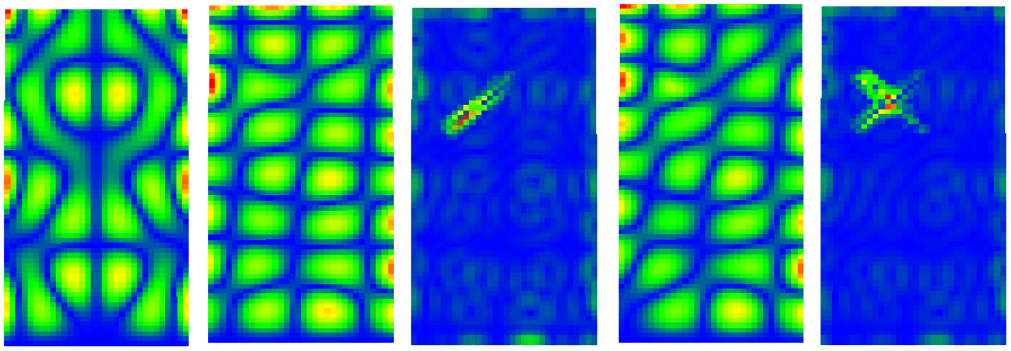

Healthy MS D1 MS Detector D2 MS Detector

44

Delta Mode (D1) Delta Mode (D2)

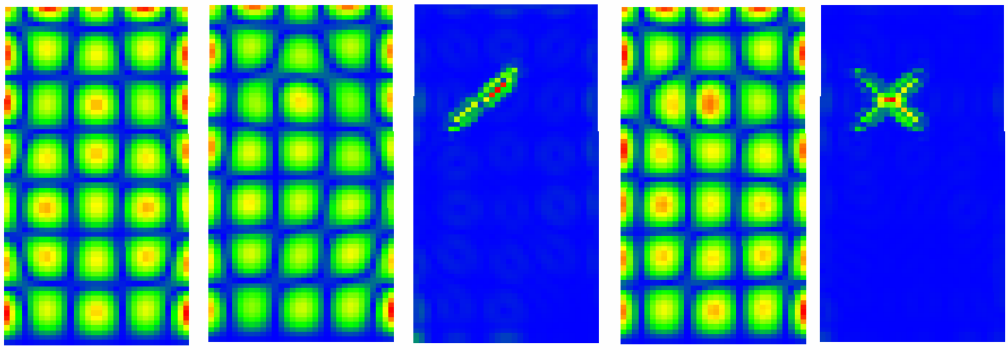

Healthy MS D1 MS Detector D2 MS Detector

46

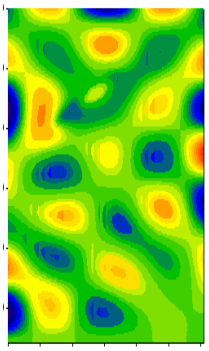

Delta Mode (D1)

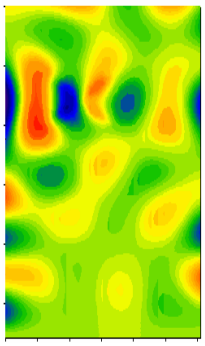

Delta Mode (D2)

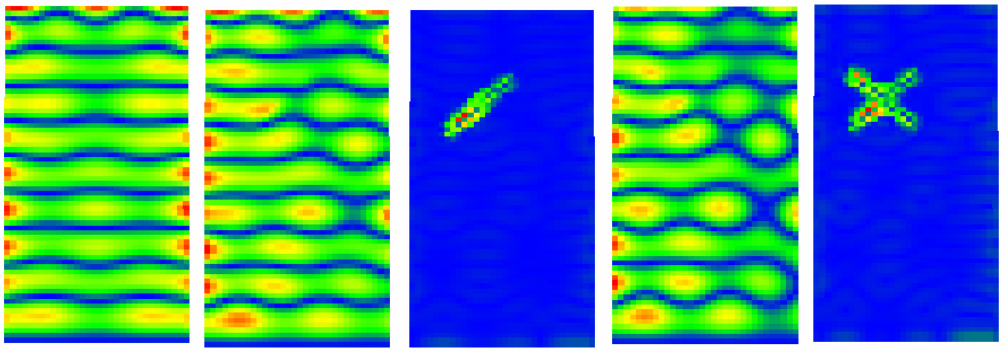

Healthy MS D1 MS Detector D2 MS Detector

47

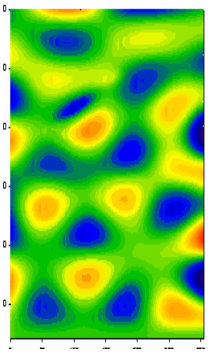

Delta Mode (D1)

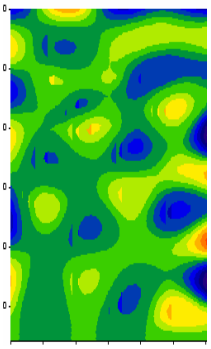

Delta Mode (D2)

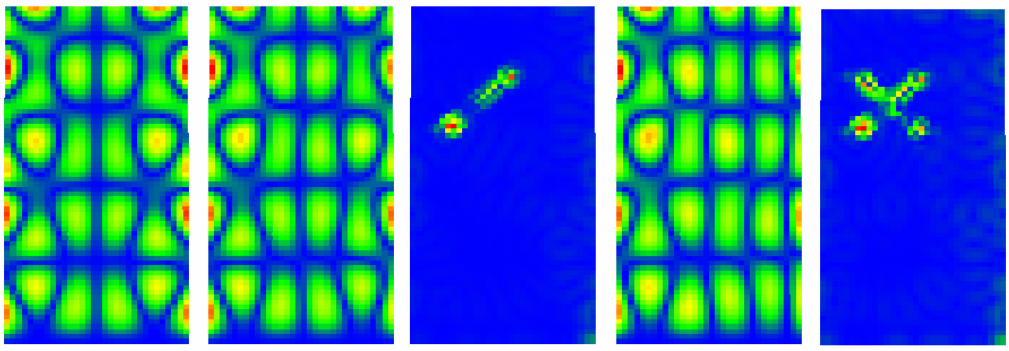

48

Healthy MS D1 MS Detector D2 MS Detector

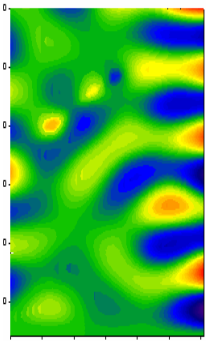

Delta Mode (D1)

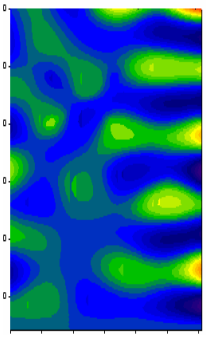

Delta Mode (D2)

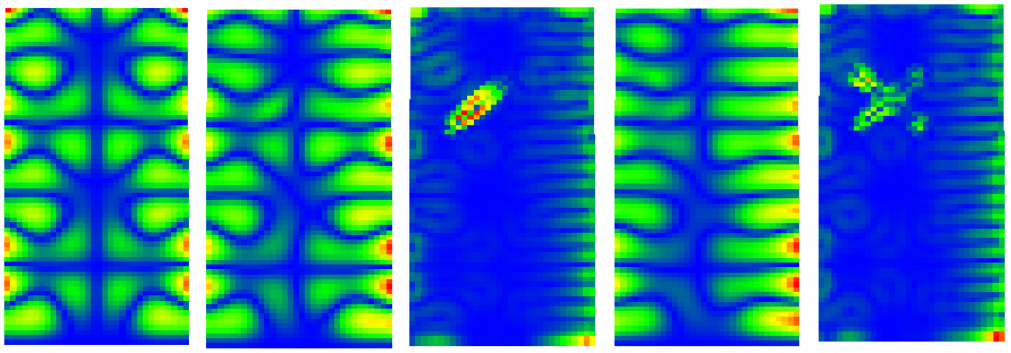

49

Healthy MS D1 MS Detector D2 MS Detector

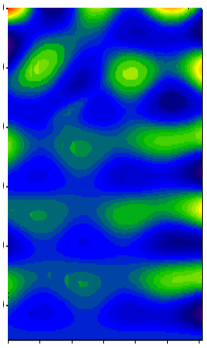

Delta Mode (D1)

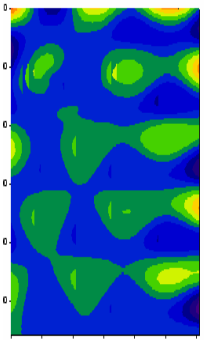

Delta Mode (D2)

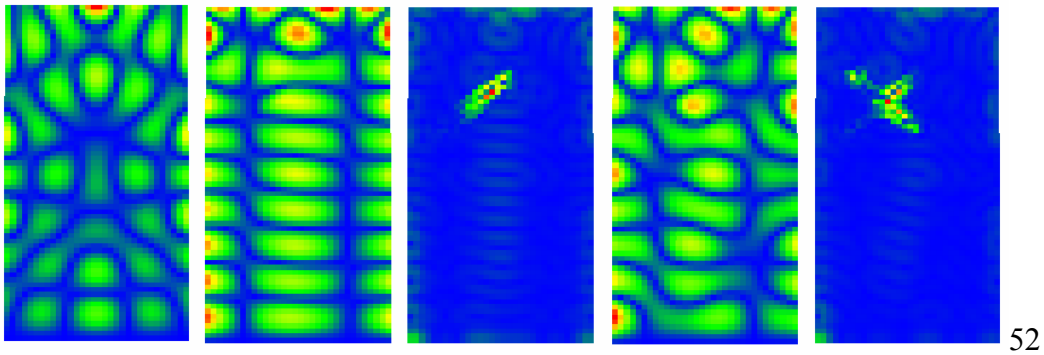

Healthy MS D1 MS Detector D2 MS Detector

52

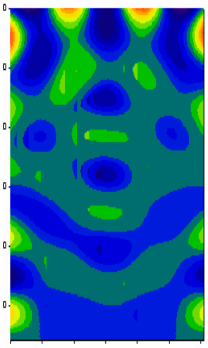

Delta Mode (D1)

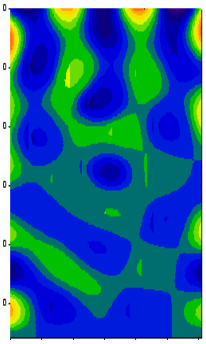

Delta Mode (D2)

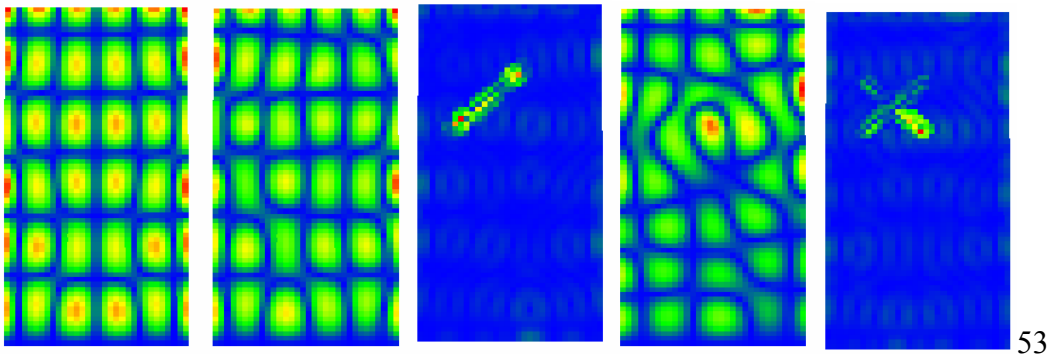

Healthy MS D1 MS Detector D2 MS Detector

53

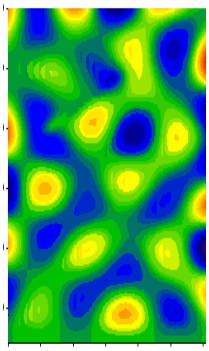

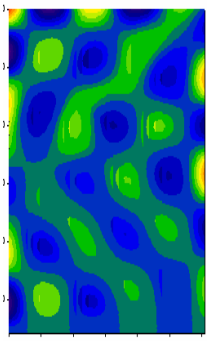

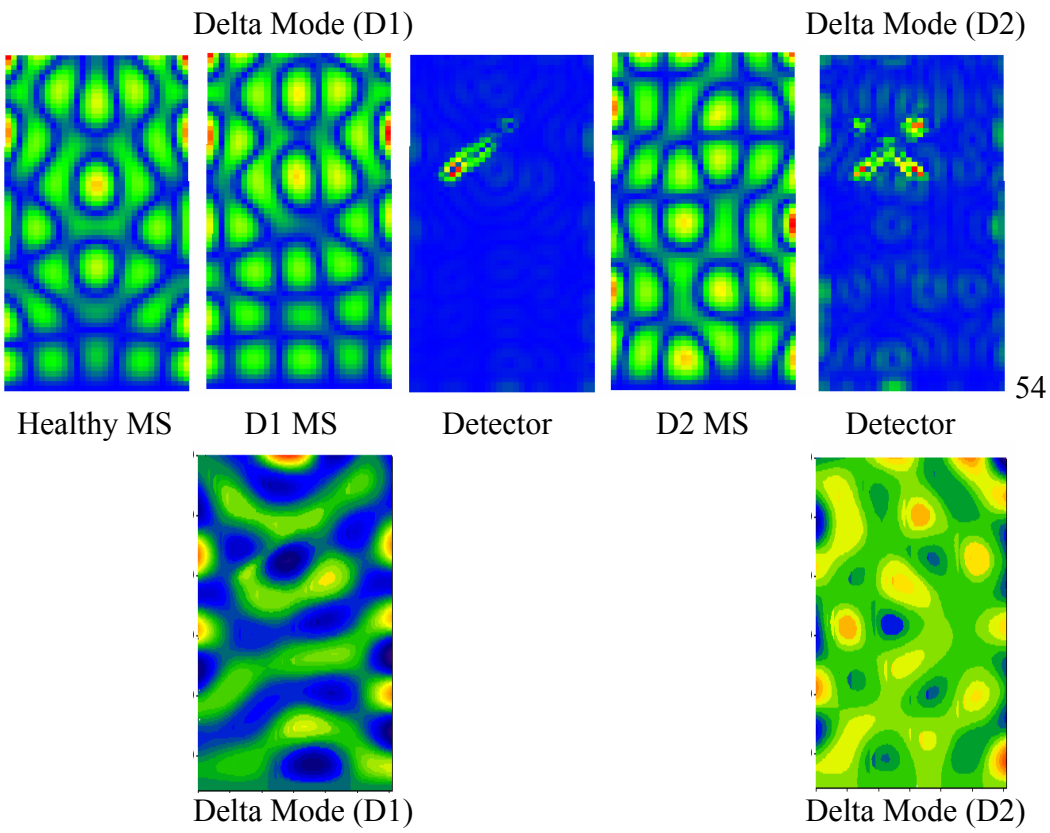
Delta Mode (D1)
Delta Mode (D2)
Healthy MS
D1 MS
Detector
D2 MS
Detector
Delta Mode (D1)
Delta Mode (D2)

54

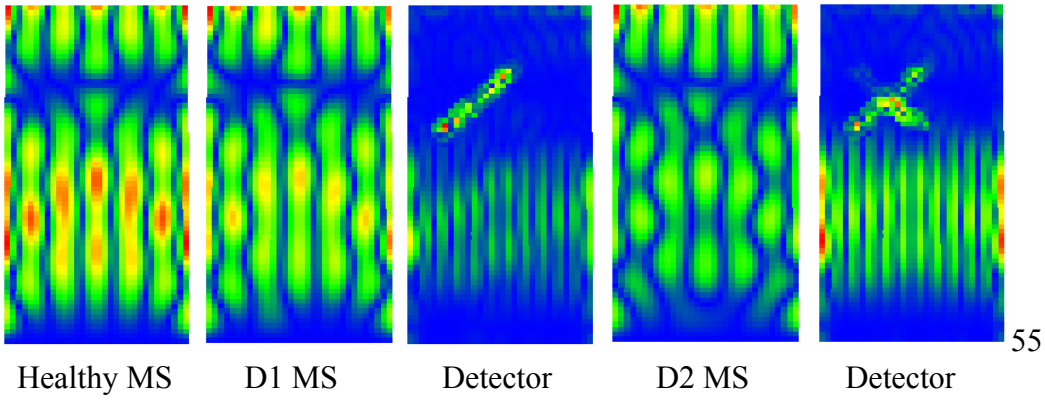
Healthy MS
D1 MS
Detector
D2 MS
Detector

55

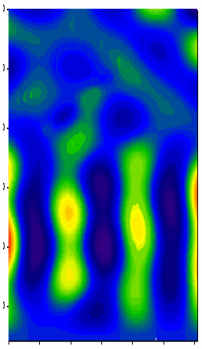

Delta Mode (D1)

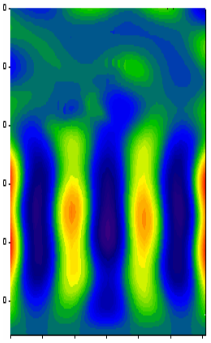

Delta Mode (D2)

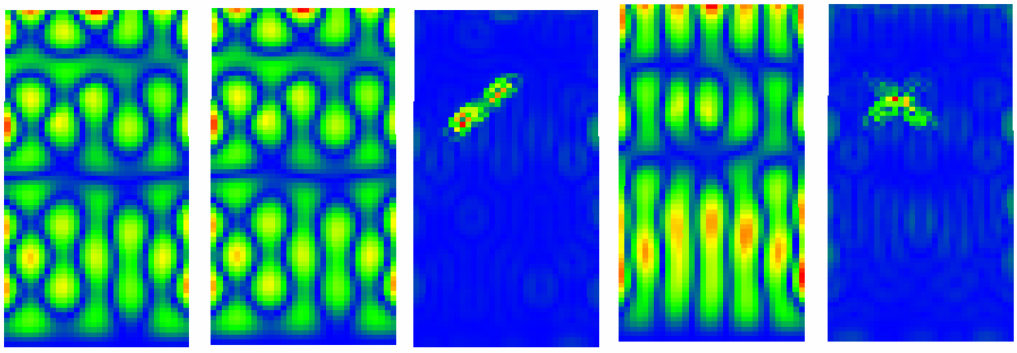

Healthy MS D1 MS Detector D2 MS Detector

56

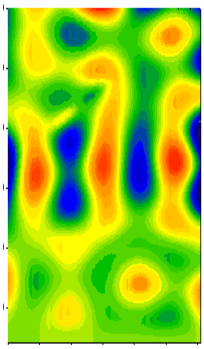

Delta Mode (D1)

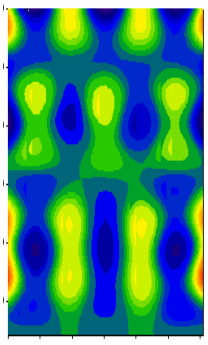

Delta Mode (D2)

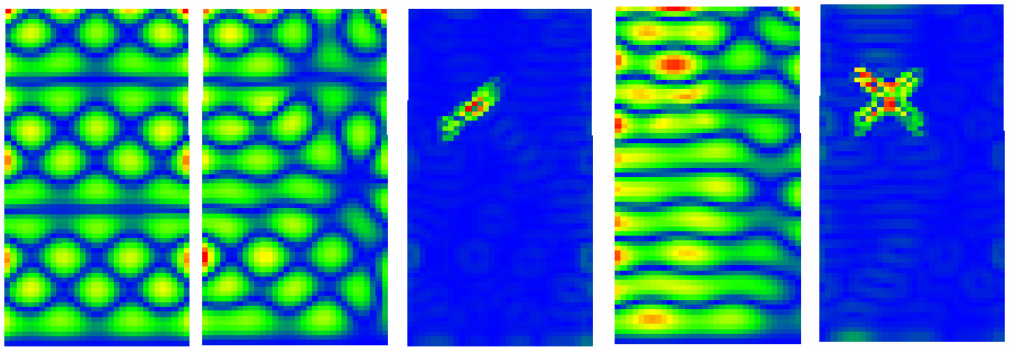

57

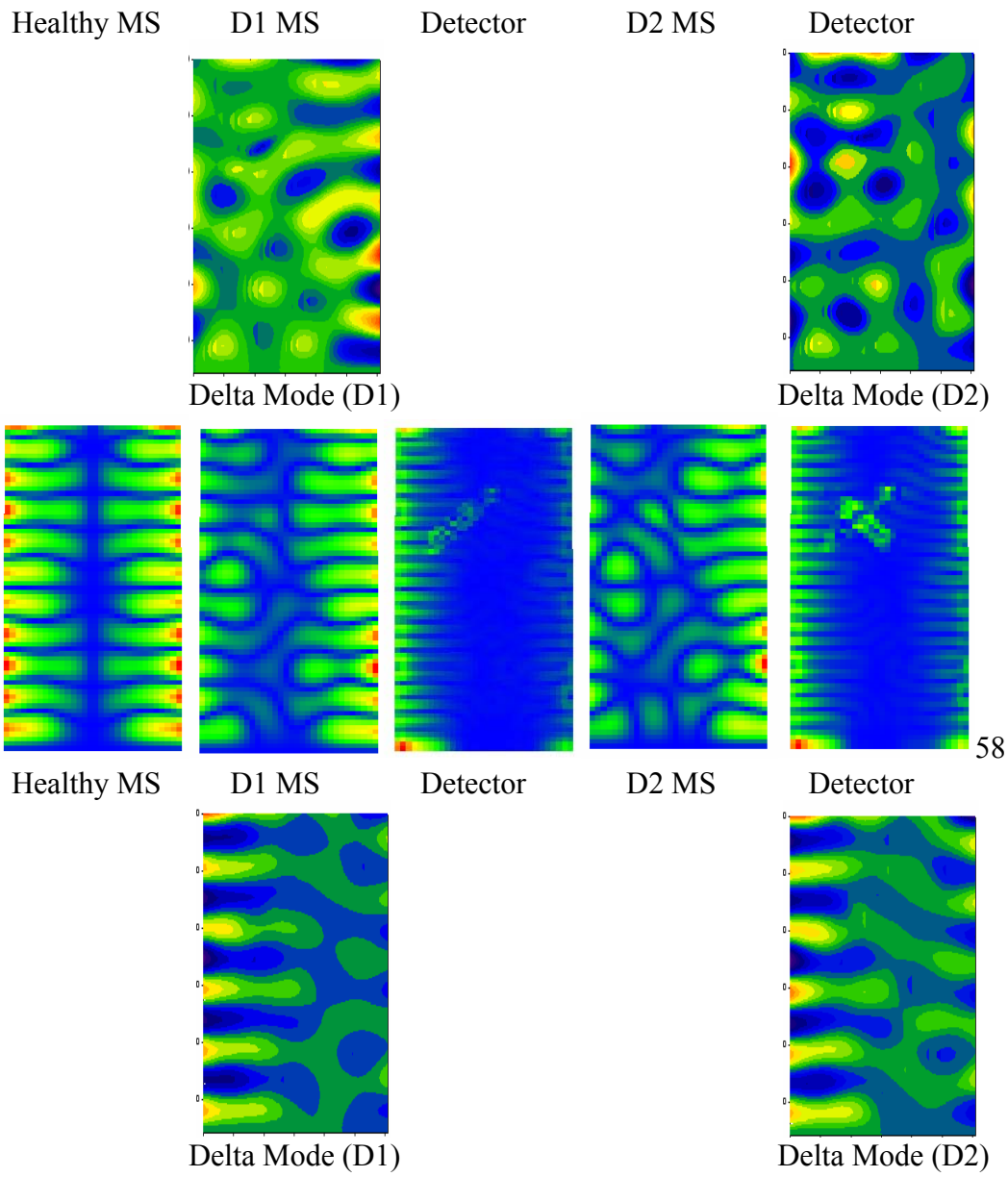
Healthy MS
D1 MS
Detector
D2 MS
Detector
Delta Mode (D1)
Delta Mode (D2)
58
Healthy MS
D1 MS
Detector
D2 MS
Detector
Delta Mode (D1)
Delta Mode (D2)

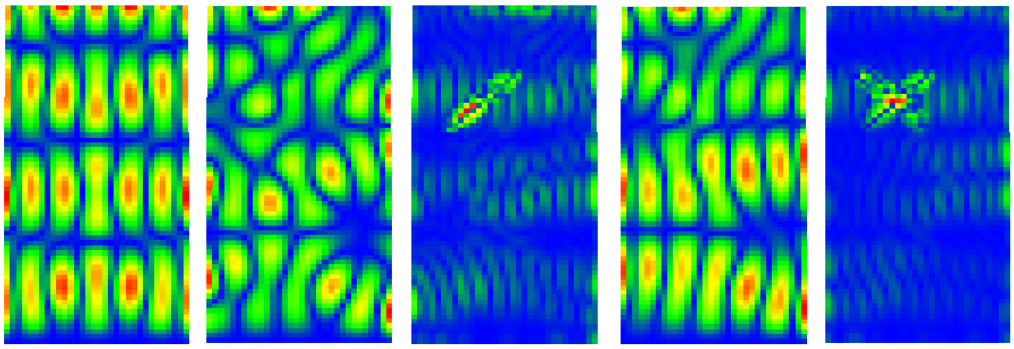

60

Healthy MS D1 MS Detector D2 MS Detector

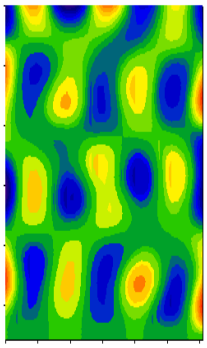

Delta Mode (D1)

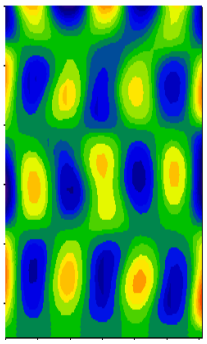

Delta Mode (D2)